Université de Toulouse

THÈSE

En vue de l'obtention du

DOCTORAT DE L'UNIVERSITÉ DE TOULOUSE

Délivré par :

Institut National des Sciences Appliquées de Toulouse (INSA de Toulouse)

Présentée et soutenue par :
Thanh Duong DAO

le 09 septembre 2013

Titre :

Procédés membranaires pour l'élimination des métaux lourds : Application de la Distillation Membranaire à l'élimination de l'Arsenic contenu dans les eaux saumâtres

---

École doctorale et discipline ou spécialité :
ED MEGEP : Génie des procédés et de l'Environnement

Unité de recherche :
Laboratoire d'Ingénierie des Systèmes Biologiques et des Procédés (LISBP)

Directeur(s) de Thèse :

Corinne Cabassud et Stéphanie Laborie

Jury :
Eric Favre - Professeur, ENSIC, Nancy (Rapporteur)
Alessandra Criscuoli - Chargée de recherche, ITM-CNR, Rende, Italie (Rapporteur)
Fabrice Gascons Viladomat - Directeur d'Ederna, Toulouse
Jean-Pierre Méricq - Maître de Conférences, Université Montpellier II, Montpellier
Corinne Cabassud - Professeure, INSA, Toulouse
Stéphanie Laborie - Maître de Conférences, INSA, Toulouse

THESE

Présentée à l'

INSTITUT NATIONAL DES SCIENCES APPLIQUEES de TOULOUSE

En vue de l'obtention du

DOCTORAT DE L'UNIVERSITE DE TOULOUSE

Ecole Doctorale MEGeP

Spécialité : Génie des Procédés et de l'Environnement

par

Thanh Duong DAO

Ingénieur de l'INSA de Toulouse

Procédé membranaires pour l'élimination des métaux lourds: Application de la Distillation Membranaire à l'élimination de l'Arsenic contenu dans les eaux saumâtres

Soutenue le 9 septembre 2013 devant le jury composé de

Eric Favre	Professeur à ENSIC, Nancy (France)	Rapporteur
Alessandra Criscuoli	Chargée de recherche, ITM-CNR , Rende (Italie)	Rapporteur
Fabrice Gascons Viladomat	Dr/Directeur d'Ederna, Toulouse (France)	Examinateur
Jean-Pierre Méricq	Maître de Conférences, Université Montpellier II (France)	Examinateur
Corinne Cabassud	Professeure à INSA, Toulouse (France)	Directrice
Stéphanie Laborie	Maître de Conférences à INSA, Toulouse (France)	Co-directrice

Laboratoire d'Ingénierie des Systèmes Biologiques et des Procédés (LISBP)
LISBP, UMR5504 CNRS, UMR792 INRA, INSA Toulouse
Mécanique, Energétique, Génie civil et Procédés (MEGeP)

RESUME :

Cette thèse de doctorat concerne l'étude de la distillation membranaire sous vide pour l'élimination de l'arsenic contenu dans les eaux souterraines. En effet, la contamination des nappes phréatiques par l'arsenic est une problématique majeure dans de nombreux pays, et en particulier au Vietnam. Dans ce pays, choisi comme cas d'étude pour ce travail, environ 13% de la population est empoisonnée par des eaux souterraines contaminées par l'arsenic. De plus, ces eaux souterraines présentent des salinités élevées (5-10 $g.L^{-1}$) dues à des infiltrations d'eau de mer dans les nappes. Ce travail de thèse a permis de démontrer la faisabilité de la distillation membranaire sous vide (DMV) pour éliminer l'arsenic contenu dans ces eaux et réduire leur salinité afin de les rendre propres à la consommation humaine. Les concentrations en As(III) dans le perméat de DMV sont toujours inférieures aux limites de la norme en eau potable (10 $\mu g.L^{-1}$), même pour de très fortes concentrations en As(III) dans l'alimentation (jusqu'à 2000 $\mu g.L^{-1}$). La DMV ne nécessite pas de pré-oxydation de l'As(III) en As(V), étape nécessaire dans de nombreux procédés conventionnels de traitement.

De plus, un couplage entre l'osmose inverse (OI) et la DMV a été étudié : l'étape d'OI permet une pré-concentration en NaCl et As(III), puis ce rétentat est alors sur-concentré grâce à la DMV. La DMV a montré de très bonnes performances pour traiter un concentrat contenant de très fortes concentrations en As(III) (7000 $\mu g/L$). La DMV permet toujours de limiter les teneurs en arsenic dans le perméat à des valeurs en-dessous de la norme. Enfin, une simulation d'un procédé global, incluant OI et DMV, et fonctionnant à un taux de conversion global de 96%, a été effectuée. Ce couplage ouvre la voie vers un traitement global de l'arsenic permettant de générer de très faibles quantités d'effluents finaux.

MOTS CLES:

Elimination arsenic, eaux souterraines, distillation membranaire sous vide, membrane hydrophobe, traitement de l'eau

ABSTRACT:

This PhD work deals with vacuum membrane distillation (VMD) for arsenic removal from groundwaters. Contamination of water resources with arsenic was identified in 105 countries. Approximately 150 million people are being exposed to arsenic contamination, and 147 million of these people live in Asia. In Vietnam, chosen as the case study of this work, 13% of the population is being in risk of arsenic poisoning. Drinking water resources present not only high arsenic concentration (1 – 3050 ppb) but also high salinity (5 – 15 g/L). This work allowed demonstrating the feasibility of VMD to remove arsenic and also salts contained in groundwaters. As(III) concentration in the permeate of VMD was always lower than the standard level for drinking water (10 $\mu g.L^{-1}$), even for high As(III) concentrations in the feed (up to 2000 $\mu g.L^{-1}$). With VMD, a pre-oxidation step was not necessary to convert As(III) into As(V), as it is the case for other conventional treatment processes.

Moreover, a coupling between reverse osmosis (RO) and VMD was studied. RO was considered as a first step to concentrate NaCl and As(III) before this retentate stream was further concentrated by the VMD. VMD could work efficiently with 99.9% of As(III) and NaCl rejections at a very high RO retentate concentrations ([NaCl] = 300 g/L and [As(III)] = 7000 ppb). Arsenic in the permeate was still lower than the required standard for drinking water. Finally, a simulation of the coupling was performed. By coupling of RO and VMD, a high global recovery of 96% could be achieved.

KEYWORDS:

Arsenic removal, brackish groundwater, vacuum membrane distillation, hydrophobic membrane, water treatment

Table of contents

TABLE OF CONTENTS

Introduction:
Research problem

Arsenic contamination of shallow groundwater is among the biggest health threats in the world. According to the latest information from International Water Association Publishing (IWA, 04/2013), contamination of water resources with arsenic are identified in 105 countries and territories in all continents: Approximately 151 million people worldwide are exposed to arsenic contamination and 147 million of these people live in Asia.

In Asia, Vietnam is one of the countries being identified as affected by arsenic contamination in drinking water resources together with India, Bangladesh, China, Cambodia, Nepal and Thailand. In Vietnam, this contamination is due to the commonly observed sources (geological structure; agriculture activities and industry, etc...), which have been widely reported in other places, but also to one more specific anthropogenic source of arsenic: the 'Operation Ranch Hand" program during Vietnam war. During all ten years of this war (1962 – 1971), Agent Blue, containing 31.1% of arsenic compounds, was sprayed as the major exterminatory chemical over Vietnam. According to the HERBS collection, the most thorough data repository of herbicide usage during the Vietnam War, approximately 4,712,920 liters of Agent Blue were sprayed in Southern Vietnam, corresponding to 235,820 liters of arsenic compounds were sprayed onto crop lands. Distribution of arsenic contamination in Vietnam is presented in the following figure A.

As a consequence, arsenic contamination was detected in many provinces of Vietnam. According to a practical survey of Ministry of Natural Resources and Environment of Vietnam (MONRE), more than one million of high arsenic-contaminated water wells are in use in the whole country, mainly gathering in both Mekong Delta (South of Vietnam) and Red River Delta (North of

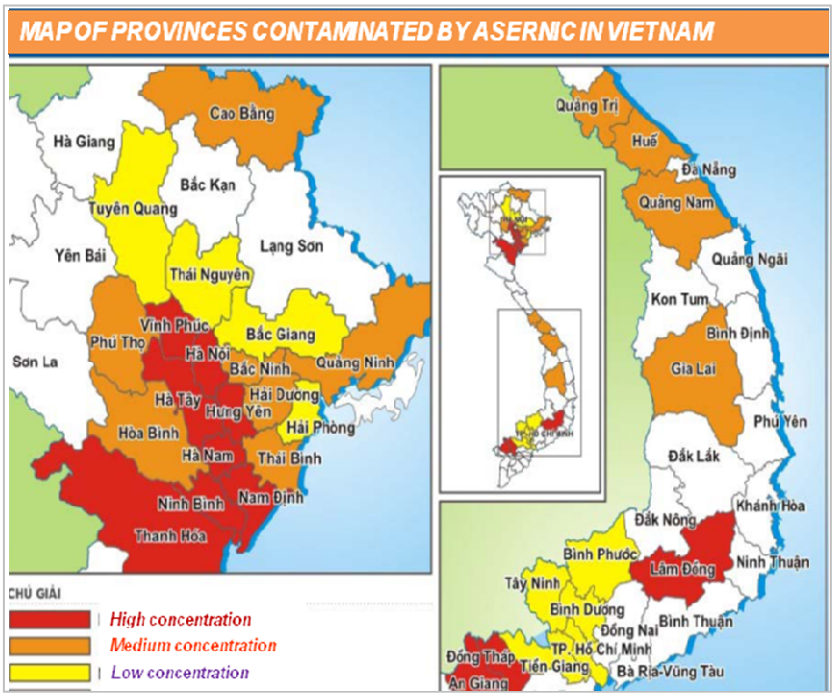

Figure A *Distribution of arsenic contamination in Vietnam*

Vietnam). With arsenic concentrations in range of [1 – 1610 ppb] and [1 - 3050 ppb] in Mekong Delta and Red River Delta respectively, around 10 – 15 million Vietnamese residents (equivalent to 13% of population) are being in risk of arsenic poisoning.

Moreover, along with arsenic contamination issue in water sources for drinking water, Vietnam is also one of the countries in the world being affected seriously by Climate change issue. According to the Climate change scenario published by MONRE in 2012, the sea level would increase in range 0.75 – 1.0 meter, leading to 40% total areas of MeKong Delta, 11% of Red River Delta and 3% of other coastal provinces would be flooded at the end of 21st century. As a consequence of seawater intrusion, the drinking water resources have high salinity of 5 – 15 g/L, much higher than the standard for drinking water. It means that desalination and arsenic removal for drinking water production can be foreseen as critical sanitary issues in the near future for Vietnam.

Regarding arsenic removal, various treatment technologies (adsorption, precipitation, ion exchange and membrane processes) can be applied efficiently to remove arsenic to meet the standard for drinking water (MCL = 10 ppb). However, one of the main drawback of these techniques is high treatment cost since a pre-oxidation step to convert As(III) into As(V) is required to ensure high arsenic removal. In addition, the reverse osmosis membrane process is quite suitable for desalination but not very efficient for As(III) removal while other conventional techniques, such as: adsorption, precipitation are useless for desalination. In this situation, membrane distillation (MD) could be considered as an interesting alternative or complementary process. Moreover, vacuum membrane distillation (VMD) is expected to produce a permeate flux, which is from 1.4 – 2 times higher than that of other membrane distillation configurations. For these reasons, the aim of this PhD study is to determine feasibility of the VMD process for removing arsenic in contaminated brackish underground waters. This work was performed at LISBP – INSA Toulouse and was supported by Hanoi University of Science and Technology (USTH) in the frame of a French-Vietnamese partnership.

Regarding scope of study, this research mainly focuses on an evaluation of potentiality and applicability of the VMD technology for arsenic rejection with the objective to produce drinking water. Arsenic contamination in Vietnam was considered as a research case-study. For that reason, synthetic feed solution with similar characteristic to the one of groundwater in

Vietnam were prepared and used for all the experiments. **It is worth noting that it was decided to focus on As(III) removal in this study to assess ability of the VMD for direct As(III) removal without any pre-oxidation step required as in the conventional treatment processes**.

Two different process configurations were considered in this work:

(1) VMD as a direct treatment to remove both salt (NaCl in this study) and As(III) from water; and

(2): Coupling of reverse osmosis (RO) and VMD, in which RO was considered as a first step to concentrate NaCl and As(III) before this retentate stream was further concentrated by the VMD.

These two configurations were compared in term of water recovery and specific energy consumption.

In general, this report includes five chapters with the following main contents:

Chapter 1 : Bibliography review;
Chapter 2 : Materials and methods;
Chapter 3 : A new method for permeability measurement of hydrophobic membrane in vacuum membrane distillation;
Chapter 4 : Direct arsenite removal by vacuum membrane distillation technology;
Chapter 5 : Coupling of reserve osmosis and vacuum membrane distillation for arsenite removal from brackish groundwater.

Chapter I:
Bibliography review

As the main objective of this research is to study feasibility of Vacuum membrane distillation for direct arsenic removal from water, this chapter mainly aims to introduce background and literature review on: (1) arsenic and (2) vacuum membrane distillation. The first section provides all general information related to arsenic compounds, including arsenic definition, arsenic chemistry, occurrence, toxicity and its mechanisms to affect people health. Furthermore, possible treatment methods that have been applied for arsenic removal such as: oxidation, coagulation, adsorption, precipitation, ion exchange and membrane processes are also introduced and compared for this application. The last section of this chapter focuses on membrane distillation and particularly on the vacuum membrane distillation process. In this part, existing industrial applications of the VMD technology are introduced. Besides that, a detailed description of transfer mechanisms (both heat and mass transfer) is presented. Finally, influences of operating conditions on the VMD performance, such as: feed temperature, permeate pressure, hydrodynamics, are summarized.

I.1 BACKGROUND OF ARSENIC

I.1.1 What is arsenic?

Arsenic is a ubiquitous element that ranks 20th in abundance in the earth's crust, 14th in the seawater, and 12th in the human body [*Mandal and Suzuki, 2002*]. This element, represented by the symbol As, is a high poisonous metal having three allotropic forms, yellow, black and grey, of which the brittle, crystalline grey is the most common. Bearing the name derived from the Greek work *arsenikon,* meaning potent [*Choong et al, 2007*], this element can be found naturally in air, water, soil, and in plants and animals and is considered as a well-known human carcinogen [*Shih, 2005*].

In the Periodic Table of elements, arsenic is located in group 5A, so it is considered as a metalloid with its toxicity similar to other heavy metals such as lead (Pb) and mercury (Hg) that can cause skin and lung cancer, peripheral vascular disease, and liver damage. Due to its smell-less, tasteless, invisible and non-evaporative characteristics in the environment, even at its lethal dose, it is impossible to detect the presence of arsenic in waters by senses. Typical physicochemical properties of arsenic and its compounds are summarized in Table 1.1.

Table 1.1 *Typical physicochemical properties of arsenic and its compounds.*

Compound	Molecular formular	Melting point, (^{0}C)	Boiling point, (^{0}C)	Density (g/cm^3)	Water solubility, (g/L)
Arsenic	As	613	-	5.727[b]	Insoluble
Arsenic trioxide	As_2O_3	312.3	465	3.738	37 at 20^{0}C
Arsenic pentoxide	As_2O_5	315[a]	-	4.32	1500 at 16^{0}C
Arsenic sulphide	As_2S_3	300	707	3.43	5.10^{-4} at 18^{0}C
DMA	$(CH_3)_2AsO(OH)$	200	-	-	829 at 22^{0}C
MMA	$(CH_3)_2AsO(OH)_2$	-	-	-	-
Lead arsenate	$PbHAsO_4$	720[a]	-	5.79	Slightly soluble
Potassium arsenate	KH_2AsO_4	288	-	2.867	190 at 6^{0}C
Potassium arsenite	$KAsO_2HAsO2$	-	-	-	Soluble

***Source**: WHO, 2011.*

DMA: Dimethylarsinic acid;

MMA: Monomethylarsonic acid;

a: decomposes;b: at 14^{0}C.

Arsenic and its compounds are used commercially and industrially as alloying agents in the manufacture of transistors, lasers and semiconductors, as well as in the processing of glass, pigments, textiles, paper, metal adhesives, wood preservatives and ammunition. They are also used in the hide tanning process and, to a limited extent, as pesticides, feed additives and pharmaceuticals [*WHO, 2011*]. As a consequence, arsenic can be found in the environment because of its presence in the earth but also because of the anthropogenic activity.

I.1.2 Arsenic chemistry

In natural, arsenic occurs in both organic and inorganic forms (see Table 1.1). The organic species (monomethylarsenic and dimethylarsenic) are abundant in seafood, less harmful to the human health and readily eliminated by the body [*Havezov and Tsekulov, 2010*]; while the inorganic forms are more prevalent in water and considered more toxic. Therefore, most of studies focus on inorganic arsenic forms.

Inorganic arsenic has four oxidation states that are: -3, 0, +3 and +5, of which the +3 and +5 states are the most abundant found in a variety of minerals and natural waters. Total inorganic arsenic is the sum of particulate and soluble forms. Size distribution of particulate and soluble

inorganic arsenic is higher than 0.45-micron and lower than 3 kDa, respectively. As a result, a 0.45 micron filter is generally supposed to remove particulate arsenic. Meanwhile, soluble, inorganic arsenic exists in either one of two valence states depending on local re-dox conditions, including:

- ***In anoxic condition as in groundwaters***: arsenic is found in its arsenite or reduced trivalent form As(III);
- ***In aerobic condition as in surface waters***: another form as arsenate or oxidized pentavalent form As(V) is found.

Both arsenite and arsenate consist of four different species, which are very unstable in natural water. Their distribution depends on the redox conditions, pH and the presence of precipitating metals, such as: iron, organic matter, as well as on microbial activity [*Ujevic et al, 2010*]. In general, under reducing conditions, the trivalent form As (III) is the dominant and As(III) exists as arsenious acid (H_3AsO_3) and arsenite ions ($H_2AsO_3^-$, $HAsO_3^{2-}$, and AsO_3^{3-}). On the contrary, under oxidizing conditions the pentavalent As(V) is the dominant as arsenic acid H_3AsO_4 and arsenate ions ($H_2AsO_4^-$, $HAsO_4^{2-}$, AsO_4^{3-}) [*Ergican et al, 2005*]. These anions have acidic characteristics, and the stability and dominance of specific species depend on the pH of the solution, as shown in the Fig 1.1.

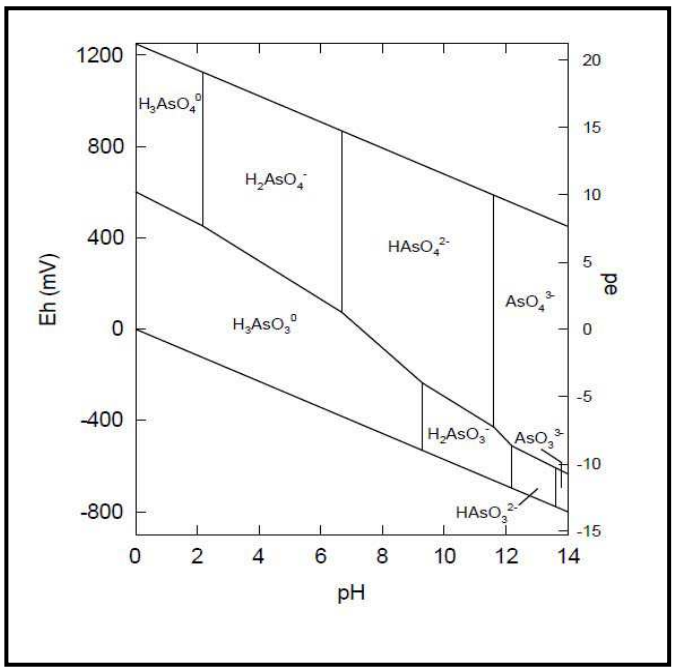

Fig 1.1. *Eh-pH diagram of aqueous arsenic species in the system As-O_2-H_20 at 25^0C and 1 bar total pressure [Smedley and Kinniburgh, 2003].*

As observed in Fig 1.1, under oxidising conditions, $H_2AsO_4^-$ is dominant at low pH (less than about pH 6.9), whilst at higher pH, $HAsO_4^{2-}$ becomes dominant (H_3AsO_4 and AsO_4^{3-} may be present in extremely acidic and alkaline conditions, respectively). On the contrary, under reducing conditions at pH less than about pH 9.2, the uncharged arsenite H_3AsO_3 will predominate. Dissociations of arsenious (H_3AsO_3) and arsenic (H_3AsO_4) acids under differing conditions are summarized in Fig 1.2 from the respective pKa values [*Mohan and Pittman, 2007*].

$$\mathbf{H_3AsO_3} \xrightarrow[\text{pKa = 9.1}]{-H^+} \mathbf{H_2AsO_3^-} \xrightarrow[\text{pKa = 12.1}]{-H^+} \mathbf{HAsO_3^{2-}} \xrightarrow[\text{pKa = 13.4}]{-H^+} \mathbf{AsO_3^{3-}}$$

$$\mathbf{H_3AsO_4} \xrightarrow[\text{pKa = 2.1}]{-H^+} \mathbf{H_2AsO_4^-} \xrightarrow[\text{pKa = 6.7}]{-H^+} \mathbf{HAsO_4^{2-}} \xrightarrow[\text{pKa = 11.2}]{-H^+} \mathbf{AsO_4^{3-}}$$

Fig 1.2. *Dissociations of As (III) and As (V).*

The dependence of inorganic arsenic species on pH range can also be illustrated as in the Fig 1.3 and Fig 1.4 below, in which the shaded area corresponds to the pH range of most ground waters [*USEPA, 2001a,b*]:

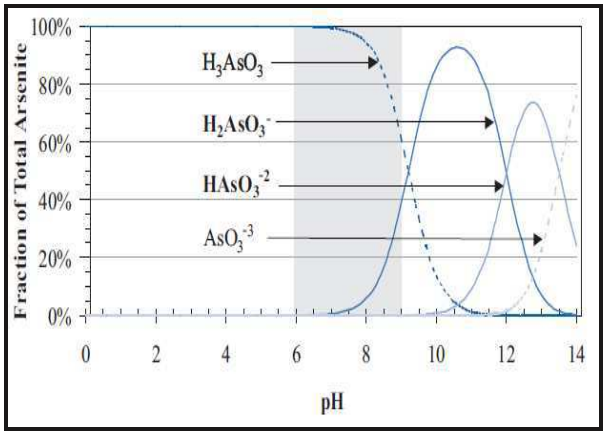

Fig 1.3. *Concentrations of the As (III) species at different pH values*

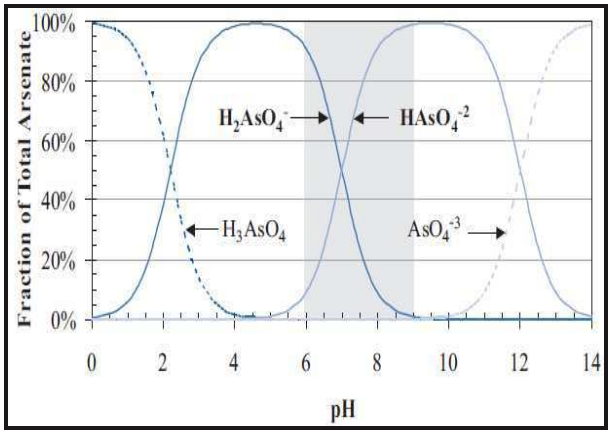

Fig 1.4. *Concentrations of the As (V) species at different pH values*

Chemical speciation is a critical step of arsenic treatment. Negative surface charge will facilitate removal of arsenic by some conventional processes as adsorption, anion exchange and co-precipitation. Since net charge of arsenite As(III) in water at a natural pH levels (6 - 9)

is neutral ($H_3AsO_3^0$), this form is hard to remove out of water. On the contrary, the net molecular charge of arsenate As(V) is negative (-1, -2) in the same range of pH, enabling it to be removed with higher efficiency. Since As(III) is normally predominant in ground waters, conversion of As(III) to As(V) is a critical step of most conventional arsenic treatment lines.

I.1.3 Arsenic occurrence

I.1.3.1 Natural sources of arsenic

In nature, arsenic is introduced into the aquatic environment by mobilization through a combination of natural processes, such as: weathering reactions and dissolution of arsenic bearing rocks, minerals and ores. The natural content in arsenic, in some common rocks and sediments that form aquifers tapped for drinking, is presented in Table 1.2.

Table 1.2 *Arsenic content in rocks and sediments.*

Rock or sediment type	Arsenic content (mg/kg)	
	Average	Range
Sandstone	4.1	0.6 – 120
Limestone	2.6	0.4 – 20
Granite	1.3	0.2 – 15
Basalt	2.3	0.2 – 113
Alluvial sand (Bengal)	2.9	1.0 – 6.2
Alluvial silt (Bengal)	6.5	2.7 – 15
Loess (Argentina)	-	5.4 – 18

Source: UNICEF, 2008

In most cases, the arsenic found in rocks and sediments is responsible for trace levels of arsenic in groundwaters. Under effect of natural geochemical conditions and processes, natural release of arsenic from aquifer materials into groundwaters might occur, which enhances the risk of drinking water contamination. The four main geochemical mechanisms that trigger the natural release of arsenic are shown in Table 1.3.

Table 1.3 *Natural geochemical mechanisms that release arsenic to groundwaters.*

Mechanisms	Characteristic geochemical conditions	Generalized geological environment	Countries where this mechanism is known to occur	Additional information
Reductive dissolution	✓ Anoxic groundwater; ✓ Low levels of dissolved oxygen, NO_3^- and SO_4^{2-}; ✓ pH~7; ✓ High iron (Fe); ✓ Also high manganese (Mn), ammonia (NH_4) and bi-carbonate (HCO_3^-).	Holocene sediments deposited in floodplain areas of rivers draining geologically-recent mountain chains.	Bangladesh, India, Vietnam, China, Cambodia, Hungary	✓ May affect large areas. ✓ 64% of known occurrences of arsenic due to this mechanism.
Alkali desorption	✓ Anoxic groundwater; ✓ pH ~ 8; ✓ Low levels of iron (Fe). Possible elevated levels of other toxic ions such as F, B, Mo, Se.	Alluvium and bedrock aquifers.	Argentina, USA, Spain, China	✓ May affect large areas.
Sulfide oxidation	✓ Anoxic groundwater; ✓ pH < 7 (sometimes extremely acidic); ✓ High levels of sulphate (SO_4^{2-}).	Areas where mineralization has taken place, often associated with rare metals, e.g., gold, tin.	Ghana, Thailand, USA	✓ Usually localized.
Geothermal	✓ High temperature ground water; ✓ High chloride (Cl^-)	Areas of geothermal activity, i.e., geologically active, often associated with volcanic rocks.	Chile, China, Nicaragua	✓ Usually localized.

***Source**: UNICEF, 2008*

Another natural source of arsenic is from the most abundant arsenical, arsenopyrite (FeAsS). Arsenopyrite is formed under high temperature in the earth's crust and has a concentration of above 100,000 ppb of arsenic. It is unstable under aerobic conditions, so it oxidizes to iron oxides and releases arsenic into groundwaters. Other notable arsenicals with the similar chemical properties are orpiments (As_2S_3) and realgar (AsS) (*Liang et al., 2009*).

I.1.3.2 Anthropogenic sources of arsenic

Human activity is another source of arsenic. Arsenic can be released from use of arsenical pesticides, application of fertilizers (which are forbidden in many countries nowadays), and disposal of industrial and animal wastes [*Mandal and Suzuki, 2002*]. On a global level, around 50,000 tons (from 1964 – 1973) of elemental arsenic were being extracted annually. During the 1970's, approximately 80% of the arsenic was used for agricultural purposes such as: insecticides, herbicides, desiccant, wood preservatives, and feed additives. At present, agricultural use of arsenic is declining, and many of these agricultural uses of arsenic compounds are even prohibited in many countries. Arsenic enters the atmosphere through anthropogenic inputs from coal combustion, herbicides use, glass production, wood preservatives, steel production, waste incineration, and smelter operations. In 1983, worldwide yearly emissions of arsenic to the atmosphere from anthropogenic sources ranged from 12000 to 25600 metric tons with a median value of 18800 metric tons [*Nriagu and Pacyna, 1988*]. In 1987, global emission of both natural and anthropogenic sources of arsenic emissions to the atmosphere was 73500 and 28100 metric tons per year, respectively. Among them, copper smelting and coal combustion accounted for 65% of anthropogenic emissions [*Chivers and Peterson, 1987*]. The global arsenic cycle is illustrated in the Fig 1.5.

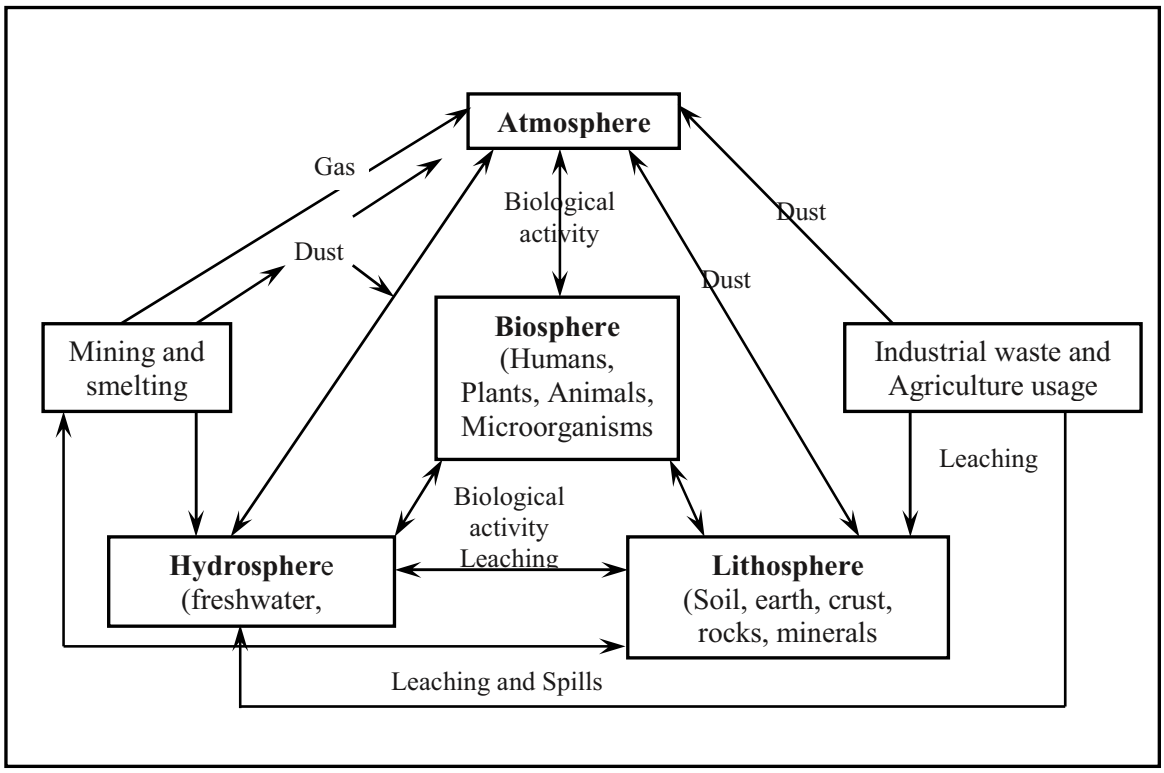

Fig 1.5 *The global arsenic cycle [from Shih, 2005]*

I.1.4 Arsenic toxicity and effects on human health

Arsenic is known as the "King of Poisons" and is mutagenic, carcinogenic, and teratogenic [Altug, 2003]. The toxicity of different arsenic species varies in the order: *arsine AsH_3 > arsenite As(III) > arsenate As(V) > Monomethylarsonate (MMA) > Dimethylarsinate (DMA)* [*Thirunavukkarasu et al, 2002*]. Among them, inorganic arsenic species are about 100 times more toxic than organic species while As (III) is about 60 times more toxic than As (V) species [*Choong et al, 2007; Villaescusa and Bollinger, 2008; Ujevic et al, 2010; Ergican et al, 2005; Havezov and Tsekulov, 2010; Shih, 2005; Jain and Ali, 2000*]. This is due to a greater thermodynamic stability of the combination with the thiol (-SH) part of proteins [*Villaescusa and Bollinger, 2008*]. The 50% lethal dose (LD^{50} – *amount of a material, given all at once, which causes the death of 50% of a group of test animal*) of arsenic species for oral administration to mice and also for an adult people are shown in Table 1.4.

Table 1.4 *The LD^{50} values for arsenic species for oral administration to mice and human.*

Arsenic species	Lethal Dose^{50}	
	Mice (mg/kg)	*Human (mg)*
Arsine - AsH_3	3	-
Arsenite – As(III)	14	100 - 200
Arsenate – As(V)	20	-
MMA	700 – 1800	-
DMA	1700 – 2600	-

Source: *Benramdanel et al, 1999.*

The toxicology of arsenic is a complex phenomenon since arsenic is also considered as an essential oligoelement at trace level also. Two types of toxicity, including acute and chronic poisons, are known from long time [*Jain and Ali, 2000*]. Some typical symptoms of both acute and chronic poisons by arsenic are summarized in Table 1.5.

Table 1.5 *Typical symptoms of both acute and chronic arsenic poisons*

Symptoms of arsenic poison	
Acute poison	***Chronic poison***
✓ Dry throat and mouth	✓ Loss of appetite;
✓ Colicky abnormal pain	✓ Nausea and some vomiting;
✓ Profuse diarrhoea	✓ Shooting pains;
✓ Dysphasia	✓ Diarrhoea;
✓ Muscular cramps	✓ Nervous weakness;
✓ Facial edema and cardiac shock	✓ Tingling of the hands and feet;
	✓ Jaundice and erythema.

Source*: Jain and Ali, 2000.*

Long-term exposure or chronic ingestion of arsenic can lead to a wide range of health problems, which are collectively called *arsenicosis* or chronic arsenic poisoning. The most widely recognized signs of chronic arsenic poisoning are *melanosis* (change in skin colour) and *keratosis* (hardening and thickening of skin into nodule). The risk of skin lesions increases both with duration of exposure and arsenic concentration. At very high concentrations, *melanosis* and *keratosis* can develop in a few years, but in most cases ten to twenty years are required. *Keratosis* often develops after *melanosis*.

While skin lesions are among the most recognized symptoms of *arsenicosis*, the highest health threats due to arsenic are cancers. Indeed arsenic is a known carcinogen, with skin, lung and bladder cancers causing the highest level of disease burden. Internal cancers can also

occur without any development of skin lesions, so simply relying on early onset symptoms to estimate the likely disease burden is not reliable [*UNICEF, 2011*].

I.1.5 Drinking water standards for arsenic

As established under the 1975 National Interim Primary Drinking Water Regulations (NIPDWRs), the former arsenic maximum contaminant level (MCL) was 50 ppb. In 1993, after considering the cancer and other human health risks associated with arsenic exposure, the World Health Organization (WHO) recommended drinking water criterion from 50 to 10 ppb [*Smith and Smith, 2004*]. This new standard recommendation has been adopted by many regulatory agencies in industrialized nations, including United States, Canada, and the European Union while many developing nations continue to retain a 50 ppb drinking water standard for arsenic. Some drinking water standards for arsenic are presented in Table 1.6.

Table 1.6 *Some drinking water standards for arsenic.*

Nation/State	Drinking water standard (ppb)	References
Australia	7	*National Health and Medical Research Council (2004)*
Canada	10	*Federal-Provincial-Territorial Committee on Drinking water (2007)*
European Union	10	*European Union (1998)*
Japan	10	*Japanese Ministry of the Environment (2008)*
United States	10	*Code of Federal Regulations (2006)*
Vietnam	10	*Ministry of Natural Resources and Environment (2009)*
Mexico	35	*Mexican Guidelines for industrial discharge waters (1996)*
Bangladesh	50	*Bangladesh Rural Advancement Committee (2000)*
Chile	50	*Caceres et al, 2005*
China	50	*Guo and Wang (2005)*
Thailand	50	*Zhang et al, 2003*
WHO	10	*World Health Organization (1998)*

***Source**: Kevin Henke, 2009.*

I.1.6 Possible treatment methods for arsenic removal

Several detailed reviews of arsenic removal technologies have been presented by Sorg and Logsdon (1974), by Jekel (1994), by USEPA (2003), by Kuan-Seong Ng et al (2004) and recently by Jain and Singh (2012). In these reviews, a variety of arsenic removal techniques from contaminated waters have been listed that are applied in both laboratory and full scale conditions. Generally, these various technologies are based mainly on the six following processes [*USEPA, 2003*]:

(i) Oxidation and filtration
(ii) Biological oxidation: oxidation of As(III) to As(V) by micro-organisms followed by precipitation with iron and manganese oxides
(iii) Co-precipitation: oxidation of As(III) to As(V) by adding an oxidizing agent followed by coagulation, sedimentation and filtration
(iv) Adsorption: adsorbents such as activated alumina, activated carbon, iron based sorbents, zero valent iron and hydrated iron oxide, etc...
(v) Ion exchange using suitable cation and anion exchange resins
(vi) Membrane technology: reverse osmosis, nano-filtration, electro-dialysis (ED) and membrane distillation (MD), recently.

As above-mentioned, As(III) is harder to be removed out of waters than As(V). In his review paper, *Kuan-Seong Ng et al., 2004* reported that As(III) removal efficiency in range of 10 – 87.5% could be achieved while it was higher for As(V). Some typical As(V) treatment efficiencies and water losses for these processes operated under normal conditions are provided in Table 1.7

Table 1.7 *Typical As(V) treatment efficiencies and water loss.*

Treatment process	As(V) removal efficiency	Water loss
Oxidation and Filtration		
Green sand	50- 90%[a]	≤ 2%
Biological oxidation	> 95%	
Co-precipitation		
Enhanced lime softening	90%	1 - 2%
Enhanced coagulation/filtration		
with Alum	< 90%	1 - 2%
with Ferric chloride	95%	1 - 2%
Coagulation assisted microfiltration	90%	5%
Adsorption		
Activated alumina	95%	1 - 2%
Iron based sorbents	up to 98%	1 - 2%
Ion exchange	95%	1 - 2%
Membrane technology		
Reverse osmosis	> 95%	15 – 50%

Source*: Jain, 2012.*

[a] *depends on arsenic and iron concentrations*

I.1.6.1 Oxidation and filtration

Coupled oxidation and filtration are often used to remove iron and manganese from waters, through the oxidation of the soluble forms of iron and manganese to their insoluble forms and then their separation and removal by filtration.

If arsenic is present in the resource water, it can be removed via three primary mechanisms: oxidation, adsorption and co-precipitation. First, soluble Fe^{2+} and As(III) are oxidized to Fe^{3+} and As (V). The As(V) adsorbs onto the iron hydroxide, and the precipitates are ultimately filtered out of solution. This process is the same for arsenic removal together with manganese; however, iron is much more efficient. The arsenic removal efficiency is strongly dependent on the initial iron concentration and ratio of iron to arsenic. In general, the Fe:As mass ratio should be at least 20:1 [*EPA website*]. These conditions customarily result in an arsenic removal efficiency of about 80 – 95%. The effectiveness of arsenic co-precipitation with iron is relatively independent of resource water pH in the range 5.5 to 8.5. However, high levels of

NOM, orthophosphates, and silicates can reduce arsenic removal efficiency by competing for sorption sites on iron hydroxide precipitates in the following order arsenate > phosphate > arsenite > silicate at pH 6.8 [*Fileds et al., 2000b; Bang and Meng, 2004*].

I.1.6.2 Co-precipitation with additional salts

This treatment process has been the most popular treatment method to remove arsenic contaminated water in numerous pilot and full scale applications [*Jain & Singh, 2012*]. Principle treatment mechanism of this method is to use coagulants such as alum [$Al_2(SO_4)_3.18H_2O$], ferric chloride [$FeCl_3$], and ferric sulfate [$Fe_2(SO_4)_3.7H_2O$] to remove arsenic from water through coagulation and flocculation. During the flocculation process, all kinds of micro-particles and negatively charged ions are attached to the flocs by electrostatic attachment. Arsenic is also adsorbed onto coagulated flocs. As As(III) occurs in non-ionized form at neutral pH, it is not subject to significant removal. Oxidation of As(III) to As(V) is thus required as a pre-treatment for efficient removal. Several studies proved that ferric salts are more effective in removing arsenic than alum on a weight basis and over a wider pH range [*Edwards, 1994; Hering et al., 1997*]. This technology can typically reduce arsenic concentration to less than 10 ppb and the doses of ferric salt below 0.010 $mg.L^{-1}$ [*Pontius, 1995*]. Logsdon et al., 1974 showed that at a feed concentration of 0.3 $mg.L^{-1}$, over 95% of As(V) was removed with ferric sulphate coagulation and 83 - 90% with alum coagulation.

I.1.6.3 Biological oxidation

The biological oxidation of iron and manganese as a treatment method for arsenic removal is a relatively new method. It is based on the fact that ground waters contaminated with arsenic are usually reducing and also containing concentrations of iron and manganese. The biological oxidation of iron or manganese results in the formation of non-soluble products (iron or manganese oxides) which are subsequently removed from water by filtration [*Mouchet, 1992*]. If arsenic is simultaneously present in water, it can be removed by sorption onto the produced oxides, which progressively creates a natural (biogenic) coating on the filter medium. Therefore, the application of this method for the removal of arsenic was named "*biological adsorptive filtration*" [*Zouboulis and Katsoyiannis et al., 2002c*].

Zouboulis and Katsoyiannis, 2004a reported that both inorganic forms of arsenic can be efficiently treated by biological oxidation in the concentration range 50 – 200 ppb. They also reported in 2006 that the arsenic removal efficiency is higher by iron oxidizing bacteria than manganese oxidizing bacteria. The difference in the removal efficiency can be attributed to the fact that iron oxides are efficient adsorbents regarding the removal of arsenic, presenting a strong tendency to create surface complexes with arsenic ions, whereas the use of manganese oxides is not equally efficient. It has also been reported that with the application of biological iron oxidation, the arsenic removal efficiency was not affected by the different initial arsenic concentrations and the final concentration of arsenic was always below 0.010 mg/L. The rates of oxidation of iron, manganese and arsenic are faster than those reported for physic-chemical oxidation, indicating the catalytic role of bacteria in removing arsenic.

The fast rate of oxidation reaction by specific bacteria, namely the *Leptothrix ochracea* and *Gallionella ferruginea*, rendered this process quite economic and environmental friendly because no additional use of chemical reagents is required. Limitations are that iron must be present in water at sufficient levels [*Damodar Pokhrel et al., 2009*].

I.1.6.4 Adsorption

Depending on the arsenic initial concentration, adsorption (mostly in packed columns) typically can reduce arsenic concentration to less than 10 ppb. As the contaminated water is passed through the column, contaminants are adsorbed onto the media's surface and pores. When the adsorption sites become saturated, the column must be regenerated or disposed of and replaced with new media.

Some commonly adsorption media used for arsenic removal include: (i) activated alumina (AA); (ii) Iron based sorbent (IBS); (iii) indigenous filters and cartridges and (iv) other miscellaneous adsorbents. Activated alumina (AA) was the first adsorptive medium to be successfully applied for the removal of arsenic from water [*EPA, 2000a,b*]. The reported adsorption capacity of AA ranges from 0.003 to 0.112 gram of arsenic per gram of AA with optimum pH range as 5.5 – 6.0 [*Jain and Singh, 2012*]. The arsenic removal efficiency could reach 98% under these conditions [*EPA, 2000a,b*]. *Ahmed et al., 2000* showed that using hybrid aluminums and composite metal oxides as adsorption media made able to treat water

containing 550 ppb of arsenic and 14 mg.L^{-1} of iron, and thus to meet the standard required (MCL = 10 ppb). However, a pre-oxidation step to convert As(III) into As(V) is also required as the selectivity of activated alumina (AA) towards As(III) is poor, owing to the overall neutral molecular charge at pH levels below 9.2.

Other adsorptive media were iron based sorbents (IBS).The affinity of this kind of media for arsenic removal is strong under natural pH condition [*Jekel, 1994; Driehaus et al., 1998; Manning et al., 2002*]. Examples of iron based sorbents (IBS) are currently available in the market, including: granular ferric hydroxide, zero valent iron, iron coated sand, modified iron and iron oxide based adsorbents. Among them, zero valent iron (ZVI) has received increased attention due to its high arsenic removal capacity. *Ramaswami et al., 2001* reported that a batch-mixed iron settling system is effective in the treatment of water containing arsenic in range of 200 – 2000 ppb at contact times of 0.5 – 3 hours, with iron dose ranging from 2500 – 625 mg/L.

I.1.6.5 Ion exchange (IE)

Ion exchange is a physico-chemical process in which ions are swopped between a solution phase and solid phase. Depending on the initial concentration, this technology typically can reduce arsenic concentrations to less than 50 ppb and in some cases to lower than 10 ppb [Jain & Singh, 2012]. Its effectiveness is sensitive to a variety of untreated water contaminants and characteristics. This technology, therefore, is used less frequently than precipitation/co-precipitation technology. Similar to other conventional processes, the efficiency of IE process is radically improved by pre-oxidation of As(III) to As(V) but the excess of oxidant often needs to be removed before the ion exchange operation in order to avoid the damage of sensitive resins. The exchange affinity of various ions is a function of the net surface charge. Therefore, the efficiency of this process for As(V) removal depends strongly on the solution pH and the concentration of other anions, most notably sulfates and nitrates. These and other anions compete for adsorption sites on the exchange resin according to the following selectivity sequence: $SO_4^{2-} > HAsO_4^{2-} > NO_3^- > CO_3^{2-} > NO_2^- > Cl^-$ [Clifford, 1999]. High level of total dissolved solid (TDS) can have adverse effects on the performance of a ion exchange system. *Wang et al., 2000* reported that the ion exchange is not an economically viable technology if the water resource contains over 500 mg/L of TDS.

I.1.6.5 Conventional membrane technologies

❖ *Pressure-driven membrane technologies*

Among the four types of pressure-driven membrane processes (microfiltration, ultrafiltration, reverse osmosis and nanofiltration), only reverse osmosis (RO) and nano-filtration (NF) are likely to effectively retain dissolved arsenic since arsenic species dissolved in water tend to have a relatively low molecular weights [*EPA, 2000a,b*]. For RO process, *Kang et al., 2000* reported that removal of arsenic compounds was strongly affected by the solution pH, especially for As(III). By using polyamide RO membrane (ES-10), the author found that an increase of As(III) rejection efficiency from 75% to more than 90% was observed for pH values rising from 7 to 10 while As(V) rejection was stable with more than 95% in all investigated range of pH (3 – 10). By changing another type of membrane with polyvinyl alcohol membrane (NTR-729 HF), same trend for As(III) rejection was observed with increase of rejection efficiency from 20 to 40% with increase of pH from 7 to 10. However, increase of As(V) rejection efficiency from 80% to 95% with increase of pH from 3 to 5, 7 and 10 was found. These observations indicated the necessity to find optimum operating pH values as well as suitable membrane.

Also by using RO process, *Narasimhan et al., 2005* had the same tendency with As(III) rejection more complete at pH > 8. RO membranes are more selective than NF membranes although it requires higher driving pressures (hence higher energy cost). RO units can be used as stand-alone arsenic treatment under most water quality conditions and are capable of achieving over 97% removal of As(V) and 92% removal of As(III) [*NSF, 2001 a,b*]. The negatively charged membranes used in most of the reported studies explain the higher rejection obtained with anionic components, like As(V), rather than with fully protonated As(III). As a result, oxidation of As(III) to As(V) is also required with this type of treatment.

However, oxidizing agents, like chlorine, could damage the membrane material [*Kartinen and Martin, 1995*]. Typical disadvantages of using membrane processes were for the previous decades the high cost due to the membrane itself, but membrane prices have decreased a lot in relation with the development of their use in water desalination. In addition, membrane fouling remains the major drawback of such system.

❖ *Thermally-driven membrane technologies*

Recently, a new comer in membrane family, namely membrane distillation (MD) process, has also been applied for arsenic removal. The principle and background of MD will be introduced and developed in part 2 of this chapter. Let's see here what is the state of use or development of this process for the removal of arsenic.

Qu et al., 2009 used direct contact membrane distillation (DCMD) configuration with self-made PVDF membranes (0.15µm) for removing As (III) and As (V) in synthetic groundwaters. The author concluded that DCMD process showed higher arsenic removal efficiency than pressure-driven processes, especially for high feed concentrations. Permeate arsenic concentration was always under the maximum contaminant limit (MCL = 10 ppb) until the feed As (III) and As (V) concentrations reached 40 ppm and 2000 ppm, respectively. The removal efficiencies were always higher than 99.95% for both types of arsenic. Permeate fluxes in these two cases were stable at 7.60 and 7.50 $kg.m^{-2}.h^{-1}$, irrespective of increase of feed concentration. A 250h experiment for As(III) rejection showed that this DCMD (with PVDF membrane) had a stable As(III) rejection. SEM analysis of the membrane before and after experiment showed that membrane morphology has been changed slightly. However, the permeability and salt rejection did not change.

The same DCMD configuration with different types of membranes (PTFE 0.22µm and PP 0.22µm) was applied for treatment of real arsenic-contaminated groundwaters collected from some arsenic-affected areas in India [*Pal and Manna, 2010]*. The highest permeate flux obtained was 49.80 $kg.m^{-2}.h^{-1}$ at a circulation velocity v = 0.052 $m.s^{-1}$; T_f = 60°C and T_p = 21°C, respectively. No arsenic was detected in the permeate after 4 days of operation (12 hours per day). An average flux decline of 12% was observed for all membranes when arsenic concentration was increased from 0 – 1200 ppb without distinction between As (III) and As (V). No experiment on membrane fouling was mentioned regardless of presence of Fe^{total} (1.2 – 1.8 ppm), Ca^{2+} (102.5 – 110.3 ppm), Na^{+} (26 – 32 ppm), in the feed solution.

Yarlagadda et al., 2011 applied direct contact membrane distillation (DCMD) for recovery potable water from As-contaminated saline ground water. Two types of membranes with PP 0.45µm and PTFE 0.22µm were used. The highest permeate flux was 90 - 95 $kg.m^{-2}.h^{-1}$ for

both PP and PTFE, respectively at the operating conditions (T_f = 80°C, T_p = 20°C, salt concentration = 1000 – 10000 ppm, [As] = 10 - 400 ppb). No identification was given of what kind of salt was present in the groundwater. The results showed influence of salt concentration to the permeate flux with 5% reduction of permeate flux when salt concentration was increased from 1000 to 10.000 ppm (rejection efficiency of 99%). A minimal decrease of flux could be observed also when As concentration increased from 10 ppb to 350 ppb, but no distinction between As (III) and As (V) was mentioned. The highest arsenic concentration in permeate was 0.17 ppb. A 12-hour operation was carried out to evaluate the effect of inorganic fouling on the membranes; but neither fouling nor flux decline was observed during this time.

Criscuoli et al., 2012 applied vacuum membrane distillation (VMD) configuration for treating pure water containing arsenic, both in the trivalent and pentavalent forms. PP (0.2 – 0.45μm) and PVDF (0.2 μm) commercial membranes were used for the experiments. Operating conditions were fixed at low feed temperature (20 – 40^0C) with Pp = 10 mbar and Re = 1700. For synthetic feed solutions containing a maximal concentration of 1 ppm for each arsenic form, no arsenic was detected in the permeate. Trans-membrane flux was strongly affected by the feed temperature and neither depended on the arsenic contents nor on the arsenic forms. The highest flux ranged between 3 and 12.5 $kg.m^{-2}.h^{-1}$ at 20^0C and 40^0C, respectively.

To sum up, a summary of these four MD published studies was presented in Table 1.8.

Table 1.8 *Summary of arsenic removal by new MD processes.*

No	Publications	Membrane	Operating conditions	Permeate flux ($Kg.m^{-2}.h^{-1}$)	Rejection rate (%)	Fouling
1	Experimental study of As removal by DCMD (*Qu et al., 2009*)	PVDF	✓ Not mentioned for arsenic removal; ✓ [As(III)] = 40 ppm; ✓ [As(V)] = 2000 ppm	✓ $J_{As(III)}$ = 7.6; ✓ $J_{As(V)}$ = 7.5;	99.95	Not affected by presence of arsenic;
2	Removal of As from contaminated groundwater by SDMD using 3 different membranes (*Pal and Manna, 2010*)	PTFE & PP	✓ T_1 = 50°C; ✓ T_2 = 21°C; ✓ v = 0.052 m/s; ✓ [As] = 0 – 1200 ppb;	✓ J_{max} = 50; ✓ 12% decline of flux when increase of feed As concentration.	100	Possible fouling by Ca^{2+}; Fe_{total} and NaCl was not mentioned
3	Potable water recovery from As, U, and F contaminated ground waters by DCMD (*Yarlagadda et al., 2011*)	PTFE & PP	✓ T_f = 80°C; ✓ T_p = 20^0C ; ✓ [As] = 10 – 400 ppb ✓ [Salt] = 1 – 10 mg/L	✓ J_{max} = 90 - 95; ✓ 5% decline of flux with increase of salt concentration.	99	No fouling with presence of inorganic components
4	Arsenic removal in solutions containing arsenic in pure water, by VMD (*Criscuoli et al., 2012*)	PP	✓ T_f = 20 - 40°C; ✓ Pp = 10 mbar; ✓ Re = 1700; ✓ [As(III)] = 0.5- 1 ppm ✓ [As(V)] = 0.5- 1 ppm	✓ J = 3 – 12: not depends on As contents or forms	100	Not affected by presence of arsenic.

I.1.7 Summary

As a summary according to most publications, it is easier to remove As(V) than As(III) . As a result, pre-oxidation step to convert As(III) into As(V) to facilitate the arsenic rejection is needed. This is a critical step for achieving optimal performance of most of the treatment processes described above. Oxidizing agents such as chlorine, bleaching powder (chloride), ozone, hydrogen peroxide or potassium permanganate can be used for this oxidation step. pH value determines the predominant arsenic species present in water and is therefore expected to be a very influencing parameter for the treatment. Many of arsenic treatment technologies require pH adjustment for optimization of performance and are effective in removing arsenic in pentavalent state. Sorption and coagulation processes are particularly sensitive to pH, and function effectively at the lower end of the natural pH range. However, use of activated alumina at a natural pH may be a cost effective option for many small water systems. A summary of the optimal pH ranges for conventional arsenic treatment technologies is introduced in the Fig 1.7.

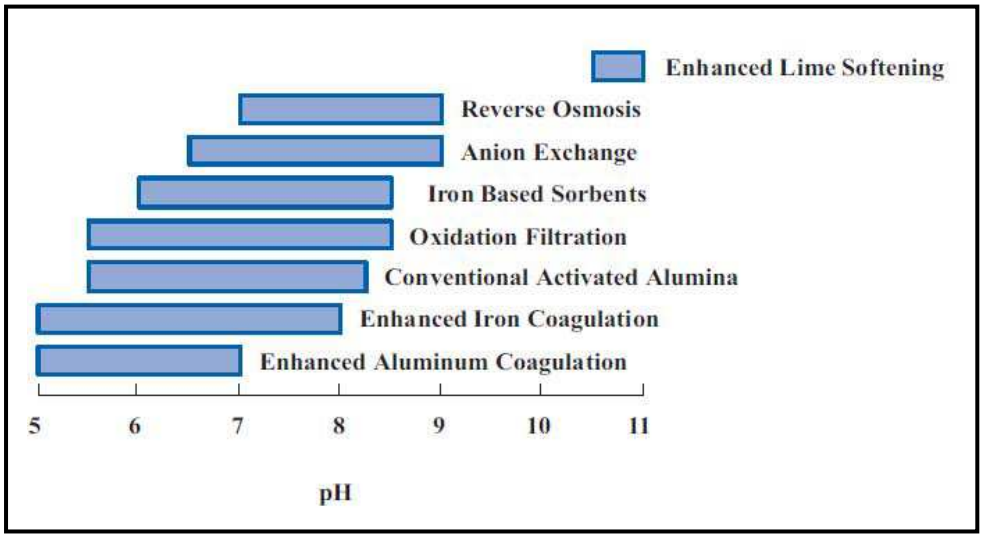

Fig 1.7 *Optimal pH ranges for arsenic treatment technologies [USEPA, 2003].*

Major disadvantages of these physico-chemical processes are the requirements of multiple chemical treatments, pre-or-post treatment of drinking water, high operating and capital costs and more importantly, regeneration of medium handling of arsenic contaminated sludge. Disposal of the sludge poses a problem in most cases. Similarly, pressure driven membrane processes (RO/NF) also have some drawbacks as:

- the need of an efficient pre-treatment, that should integrate both a pre-oxidation step to convert As(III) into As(V) is also required and a clarification step to prevent membrane fouling
- the problem of concentrate disposal
- a limited recovery due to osmotic effects
- membrane bio-fouling inducing a flux decline and necessity of chemical cleanings.

On contrary, membrane distillation technologies show very high treatment efficiency for arsenic, irrespective of its forms. It means that pre-oxidation step to convert As(III) into As(V) seems not necessary for this process. Moreover, feasibility of MD process for desalination has been reported in many previous publications [*Cabassud and Wirth, 2003*; *Méricq et al., 2009-2010; Safavi and Mohammadi, 2009*]. On the basis of computations, it was concluded that for a really high permeable membrane, VMD can compete with RO on energy consumption (less than 2 kWh/m^3) with the same level of permeate flux (between 5 – 15 $kg.m^{-2}.h^{-1}$) [*Cabassud and Wirth, 2003*]. Moreover salinity and high salt concentrations do not alter the process efficiency because osmotic effects are not limiting. For that reasons, membrane distillation (MD) process could be considered as a good alternative process to reduce the complexity of the treatment plant in comparison with the other membrane processes. Background information on the membrane distillation technology, especially for vacuum membrane distillation will be discussed in the following sections.

I.2 VACUUM MEMBRANE DISTILLATION PROCESS

I.2.1 Background on membrane distillation technology

I.2.1.1 Introduction

Membrane distillation (MD) is a new comer of the membrane family. Although the discovery of MD phenomenon can be traced back to the 1960s, it has not received more attention until the 80s when techniques for membrane fabrication gained remarkable development. Today, MD is considered as a potential alternative to some traditional separation techniques, and is believed to be effective in the fields of desalination, concentration of aqueous solution, etc…

MD is a thermally-driven process, in which only vapour molecules are transported through the pores of hydrophobic membranes. The liquid feed to be treated by MD must be maintained in direct contact with one side of the membrane without penetrating its pores. The hydrophobic nature of the membrane can prevent liquid solutions from entering its pores due to the surface tension forces if the applied transmembrane pressure is smaller than the membrane liquid entry pressure (LEP). As a result, a liquid/vapour interface is formed at the entrance of each membrane pore. If the solution contains at least one volatile component, temperature difference between the pore inlet and outlet produces a vapour pressure gradient within the pores and then a diffusion of the vapour molecules of volatile component (produced by evaporation from the feed solution at the vapour – liquid interface) that are migrating from the feed side to the permeate side of the membrane. In this way the solution from the feed side is concentrated in non volatile compounds. In summary, MD is, by its nature, a combination of membrane separation and evaporation/condensation process and a micro-porous hydrophobic membrane is employed to act as the support of vapour liquid interfaces.

In comparison with separation processes such as osmotic distillation and evaporation, *Lawson and Lloyd, 1996* reviewed the features of MD process as follows:

- The membrane should be porous;
- At least one side of the membrane should be in contact with the liquid to be dealt with;

- For each component, the driving force of this membrane operation is a partial pressure gradient in the vapour phase;
- The membrane should not be wetted by the liquid;
- No capillary condensation of vapour takes place inside the membrane pores;
- The membrane does not alter the vapour-liquid equilibrium of different components in the feed.

The term "*membrane distillation*" arises from the similarity of this process to the conventional distillation. Both processes depend on vapour-liquid equilibrium as the basis of separation and latent heat should be applied to produce vapour phase. However, the remarkable difference between these two processes is that in membrane distillation the contact area between the liquid and the gas phase in controlled by the membrane material, and there is no mixture between the gas phase and the liquid phase (no bubbles nor foaming), which are separated by the membrane. Some advantages of MD in comparison with other membrane processes are as follows [*Couffin et al., 2000, Wirth et al, 2003, Lei et al., 2005*]:

- ***High treatment efficiency***: In general, owing to the process principle, almost 100% of non-volatile components in the aqueous feed like, for example, all dissolved compounds (i.e. ions, macromolecules) but also colloids and bacteria are able to be rejected, while pressure-driven membranes separation processes such as RO, MF and UF can not obtain such a high rejection level of dissolved species;

- ***Mild operation condition***: Although the feed needs to be heated to establish a temperature gradient between the two sides of the membrane, it is not necessary to increase the feed temperature to its boiling point. In some cases, MD can be performed well at the feed temperature ranging from 50°C – 80°C with satisfactory mass transfer. Therefore, low-grade waste heat energy sources, such as the cooling water from engines and the condensed water of low-pressure vapour, are good energy sources for MD. But the most attraction is the alternative energy sources such as solar and geothermal energy. Moreover, the low operation temperature also makes MD a potential technology for the concentration of heat-sensitive substances in the field of food and pharmacy. Besides that, low operation pressure of the MD process results in small equipment and operation cost, low requirement for membrane mechanics and increased process safety.

- ***Small space required***: Compared to conventional distillation or evaporation, a large vapour-liquid interface area per unit volume is available in MD. Both MD and conventional distillation (or evaporation) requires a large vapour-liquid interface area. In distillation column or evaporators, this relies on the vapour space within the equipments. But in MD, the vapour-liquid interface area is provided by the membrane which can be densely packed in the membrane module and by the pores themselves. The vapour space in the module is the pore volume of micro-porous membrane. As a result, the size of MD equipment is small.

- ***Less risky of membrane fouling***: In MD the hydrophobic membrane acts merely as a support for a vapour-liquid interface and does not distinguish between solution components on a chemical basis, nor does not act as a sieve. Therefore, MD membranes can be fabricated from chemically resistant polymers such as polytetrafluoroethylene (PTFE), polypropylene (PP), and polyvinylidenedifluoride (PVDF). Further, membrane fouling is less of a problem in MD than in other membrane separations because the pores are relatively large compared to the 'pores' or diffusion pathways in RO or UF, and are not as easily clogged.

However, the MD has for a long time be considered as a process allowing a low permeate flux compared to reverse osmosis is often considered, but some studies, including the ones of Wirth and Méricq at INSA-LISBP on the application of desalination have shown that for highly permeable membranes [*Cabassud et al, 2003*] and for a correctly chosen set of operating conditions, MD could compete with RO [*Wirth et al, 2003, Méricq et al, 2009*] in terms of flux if the thermal energy can be provided to the system.

In the last years some membranes and modules have been specifically designed for membrane distillation by different companies and some large scale demonstration plants are being built in different places worldwide (Singapore, North Sea…).

I.2.1.2 Membrane distillation configurations

Basically, there are four main configurations developed to perform MD process, i.e. direct contact membrane distillation (DCMD), air gap membrane distillation (AGMD), sweeping

gas membrane distillation (SGMD) and vacuum membrane distillation (VMD). The differences among these configurations are the way how trans-membrane partial pressure difference is generated as well as how the vapour (migrating from the vapour-liquid interface of the membrane surface at the feed side to that at the permeate side) is condensed and/or removed out of the module. Schemes of all these configurations are presented in the Fig 1.8.

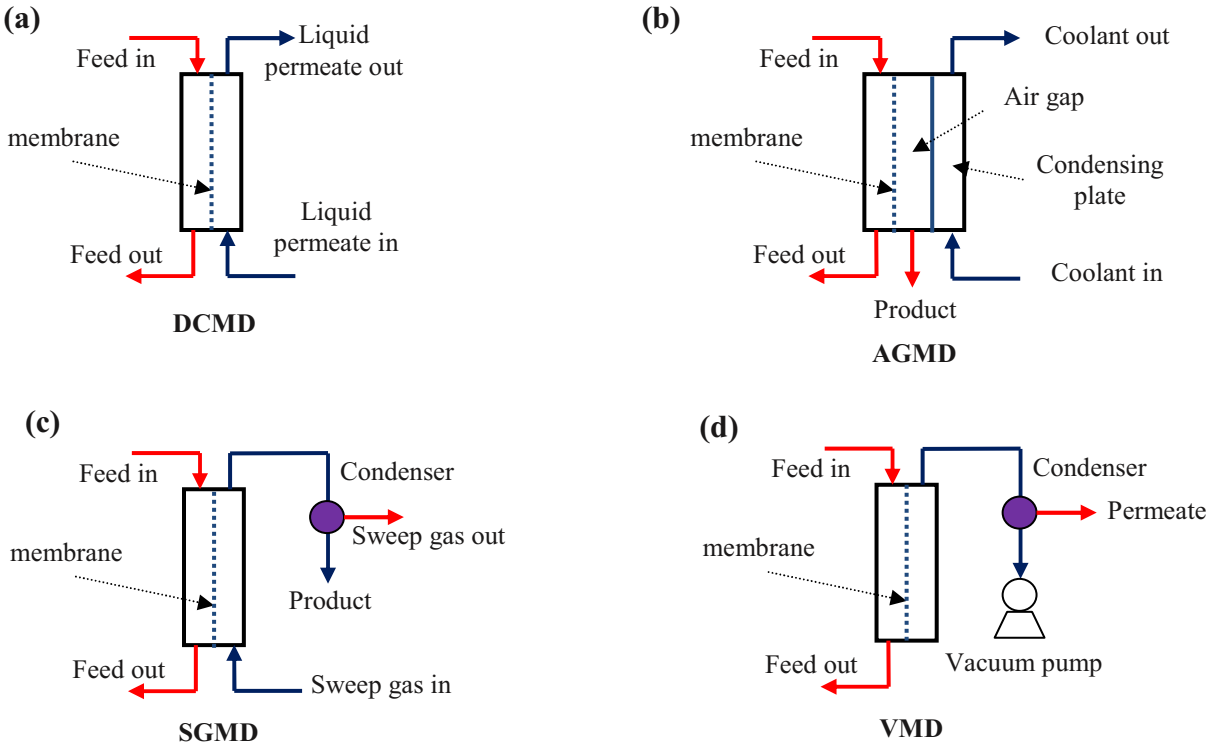

Fig 1.8 *MD configurations: (a) DCMD; (b) AGMD; (c) SGMD and (d) VMD [Lawson and Lloyd, 1997; Cabassud, 2000; Bourawi et al., 2006]*

❖ *Direct contact membrane distillation (DCMD)*

The DCMD configuration is illustrated in Fig 1.8a, where two chambers are separated by a flat sheet micro porous membrane. Trans-membrane partial pressure difference is generated by the difference in temperature between hot and cold liquid at two sides of the membrane, respectively. Because of the hydrophobic characteristic of membrane, only volatile molecules evaporate at the liquid/vapour interface, pass through the membranes pores in vapour phase and condense in the cold liquid/vapour interface inside the membrane module. Due to direct contact of permeate flow in cooling chamber, high heat loss by conduction is the main drawback of this design [*Lei et al., 2005; Alkhudhiri et al., 2012*]. DCMD is considered as the

simplest MD configuration with many applications in desalination [*Lawson and Lloyd, 1997*], in food industries [*Gunko, 2006*] and in acid manufacturing [*Tomaszewska et al., 1995*].

❖ *Air gap membrane distillation (AGMD)*

The air gap membrane distillation configuration is shown in Fig 1.8b, where an air gap is introduced by using a plate to compartment the cooling chamber from the membrane. Trans-membrane partial pressure difference is generated by difference in temperature between hot feed liquid and cold surface at the permeate side of the membrane. A stagnant air gap is placed between the membrane and a condensation surface. By this way, the vapour molecules, migrated out of the membrane pores, have to pass through the air gap and then condense on the plate before draining out of the air gap by gravity. The benefit of this design is the reduced heat loss by conduction [*Alkhudhiri et al., 2012]*. However, existence of the stagnant air presents a new resistance to mass transfer which in turn results in a low permeate flux across the membrane. This configuration is suitable for desalination [*Banat and Simandl, 1998*] and removing volatile compounds from aqueous solutions [*Banat and Simandl, 1999; Garcia-Payo et al., 2000*].

❖ *Sweeping gas membrane distillation (SGMD)*

The sweeping gas membrane distillation configuration is illustrated in Fig 1.8c, where a cold inert gas is used to sweep into the cooling chamber and making the air flow tangentially over surface of the membrane instead of using a stagnant air layer to compartment the membrane and the condensing surface. This solution is considered as a new approach to overcome the mass transfer resistance occurred in AGMD. Compared with that in static air layer, the mass transfer in the air stream would be promoted greatly. The vapour of volatile component is taken out of the chamber by the air stream, and then condenses in an external condenser. Therefore, SGMD can be looked on as the combination of the low heat loss of AGMD and the high mass transfer coefficient of DCMD [*Lei et al., 2005*]. This configuration is useful for removing volatile compounds from aqueous solution [*Walton et al., 2004*]. The main disadvantage of this configuration is that a small volume of permeate diffuses in a large sweep gas volume, requiring a large condenser [*Alkhudhiri et al., 2012*].

❖ *Vacuum membrane distillation (VMD)*

The VMD configuration is illustrated in Fig 1.8d, where vacuum is applied in the permeate side of the membrane module by means of a vacuum pump. In this variant, the feed solution in direct contact with the membrane surface is kept at pressure lower than the liquid entry pressure (LEP); at the other side of the membrane, the permeate pressure is often maintained below the equilibrium vapour pressure of volatile molecules owing to a vacuum pump to be separated from the feed solution. The total pressure difference between the two sides of the membrane causes a convective mass flow through the pores that contributes to the total mass transfer of VMD. In this case, condensation takes place outside of the membrane module by an external condenser. The heat lost by conduction is negligible, which is considered as a great advantage [*Lawson and Lloyd, 1997*]. Feasibility of VMD for desalination of seawater has been reported recently [Cabassud, 2000; *Méricq et al, 2009 – 201; Cabassud and Wirth, 2003; Safavi and Mohammadi, 2009]*.

As this study intends to apply the VMD process for arsenic removal from water, its applications and transfer mechanisms will be mentioned in details in the next following parts.

I.2.2 Applications of the vacuum membrane distillation process

The first potential applications of VMD were the extraction of volatile organic compounds (VOCs) from aqueous solutions such as chloroform, benzene, toluene, methyltert-butyl ether (MTBE), TCS, 2, 4-dichlorophenol, 1,1,1-tricholoethane, tetracholoroethylene, etc [*Soni et al, 2008; Couffin et al, 1998; Urtiaga et al, 2000,2001; Wu et al, 2006*]. Treatment of aqueous alcohol solutions by VMD is also an important application [*Izquierdo-Gil and Jonsson, 2003]*. Recently, other research areas involving aqueous solutions containing non-volatile compounds have also been considered, such as: desalination [*Cabassud and Wirth, 2003;Xu et al., 2006;Méricq et al, 2009 – 2011; Safavi and Mohammadi, 2009; Tang et al., 2010*] for production of distilled water or concentration of aqueous sucrose solutions [*Al-Asheh et al, 2006*], treatment of dye solutions [*Banat et al, 2005*; *Criscuoli et al., 2008*], concentration of ginseng extracts in aqueous solutions [*Zhao et al, 2008 – 2011*] and ethylene glycol from used coolant liquids [*Mohammadi and Akbarabadi, 2005*]. Moreover, VMD process was used for ammonia removal [*El-Bourawi et al, 2007*] and for concentration of fruit juices and recovery

of volatile aroma compounds [*Diban et al, 2009*]. Additionally, attempts were made to couple VMD technology with renewable energy sources or with other membrane processes [*Méricq et al, 2010; Sarbatly and Chiam, 2013*].

Regarding arsenic rejection, VMD has just applied for this application [*Criscuoli et al., 2012*]. More details of this study had been presented in the previous section I.1.6.5.

I.2.3 Transfer mechanisms in the VMD process

In MD process, both heat and mass transfers through porous hydrophobic membranes are involved simultaneously. The mass transfer occurs through the pores of the membrane whereas heat is transferred through both the membrane matrix and its pores. One must pay attention that only water vapour or volatile compounds are transported through the membrane pores from the feed side to the permeate side as the membrane is hydrophobic. In addition, there is a presence of fluid boundary layers adjoining both the feed and permeate sides giving rise to the phenomena called temperature polarization and concentration polarization. Depending on each specific variant of MD, these phenomena will affect to MD performance or not. The next parts will present these mechanisms in more detail, especially in case of VMD variant as presented in Fig 1.9

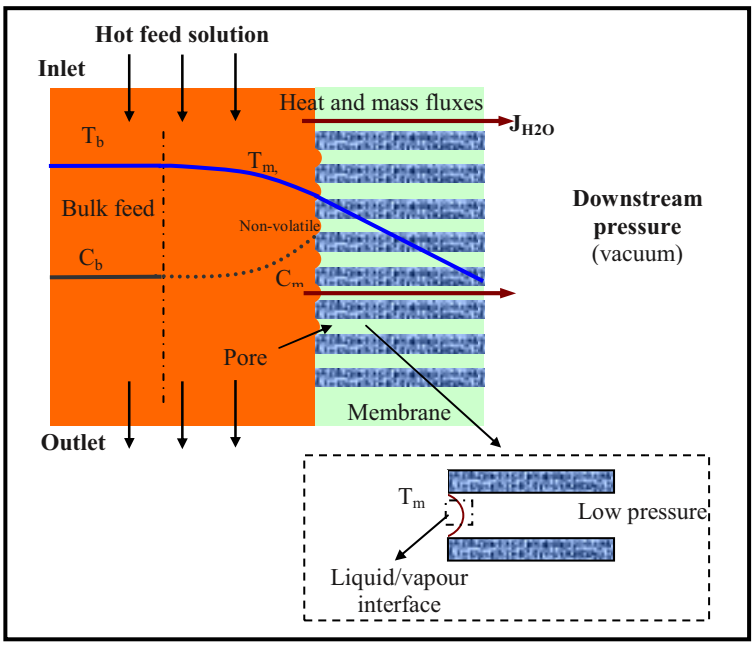

Fig 1.9 *Heat and mass transfer through a porous hydrophobic membrane in VMD [Khayet and Matsura, 2011]*

I.2.3.1 Heat transfer

In general, the heat transfer process in MD includes four steps: (1) heat transferred from the feed solution to the membrane surface across thermal boundary of the feed side; (2) heat transport by conduction through the membrane matrix and the gas filled pores considered heat loss in MD; (3) heat associated to the latent heat of vaporization and therefore to the mass transfer through the membrane pores and (4) heat transfer through thermal boundary of the permeate side, and the corresponding regions are the thermal boundary layer of the feed side, the membrane itself and the thermal boundary layer of the permeate side [*El-Bourawi et al., 2006*]. The heat fluxes for these regions are schematically represented in Fig 1.10 in an electrical analogue.

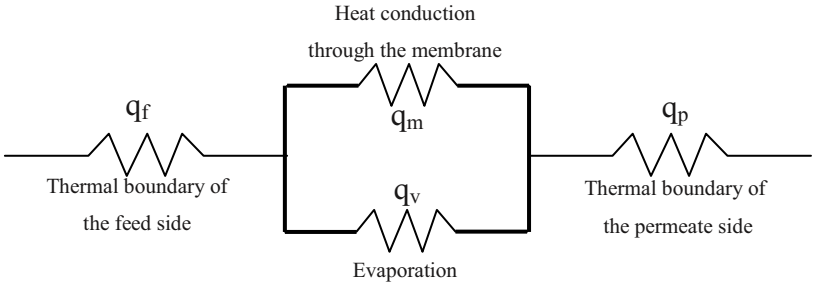

Fig 1.10 *Schematic representation of heat transfer in MD [from Lei et al., 2005].*

❖ *Heat transfer through thermal boundary layers (temperature polarization)*

Heat transfer across the boundary layers is often the rate limiting step for mass transfer in MD, because such a large quantity of heat must be supplied to the surface of the membrane to vaporize the liquid [*Lawson and Lloyd, 1997*]. The heat flux, q_f depending on the heat transfer coefficient in the boundary layer, h_f and the temperature difference between the feed bulk and membrane surface, can be written as:

$$q_f = h_f \Delta T_f = h_f (t_f - t_{fm}) \quad (1\text{-}1)$$

where:

- q_f : heat flux transfer through the thermal boundary layer of the feed side ($W.m^{-2}$);
- h_f : heat transfer coefficient in the boundary layer of the feed side ($W.m^{-2}.K^{-1}$);
- t_f : feed temperature of aqueous solution at the bulk (K);
- t_{fm}: feed temperature of aqueous solution at the membrane surface (K).

Within the boundary layers as illustrated in Fig 1.11, the feed temperature decreases from the value of t_f in the bulk to the value of t_{fm} at the surface of the membrane. This phenomenon is referred as the temperature polarization when each thermal boundary layer imposes a resistance to heat transfer and also affects negatively the driving force for mass transfer leading to decrease of the MD flux. In specific case of VMD, the temperature polarization coefficient is given as follows [*Wirth's thesis, 2002; Banat et al., 2003; Méricq's thesis, 2009*]:

$$\Theta = \frac{t_f - t_{fm}}{t_f - t_p} \tag{1-2}$$

where:

- t_f : feed temperature of aqueous solution in the bulk (K);
- t_{fm} : feed temperature of aqueous solution at the membrane surface (K);
- t_p : temperature at the permeate side (K);

This coefficient can be used to determine the dominant limitation of the process. According to the equation, if coefficient Θ tends to zero, equivalent to t_{fm} approaches t_f, the resistance to heat transfer within the feed boundary layer is negligible. The process is then controlled by the resistance to heat transfer caused by the membrane. And if coefficient Θ tends to 1, corresponding to t_p approaches t_{fm}, the resistance to heat transfer within the membrane is negligible. In this case, the process is controlled by resistance in the feed side.

Similarly within the thermal boundary layer at the permeate side, heat flux is produced in the similar manner as at the feed side, which can be written as:

$$q_p = h_p(t_{pm} - t_p) \tag{1-3}$$

where:

- h_p : heat transfer coefficient in the boundary layer of the permeate side ($W.m^{-2}.K^{-1}$);
- t_{pm} : temperature at the membrane surface from permeate side (K);
- t_p : temperature at the permeate side (K).

This equation, however, is not applicable for VMD because of no existence of the thermal boundary layer at the permeate side in VMD. Within the MD module, two fluids with different temperatures are separated by a macro-porous membrane (with the thickness of ∂), so two thermal boundary layers appear at the feed side (with the thickness of ∂_f) and the permeate side (with the thickness of ∂_p) of the membrane respectively, as shown in Fig 1.11.

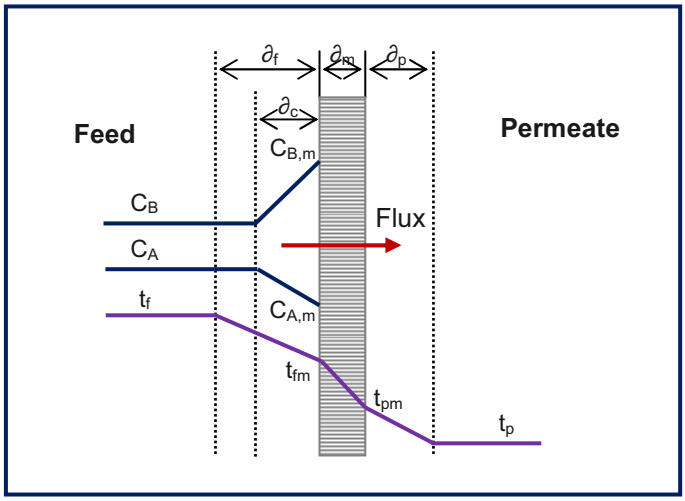

Fig 1.11 *Schematic representation of temperature and concentration profiles of the boundary layers adjacent to the hydrophobic membrane [Lei et al., 2005].*

In the MD literature, boundary layer heat transfer coefficients are almost estimated from the empirical correlations that relate the dimensionless Nusselt number with the Reynolds and Prandtl numbers.This factor could be given as follow [*Lawson and Lloyd, 1997*]:

$$Nu = \frac{h_f d}{k^T} = 0.023\,\mathrm{Re}^{0.8}\,\mathrm{Pr}^{1/3}\left(\frac{\mu}{\mu_m}\right)^{0.14} \qquad (1\text{-}4)$$

where:

- Nu : Nusselt number (-);
- Re : Reynolds number (-);
- Pr : Prandtl number (-);
- d : hydraulic diameter (m);
- k^T : thermal conductivity of liquid ($W.m^{-1}.K^{-1}$);
- μ : bulk liquid viscosity (Pa.s);
- μ_m : liquid viscosity at the membrane surface (Pa.s).

❖ *Heat transfer by conduction through the membrane*

In this case, the heat transfer within the membrane is due to: (1) the latent heat accompanying vapour flux; and (2) the heat transferred by conduction across both the membrane material and the gas-filled membrane pores. The latent heat transferred from the feed side to the permeate side with the flux determined by the equation 1-5:

$$q_v = N.\Delta H \tag{1-5}$$

where:

- N : the mass transfer flux through the membrane ($mol.m^{-2}.s^{-1}$);
- ΔH : the latent heat of the volatile component ($J.mol^{-1}$);
- q_v : fraction of the heat energy transferred to the membrane surface and through the membrane in the form of latent heat ($W.m^{-2}$).

Besides the heat flux represented by q_v, due to the temperature difference between the two surfaces of the membrane, heat is also conducted through the membrane material and the gas that fills the pores with the flux q_m given by equation 1-6:

$$q_m = h_m (t_{fm} - t_{pm}) \tag{1-6}$$

where:

- t_{fm} : the temperatures of the feed aqueous solution at the membrane surface (K);
- t_{pm} : the temperatures of the permeate at the membrane surface (K);
- h_m : the heat transfer coefficient of the membrane ($W.m^{-2}.K^{-1}$), depending on its characteristics (thickness and porosity) and the materials of which the membrane is fabricated [*Soni et al, 2008*] , and can be determined by :

$$h_m = \frac{\lambda_m}{\delta_m} = \frac{\varepsilon.\lambda_g + (1-\varepsilon).\lambda_s}{\delta_m} \tag{1-7}$$

where:

- λ_m : the average heat conductivity of the membrane material ($W.m^{-1}.K^{-1}$);

- ε : the porosity of the membrane (-);
- δ_m : thickness of the membrane (m);
- λ_s : the heat conductivity of membrane material ($W.m^{-2}.K^{-1}$).
- λ_g : the heat conductivity the gas that fills the pores($W.m^{-2}.K^{-1}$).

The heat conductivity of some material or gas involved in MD is listed in the Table 1.9. It showed that temperature has only a minor effect on the heat conductivity.

Table 1.9 *Heat conductivity of some materials or gas involved in MD [Lei et al., 2005].*

Temperature (^0K)	PVDF ($W.m^{-1}.K^{-1}$)	PTFE ($W.m^{-1}.K^{-1}$)	PP ($W.m^{-1}.K^{-1}$)	Air ($W.m^{-1}.K^{-1}$)	Water vapour ($W.m^{-1}.K^{-1}$)
296	0.17 – 0.19	0.25 – 0.27	0.11 – 0.16	0.026	0.020
348	0.21	0.29	0.20	0.030	0.022

In summary, the total heat flux transferred through the membrane matrix whether it is considered efficient heat (heat for evaporation) or heat lost by conduction can be described as follows:

$$Q_m = q_v + q_m = h_m(t_{fm} - t_{pm}) + N.\Delta H \quad (1\text{-}8)$$

It is worth quoting that of the total heat flux transferred through the membrane, typically 50 – 80% is consumed as latent heat for permeate production, while the remainder is lost by thermal conduction. In fact, the heat lost by thermal conduction through the membrane matrix becomes less significant when the MD system works under high operating temperature [*Lei et al., 2005*]. Moreover, the thermal conductivity of air/gases in an order of magnitude lower than that of the membrane material. The heat lost by conduction through the membrane, therefore, can be minimized by using membranes with high porosity (i.e. high void volume) [*Bourawi et al., 2006*].

In VMD, the boundary layer resistance in the permeate side and the contribution of the heat transported by conduction through the membrane are frequently neglected *[Mengual et al, 2004*]. This implies a decrease in the heat conducted through the membrane and enhancement of the VMD performance.

I.2.3.2 Mass transfer

In general, the mass transfer in MD consists of two steps: (1) the first step is across the boundary layers at the both sides of the membrane; and (2) the other is across the membrane. The latter is somewhat complicated and includes several basic mechanisms. The trans-membrane mass transfer may be explained according to different possibilities: the Knudsen flow model, the Poiseuille (viscous) flow model, the ordinary molecular diffusion flow model, and/or the combination of these above mechanisms as often summarized as the Dusty Gas Model [*Mengual et al, 2004; Lawson and Lloyd, 1997*]. The surface diffusion mechanism, which occurs in the process of gas mass transfer through porous medium, is not included because it has little influence on the whole process due to the weak molecule-membrane interaction [*Lei et al, 2005*]. The relationship of all the possible basic mass transfer mechanisms in an electrical analogy and their descriptions are illustrated in the Fig 1.12 and Fig 1.13.

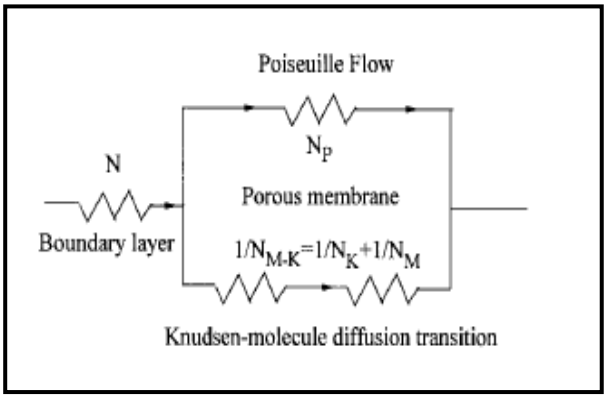

Fig 1.12 *Schematic representation of mass transfer in MD [Lei et al., 2005]*

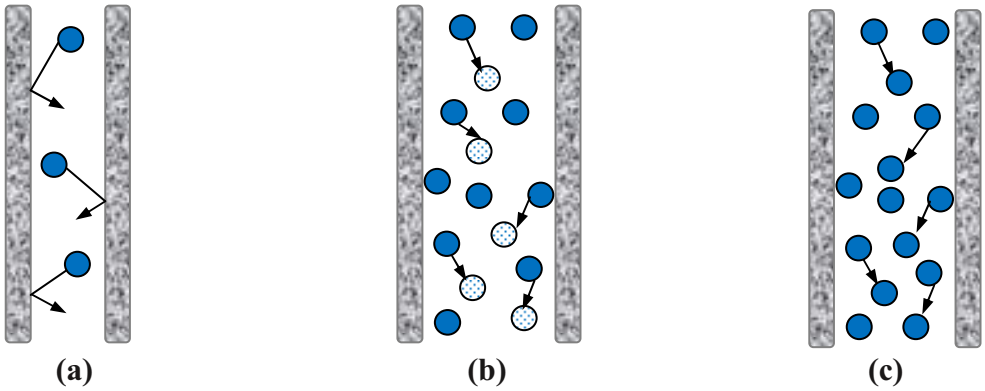

Fig 1.13 *Transport mechanism through a membrane pore used in MD process: (a) Knudsen flow; (b) Molecular diffusion flow and (c) Poiseuille flow* [*from Khayet and Matsura, 2011*]

❖ *Mass transfer in the membrane*

The driving force of mass transfer in a porous membrane is the partial pressure difference between the two sides of the membrane. In VMD, the driving force is maintained by applying a continuous vacuum below the equilibrium vapour pressure at the permeate side. The feed solution is brought into contact with one side of the membrane (i.e. upstream side). In the case of mass transport of a single compound (i.e. water) through the membrane, the permeate flux, J is written as:

$$J_{H2O} = k_k * \Delta P = k_k * (\alpha_{H2O} X_{H2O} P_m^* - P_p) \quad (1\text{-}9)$$

where:

- J_{H20} : molar flux of water ($mol.s^{-1}.m^{-2}$);
- ΔP : partial pressure difference on both sides of the membrane (Pa);
- P^*_m : partial pressure of water vapour at the membrane's conditions (Pa);
- P_p : partial pressure at the permeate side, which equal to vacuum pressure (Pa);
- k_k :mass transfer coefficient in the membrane, which depends on geometric characteristics of the membrane ($s.m^{-1}.mol.kg^{-1}$);
- α_{H2O} : the activity of the water (α_{H2O} = 1 for distilled water),
- X_{H2O} : mole fraction of water in the feed (-).

The water vapour pressure at the liquid/vapour interface (Pa) may be related with the temperature (K), by using the Antoine's equation:

$$P_m^* = B_1 * \exp(A_1 - \frac{A_2}{T_m + B_2 + A_3}) \quad (1\text{-}10)$$

(with A_1 = 18.3036; A_2 = 3816.44; A_3 = - 46.13; B_1 = 133.32 and B_2 = 273.15)

where B_1 and B_2 are the coefficients to convert unit mmHg and C into Pa and K, respectively; T_m is the temperature at the membrane surface (K);

In order to determine what kind of transfer mechanism is dominant in the mass transfer within the membrane, Knudsen number (Kn), which is defined as the ratio of the mean free path (λ) of the transported molecules to the pore size of the membrane, should be used. The mean free path (λ) of molecules can be calculated using the following expression:

$$\lambda = \frac{R * T}{N_A \sqrt{2} \pi p \sigma^2} \tag{1-11}$$

Where:

- R : ideal gas constant (R = 8.314 J.mol^{-1}.K^{-1});
- T : the absolute temperature (K);
- N_A : Avogadro constant (N_A = 6.02214129 x 10^{-23} mol^{-1});
- p : the mean pressure within the membrane pores (Pa);
- σ : the collision diameter or average diameter of water molecule (σ = 2.641 Å for water vapour).

In the VMD process, the ordinary molecular diffusion resistance is neglected because it is proportional to the partial pressure of air in the membrane pores and in VMD only traces of air are present within the membrane pores. Thus, the mass transport mechanisms through porous and hydrophobic membranes in VMD are only Knudsen flow model, Poiseuille (viscous) flow model and their combination [*Izquierdo-Gil and Jonsson, 2003; Urtiaga et al, 2001; Khayet and Matsuura, 2004*]. In VMD, all mechanisms can occur simultaneously, depending on the operating condition with the three possible following cases:

When r < 0.05λ, the molecule – pore wall collisions are dominant in comparison with the molecule-molecule collisions, and Knudsen type diffusion of the vapour molecules through the membrane pores is applied by the following equation [*Bandini and Saavedra, 1997; Cabassud and Wirth, 2003; Mengual et al., 2004*]:

$$k_k = \frac{2}{3RT} \frac{\varepsilon r}{\tau \delta} \sqrt{\frac{8RT}{\pi M_{H2O}}} = \frac{K_M}{\sqrt{M_{H2O}}} \tag{1-11}$$

where

- r : the mean pore radius (m)

- R : ideal gas constant (R = 8.314 J.mol^{-1}.K^{-1})
- T : the absolute temperature (K)
- ε : membrane porosity (-)
- τ : the pore tortuosity (-)
- δ : the membrane thickness
- K_M : Knudsen permeability (s.mol$^{-1/2}$.m^{-1}.kg$^{-1/2}$).

When 0.05λ < r < 50λ, the transition flow dominates and the following equation corresponding to the combined Knudsen/Poiseuille mechanism is considered [*Lawson and Lloyd, 1996; Banat and Simandl, 1994*]:

$$k_k = \frac{1}{RT\delta}\left(\frac{2\varepsilon r}{3\tau}\sqrt{\frac{8RT}{\pi M_{H2O}}} + \frac{\varepsilon r^2}{8\tau\eta}\bar{p}\right) \tag{1-14}$$

where η is the viscosity of water vapour and $\bar{p}$ is the average pressure in the membrane pores. In this case, the contribution of the viscous flow in the total permeate flux can be estimated by the ratio of the viscous and Knudsen terms:

$$\kappa_i^{v/K} = 0.2\frac{\bar{p}\bar{r}}{\nu\eta_i} \tag{1-15}$$

where ν is the mean molecular speed of vapour molecules.

When (r > 50λ), molecule – molecule collisions are dominant over the molecule – pore wall collision (Knudsen flow), the mass transport takes place via Poiseuille type of flow also called viscous flow can be calculated using the following expression [*Khayet and Matsuura, 2004*]:

$$k_k = \frac{\varepsilon r^2}{\tau\delta}\frac{\bar{p}}{8\eta\ RT} \tag{1-16}$$

where η is the viscosity of water vapour and $\bar{p}$ is the average hydrostatic pressure in the membrane pore.

As a matter of fact, the Knudsen type of diffusion is commonly considered as the predominant mass transfer mechanism in VMD by the majority of authors [*Mengual et al, 2004; Couffin et al, 1998; Urtiaga et al, 2000; Sarti et al, 1993; Wirth and Cabassud, 2003; Bourawi et al, 2006; Méricq et al, 2010*]. This is because the membranes for the VMD process should have small pore sizes in order to avoid their wetting when contacted with feed solutions, which often are aqueous solutions of organic liquids with low surface tension. Moreover, the calculated values of the mean free path of the transported molecules through the membrane pores is higher in VMD than in SGMD or DCMD configurations because of the low pressure applied on the permeate side (the mean free path value is proportional to the pressure).

❖ *Mass transfer through the feed boundary layer*

The mass transfer through the feed boundary layer can be affected by a presence of fluid boundary layers adjoining both the feed and permeate membrane sides, giving rise to the phenomenon called concentration polarization. This phenomenon is defined as the increase of solute concentration on the membrane surface to the bulk solute concentration.

When an aqueous solution containing non-volatile is used as feed, the concentration of the solute at the feed-side membrane surface becomes greater than in the bulk. It means the concentration polarization appeared and resulted in reduction of both driving force and permeate flux. The solute concentration polarization coefficient (ξ) is defined as [*Lawson and Lloyd, 1996*]:

$$\xi = \left(\frac{\chi_{fm} - \chi_p}{\chi_f - \chi_p} \right) \tag{1-17}$$

where:

- χ_{fm} : the mole fraction of the solute at the membrane surface;
- χ_f : the mole fraction of the solute at the bulk;
- χ_p : the mole fraction of the solute at the permeate side;

The molar flux N through the feed side boundary is calculated based on Fick's law as follows:

$$N = k_f c \ln\left(\frac{\chi_{fm} - \chi_p}{\chi_f - \chi_p}\right) \quad (1\text{-}18)$$

where:

- N : molar flux (mol.m^{-2}.s^{-1})
- k_f : mass transfer coefficient in the feed boundary layer (m.s^{-1});
- c : molar concentration at bulk liquid phase (mol.m^{-3});

The coefficient k_f can be estimated from Sherwood number (Sh):

$$Sh = \frac{k_f d}{D} = a\,\mathrm{Re}^b\, Sc^c \left(\frac{d}{L}\right)^d \quad (1\text{-}19)$$

where:

- L : length of the feed channel;
- D : diffusive coefficient of the solute in the solution (m^2.s^{-1});
- Sh : Sherwood number (-);
- d : hydraulic diameter (m);
- Re : Reynolds number (-)
- Sc : Schmidt number:

$$\mathrm{Re} = \frac{\rho u d}{\mu} \quad (1\text{-}20) \text{ and } \quad Sc = \frac{\mu}{\rho D} \quad (1\text{-}21)$$

where ρ is density, μ is viscosity, u is feed velocity.

I.2.4 Effects of operating parameters on the VMD performance

As the objective of this study is to focus on arsenic and salt rejection, so it is worth noting that most of the results reviewed below are only for non-volatile compound.

I.2.4.1 Effect of feed temperature

The feed temperature is a very sensitive operating parameter, which significantly affects both the permeate flux and the total energy requirement. The feed temperature in VMD is normally in range of 20 – 80^{0}C. The permeate flux increases exponentially with increase of the feed temperature due to dependence of partial vapour pressure at the membrane surface on the feed temperature (Antoine equation). Thermal efficiency, defined as the ratio of the heat that contributes to evaporation and the total heat transferred from the feed to the permeate, increases with increase of feed temperature although the temperature polarization effect also increases [*Lawson and Lloyd, 1996; Bandini et al., 1992; Cabassud and Wirth, 2003; Khayet et al., 2003; Criscuoli et al., 2008*]. Besides, the permeate flux is highly sensitive to the feed temperature especially at high value of vacuum pressure [*Banat et al., 2003*]. Effect of feed temperature on the permeate flux achieved in several recent VMD studies was summarized in Table 1.10.

Table 1.10 *Effect of feed temperature on the VMD permeate flux*

Reference	Membrane type	Solution	Operating conditions	T_f (^{0}C)	Permeate kg.m^{-2}.h^{-1}
Criscuoli et al., 2008	PP (0.2 µm)	Pure water	Pp = 10 mbar Q = 150 L.h^{-1}	53.9 → 59.3	29.7 → 51.4
Safavi et al 2009	PP (0.2 µm)	NaCl (300 g.L^{-1})	Pp = 40 mbar Q = 30 mL.s^{-1}	25 → 55	5.5 → 9.23
Tang et al, 2010	PP	NaCl (0.5 mol.L^{-1})	Pp = 3 kPa Q = 50 L.h^{-1}	40 → 80	≈ 4 → 28.92
Méricq et al., 2010	PTFE (0.2 µm)	Seawater (300 g.L^{-1})	Pp = 500 Pa Re = 4000	20 → 70	1.33 → 22.30
Criscuoli et al., 2012	PP (0.2 µm)	As(III) (1 ppm)	Pp = 10 mbar Re = 1700	20 → 40	2.3 → 9

Regarding energy consumption, higher feed temperature requires higher energy consumption, especially for heating. By applying VMD for desalination of seawater, *Méricq et al, 2010* reported that increase in feed temperature from 20 to 70°C increased the permeate flux but the total energy requirement was also drastically increased with more than 98% of the total energy requirement was heat energy at T_f = 70°C. Similar trend could be observed in literature [*Criscuoli et al., 2008; Sarbatly and Chiam, 2013*]. .

I.2.4.2 Effects of downstream (vacuum) pressure

In VMD, decrease of vacuum pressure can lead to increase of trans-membrane pressure difference (i.e. driving force) and as a result, permeate flux also increases. In that case, the risk of membrane pore wetting becomes higher. Evaporation efficiency also increases with decrease of vacuum as almost 90% achieved at 10 mbar of vacuum [*Criscuoli et al., 2008*]. Effect of vacuum pressure on the permeate flux achieved in several recent VMD studies was summarized in Table 1.11.

Table 1.11 *Effect of vacuum pressure on the VMD permeate flux*

Reference	Membrane type	Solution	Operating conditions	Pp (Pa)	Permeate $Kg.m^{-2}.h^{-1}$
Criscuoli et al., 2008	PP (0.2 µm)	Pure water	Tf = 59.2^{0}C Q = 235 $L.h^{-1}$	6000 → 1000	50.5→56.2
Safavi et al 2009	PP (0.2 µm)	NaCl (300 $g.L^{-1}$)	T_f = 40^{0}C Q = 30 $mL.s^{-1}$	12000 → 4000	1.5 → 7.5
Méricq et al., 2009	PTFE (0.1 µm)	Seawater (300 $g.L^{-1}$)	Tf = 40^{0}C Re = 4500	1500 → 100	18 → 27
Méricq et al., 2010	PTFE (0.2 µm)	Seawater (300 $g.L^{-1}$)	T_f = 50^{0}C Re = 4500	6100 → 600	2.2 → 10

Decrease of vacuum can influence the specific energy consumption, defined as the ratio between energy consumption and permeate flow-rate. *Criscuoli et al, 2008* reported that energy consumption increased from 223.9 to 441.2 W with decrease of vacuum pressure from 60 to 10 mbar, corresponding to increase of specific energy consumption from 1.10 to 1.98 kWh/kg. Constant specific energy consumption with decrease of vacuum was observed in study by *Méricq et al., 2009*. However, it was attributed to small range of decrease of vacuum applied (i.e. 1500 – 100Pa) .Therefore, it is advisable to determine the optimum downstream pressure taking into account economic considerations.

I.2.4.3 Effect of feed inlet concentration

In all MD configurations, the increase of non-volatile solute concentration in the aqueous feed solution can result in reduction of the permeate flux. This observation seems very clear in case of salt due to the decrease of water vapour pressure as well as to the contribution of the concentration polarization effect [*Cabassud and Wirth, 2003; El-Bourawi et al., 2006*]. However this tendency seems to be not applicable in case of aqueous feed solution containing arsenite with increase of As(III) concentration in range of 0 to 5 ppm [*Criscuoli et al, 2012*]. In this case, low feed As(III) concentration, which is not high enough to alter water activity coefficient can be the reason.

VMD can perform well for highly concentrated aqueous solutions of salts (i.e. for RO brine from 50 – 300 $g.L^{-1}$ salt concentration) [*Cabassud and Wirth, 2003*; *Méricq et al, 2010; Mohammadi and Safavi, 2009*]. The permeate flux decreases as the feed salt concentration increases and this leads to salt crystallization and scaling. *Mohammadi and Safavi, 2009* and *Méricq et al, 2010* concluded that the effect of scaling in desalination by VMD was not remarkably strong. No significant difference was detected between permeability of the membrane (PTFE) before and after washing, confirming that scaling is reversible and occurs only on the membrane surface. Effect of salt concentration on the permeate flux achieved in several recent VMD studies was summarized in Table 1.12.

Table 1.12 *Effect of vacuum pressure on the VMD permeate flux*

Reference	Membrane type	Solution	Operating conditions	Concentration $g.L^{-1}$	Permeate $Kg.m^{-2}.h^{-1}$
Cabassud and Wirth, 2003	PVDF (0.2 µm)	NaCl	Tf = 25^0C Pp = 100 Pa Re = 4000	30 → 100	15 → 5
Safavi et al 2009	PP (0.2 µm)	NaCl	T = 40^0C P = 40 mbar Q = 30 $mL.s^{-1}$	100 → 300	11.41 → 9.23
Méricq et al., 2010	PTFE (0.2 µm)	Seawater	Pp = 500 Pa Re = 4000	95 → 300	25 → 15
Criscuoli et al., 2012	PP (0.2 µm)	As(III)	T_f = 40^0C Pp = 10 mbar Re = 1700	0 → 5 ppm	stable: 9

I.2.4.4 Effect of feed flow rate

Increase of feed flow rate can increase heat transfer efficiency of the feed boundary layer and VMD permeate flux by lessening temperature and concentration polarization effects. More precisely, increase of feed flow rate results in significant increase of VMD permeate flux, especially in the laminar and transitional flow regimes. Effect of feed flow-rate on the permeate flux achieved in several recent VMD studies was summarized in Table 1.13

Table 1.13 *Effect of feed flow-rate on the VMD permeate flux*

Reference	Membrane type	Solution	Operating conditions	Reynolds number	Permeate $Kg.m^{-2}.h^{-1}$
Méricq et al., 2010	PTFE (0.2 µm)	Seawater (300 $g.L^{-1}$)	Pp = 500 Pa $T_f = 50^0C$	350 → 6100	8 → 9.8
Criscuoli et al., 2012	PP (0.2 µm)	As(III) (1 ppm)	Pp = 10 mbar Re = 1700	700 → 1700	8 → 9

I.2.5 Hydrophobic membranes used in MD process

Although being introduced in the late 1960s, the development of MD process was made only in the early 1980s when newer, more suitable membranes became available. Until now, the commercial macro-porous hydrophobic membranes made of PP (Polyethylene), PVDF (Poly vinylidene fluoride) and PTFE (Polytetrafluoroethylene), available in tubular, capillary or flat sheet forms have been widely used in MD process. List of some commercial membranes used commonly in MD are summarized in the Table 1.14 and 1.15 [*M.Khayet &T. Matsuura, 2011].*

Table 1.14 *Flat sheet commercial membranes commonly used in MD process*

Membrane trade name	Manufacturer	Material	Membrane thickness (μm)	Mean pore size (μm)	Porosity (%)	LEP of water (kPa)
TF200	Gelman	PTFE/PP	178	0.20	80	282
TF450				0.45		138
TF1000				1.00		48
Taflen		PTFE	60	0.8		-
GVHP	Millipore	PVDF	110	0.22	75	204
HVHP			140	0.45		105
FGLP		PTFE/PE	130	0.2	70	280
FHLP			175	0.5	85	124
FALP			150	1.0	85	48.3
Gore		PTFE	64	0.2	90	368
			77	0.45	89	288
		PTFE/PP	184	0.2	44	463
Enka		PP	100	0.1	75	-
			140	0.2		
Celgard 2500	Hoechst Celanese Co.		28	0.05	45	
Celgard 2400			25	0.02	38	
Metricel	Gelman		90	0.1	55	
Vladipore		-	120	0.25	70	-
3MA	3M corporation	PP	91	0.29	66	-
3MB			81	0.40	76	
3MC			76	0.51	79	
3MD			86	0.58	80	
3ME			79	0.73	85	
Teknokrama		PTFE	-	0.2	80	-
				0.5		
				1.0		
G-4.0-6-7	GoreTex Sep GmbH	PTFE	100	0.2	80	463

Table 1.15 *Capillary commercial membranes commonly used in MD*

Membrane Trade name	Manufacturer	Material	Membrane thickness (µm)	Mean pore size (µm)	Porosity (%)	LEP of water (kPa)
Accurel® S6/2	AkzoNobel Microdyn	PP	450	0.2	70	140
MD020TP2N	Enka Microdyn		1550	0.2	75	-
Accurel® BFMF06-30-33	Enka A.G. Euro-Sep		200	0.2	70	
Celgard X-20	Hoechst Celeanese Co.		25	0.03	35	
Sartocon® Mini SM 3031 750701W	Sartorius	Polyolefine	-	0.22	-	
PTFE	Sumitomo Electric	POREFLON	550	0.8	62	
PTFE	Gore-Tex	TA001	400	2	50	

In general, based on the previous published studies *Khayet and Matsuura, 2011* summarized the requirements which a membrane should satisfy for being used for MD:

a) The membrane can be single layer or multi-layers, but at least one of the layers should be made of hydrophobic material and be porous.

b) The pore size range may be from 10 nanometres to 1 micrometer and the porosity should be as high as possible since MD permeate flux increases with the increase of the pore size and/or porosity. However, the Liquid Entry Pressure (LEP) should be as high as possible. The LEP is characteristic of a given membrane. A membrane should be made of material of low surface energy or high hydrophobicity (i.e. large contact angle to water) and small maximum pore size to have high LEP.

c) The tortuosity factor (i.e. defined as ratio of average pore length to the membrane thickness) should be small since the permeate flux decreases with increase of membrane's tortuosity.

d) The thickness of the single-layer membrane should have an optimized value as the thickness is inversely proportional to the rate of mass and heat transport by conduction through the membrane. While a high mass transport is favoured for the MD process, a high heat transport is considered to be a heat loss. Therefore, a compromise should be made, between the mass and the heat transfer, by properly adjusting the membrane thickness.

e) The thermal conductivity of the membrane material should be as low as possible. Since the thermal conductivity of commercial membranes are almost in the same order of magnitude (between 0.04 and 0.06 $W.m^{-1}.K^{-1}$), it is possible to diminish the membrane heat transfer by conduction using membrane of high porosities. It was explained by the conductive heat transfer coefficients of gases entrapped in the pores are an order of magnitude smaller than most of the used membrane;

f) The membrane as a whole should be exhibit good thermal stability.

g) The membrane material should have excellent chemical resistance to various feed solutions. If the membrane has to be cleaned, resistance to acid and base is necessary.

h) The membrane should have a long life with stable MD performance (permeability and selectivity) when used commercially.

i) And finally, another important requirement is that the membrane should be cheap.

I.2.6 Conclusions

The MD process in general and its VMD variant in particular is an advanced technology that seems to be suitable for both direct arsenic removal and desalination. Among the four variants of MD process, VMD is expected to provide higher permeate flux than that of other membrane distillation configurations. As a consequence, a study to determine feasibility of the VMD process for arsenic rejection from brackish groundwater is proposed. Several published studies have proven its feasibility either in arsenic treatment or in desalination. However, the achieved permeate flux is still a question due to its dependence on the type of hydrophobic membrane employed. Moreover, effect of arsenic concentration in feed solution to the permeate flux is still a doubtful question because of the opposite conclusions. Besides that, most of the studies used synthetic solution with either pure water or distilled water so influences of salt, calcium and organic matter to membrane fouling or wetting have not been studied carefully, especially for the case of VMD configuration. For that reasons, this study will test the influences of the operating parameters on the VMD performance for arsenic removal with presence of NaCl. Membrane fouling will also be taken into consideration with presences of calcium and organic matter. Furthermore, an integrated process by coupling of RO and VMD processes for direct As(III) removal for a higher global recovery of clean water will also be studied.

Chapter II:
Materials and Methods

In this research, performances of both reverse osmosis (RO) and vacuum membrane distillation (VMD) processes for direct arsenic removal were studied. This chapter, thus, will introduce all the material and experimental protocols used in RO and VMD experiments. Detailed descriptions of the RO and VMD pilots used for the study are also presented. As membrane plays an important role in the MD process, permeability measurement methods of the employed hydrophobic membranes will be studied in detail and intended to be a separate subject of Chapter 3.

II.1. THE EXPERIMENTAL PILOTS

II.1.1. The vacuum membrane distillation (VMD) pilot plant

In general, the experimental VMD pilot plant consists of the following components as illustrated in Fig 2.1:

- A thermostatic feed tank, including a stirrer and a condenser;
- A heat exchanging group, including a heating bath and a heat exchanger;
- A pump system;
- A condensing unit in the permeate side, including two parallel liquid nitrogen traps;
- A vacuum group, including a vacuum pump, vacuum manometer and a condenser;
- A flat sheet membrane module;
- A data acquisition system.

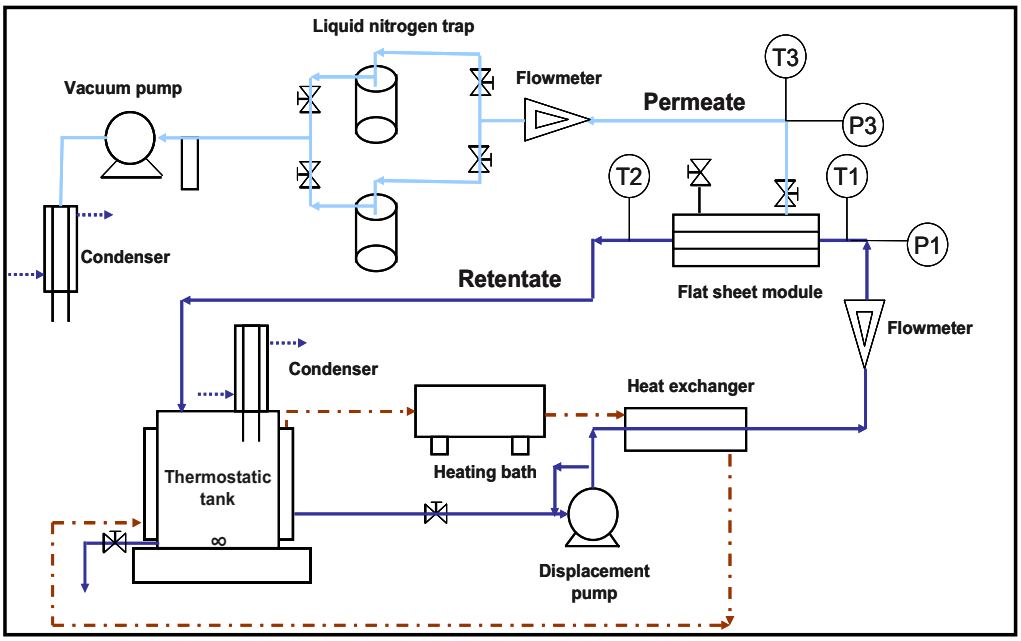

Fig 2.1 *Schematic diagram of the VMD pilot plant.*

Fig 2.2 *Photo of the experimental VMD pilot plant.*

All the tests were carried out with a bench-scale batch pilot plant as illustrated in the Fig 2.2. In principle, feed water was introduced into a thermostatic feed tank, where its temperature was controlled in range of 25 - 60°C owing to a heating group. Feed solution was, then, pumped through the membrane module by a pump (A/B Pompes). Vacuum or low permeate pressure Pp was obtained using a vacuum pump. Permeate water vapour flux passing through the membrane was measured by a BRONKHORST water thermal mass flow meter with capacity of $0 \div 60$ g.h^{-1}. Temperature and pressure measurements at inlet and outlet, and at the permeate side of the membrane module were also conducted and recorded in the data acquisition system.

II.1.1.1. The thermostatic feed tank

The feed tank, with volume of 4L, is made of stainless steel. Feed solution temperature inside this tank can be adjusted to expected values owing to a heat exchanging system as well as maintained at a stable value owing to a jacket to isolate with the outside environment. A condenser, used for water condensation process, is installed above the tank to prevent water loss by evaporation. A magnetic stirrer is

included to ensure the homogenization of the feed solution, both in temperature and concentration.

II.1.1.2. The heat exchanging group

This group consists of a heating bath and a heat exchanger. This digital heating bath can heat the water temperature in range of 25°C ÷ 150°C with accuracy of 0.1°C (Bioblock Scientific, France) before providing hot water into the jacket of the feed tank and the heat exchanger. The heat exchanger can control and regulate the feed solution temperature to a fixed value as expected. In order to prevent heat loss and water condensation in pipes by conduction to the outside environment, a thermal insulation of the pipelines with a sleeve insulation made from synthetic rubber is also designed.

II.1.1.3. The pump system

The pump system is equipment with an A/B pump that can maintain a constant liquid flow at the inlet of membrane module while the remaining is circulated back to the feed tank. This pump has capacity to provide a flow-rate in range of 25 ÷ 250 $L.h^{-1}$ determined by using a magnetic flow-meter.

II.1.1.4. The condensing unit

The condensing unit, located in the permeate side, includes two components: (1) a system of two parallel liquid traps located between the permeate effluent and the vacuum pump, and (2) a condenser located after vacuum meter. The two liquid traps are used for condensation of vapour water and recovery of permeate while the condenser can help to collect the vapour water passing through the two liquid trap as permeate. It, thus, helps to avoid

possible penetration of steam into the vacuum pump. Permeate flow-rate is measured by a mass flow-meter located before the two liquid trap.

It is worth noting that the two liquid traps are located in parallel and operated alternatively. This alternative operation helps to prevent the decrease of vacuum pressure when opening the liquid trap for sample collection and, thus, ensure the continuity of permeate flow-rate measurement. Each of these two liquid traps can be isolated and removed from the system via two valves located upstream and downstream of the trap while the second one is still being used. In order facilitate the vapour water condensation, liquid nitrogen at -196°C is poured into two Dewar, which are then placed under the two liquid traps. The low temperature of liquid nitrogen helps to condense almost the steam, which is found in solid form (ice) and can be retrieved for analysis after fusion.

II.1.1.5. The vacuum group

The vacuum group includes a pressure meter and a roots vacuum pump (RP 15C Vario Vaccubrand), which can provide a theoretical vacuum limit of 100 Pa for a flow-rate of 15 $N.m^3.h^{-1}$. This pump is operated by two symmetric rotary pistons, which can cause displacement of air (or steam) from the permeate circuit to the outlet of the pump. The vacuum pressure can be adjusted by a manual diaphragm valves with an accuracy of 100 Pa.

II.1.1.6. The membrane module

The VMD pilot in this study was designed as a flat sheet membrane module. Its structure was described in Fig 2.3.

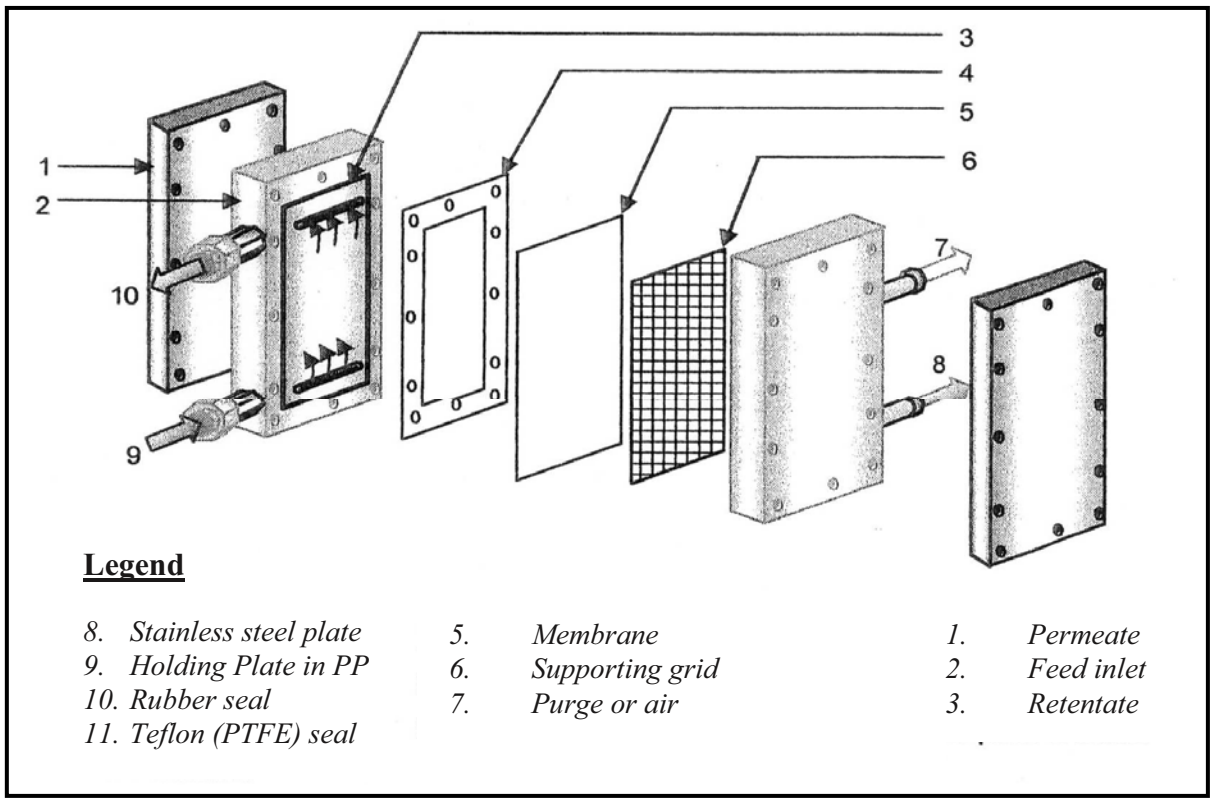

Fig 2.3 *Inside structure of the flat sheet membrane module.*

This membrane module has a rectangular shape with two polypropylene (PP) sheets restrained between two stainless steel plates to ensure tightness of this module. In order to prevent heat loss by conduction into the environment, the membrane module is isolated by using a thin multilayer insulation thermal reflector (Trisoreflex) to cover around its outside. Inside the module, a flat sheet membrane with available area of 5.78×10^{-3} m^2 (L x W = 16.5 cm x 3.5 cm) is restrained between the two PP plates. Gap between the membrane and module wall is 1 mm, allowing a range of feed stream flow-rate from 1.93×10^{-6} to 1.93×10^{-5} $m^3.h^{-1}$, corresponding to 0.2 – 2 $m.s^{-1}$ of feed velocity. In this range of feed velocity, hydrodynamic flow pattern corresponds to range of Reynolds number from 400 – 3900 (from laminar to turbulence regime) at $T_f = 25^0C$. In addition to that, with the increase of T_f from 25 – 60^0C, this range of Reynolds number could increase from 400 – 8750.

In this study, two different types of hydrophobic membrane were used: PTFE flat-sheet membrane (Fluoropore) and PVDF flat-sheet membrane (Durapore), provided by Millipore Corporation, France. The membrane structure and its characteristics were given in Fig 2.4 and Table 2.1.

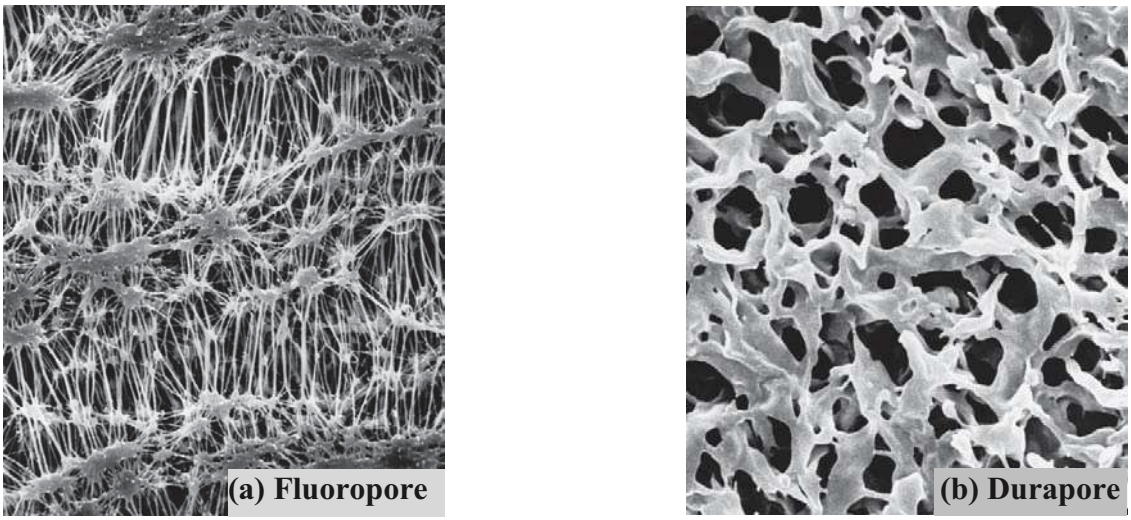

Fig 2.4 *The employed hydrophobic membranes: (a) Fluoropore membrane (PTFE - Polytetrafluoroethylene), and (b) Durapore membrane (PVDF - Polyvinylidene fluoride)*

Table 2.1 *Characteristics of the hydrophobic membranes employed.*

Hydrophobic membranes	Fluoropore	Durapore
Material	PTFE	PVDF
Nominal pore size, μm	0.22	0.22
Thickness, mm	0.175	0.125
Porosity, %	70	75
Contact angle, °	123.9	136.3
Liquid entry pressure, bar	4.2	2.6

Note:

- ✓ *Contact angle: determined by Contact Angle Meter (Digidrop);*
- ✓ *LEP: determined by Amicon filtration unit of Millipore 8050 connected with a compressed air system.*
- ✓ *Other parameters: provided by the Millipore manufacturer.*

II.1.1.7. The instruments

In order to determine operating parameters such as temperature, pressure and permeate flow-rate at different points of the pilot, some instruments are used as follows:

Three temperature probes (PT 100 probe with an accuracy of ± 0.5°C) are installed at the inlet and outlet of the membrane module on the feed side and at the outlet of the membrane module on the permeate side (corresponding to T_1, T_2 and T_3 in the Fig 2.1, respectively). These probes are directly connected to the acquisition system to record the three temperature values simultaneously. A temperature calibration using a reference thermal-meter is recommended to determine the difference between temperature probes and acquisition system. The obtained calibration curve is presented in the Appendix section.


Vacuum pressure manometer

Similar to the temperature measurement, three digital pressure gauges, with an accuracy of ± 400 Pa, are installed to measure pressures at inlet and outlet of the membrane module on the feed side and at the outlet of the membrane module on the permeate side (corresponding to P_1, P_2 and P_3 in the Fig 2.1, respectively). Furthermore, a digital manometer is positioned between the condensing unit (liquid nitrogen traps) and the vacuum pump to measure vacuum pressure with an accuracy of 100 Pa. The pressure sensor is calibrated using a needle manometer with detection limit at –1 bar and with an accuracy of 0.005 bars. The obtained calibration curve is presented in the Appendix.

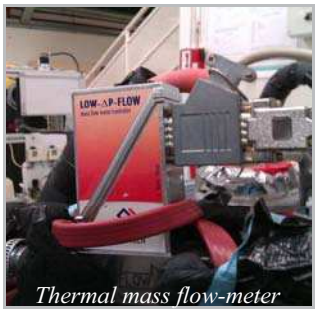

Thermal mass flow-meter

In order to facilitate a continuous operation, a thermal mass flow-meter (Bronkhorst), which has ability to run at a low flow-rate of water vapour under vacuum condition, is used and placed before the liquid nitrogen traps. The measuring range of the flow-meter is between 0 – 60 $g.h^{-1}$ with 0.6 % of the measurement uncertainty.

II.1.1.8. The data acquisition system

This system includes a computer with acquisition software to show values of the operating parameters (temperature, pressure and permeate flow-rate), which are measured directly by temperature probes and pressure gauges located at the inlet, outlet and permeate side of the membrane module. All data are recorded after each 5 seconds and then transferred into Excel spreadsheet file for further analysis.

II.1.1.9. The operating conditions

Range of operating conditions for all VMD experiments was summarized in Table 2.2.

Table 2.2 *Range of operating conditions in all VMD experiments.*

Feed temperature (°C)	Permeate pressure (Pa)	Feed flow-rate ($L.h^{-1}$)	Reynolds number (-)
25 ÷ 60	2500 ÷ 7500	25 ÷ 250	400 - 8750

II.1.2. The Reverse Osmosis (RO) pilot plant

II.1.2.1. The experimental set-up

The experimental RO pilot consists of the following components:

- A nitrogen gas cylinder;
- A filtration cell;
- A stirrer controller ;
- A balance;
- A data acquisition system.

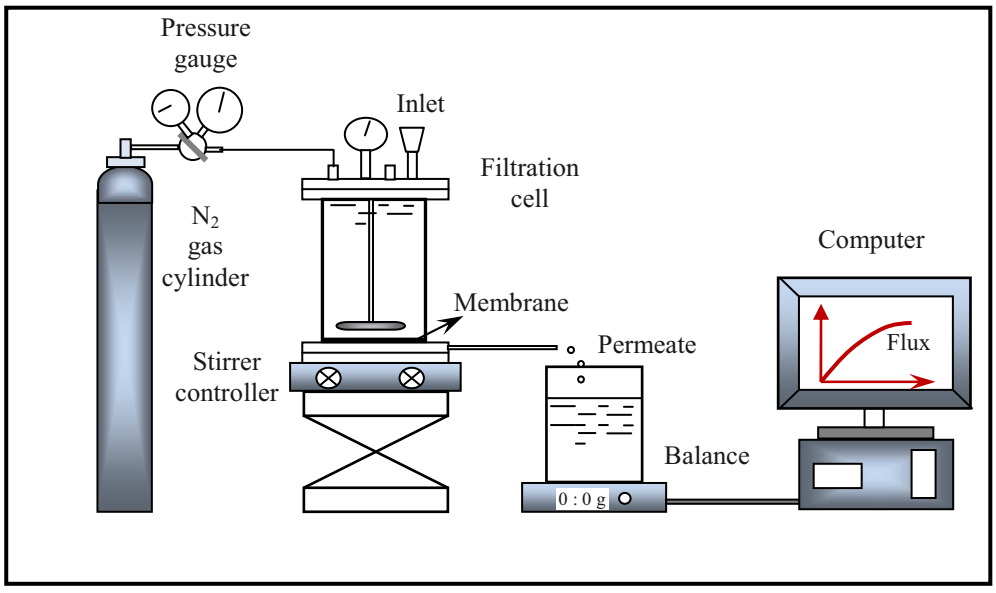

Fig 2.5 *The experimental RO set-up*

A batch pilot reactor, as described in the Fig 2.5, was employed. Feed water was introduced into the cell before each experiment. A flat-sheet membrane of 9 cm in diameter was used. The cell has an area of 63.6 cm^2 filter and a total volume of 500 ml. A circuit of nitrogen gas was used to impose a trans-membrane pressure of between 0 and 36 bars. A magnetic stirrer was used to stir liquid continuously on the surface of the membrane in order to limit the effect of concentration polarization. Permeate flow was determined owing to a regular electronic balance (Sartorius 1500S), which is connected to a computer.

Detailed structure of the filtration cell (0.5L) used for the experiments was described in the Fig 2.6. Inside the cell, a RO (osm-ESPA) thin film composite polyamide membrane module with active area of 38.5 cm^2 was employed. Main characteristics of this kind of membrane were described in the Table 2.3. The membrane with higher salt retention presents also the lower water permeability. Moreover, this membrane has negative surface charge and tends to be hydrophobic.

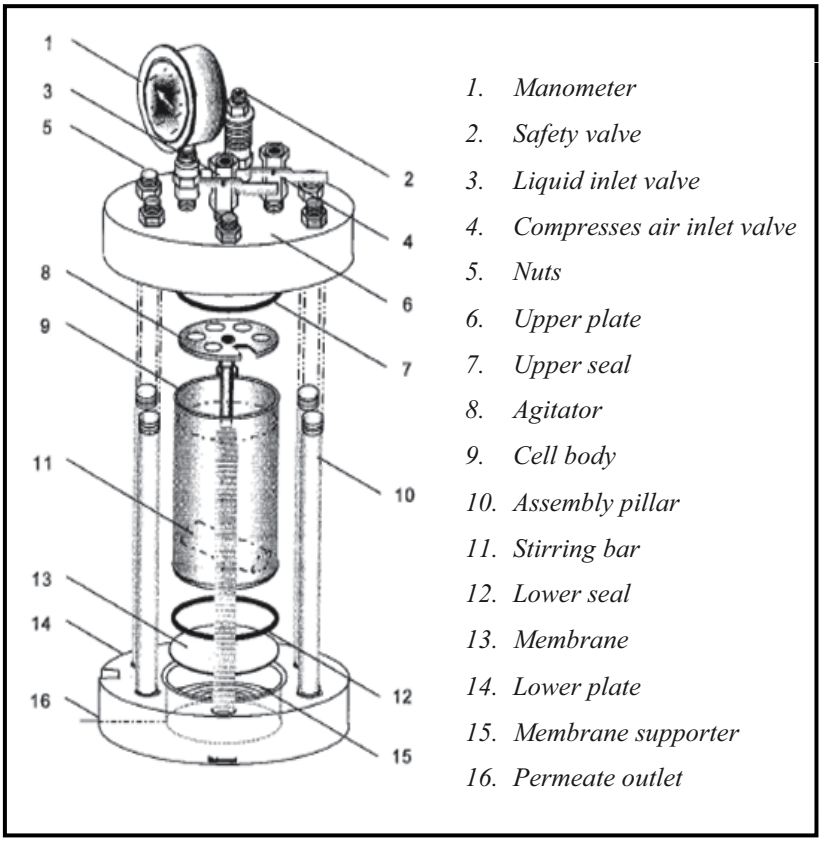

Fig 2.6 *The RO filtration cell.*

Table 2.3 *Characteristics of the employed osm-ESPA membrane.*

No.	Specification	Value
1	Manufacturer	Hydranautics
2	Classification	Reverse osmosis
3	Material	Polyamide
4	MWCO ($g.mol^{-1}$)	< 200
5	Salt retention	> 98.7% $CaCl_2$
6	Water permeability at 20°C: (L.h-1.m-2.bar-1)	3.6
7	Contact angle (°)	69
8	Zeta potential at pH 7 (mV)	-7.7
9	Average roughness (nm)	130.2

II.1.2.2. The operating conditions

Range of operating conditions for the RO experiments was summarized in Table 2.4.

Table 2.4 *Range of operating conditions in all RO experiments.*

pH	Pressure (bar)	Recovery rate (%)
7 ÷ 10	24 ÷ 32	14 ÷ 86

II.1.2.3. The RO experimental protocols

❖ *Determination of the RO permeate flux*

As stated above, the objective of this part was to study direct As(III) rejection performance of the osm-ESPA membrane by using a batch-mode RO reactor. Scheme of the experimental RO set-up was presented in Fig 2.5 and Fig 2.6. In operation of the RO process, a trans-membrane pressure (ΔP), which should be higher than the osmotic pressure (ΔΠ), was required to produce permeate flux. Theoretically, the RO permeate flux could be considered into two different terms: (1) flux of solvent and (2) flux of solute. Between them, flux of solvent, defined as the volumetric flow rate of a fluid through a given area, is linearly proportional to the effective pressure difference across the membrane and can be calculated according to the following equation:

$$J_w = K_w * (\Delta P - \Delta \Pi) = K_w * P_D \quad (2\text{-}1)$$

where

- ✓ J_w : water flux passing through the RO membrane ($kg.m^{-2}.h^{-1}$);
- ✓ K_w : water transport coefficient or membrane permeability ($kg.m^{-2}.h^{-1}.Pa^{-1}$);
- ✓ ΔP : pressure difference across the membrane (Pa);
- ✓ $\Delta \Pi$: osmotic pressure difference across the membrane (Pa);
- ✓ P_D : applied driving pressure, defined as the pressure difference between trans-membrane pressure (ΔP) and osmotic pressure ($\Delta \Pi$).

Experimentally by using a batch-mode RO reactor, the RO permeate flow-rate in this study was determined directly by an electronic balance, which is connected to a computer. These data will be used to recalculate value of the RO permeate flux.

Meanwhile, flux of solute through the membrane is proportional to the effective solute concentration difference across the membrane and can be calculated according to the following equation

$$J_s = K_s * (C_m - C_p) \quad (2\text{-}2)$$

where

- ✓ J_s : flux of solute passing through the RO membrane ($g.m^{-2}.h^{-1}$);
- ✓ K_s : salt permeability coefficient (a function of the salt diffusivity through the membrane);
- ✓ C_m : molar concentration of solute at the membrane surface;
- ✓ C_p : molar concentration of solute in the permeate;

❖ *Determination of osmotic pressure*

Osmotic pressure is defined as the amount of pressure required to stop the process of osmosis in the experimental set-up. This pressure is generated by existence of a significant amount of salts in the solution, and therefore, proportional to the salt concentrations according to the equation below:

$$\Pi = i.M.R.T \quad (2\text{-}3)$$

where

- ✓ Π : osmotic pressure (bar);
- ✓ I : the van't Hoff factor, an unitless value representing degree of dissociation of

molecules in solution. This value depends on the number types of ions in the solution;

- ✓ M : molarity (mol.L^{-1});
- ✓ R : ideal gas constant, R = 0.08206 L.bar.mol^{-1}.K^{-1};
- ✓ T : solute temperature (K).

By calculation, the osmotic pressure of feed solution at different NaCl concentrations at 25^0C were estimated according to the equation **y = 0.7426x** as presented in Fig 2.7. It is worth noting that the van't Hoff factor i was chosen at value of 1.8 for NaCl rather than 2 because of a concept called "ion pairing". In solution, a certain number of Na^+ ions and Cl^- ions will randomly come together and form NaCl ion pairs. This reduces the total number of particles in solution, hereby reducing the van 't Hoff factor. Finally, for the used synthetic feed solution ([As(III) = 300 ppb;[NaCl] = 10 g/L), the estimated osmotic pressure at 25^0C was around Π = 7.4 bar.

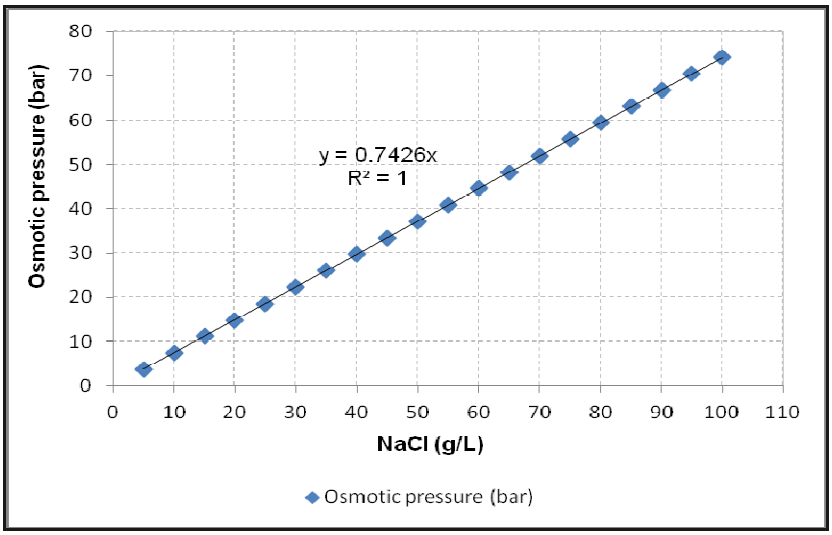

Fig 2.7 *Osmotic pressure as a function of NaCl concentration in solution.*

However in this study where a batch-mode RO reactor was applied, the feed NaCl concentration increased during the filtration, bringing about increase of the osmotic pressure also, which is proportional to salt concentration in the bulk and hydrodynamic condition. A batch mode RO experiment with brackish water ($[NaCl]_{initial}$ = 10 g/L) at fixed trans-membrane pressure TMP = 24 bars was conducted to study on the variation of osmotic pressure during the filtration. The permeate flux was measured by factor of recovery (Y_{RO}),

defined as ratio of volume of permeate and initial feed solution volume, and expressed in the equation 2- 4. Variation of osmotic pressure as function of FRV was illustrated in Fig 2.8.

$$Y_{RO} = \frac{V_{permeate}}{V_{feed}} \tag{2-4}$$

where

- ✓ V_{feed} : Initial volume of feed solution (mL);
- ✓ $V_{permeate}$: Volume of permeate (mL).

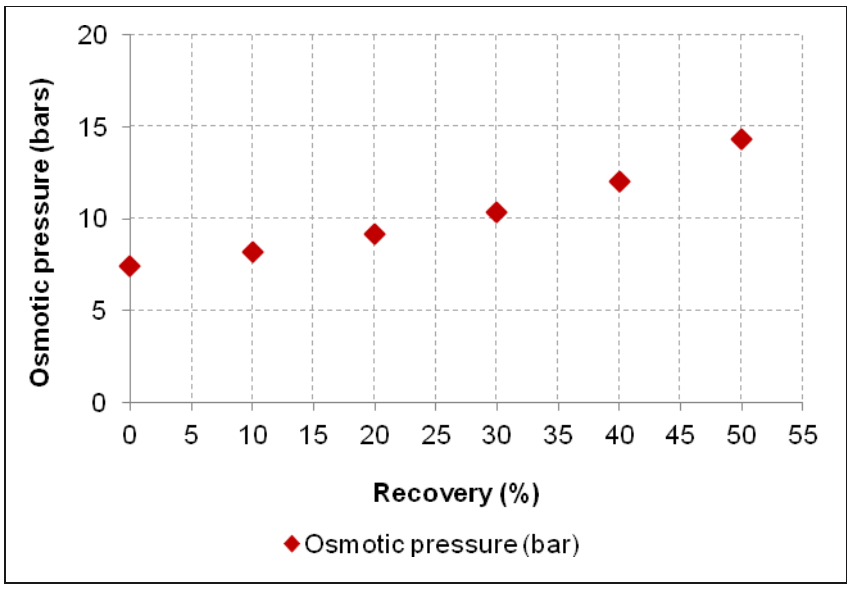

Fig 2.8 *Variation of osmotic pressure as a function of recovery ($[NaCl]_{initial}$ = 10 $g.L^{-1}$).*

In comparison the RO performance, the membrane permeability K, defined as specific flux, is approximated by taking the overall system flux and dividing by the applied driving pressure P_D and expressed by the following equation 2-5:

$$K = \frac{J}{P_D} \tag{2-5}$$

Normalized permeability of the RO membrane, at T = 20^0C, was calculated by the following equation 2-6:

$$K_{20^0C} = \frac{K}{K_0} \tag{2-6}$$

where

- ✓ K_0: initial permeability value at the beginning of filtration process at applied driving pressure and initial osmotic pressure ($kg.m^{-2}.h^{-1}.Pa^{-1}$);

II.2. PREPARATION OF SYNTHETIC BRACKISH WATERS

In this study, synthetic solutions were used for all experiments. Depending on specific objective of each test, different synthetic feed solutions were made from the chemicals listed in Table 2.5.

Table 2.5 *List of chemicals used in the study (commercial products).*

Chemical	Source
Sodium arsenite solution – $NaAsO_2$ ([As(III)] = 5g/L)	Subra – France
Sodium hydrogenarseniate – $Na_2HAsO_4.7H_2O$ ACS 98.0 – 102 %	Subra – France
Sodium chloride – NaCl 98%	VWR – Belgium
Humic acid sodium salt (HASS) – $C_9H_8Na_2O_4$ 50%	Carl Roth – Germany
Calcium sulphate – $CaSO_4.2H_2O$ (Gypsum) 99%	Aldrich, USA

In order to facilitate the sample preparation, arsenite mother solution was prepared by diluting 4 ml sodium arsenite solution (commercial product) into deionised water to make 01 L arsenite mother solution ([As(III)] = 20 mg/L). This mother solution, then, were used to prepare synthetic feed solutions at different arsenic concentrations depending on the objective of the experiments. Compositions of some feed solutions used in the study were listed in the Table 2.6.

Table 2.6 *Compositions of some feed solutions used in the study.*

Feed solutions	As(III) (ppb)	NaCl (g/L)	$CaSO_4$ (g/L)	HASS (mg/L)	pH -	Ec (mS/cm)	TOC (mg/L)
Deionised water	-	-	-	-	6.9	1.10^{-3}	-
Brackish water	-	10	-	-	6.7	18.12	-
As(III) + NaCl	100	10	-	-	6.8	17.98	-
As(III) + NaCl	300	10	-	-	6.8	16.40	-
As(III) + NaCl + $CaSO_4$	300	10	0.5	-	6.5	15.92	-
As(III) + NaCl + HASS	300	10	-	20	6.7	16.95	7.5
As(III) + NaCl + HASS	7000	300	-	165	6.0	247	50

II.3. THE ANALYTICAL METHODS

II.3.1. Electrical conductivity (EC) measurement

EC is the ability of a liquid/solution to conduct electricity. EC measurement, thus, can quantify the overall presence of salts in the water. In this work, conductivity measurement was made with a conductivity meter CDM 210 Lab (WTW, Germany). This device can work in a conductivity range of 0.01 mS/cm to 1400 mS/cm with a precision of 0.2%. Conductivities of feed solution, retentate and permeate were measured to estimate salts removal efficiencies.

II.3.2. Total organic carbon (TOC) measurement

TOC measurement is conducted to quantify the presence of organic contaminants (carbon based) in waters since organic contaminants are non-ionic and not detected by standard conductivity measurement. In this study, TOC measurement was performed with a TOC-meter (Shimadzu, Japan). The principal measurement is as follows: firstly, the sample is acidified with sulphuric acid (H_2SO_4) and purged with inert gas to remove inorganic carbon (IC) and the potential volatile organic carbon remaining, the inorganic carbon in the sample is converted to carbon dioxide, and the inorganic carbon concentration is obtained by detecting with the infra red gas analyzer (Non Dispersive Infra Red – NDIR). The sample is then delivered to a combustion furnace, which is supplied with purified air. There, combustion through heating to 680^{0}C with thermal platinum catalyst, where the sample decomposes and is converted to carbon dioxide. The carbon dioxide generated is cooled and dehumidified, and then detected by the NDIR. The total carbon (TC) concentration in the sample is obtained through comparison with a calibration curve formula. The TOC concentration is then calculated by subtracting the IC concentration from the obtained TC concentration. The uncertainty of the TOC meter is 0.1 mg.L^{-1} with lower limit of detection is 1.0 mg.L^{-1} for saline water.

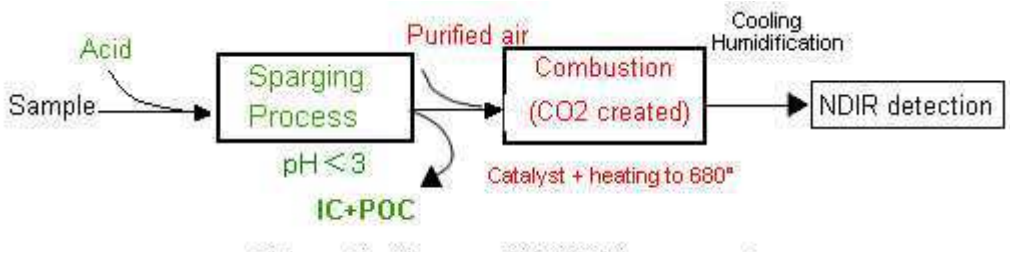

Fig 2.6 Schematic diagram of non-purgeable organic carbon NPOC

II.3.3. Arsenic measurement

Total arsenic concentration in the feed as well as in the permeate obtained was measured by an Optical Emission Spectrophotometer (ICP/OES Optima 2100DV – Perkin Elmer) with 5 ppb of quantitative detection limit. Analytical method followed the ISO 11885:2007 (Water quality -- Determination of selected elements by inductively coupled plasma optical emission spectrometry (ICP-OES)).

II.3.4. Scanning electronic microscopy & Electron detection scan measurements

Membrane's surface topographies and chemical compositions of blank or used membranes were performed by SEM and EDS measurements, respectively. A sample preparation procedure was needed before the measurements. Firstly, the membranes to be tested were dried for 24 hours at the room temperature and then coated with a thin carbon layer. This conductive carbon layer (thickness of a few Angstroms) was used to prevent accumulation of energy supplied by the electrons on the non-conductive membrane and also from its deterioration. The membrane surface, side exposed to the feed solution, was observed before and after experiments. This SEM measurement was conducted through JEOL 5410 LV Instrumentation, which was operated under a vacuum (approximately $3x10^{-3}$ Pa).

Subsequently, the qualitative identifications of elements present on the membrane surface were carried out by EDS measurement performed with a Bruker probe SDD Quantax of 30 mm^2. By sending electrons to a point on the membrane surface, an emission spectrum of the elements present at that point is obtained. Each item can be identified by its emission line (primary, secondary or tertiary), whose position is fixed on the spectrum. With a presence of an element, a peak is visible, however, it should be emphasized that this is just a qualitative measure. The peak intensities can be compared on the same response spectrum but not between two different response spectra. Peak positions of elements that can be detectable on the full emission spectrum were presented in Fig 2.7.

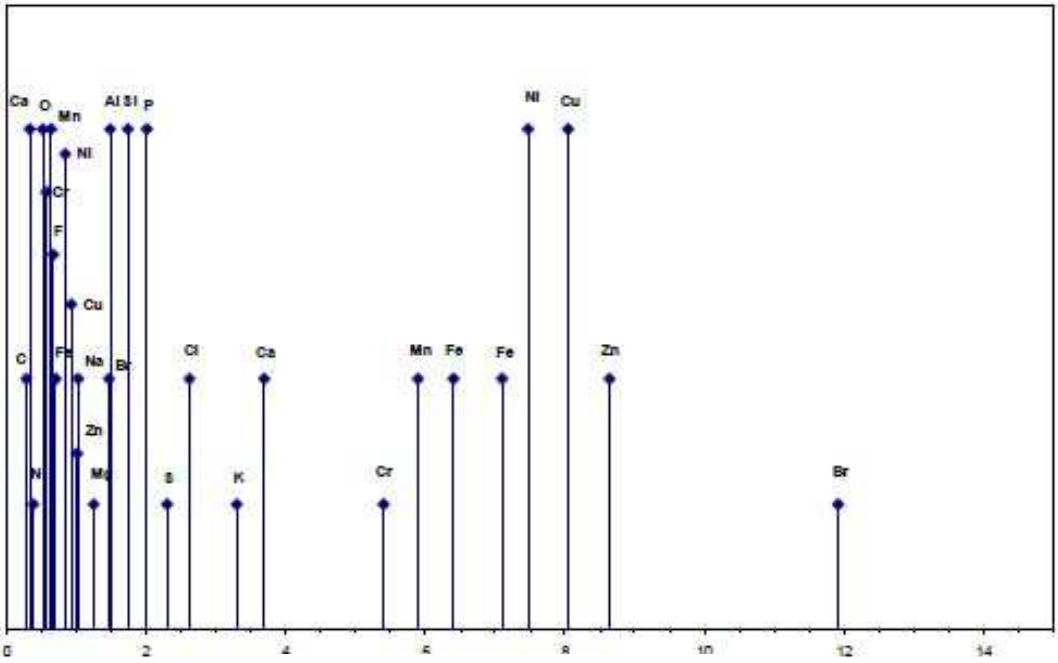

Fig 2.7 *Spectrum of ray emission of different elements.*

Chapter III:

A new method for permeability measurement of hydrophobic membrane in Vacuum membrane distillation

Extract of the article:" A new method for permeability measurement of hydrophobic membranes in Vacuum Membrane Distillation process" published in journal of WATER RESEARCH, Volume 47, Issue 6, 15 April 2013, Pages 2096 - 2104

Hydrophobic membrane plays an important role in membrane distillation process, in which choosing an appropriate membrane for a given application is a crucial step for all researchers and/or users. In membrane speciality, choice of a suitable membrane is a compromise between various membrane characteristics, such as: liquid entry pressure (LEP), mean pore size, pore size distribution, membrane thickness, porosity, pore tortuosity, membrane thermal conductivity and especially membrane permeability. Among them, permeability is not always fully provided by membrane manufacturers and, thus, must be obtained from experimental measurements.

In practice, two common measurement methods, namely Gas permeation test and pressure variation method (the temperature is fixed and the permeate pressure varies to create the driving force for mass transfer) have being applied for determining permeability of a hydrophobic membrane. These methods, however, showed some drawbacks with inaccuracy result or unstable operation, respectively (more discussions in the following section). As a consequence, finding out a new measurement method to overcome the shortcomings of these existing methods is needed.

In this chapter, in the following of Jean-Pierre Méricq's PhD thesis, a new method for permeability measurement of hydrophobic membranes used in Vacuum Membrane Distillation, instead of common measurement methods, was proposed. As VMD is a thermally-driven process, the idea of this work is to propose a new water vapour permeability measurement method based on variation of feed temperature at a fixed vacuum pressure. This new method showed a greater stability and simplicity than the existing pressure variation method by not only allowing a wide range of feed temperature (25°C ÷ 60°C) to be scanned continuously, but also avoiding fluctuations of the system as observed in the pressure variation test. Permeabilities of both Fluoropore and Durapore hydrophobic membranes were measured by this new method and also by the existing pressure variation test. A comparison between these two methods was also presented to assess the feasibility and applicability of this new method. In summary, a publication with four main parts will be the main content of this Chapter 3 as follows:

(i) Theory as basic principle to determine permeability of a hydrophobic membrane;
(ii) Experimental results obtained by the pressure variation method;

(iii) Experimental results obtained by the temperature variation method;

(iv) After all, a comparison between the two methods and conclusions.

WATER RESEARCH 47 (2013) 2096–2104

Available online at www.sciencedirect.com

SciVerse ScienceDirect

journal homepage: www.elsevier.com/locate/watres

A new method for permeability measurement of hydrophobic membranes in Vacuum Membrane Distillation process

T.D. Dao [a,b,c], J.-P. Mericq [a,b,c], S. Laborie [a,b,c,*], C. Cabassud [a,b,c]

[a] Université de Toulouse, INSA, UPS, INP, LISBP, 135 Avenue de Rangueil, F-31077 Toulouse, France
[b] INRA, UMR792 Ingénierie des Systèmes Biologiques et des Procédés, F-31400 Toulouse, France
[c] CNRS, UMR5504, F-31400 Toulouse, France

ARTICLE INFO

Article history:
Received 19 October 2012
Received in revised form
21 January 2013
Accepted 22 January 2013
Available online 31 January 2013

Keywords:
Vacuum Membrane Distillation
Mass transfer coefficient
Permeability measurement
Hydrophobic membrane
Knudsen diffusion
Methodology

ABSTRACT

In this paper, a new method for permeability measurement of hydrophobic membranes used in Vacuum Membrane Distillation, instead of common measurement methods, was proposed. As VMD is a pressure and temperature driven process, the idea of this work is to propose a new water vapour permeability measurement method based on variation of feed temperature at a fixed vacuum pressure. This new method showed a greater stability and simplicity than the existing pressure variation method by not only allowing a wide range of feed temperature (25 °C ÷ 60 °C) to be scanned continuously, but also avoiding fluctuations of the system as observed in the pressure variation test. Permeabilities of two different kinds of hydrophobic membranes were measured by this new method and also by the existing pressure variation test. A comparison between these two methods was also presented to assess the feasibility and applicability of this new method.

1. Introduction

Membrane Distillation (MD) is a thermally-driven separation process, in which only vapour molecules are able to pass through a porous hydrophobic membrane (Yasuda and Tsai, 1974; Lawson and Lloyd, 1996; Couffin et al., 1998; Boi et al., 2005; El-Bourawi et al., 2006; Khayet and Matsuura, 2011; Alkhudhiri et al., 2012). When a heated aqueous solution is brought into contact with one side of the membrane (i.e. feed side), the hydrophobic nature of the membrane prevents penetration of the liquid aqueous solution into the pores, resulting in the formation of a vapour–liquid interface at the pore inlet. Driving force in this process is the water vapour partial pressure difference through the membrane. Water vaporizes at the pore inlet and vapour molecules go through the membrane which acts merely as a physical barrier between the two phases. The water vapour partial pressure difference can have different origins according to different MD configurations: Direct Contact Membrane Distillation (DCMD); Air Gap Membrane Distillation (AGMD); Sweeping Gas Membrane Distillation (SGMD); Thermostatic Sweeping Gas Membrane Distillation (TSGMD), a combination process between AGMD and SGMD; and Vacuum Membrane Distillation (VMD) (Lawson and Lloyd, 1997; Khayet, 2001, 2004; Garcia-Payo, 2002; El-Bourawi et al., 2006; Khayet and Matsuura, 2011; Alkhudhiri et al., 2012). DCMD is the simplest and the most widely studied configuration (Lawson and Lloyd, 1997; El-Bourawi et al., 2006; Khayet and Matsuura, 2011). However,

* *Corresponding author*. Université de Toulouse, INSA, UPS, INP, LISBP, 135 Avenue de Rangueil, F-31077 Toulouse, France. Tel.: +33 5 61 55 97 73; fax: +33 5 61 55 97 60.
E-mail address: Stephanie.laborie@insa-toulouse.fr (S. Laborie).
0043-1354/$ – see front matter © 2013 Elsevier Ltd. All rights reserved.
http://dx.doi.org/10.1016/j.watres.2013.01.040

the main drawback of this MD variant is the irreversible conductive heat loss through the membrane, particularly when thin membranes are used in order to reduce the resistance to mass transfer. On the contrary, VMD configuration has a very low conductive heat loss, which allows obtaining higher permeate flux than in DCMD (Khayet and Matsuura, 2011). Fig. 1 shows heat and mass transfer through a porous hydrophobic membrane in a VMD system with a tangential flow cell.

Since its appearance in the late of the 1960s and its development in the early of 1980s with growth of membrane engineering, MD claims to be a cost effective separation process that can utilize low-grade waste and/or alternative energy sources such as solar and geothermal energy. Many scientific studies have proved its high treatment efficiency (Lawson and Lloyd, 1997; El-Bourawi et al., 2006; Mericq et al., 2009; Khayet and Matsuura, 2011). However, from the commercial point of view, MD process has not been popularized yet in industry or environmental treatment regardless of availability of many scientific research conducted. One of the main reasons for this limitation is lack of appropriate hydrophobic membranes to provide higher permeate flux (El-Bourawi et al., 2006; Susanto, 2011). Choice of a hydrophobic membrane for a given MD application is a compromise between various membrane characteristics, such as: liquid entry pressure (LEP), mean pore size, pore size distribution, membrane thickness, porosity, pore tortuosity, membrane thermal conductivity and especially membrane permeability. In other words, permeate flux strongly depends on the characteristics of used membranes (El-Bourawi et al., 2006). So far, suitable commercial macroporous hydrophobic membranes are made of polytetrafluoroethylene (PTFE), polypropylene (PP), polyvinylidene fluoride (PVDF) and polyethylene (PE). However, these membranes were developed for micro-filtration (MF) applications and its manufactured data (rejection and hydraulic permeability) are characteristics for MF. Moreover, permeability is not always fully provided by membrane manufacturers (Khayet and Matsuura, 2011). This explains why permeability measurement of hydrophobic membranes is being considered as an essential step to help researchers or customers to select the most appropriate membranes.

Permeability is an important parameter in choosing a suitable hydrophobic membrane for a given MD application. In case of a hydrophobic membrane for MD, permeability is defined as ability of the membrane to allow vapour water to pass through its pores (Tanikawa et al., 2006). Since membrane structural characteristics are not always precisely known and permeability depends on predominant transfer mechanism occurring through the membrane pores (Lawson and Lloyd, 1997; Cabassud and Wirth, 2003; Lei et al., 2005; El-Bourawi et al., 2006; Khayet and Matsuura, 2011), this value cannot be accurately calculated and thus must be obtained from experimental measurements.

Up to now, the common method is to determine gas permeability by Gas Permeation Test (Yasuda and Tsai, 1974; Kong and Li, 2001; Alkhudhiri et al., 2012) and then to calculate water permeability (Yasuda and Tsai, 1974; Loosveldt et al., 2002). Permeation rate through the membrane of a gas fluid (generally nitrogen gas or air) at room temperature is measured while operating pressures are varied. Permeation coefficient is

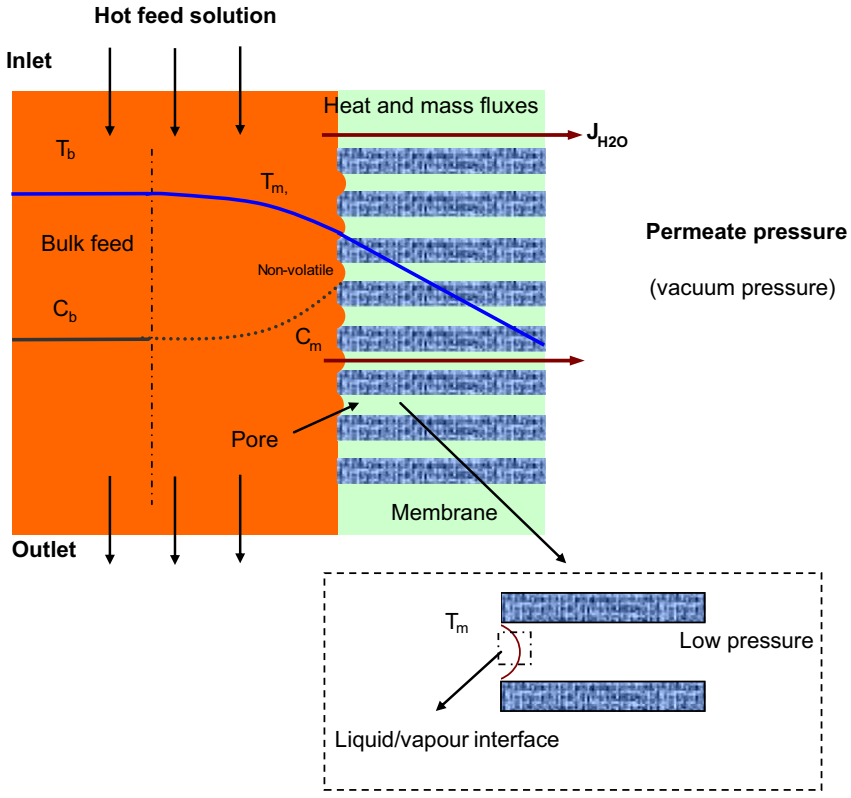

Fig. 1 – Heat and mass transfer through a porous hydrophobic membrane in VMD (Khayet and Matsuura, 2011).

then calculated at different operating pressures based on the permeation rates measured (Kong and Li, 2001). This method has several advantages: (i) Commercial gas flow-metres that cover wide range of flow rate for any kind of gas are available; (ii) Nitrogen gas is chemically inert, and it is only necessary to consider the mechanical effects for the permeability changes with an increase of confining pressure (Tanikawa et al., 2006). However, the risk of this method is that it neither takes into consideration possible interactions between water and the membrane material nor it is based on the mass transfer mechanisms that occur during membrane distillation process. This problem can lead to an inaccuracy in membrane permeability value, which was converted from gas permeability achieved. Zhang et al. (2012) measured gas (N_2) and water permeation properties of a silicon nitride hollow fibre membrane and showed a significant difference between gas and water permeabilities (Zhang et al., 2012). Two other studies conducted by Tanikawa et al. (2006) on porous sedimentary rocks and by Loosveldt et al. (2002) on mortar had also the same tendency. In case of porous sedimentary rocks, gas (N_2) permeability was 2–10 times higher than water permeability on the same specimen (Tanikawa et al., 2006) while it was in range of $1 \div 2$ in an order of magnitude in case of mortar (Loosveldt et al., 2002). These phenomena were explained by "slip" flow of gas at pore walls which enhances gas flow when pore sizes are very small (i.e. Klinkenberg effect) (Tanikawa et al., 2006) or by other phenomena such as rehydration, dissolution and migration of fine elements or water adsorption in the thinnest pores (Loosveldt et al., 2002).

Another approach to characterize a membrane used in VMD is to give the permeate flux obtained with the membrane in a given experimental conditions, as reported in many references. However, due to dependence of the flux on other operating parameters such as: feed temperature, permeate pressure, hydraulic regime, etc…, it is sometimes inaccurate to generalize this parameter in all the range of conditions. As a consequence, permeability, which is the mass transfer coefficient of the process, is recommended as a key factor to characterize a hydrophobic membrane.

By analogy with permeability measurement in "pressure-driven" processes, the permeability in VMD can be determined by varying vacuum pressure and measuring the corresponding pure water permeate flux (Wu et al., 2007). But this method presents some limitations which will be detailed in the following sections. So, as VMD is a pressure and temperature driven process, the idea of this work is to propose a new water vapour permeability measurement method based on a variation of feed temperature. Permeabilities of two different kinds of hydrophobic membranes were measured by this new method and also by the existing pressure variation test. A comparison between these two methods was presented to assess the feasibility and applicability of the new method. It is worth noting that application of these measurement methods is limited in specific case of VMD process only.

2. Theory

Generally, a macro-porous hydrophobic membrane is characterized by four main parameters, i.e. the thickness, δ (m), the mean pore size (diameter d or radius r, (m)) or its distribution, the porosity, ε (defined as porous volume fraction relative to the total membrane volume) and the tortuosity, χ (defined as the ratio of pore length to membrane thickness). Influences of each parameter to the permeability of the membrane were summarized by Lei et al. (2005) as follows:

Permeability $\propto r^{\alpha}\varepsilon/\chi\delta$, where α may be equal to 1 or 2, depending on the predominant mass transfer mechanism within the membrane pores with Knudsen number, $Kn > 1$ or $Kn < 0.01$, respectively (Lei et al., 2005). Knudsen number is defined as the ratio of the mean free path (i.e. the average distance of a particle before collision with another) to the pore size. Generally, the different types of trans-membrane mass transfer mechanisms in MD process include Knudsen flow (diffusion by collapsing between gas molecules and pore sides), viscous or Poiseuille flow, ordinary molecular diffusion and/or the combination among them (Mengual et al., 2004; Khayet and Matsuura, 2011). In VMD process, due to the vacuum pressure applied at the permeate side of the membrane, the mean free path of water molecules is considerably larger than pore size of the hydrophobic membranes (0.1–1 μm) used in MD process. Consequently, mass transfer through the membrane is generally dominated by Knudsen mechanism (Cabassud and Wirth, 2003; Lei et al., 2005; Safavi and Mohammadi, 2009; Mericq et al., 2009; Khayet and Matsuura, 2011; Alkhudhiri et al., 2012). In the case of pure water, the permeate flux J_{H_2O} through the membrane is written as:

$$J_{H_2O} = k_k * \Delta P_{H_2O} = k_k * \left(P_m^* - P_p\right) \quad \text{(i)}$$

where J_{H_2O} is molar flux of water; ΔP_{H_2O} is difference in partial pressure of water on both sides of the membrane; P_m^* is vapour pressure of pure water at the membrane's conditions; P_p is partial pressure of water in the permeate side (equal to vacuum pressure as the permeate is only composed of water) and k_k is mass transfer coefficient of the membrane.

The mass transfer coefficient k_k is expressed in the following equation:

$$k_k = \frac{2}{3}\frac{\varepsilon \cdot r}{\chi\delta RT_m}\sqrt{\frac{8RT_m}{\pi M_{H_2O}}} = \frac{K_M}{\sqrt{M_{H_2O}}} \quad \text{(ii)}$$

where ε is porosity of the membrane; r is radius of the pores; χ is tortuosity factor; δ is thickness of the membrane; R is ideal gas constant; M_{H_2O} is molar mass of water, K_M is Knudsen permeability and T_m is temperature at the membrane surface. Owing to vacuum pressure applied, the boundary layer in the permeate side is negligible, which implies a reduction in the heat conducted through the membrane in VMD.

It is well established that temperature polarization phenomenon can be diminished by creating a turbulent regime in the feed side of the membrane (El-Bourawi et al., 2006; Khayet and Matsuura, 2011). Previously, with the same membranes and experimental device as in the present study, Mericq et al. (2010) has demonstrated the insignificancy of temperature polarization on the feed side of the membrane in the case of highly concentrated brines. In this study, by using the same modelling in the case of pure water, the T-polarization coefficient (TPC) was calculated as a function of the Reynolds number. This ratio between T_m – temperature at the membrane surface – and T_b – bulk temperature – was demonstrated to be higher than 0.98 for

a Reynolds number equal or higher than 3000 (for a bulk temperature of 40 °C and a permeate pressure of 2500 Pa). This proved that the temperatures at the membrane surface and in the bulk could be considered as the same and thus that the T-polarization phenomenon could be neglected.

In all cases to facilitate the comparison, permeability is expressed at the same reference temperature $T_{ref} = 20$ °C by using the following equation (Mericq et al., 2009):

$$K_M(T_{ref}) = K_M(T)\sqrt{\frac{T}{T_{ref}}} \quad \text{(iii)}$$

where $K_M(T)$ and $K_M(T_{ref})$ are Knudsen permeability values at temperature T and at reference temperature T_{ref}, respectively;

In combination of three Equations (i), (ii) and (iii), a general equation for permeate flux calculation can be proposed as Equation (iv). According to this equation, determination of permeability of hydrophobic membrane K_M can be performed by varying of trans-membrane partial pressure ΔP_{H_2O} while recording the variation of corresponding permeate flux, J_{H_2O}: slope of the line showing correlation between J_{H_2O} and ΔP_{H_2O} is used to calculate the permeability KM of the membrane. Variation of partial trans-membrane pressure ΔP_{H_2O} can be conducted by either varying vacuum pressure at a constant bulk temperature (namely **pressure variation method**) or on the contrary by varying bulk temperature at a fixed vacuum pressure (namely **temperature variation method**).

$$J_{H_2O} = \frac{K_M(T)}{\sqrt{M_{H_2O}}}\Delta P_{H_2O} = \frac{K_M(T_{ref})}{\sqrt{M_{H_2O}}}\sqrt{\frac{T_{ref}}{T}}\Delta P_{H_2O} \quad \text{(iv)}$$

2.1. *Pressure variation method (PV method)*

In this method, variation of trans-membrane partial pressure difference ΔP_{H_2O} was conducted by varying permeate pressure at a constant bulk temperature. Different values of the permeate flux, J_{H_2O} could be achieved corresponding to each different value of the permeate pressure P_p. In this case, the two parameters J_{H_2O} and ΔP_{H_2O} (in the Equation (iv)) are variables while the other one, $(K_M(T_{ref})/\sqrt{M_{H_2O}})\sqrt{T_{ref}/T}$ is a constant. The plot showing relationship between two factors J_{H_2O} and ΔP_{H_2O} provided a straight-line with slope of this straight-line, giving the value of mass transfer coefficient k_k (Equation (i)). This value was then used to calculate the Knudsen permeability, K_M at reference temperature, $T_{ref} = 20$ °C by the Equation (v).

$$K_M(T_{ref}) = k_k\sqrt{M_{H_2O}}\sqrt{\frac{T}{T_{ref}}} \quad \text{(v)}$$

It is worth noting that varying vacuum pressure might change the mean free path, leading to changing of mass transfer mechanism within the membrane pores. At the experimental conditions ($T_b = 40$ °C and vacuum pressure in range of 7000–2500 Pa), the mean free path were calculated to be in range of [2.2–7.6 μm], which are much higher than average membrane pore (0.2 μm). It proved that at these given operating conditions, Knudsen diffusion is still the main mechanism of mass transfer within the membrane pores.

2.2. *Temperature variation method (TV method)*

Contrary to the PV method, the variation of trans-membrane partial pressure difference ΔP_{H_2O} in this method was conducted by varying bulk temperature at a fixed initial permeate pressure. Different value of the permeate flux J_{H_2O} can be achieved corresponding to each different value of the bulk temperature. In this case, the two parameters, J_{H_2O} and $\sqrt{T_{ref}/T}\,\Delta P_{H_2O}$ (in the Equation (iv)) are variables while the other one, $K_M(T_{ref})/\sqrt{M_{H_2O}}$ is a constant. The plot showing relationship between two factors J_{H_2O} and $\sqrt{T_{ref}/T}\,\Delta P_{H_2O}$ provides a straight-line with its slope, α giving directly value of Knudsen permeability K_M at reference temperature, $T_{ref} = 20$ °C by the Equation (vi).

$$K_M(T_{ref}) = \alpha\sqrt{M_{H_2O}} \quad \text{(vi)}$$

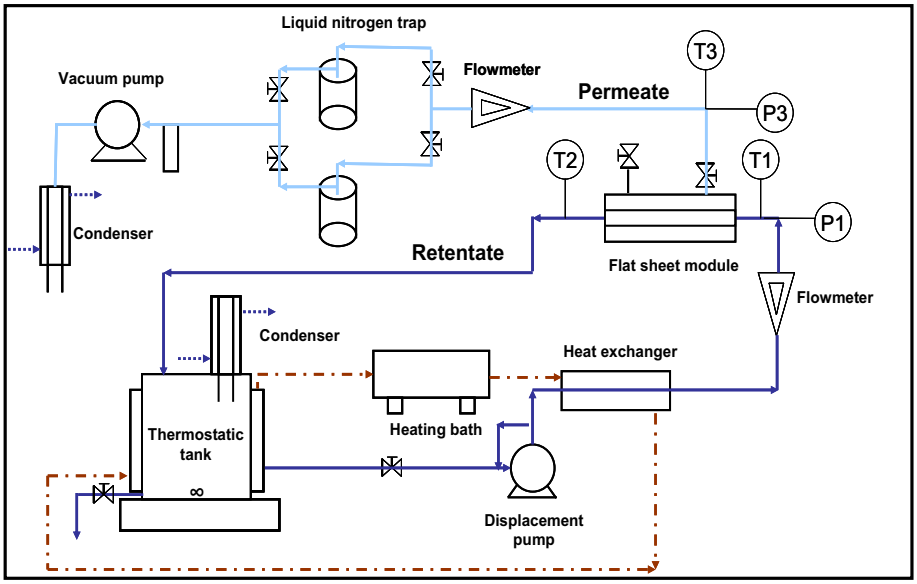

Fig. 2 – Experimental VMD set-up (Mericq et al., 2010).

Table 1 – Characteristics of the hydrophobic membranes employed.

Hydrophobic membranes	Fluoropore	Durapore
Material	PTFE	PVDF
Nominal pore size, μm	0.22	0.22
Thickness, mm	0.175	0.125
Porosity, %	70	75
Contact angle, (°)	123.9	136.3
Liquid entry pressure, bar	4.2	2.6

Note:
✓ Contact angle: determined by Contact Angle Meter (Digidrop).
✓ LEP: determined by Amicon filtration unit of Millipore 8050 connected with a compressed air system.
✓ Other parameters: provided by the Millipore manufacturer.

3. Experimental

3.1. Set-up

All the tests were carried out with a bench-scale batch pilot plant as described in Fig. 2. Feed water was introduced into a 4 L thermostatic tank where the temperature was controlled in range of 25–60 °C by a heating group. Feed was pumped through the module by a displacement pump (A/B Pompes) with capacity in range of 0 ÷ 250 L h^{-1}. The feed pressure (both inlet and outlet of the module) was equal to the atmospheric pressure for all experiments. Vacuum or low permeate pressure Pp (2500 ÷ 10,000 Pa) was obtained using an RP15C (Vario Vacuubrand) pump. Temperature and pressure measurements were made at the inlet (T_{inlet}), outlet (T_{outlet}), and permeate side ($T_{permeate}$) of the membrane module. Permeate vapour flux J_{H_2O} passing through the membrane was measured by a BRONKHORST water thermal mass flow metre with capacity of 0 ÷ 60 g h^{-1}

3.2. Hydrophobic membranes

In this study, two different types of hydrophobic membrane were used: PTFE flat-sheet membrane (Fluoropore) and PVDF flat-sheet membrane (Durapore) provided by Millipore Corporation, France. Effective membrane area was 5.78×10^{-3} m^2 (rectangle of 3.5 cm × 16.5 cm) and the feed flow channel was 1 mm in width. The membrane characteristics were given in Table 1. It is worth noting that the experiments were performed with different samples of virgin membranes.

3.3. Feed solution

Deionised water was employed in the experiments.

3.4. Operating conditions and procedures

For both methods (PV and TV), the feed flow rate was fixed at 150 L h^{-1} corresponding to a Reynolds number of 3000 (see Section 2). As previously explained, in these conditions, the Temperature Polarization Coefficient (T_m/T_b) was calculated to be close to 1 and thus, membrane temperature T_m was taken equal to T_b. In all experiments, the bulk temperature T_b was considered as the mean temperature between inlet and outlet temperatures inside the module.

$$T_b = \frac{T_{inlet} + T_{outlet}}{2}$$

Indeed, for the relative short effective length of membrane employed (L = 16.5 cm), the ratio between outlet and inlet temperatures was always higher than 0.975 (see Figs. 3b and 5b). This proved that there was almost no temperature profile along the membrane module.

In the PV method, the temperature in the feed tank was fixed at 40 °C. The permeate pressure (P_p) was then decreased from 7000 to 2500 Pa, step by step until the permeate flux reached its steady state at each corresponding permeate pressure. This measurement range was chosen based on vapour pressure of pure water in the feed side of membrane (P^*_M = 7400 Pa), which was calculated by the Antoine equation at membrane temperature of 40 °C. For the different measurement points, the operational parameters as inlet temperature (T_{inlet}), outlet temperature (T_{outlet}), permeate side temperature ($T_{permeate}$), permeate pressure (P_p) and permeate flux (J_{H_2O}) were measured.

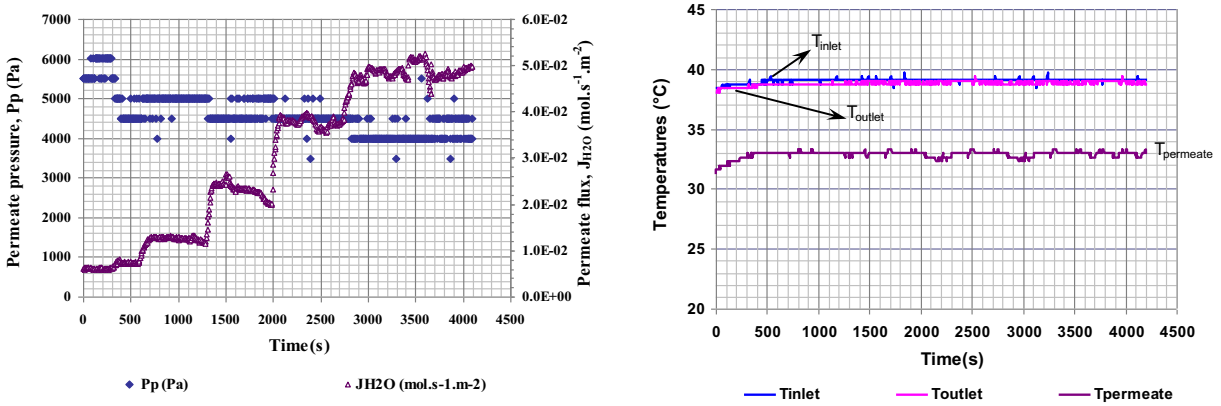

a b

Fig. 3 – Example of permeability measurement by PV method (Durapore membrane; T_m = 38 °C; Re = 3000; P_p = 7000 ÷ 2500 Pa): (a) Permeate flux and permeate pressure with time; and (b) evolution of temperatures with time.

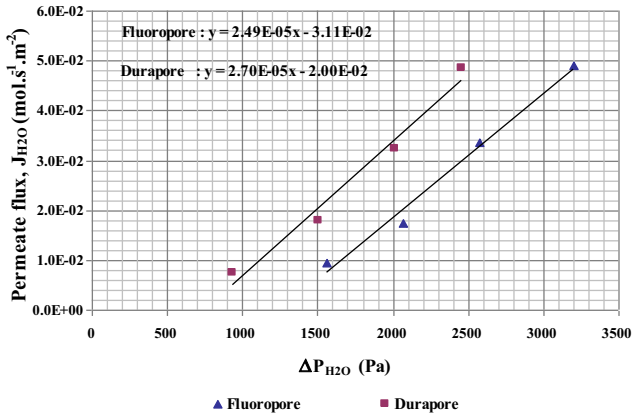

Fig. 4 – Example of permeability measurement by PV method (Durapore and Fluoropore membranes; T_m = 38 °C; Re = 3000; P_p = 7000 ÷ 2500 Pa): Knudsen permeability.

In the TV method, the permeate pressure P_p was initially fixed at a value of 2500 Pa (i.e. the lowest vacuum pressure, which the employed vacuum pump could create). Temperature in the feed tank was increased continuously over a range of 25 ÷ 60 °C by a heating group that heated the liquid slowly and steadily until its temperature reached the final value. Operational parameters as inlet temperature, outlet temperature, permeate side temperature, permeate pressure (P_p) and permeate flux (J_{H_2O}) were also measured continuously.

4. Results and discussions

4.1. *Pressure variation method (PV method)*

In order to test the stability of this PV method, tens of experiments have been conducted. For the different measurement points, the corresponding permeate flow was measured and the trans-membrane partial pressure difference was calculated. Fig. 3a showed a typical relationship between permeate pressure Pp and permeate flux J_{H_2O} achieved by this PV method: each decrease of the permeate pressure P_p applied was correspondent to each increase of the permeate flux J_{H_2O} achieved. It is worth noting that the permeate flux J_{H_2O} achieved was correspondent to the temperature at membrane surface T_m, which governs the water vapour pressure at the solution/membrane interface. As above-mentioned, the temperatures at inlet and outlet of the membrane modules were very closed, which confirmed the absence of temperature profile along the membrane (Fig. 3b).

The permeate flux was then represented as a function of the trans-membrane partial pressure difference ΔP_{H_2O} as shown in Fig. 4. Slope of the curve gave the value of transfer coefficient k_k (Equation (v)) which was used to determine the value of the Knudsen permeability K_M (T_m = 38 °C in that example) (Equation (ii)). This value was then expressed at the reference temperature T_{ref} = 20 °C by Equation (iii). An example of permeability determination with the two hydrophobic membranes by this PV method was presented in Fig. 4.

Fig. 4 showed a linear relationship between permeate flux J_{H_2O} and trans-membrane partial pressure ΔP_{H_2O}. Difference in permeability of various hydrophobic membranes employed (Fluoropore and Durapore membranes) was clearly demonstrated. Results of permeability achieved with these two membranes were presented in Table 2. By the PV method, Fluoropore membrane provides a higher average permeability than the other one with 4.06 × 10^{-6} s mol$^{1/2}$ m^{-1} kg$^{-1/2}$ in comparison to 3.45 × 10^{-6} s mol$^{1/2}$ m^{-1} kg$^{-1/2}$. By taking into consideration the membrane characteristics given by the manufacturer (i.e. porosity and thickness), this result was unpredictable. Indeed with the quite same porosities and lower thickness for Durapore membrane (Table 1), the permeability value of this Durapore membrane was expected to be higher. This unpredicted result could be explained by influences of other parameters (i.e. tortuosity and pore size distribution, which were not provided by the manufacturer), except for the porosity and thickness factors. This result finally consolidated the reasoning why permeability measurement is really necessary to characterize a hydrophobic membrane, and thereby to prove the interest of the proposed protocol.

By calculation, low standard deviations with 0.6 and 0.5 for Durapore and Fluoropore membranes respectively, offered a high reproducibility of the permeability results determined. However, there were some disadvantages in operating this PV method. Because of uncertainty of the permeate pressure applied (±400 Pa), fluctuation of permeate flux J_{H_2O} could be observed and normally the permeate flux took a certain time to reach its steady state (Fig. 3a). The uncertainty on the permeate pressure value also caused a deviation of the abscissa of the line, representing the evolution of the obtained permeate flux with trans-membrane pressure. This deviation could be observed in Fig. 4, where its trend line did not tend to pass through zero. However, it has been validated that the slope of the curve was still the same so the value of K_M was not affected. In addition, because the variation of permeate pressure (vacuum) was conducted manually by using a valve, which could modify the suction of vacuum pump, it was quite difficult and time-consuming to reach the expected permeate pressure values. Practical experiments showed that it took

Table 2 – Standard deviations for both Durapore and Fluoropore membranes by the pressure variation method.

Membrane	Permeability (10^{-6} s mol$^{1/2}$ m^{-1} kg$^{-1/2}$)	Standard deviation	95% confidence interval		Number of tests
	Mean value	(10^{-6} s mol$^{1/2}$ m^{-1} kg$^{-1/2}$)	Low	High	
Durapore	3.45	0.6	3.00	3.89	8
Fluoropore	4.06	0.5	3.55	4.56	4

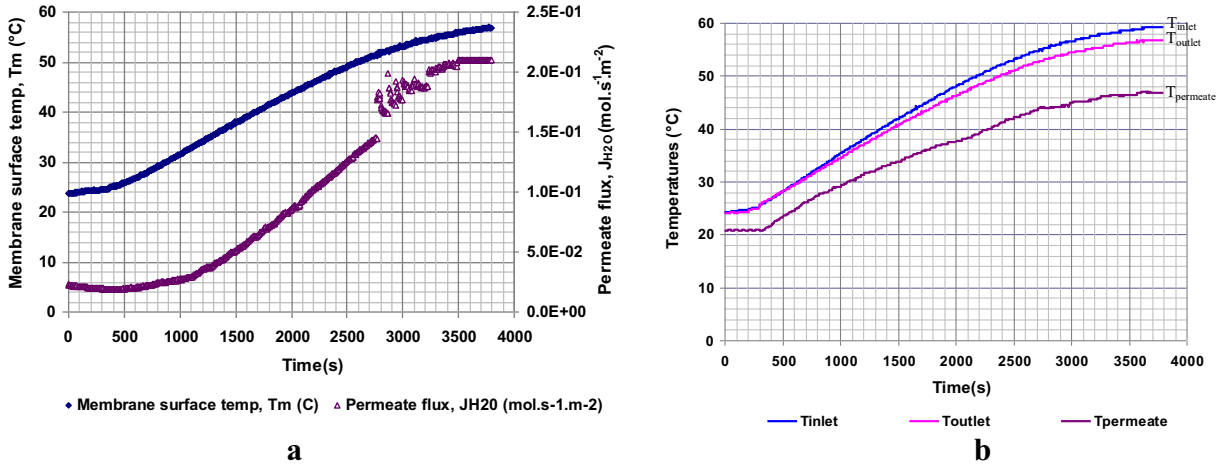

Fig. 5 – Example of permeability measurement by TV method (Fluoropore membrane; P_p = 2500 Pa; T_m = 25 ÷ 58 °C; Re = 3000): (a) Membrane surface temperature and permeate flux with time; and (b) evolution of temperatures with time.

approximately 70 min or even more to finish one measurement, depending on accuracy of each permeate pressure adjustment. In other words, this method was quite dependent on sensitivity of the valve or on technical skill of operator.

Because of the above observations, a new method for measuring permeability was thus proposed.

4.2. *Temperature variation method (TV method)*

As above-mentioned, this measurement method was operated by fixing the permeate pressure Pp at an initial value while the tank temperature was varied continuously by means of heating group. Advantage of this measure is to help the system avoid fluctuations of operating parameters (as observed in the PV method), owing to low uncertainty of the temperature during its continuous variation. Relationship between the membrane surface temperature, T_m and its corresponding permeate flux J_{H_2O} is shown in Fig. 5a. It is worth noting that presence of air available inside the pipe when starting the experiment could lead to a decrease of permeate flux at the beginning of the experiment (in the first-five minutes) as illustrated in Fig. 5a. Nevertheless, this part of the graph should not be considered for the following result discussion.

Dependence of permeate flux J_{H_2O} on the membrane surface temperature T_m could be observed. At low T_m values (i.e. 25 ÷ 30 °C), the permeate flux J_{H_2O} was stable and started to increase steadily with increase of T_m in range of 30 ÷ 50 °C. At higher value of T_m (i.e. above 50 °C), the permeate flux J_{H_2O} increased dramatically and unstably. This was explained by the fact that at high temperature (around 50 °C), a high amount of vapour was produced and passed through the membrane leading to an increase of the permeate pressure as illustrated in Fig. 6. Indeed, when the permeate flux increased, the vacuum pump had to evacuate a larger quantity of steam and could no longer sustain the permeate pressure initially fixed. The variations of permeate pressure value were then taken into account in the calculation of ΔP_{H_2O}.

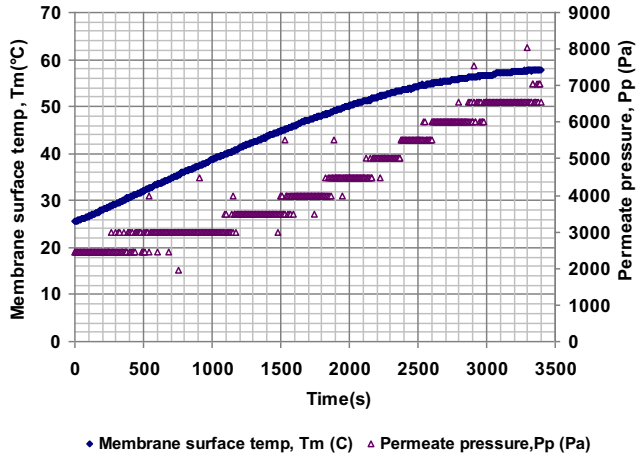

Fig. 6 – Example of permeability measurement by TV method (Fluoropore membrane; P_p = 2500 Pa, T = 25 ÷ 58 °C): membrane surface temperature and permeate pressure with time.

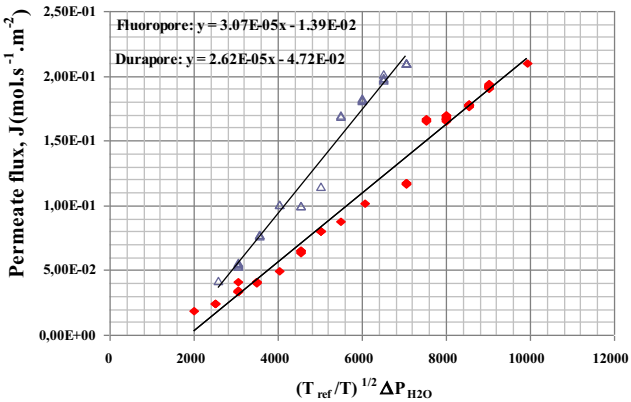

Fig. 7 – Example of permeability measurement by TV method (Fluoropore membrane; P_p = 2500 Pa; T_m = 25 ÷ 58 °C; Re = 3000): Knudsen permeability determination.

Table 3 – Standard deviation for both Durapore and Fluoropore membranes by the temperature variation method.

Membrane	Permeability (10^{-6} s mol$^{1/2}$ m^{-1} kg$^{-1/2}$)	Standard deviation	95% confidence interval		Number of tests
	Mean value	(10^{-6} s mol$^{1/2}$ m^{-1} kg$^{-1/2}$)	Low	High	
Durapore	3.41	0.6	3.03	3.79	9
Fluoropore	3.81	0.6	3.37	4.26	6

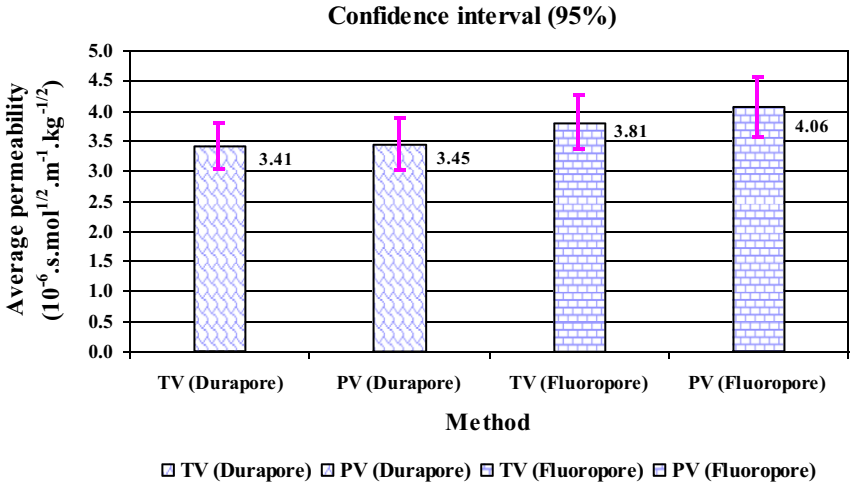

Fig. 8 – Average permeability values and confidence intervals (95%) obtained by two different methods (Durapore and Fluoropore membranes).

The permeate flux was then plotted versus the transmembrane partial pressure difference of water multiplied by the root of the ratio of temperatures in K, $\sqrt{T_{ref}/T}\,\Delta P_{H_2O}$. Slope of the straight line obtained gave directly the value of the Knudsen permeability to the reference temperature of 20 °C. Fig. 7 presented the permeability determination for both Durapore and Fluoropore membranes with results presented in Table 3. It is worth noting that similar deviation of the abscissa of the line in Fig. 4 was also observed in this case. And it was also attributed to the uncertainty of the permeate pressure measurement (±400 Pa). Similar to the PV method, Fluoropore membrane in this case once again showed a higher average permeability than Durapore membrane with 3.81×10^{-6} s mol$^{1/2}$ m^{-1} kg$^{-1/2}$ in comparison with $3.41 \cdot 10^{-6}$ s mol$^{1/2}$ m^{-1} kg$^{-1/2}$. Low standard deviation with 0.6 for measurements of both types of membrane one more time offered a high reproducibility of the permeability results.

As the temperature continuous variation was conducted automatically by means of heating system, it helped handling of this TV method much simpler, easier and even faster than the PV method. Time consumption for this TV method was mainly for increase of the temperature in range of measurement (25 ÷ 60 °C). With support of means of heating bath, it normally took 50 ÷ 60 min to finish one measurement as shown in Fig. 5.

4.3. *Comparison between the two methods*

As an illustration of Tables 2 and 3, Fig. 8 showed average permeability values and its confidence intervals (95%) obtained for both Durapore and Fluoropore hydrophobic membranes by the two different measurement methods. In a comparison between the two methods, it is quite interesting to observe that the standard deviations of both measurement methods (also for both types of Durapore and Fluoropore membrane) were rather low and more or less the same, irrespective of number of tests conducted. It showed a high reproducibility of permeability values of the both methods. For the both membranes, in addition, the average permeability value obtained by one method was always in confidence interval (95%) of the other (and vice versa) with a gap between the average permeability obtained by the two methods representing only 6%. This proved homogeneity and accuracy of measuring permeability of hydrophobic membranes by the two different methods.

Except for providing permeability results similar to the PV method, the TV method showed a higher simplicity and stability in permeability measurement than that of the PV one (as stated above). This could lead to an interest in measuring permeability of hydrophobic membrane by the TV method.

5. Conclusions

In VMD process where Knudsen mechanism is predominant, hydrophobic membrane permeability can be measured by pressure variation (PV) and temperature variation (TV) methods. However, the TV method has several advantages over the measurement of permeability by the other. First, it allows scanning easily a range of measurement (temperature

range) continuously unlike the PV method, which was done manually by steps. Thanks to the heating unit, this method is conducted automatically, which is quite simpler and more convenient for operators. In addition, the temperature change does not create sudden changes as observed in the PV method. These reasons lead to a conclusion that temperature variation method could be an interesting tool for determining permeability of hydrophobic membranes.

Acknowledgement

This research was financed by Cooperative Program for Higher Education between French Government and Vietnamese Government.

Nomenclature

J_{H_2O}	molar flux of water, mol s^{-1} m^{-2};
ΔP_{H_2O}	difference in partial pressure of water on both sides of the membrane, Pa;
P_m^*	vapour pressure of pure water at the membrane's conditions, Pa;
P_p	partial pressure of water in the permeate side (vacuum pressure) for VMD, Pa
k_k	mass transfer coefficient in the membrane, s m^{-1} mol kg^{-1}
ε	porosity of the membrane;
r	radius of the pores, m;
χ	tortuosity factor;
δ	thickness of the membrane, m;
R	ideal gas constant, $R = 8.314$ J mol^{-1} K^{-1};
T_b	temperature in the feed bulk, K;
T_{inlet}	temperature at the inlet of membrane module, K;
T_{outlet}	temperature at the outlet of membrane module, K;
$T_{permeate}$	temperature at the permeate side of membrane module, K;
C_b	concentration of non-volatile compound in the feed bulk, mol L^{-1};
C_m	concentration of non-volatile compound at the membrane surface, mol L^{-1};
T_m	temperature at the membrane surface, K;
M_{H_2O}	molar mass of water, kg mol^{-1};
K_M	Knudsen permeability, s $mol^{1/2}$ m^{-1} $kg^{-1/2}$;
$K_M(T_{ref})$	Knudsen permeability at reference temperature T_{ref}, s $mol^{1/2}$ m^{-1} $kg^{-1/2}$.
T_{ref}	reference temperature at 20 °C, K;

REFERENCES

Alkhudhiri, A., Darwish, N., Nidal, Hilal, 2012. Membrane distillation: a comprehensive preview. Desalination 287, 2–18.

Boi, C., Bandini, S., Sarti, G.C., 2005. Pollutants removal from wastewaters through membrane distillation. Desalination 183, 383–394.

Couffin, N., Cabassud, C., Lahoussine-Turcaud, V., 1998. A new process to remove halogenated VOCs for drinking water production: vacuum membrane distillation. Desalination 117, 233–245.

Cabassud, C., Wirth, D., 2003. Membrane distillation for water desalination: how to choose an appropriate membrane? Desalination 157, 307–314.

El-Bourawi, M.S., Ding, Z., Ma, R., Khayet, M., 2006. A framework for better understanding membrane distillation separation process. Journal of Membrane Science 285, 4–29.

Garcia-Payo, M.C., 2002. Separation of binary mixtures by thermostatic sweeping gas membrane distillation: II. Experimental results with aqueous formic acid solutions. Journal of Membrane Science 198 (2), 197–210.

Kong, J., Li, K., 2001. An improved gas permeation method for characterising and predicting the performance of microporous asymmetric hollow fibre membranes used in gas absorption. Journal of Membrane Science 182, 271–281.

Khayet, M., Khulbe, K.C., Matsuura, T., 2004. Characterization of membranes for membrane distillation by atomic force microscopy and estimation of their water vapour transfer coefficient in vacuum membrane distillation process. Journal of Membrane Science 238, 199–211.

Khayet, M., 2001. Membranes and theoretical modelling of membrane distillation: a review. Advances in Colloid and Interface Science 164 (1–2), 56–88.

Khayet, M., Matsuura, T., 2011. Membrane Distillation – Principles and Applications. Elsevier Publication, Great Britain.

Lawson, K.W., Lloyd, D.R., 1996. Membrane distillation. I. Module design and performance valuation using vacuum membrane distillation. Journal of Membrane Science 120, 111.

Lawson, K.W., Lloyd, D.R., 1997. Membrane distillation: a review. Journal of Membrane Science 124, 10–025.

Loosveldt, H., Lafhaj, Z., Skoczylas, F., 2002. Experimental study of gas and liquid permeability of a mortar. Cement and Concrete Research 32, 1357–1363.

Lei, Z., Chen, B., Ding, Z., 2005. Special Distillation Processes. Elsevier Publication, China.

Mengual, J.I., Khayet, M., Godino, M.P., 2004. Heat and mass transfer in vacuum membrane distillation. International Journal of Heat and Mass Transfer 47, 865–875.

Mericq, J.P., Laborie, S., Cabassud, C., 2009. Vacuum membrane distillation for an integrated seawater desalination process. Desalination and Water Treatment 9, 293–302.

Mericq, J.P., Laborie, S., Cabassud, C., 2010. Vacuum membrane distillation of seawater reverse osmosis brines. Water Research 44, 5260–5273.

Safavi, M., Mohammadi, T., 2009. High-salinity water desalination using VMD. Chemical Engineering Journal 149, 191–195.

Susanto, H., 2011. Towards practical implementations of membrane distillation. Chemical Engineering and Processing 50, 139–150.

Tanikawa, W., Shimamoto, T., Klinkenberg, 2006. Effect for gas permeability and its comparison to water permeability for porous sedimentary rocks. Hydrology and Earth System Sciences 3, 1315–1338.

Wu, B., Li, K., Teo, W.K., 2007. Preparation and characterization of poly(vinylidene fluoride) hollow fiber membranes for vacuum membrane distillation. Journal of Applied Polymer Science 106, 1482–1495.

Yasuda, H., Tsai, J.T., 1974. Pore size of microporous polymer membranes. Journal of Applied Polymer Science 18, 805–881.

Zhang, J.-W., Fang, H., Hao, L.-H., Xu, X., Chen, C.-H., 2012. Preparation of silicon nitride fibre membrane for desalination. Material Letters 68, 457–459.

Chapter IV:

Direct arsenite removal from brackish groundwater by Vacuum membrane distillation technology

IV.1. INTRODUCTION

This 21st century has witnessed big attempts of scientists/environmentalists in facing with deficiency of clean water through removing arsenic contamination in drinking water sources and desalinating the seawater. As a ubiquitous element in the earth's crust, arsenic can be found everywhere in the world at different levels, depending on regional geological structure or its originating sources. Unfortunately, this element is very difficult to be detected in water as it is tasteless, invisibleness and odourless. As a result, more than 151 millions people over 105 countries around the world, especially Bangladesh, Argentina, India, Mexico, Mongolia, Thailand, Taiwan and Vietnam are being infected by acute and chronic exposure of arsenic via drinking water [*Figoli et al., 2010; Murcott, 2013*]. Long-term of inorganic arsenic exposure can cause severe human health problems, including: skin lesions (hyperkeratosis and pigmentation changes, diabetes, circulatory disorders) and cancer of bladder, lung, and kidney and skin [*Geucke et al., 2009*]. After considering the cancer and risks in human health associated with arsenic exposure, the World Health Organization (WHO) lowered their recommended drinking criteria from 50 to 10 ppb in 1993 [*Smith and Smith, 2004*], which has been adopted in many countries in the world.

Parallel to this sanitary environmental issue, desalination from seawater to produce drinking water became quite popular in many countries. Under impacts of Climate change, saline intrusion of seawater to surface and groundwater is becoming an urgent issue in many countries in the world, especially in South-east Asia countries. For example in particular case of Vietnam, more than one millions of water wells with high concentration of arsenic are in use at both MeKong Delta ([As] = 1 - 1610 ppb) and Red River Delta ([As] = 1 - 2050 ppb), equivalent to 13.5% of Vietnamese population are in hazard poisoned by arsenic [*Nguyen, 2008; Hug, 2008; Shinkai et al, 2007*]. These water sources are being intruded by seawater, leading to both arsenic contamination and high salinity. It can be foreseen that desalination and arsenic removal in the brackish groundwater is going to be one of the main issues for the environmentalists in the near future. This is also the main objective of this study to find out an innovative, advanced treatment technology to satisfy both these requirements.

In this study, vacuum membrane distillation (VMD) technology – one of four variants of membrane distillation (MD) process was introduced as the key possible process to solve the problem. As a thermally-driven separation process, in which only vapour molecules are able

to pass through a porous hydrophobic membrane owing to partial pressure difference through the membrane, this technology was expected to solve efficiently both arsenic contamination and desalination in brackish groundwater. In fact, several relevant VMD studies have been performed, but these studies focused either on arsenic rejection in pure water or on desalination of seawater [*Criscuoli et al., 2012, Mericq et al., 2010*]. Consequently, this experimental study will be performed in order to test arsenic rejection efficiency of the VMD process under presence of NaCl in feed solution. For that reason, synthetic feed solution at different As(III) concentrations (i.e. in range of 300 – 2000 ppb) and fixed salinity corresponding to a brackish water (10 $g.L^{-1}$ NaCl) will be used in this study. The selected feed solutions are chosen to be representative of groundwater composition in Mekong Delta (Vietnam). Influences of operating conditions (i.e. feed temperature, vacuum pressure, hydrodynamic condition) on the VMD performance will be investigated. Possible scaling and fouling phenomena on the membrane surface caused by organic matter and salts will be also studied. Most of the comments and/or conclusions in this chapter are based on experimental results obtained with the VMD pilot plant introduced in chapter 2. This chapter introduces different steps of experiments which aim:

a) To test influence of feed As(III) concentration on the VMD performance, both in terms of As (III) rejection and permeate flux obtained. Desalination of brackish water is also taken into consideration;

b) To determine influences of the operating conditions (feed temperature, vacuum pressure, and hydrodynamics) on the VMD permeate flux. The objective is to select optimal operating conditions for further study according to these experimental results. For these experiments, both pure water and synthetic brackish water containing As(III) are used as feed solutions to determine if the permeate flux is affected by presence of As(III);

c) To study on possible fouling effects to the permeate flux, in turn with presence of organic matter and calcium in feed solutions.

IV.2. RESULTS AND DISCUSSIONS

IV.2.1. Effect of feed As(III) concentration on the VMD performance

Main objective of this part is to assess preliminarily performance of the VMD process for both As(III) rejection and desalination in brackish groundwater for a given set of operating conditions (Fluoropore membrane, [NaCl] = 10 $g.L^{-1}$; Pp = 4500 Pa, T_f = 40°C and Re = 3400). Explanation for choice of Fluoropore membrane was already mentioned in Chapter 3. Experiments at different As(III) concentrations in a synthetic water containing NaCl (without organics) were performed. Compositions of the feed solutions were listed in the Table 4.1.

Table 4.1 *Compositions of the three synthetic feed brackish solutions*

No	Feed solutions	As(III) (ppb)	NaCl ($g.L^{-1}$)	pH	Ec (mS/cm)
I	NaCl + As(III) 300	300	10	6.8	16.40
II	NaCl + As(III) 1000	1000	10	6.8	16.39
III	NaCl + As(III) 2000	2000	10	6.8	16.77

The effects of feed As(III) concentration were assessed through two parameters: (1) As(III) rejection rate and (2) the obtained permeate flux. Reasons for choice of the operating parameters will be discussed in the following section IV.2.2. Results of As(III) rejection by VMD process were presented in Fig 4.1a.

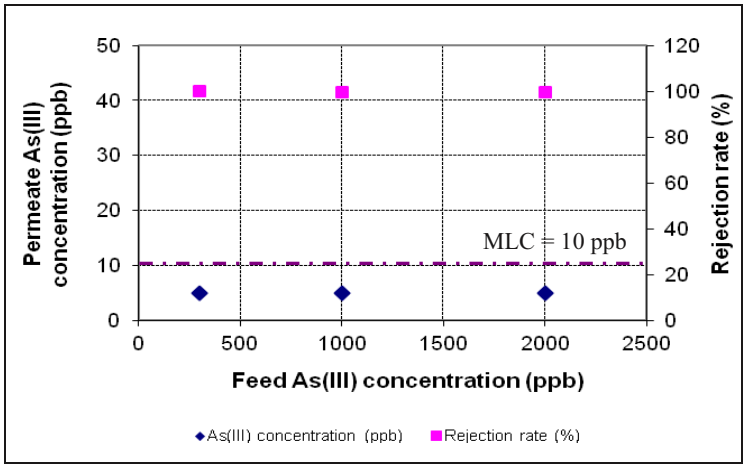

Fig 4.1a *Effects of feed As(III) concentration to VMD performance (Fluoropore membrane, [NaCl] = 10 $g.L^{-1}$, T_f = 40^{0}C, Pp = 4500 Pa, Re = 3400).*

In this figure, with the increase of the feed As(III) concentrations in the range [300 - 2000 ppb], permeate As(III) concentrations were detected to be always lower than the maximum contaminant level (MCL) required in the standard for drinking water (MCL = 10 ppb). Within

the given As(III) concentration range, it proved the independence on As(III) removal efficiency of the VMD process to the feed As(III) concentration with over 99.5 % rejection rate achieved, irrespective of feed concentrations. This conclusion was also consolidated by the same tendency in study performed by *Criscuoli et al., 2012*, where the maximum feed As(III) concentration was 5000 ppb, in pure water.

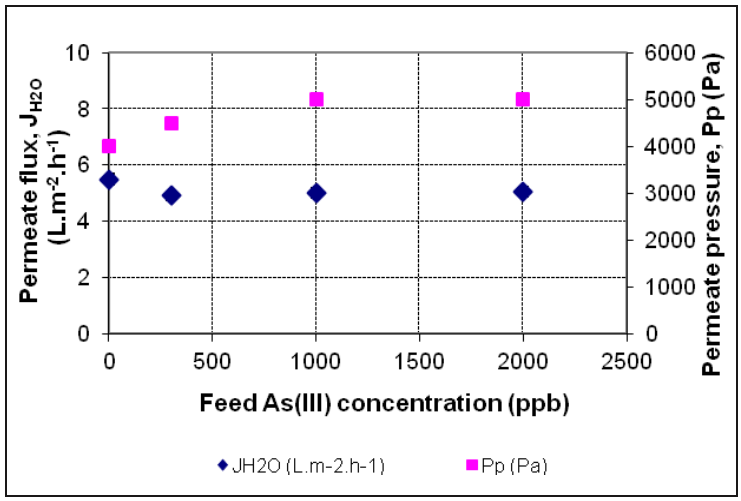

Fig 4.1b *Effects of feed As(III) concentration to VMD permeate flux (Fluoropore membrane, [NaCl] = 10 g/L, $T_f = 40^0$C, Pp = 4500 Pa, Re = 3400).*

Regarding the permeate flux, Fig 4.1b showed stability of the permeate flux obtained ($J_{H2O} \approx$ 5.0 L.m^{-2}.h^{-1}), irrespective of feed As(III) concentration, in the range of our study. A slight difference was observed in comparison with permeate flux obtained with pure water (J_{H2O} = 5.5 L.m^{-2}.h^{-1}). Two reasons could explain this difference: (1) presence of NaCl in the feed solutions (i.e. 10 g.L^{-1}) caused reduction of water activity coefficient, and then, lowered trans-membrane pressure (i.e. driving force); or (2) variation of vacuum pressure as illustrated in Fig 4.1b. When a non-volatile solute is considered, the most likely effect of the feed concentration is to result in a decrease in the permeate flux. This is attributed to the fact that the addition of non-volatile solute to water reduces the partial vapour pressure and consequently reduces the driving force of MD process. Besides that, contribution due to effect of the concentration polarization (i.e. by formation of a boundary layer on the feed membrane surface) can be considered although their effect is very small compared to that of the temperature polarization [*El-Bourawi et al., 2006*].

In our case, the permeate fluxes, were stable and not dependent on increase of the feed As(III) concentration. This is probably due to quite low feed As(III) and NaCl concentrations, which

were not high enough to cause significant decrease of water activity coefficient. In this part, the water activity coefficients of the brackish solution and of the brackish solutions containing As(III) at different concentrations were estimated and presented in Table 4.2. In this case, the calculation considered that concentration of solutes in the feed is equal to the one at the membrane surface (i.e. $C_m = C_f$). It means that the concentration polarization is negligible in this case. It is worth noting that two different methods were applied for this calculation, both by PHREEQC software and by the empirical equation cited in literature [*Lawson and Lloyd, 1997*]. This empirical equation, which was used to determine the activity of water in NaCl solution, is presented in the following equation 4.1. Quite similar results obtained by these two different methods prove high certainty of this coefficient.

$$\alpha_{H2O} = 1 - 0.5\chi_{NaCl} - 10\chi_{NaCl}^2 \quad (4\text{-}1)$$

where α_{H2O} is the activity coefficient of water and χ_{NaCl} is the mole fraction of NaCl.

As observed in Table 4.2, decrease of the water activity coefficient was mainly caused by presence of NaCl in the feed solution. Meanwhile, presence of As(III) at the given concentrations did not have any effect and induced the same value of water activity coefficient for all three As(III) concentrations, which were very small. In general with a very slight decrease of water activity coefficient (less than 1%) in comparison with the one of pure water, influences of As(III) at the given concentrations in the feed solution could be neglected. Same tendency was also observed in the study of *Criscuoli et al., 2012*, where same permeate fluxes were obtained, irrespective of feed As(III) concentrations in range of 0 – 5000 ppb.

Table 4.2 *Water activity coefficients of the different feed brackish solutions*

Feed solutions	As(III) (ppb)	NaCl ($g.L^{-1}$)	T_f (^0C)	Density kg/m^3	Activity coefficient of water, α_{H20}	
					PHREEQC software	Empirical equation
Pure water	0	0	40	992.25	1	1
NaCl	0	10	40	999.60	0.994	0.998
NaCl + As(III) 300	300	10	40	999.60	0.994	0.998
NaCl + As(III) 1000	1000	10	40	999.60	0.994	0.998
NaCl + As(III) 2000	2000	10	40	999.60	0.994	0.998

In conclusion, at the given concentrations (between 300 and 2000 ppb), the feed As(III) concentration did not affect the VMD performance, both in As(III) rejection and permeate flux obtained.

Concerning the presence of NaCl, at the given NaCl concentration (i.e. 10 $g.L^{-1}$), analytical results showed that more than 99.5% of NaCl could be retained in the feed side of the membrane, which indicates high salt removal of the VMD process. However, as said before, with the increase of bulk salt concentration, the permeate flux tends to decrease due to reduction of water vapour pressure with addition of solute in water as well as to the contribution of the concentration polarization effect. By using the VMD modelling for the same experimental setup (VMD pilot plant, Fluoropore membrane, $T_f = 50^0C$, Re = 4000), Mericq et al., 2010 reported that the concentration polarization coefficient (C_f/C_m) was in range of [0.970 – 0.987], even if for a feed solution at much higher salt concentration (i.e. 95 $g.L^{-1}$). It proved that at lower feed salt concentration, impact of concentration polarization on the permeate flux was insignificant and could indeed be neglected.

In summary, VMD process could be considered as an effective treatment solution both for direct As(III) removal and desalination in brackish water, avoiding the pre-oxidation step to convert As(III) into As(V) as for the conventional technologies. However, high permeate flux achievement, which mainly depends on many factors such as: membrane permeability, feed temperature, vacuum pressure, hydrodynamic condition, etc…, is still a challenge for its practical application. Thus, choice of the optimal operating conditions for VMD performance is necessary and will be discussed in the next section.

IV.2.2. Influences of the process operating conditions on the VMD

❖ *Effects of the feed temperature*

Theoretically, the feed temperature is a very sensitive operating parameter, which significantly affects both the permeate flux and the total energy requirement [*El-Bouwari et al., 2006*]. In these experiments, influences of the feed temperature were tested within the range of [25 – 55°C] with three synthetic feed samples: (1) pure water; (2) brackish water ([NaCl] 10 $g.L^{-1}$), and (3) As(III) contaminated brackish solutions ([As(III)] 300 ppb + [NaCl] 10 $g.L^{-1}$). These experiments were carried out at fixed permeate pressure and fixed feed flow

velocity (Pp = 4500 Pa and u = 1.19 m/s or Re = 2300 – 5200 for 25 and 55°C, respectively). Regarding hydrodynamic condition, it is worth noting that increase of feed temperature will change density and viscosity of the feed brackish solution, leading to a variation of Reynolds number as a function of temperature, even in case the feed flow velocity was fixed. Relation between the feed temperature and the VMD permeate flux was presented in the Fig 4.2. Uncertainty of the measurement was small with 0.5%.

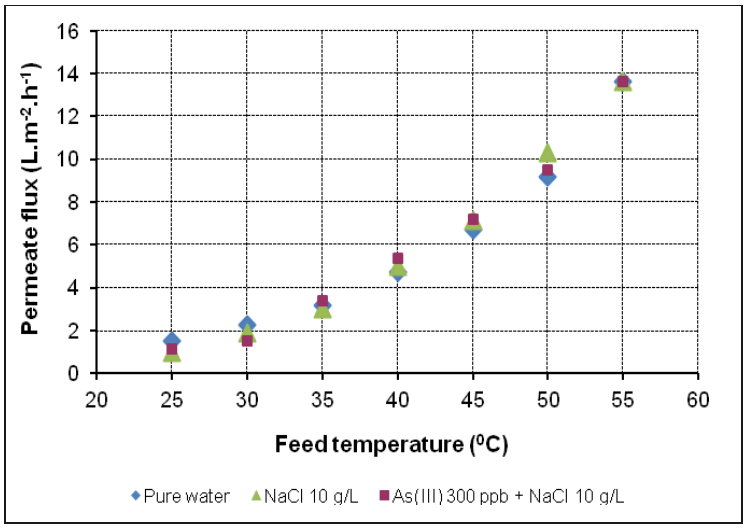

Fig 4.2 *Variation of VMD permeate flux as a function of feed temperature (Fluoropore membrane, T_f = 25 – 55^{0}C, Pp = 4500 Pa and Re = 2300 – 5200).*

As expected, for each solution, an exponential increase of the VMD permeate flux was observed with the increase of the feed temperature. It is attributed to the major influence of the feed temperature to the water vapour partial pressure (Antoine equation) and consequently to the trans-membrane pressure difference. For a better understanding, equation 4-2 showing the permeate flux as a function of feed temperature is given as follows:

$$J_{H2O} = \frac{K_M(T)}{\sqrt{M_{H2O}}}\Delta P_{H2O} = \frac{K_M(T_{ref})}{\sqrt{M_{H2O}}}\sqrt{\frac{T_{ref}}{T}}(P_m^* - P_p) \qquad (4\text{-}2)$$

where J_{H2O} *is molar flux of water;* ΔP_{H2O} *is difference in partial pressure of water on both sides of the membrane;* P_p *is vacuum pressure at the permeate side;* M_{H2O} *is molar mass of water;* K_M *is Knudsen permeability;* $K_M(T_{ref})$ *is Knudsen permeability at reference*

temperature $T_{ref} = 20^0C$; P^*_m is vapour pressure of water at the membrane's conditions, which is related to the feed temperature as mentioned by the Antoine's equation:

$$P_m^* = B_1 * \exp(A_1 - \frac{A_2}{T_m + B_2 + A_3}) \quad (4\text{-}3)$$

(with $A_1 = 18.3036$; $A_2 = 3816.44$; $A_3 = -46.13$; $B_1 = 133.32$ and $B_2 = 273.15$)

where B_1 and B_2 are the coefficients to convert unit mmHg and ^0C into Pa and ^0K, respectively; T_m is the temperature at the membrane surface.

In case of Fluoropore membrane, and for the given operating conditions, the obtained permeate flux increased from 0.8 to 13.6 $L.m^{-2}.h^{-1}$ for an increase of the feed temperature from 25 to 55°C. Moreover the three curves were very close which meant that on all the range of the feed temperature, influences of NaCl and As(III) on the VMD permeate flux were insignificant and could be neglected. It also meant that there was no effect of concentration polarization on the permeate flux at the given feed concentrations.

Regarding the total energy requirement, by applying the same VMD pilot plant for desalination of seawater, *Mericq et al., 2009* reported that more than 96% to 99% of the total energy requirement was heat energy within the range of feed temperature of 25 – 65°C. It meant that operating at higher feed temperature could provide higher permeate flux, but also require higher energy consumption, especially for heating. Moreover in practical operation of the VMD pilot plant, the permeate flux was quite sensitive to high feed temperature at low vacuum pressure, leading to fluctuation of permeate flux measured. For those reasons, feed temperature at $T_f = 40$°C was chosen in this study as an operating parameter for all remaining experiments. This value could be considered as a good compromise between the permeate flux obtained and energy requirement.

❖ *Effects of the hydrodynamic condition*

The temperature and concentration polarization influences are affected by the feed flow-rate and the flow pattern and can be reduced by increasing velocity and thus Reynolds number. This helps to increase the mass transfer coefficient of the feed boundary layer, leading to a significant increase of the permeate flux, especially in the laminar and transitional flow patterns. Further increases in the Re number may result only in a marginal gain of the VMD

permeate flux (Khayet and Matsura, 2011). In this study, effects of hydrodynamic conditions on the permeate flux, both for pure water and brackish solution containing As(III), were determined by varying feed flow-rate in range of [25 - 250 $L.h^{-1}$] at fixed values of the feed temperature and permeate pressure ($T_f = 40^0C$, Pp = 4500 Pa). This is equivalent to increase of Reynolds number value from 680 to 5200, corresponding to change of feed flow from laminar to turbulent pattern.

As illustrated in Fig 4.3, the permeate flux increased with increasing of the feed flow-rate and approached an asymptotic value at a Reynolds number of 3400. This asymptote permeate flux value was 5.2 $kg.m^{-2}.h^{-1}$ for Fluoropore membrane at feed temperature T_f = 40°C and permeate pressure Pp = 4500 Pa. Theoretically, effects of both concentration and temperature polarizations could be the reasons of the observed phenomenon. However, as there was no concentration polarization in case of pure water while same curve was obtained with arsenic-contaminated brackish solution as observed in Fig 4.3, it could be concluded that concentration polarization was limited, and as a consequence, only effect of the temperature polarization was found in this case. This was attributed to increase of feed flow-rate, leading to change of feed flow from laminar to turbulent pattern and thereby reducing the temperature polarization effect at the membrane feed side. At high Reynolds number (Re = 3400, beginning of turbulent pattern), the temperature polarization effect was negligible. That explained why the obtained permeate flux was maintained at the asymptote value (J_{H2O} = 5.2 $kg.m^{-2}.h^{-1}$) and no longer being affected by the feed flow-rate. This phenomenon was the same for both cases of pure water and arsenic-contaminated brackish solutions.

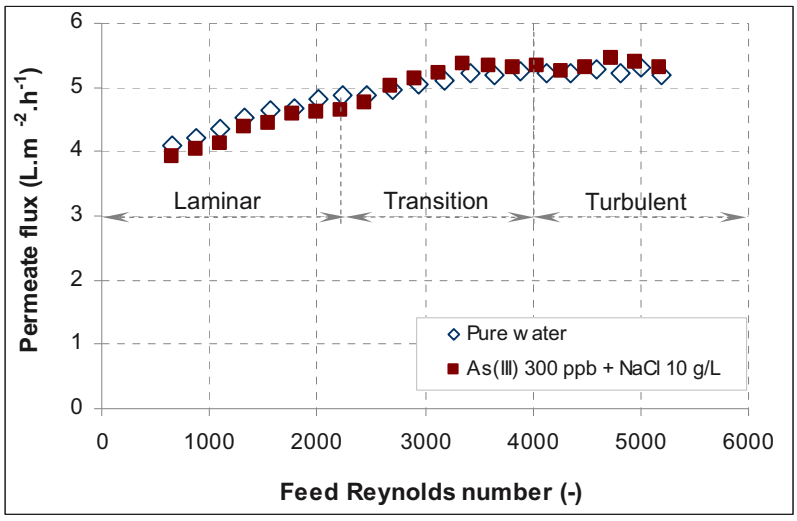

Fig 4.3 *Variation of VMD permeate flux with Reynolds number*

(Fluoropore membrane, $T_f = 40^0C$, Pp = 4.500 Pa, Re = 680 - 5200).

To sum up, in all cases, effect of concentration polarization was non-measurable for arsenic-contaminated brackish solution. Meanwhile, temperature polarization played an important role and thus hydrodynamic conditions influenced the VMD permeate flux, especially in the laminar and a part of transition patterns. At Re < 3400, the effect of temperature polarization was significant, leading to increase of the permeate flux as a function of feed flow-rate. However at Re > 3400, effect of temperature polarization was negligible and feed flow-rate showed no influence on the permeate flux with an asymptotic permeate flux value reached. It meant that operating at higher Re number (Re > 3400) is meaningless as more energy consumption is required without increase of the permeate flux. As a consequence, in order to reduce the energy consumption, Reynolds number at 3400, corresponding to the feed flow-rate Q = 150 $L.h^{-1}$ was chosen for all the remaining experiments.

❖ *Effects of the permeate (vacuum) pressure*

In general, the permeate flux increases with a decrease in the permeate pressure at fixed temperature and thus of the driving force in all MD systems. With respect to feed solutions containing volatile solutes, different permeate compositions can be obtained depending on the permeate pressure. The permeate pressure, thus, should be maintained higher than the water vapour pressure if high separation factors in favour of the volatile solutes are required *[Khayet and Matsura., 2011]*.

On the contrary with presence of non-volatile compounds in the feed solution, the permeate pressure can be lowered as much as possible to get the highest permeate flux provided that no membrane pore wetting occurred. In this study, an experiment with presence of non-volatile compounds of As(III) and NaCl was conducted. A linear relationship between permeate flux obtained and applied permeate pressure, as presented in Fig 4.4, was observed.

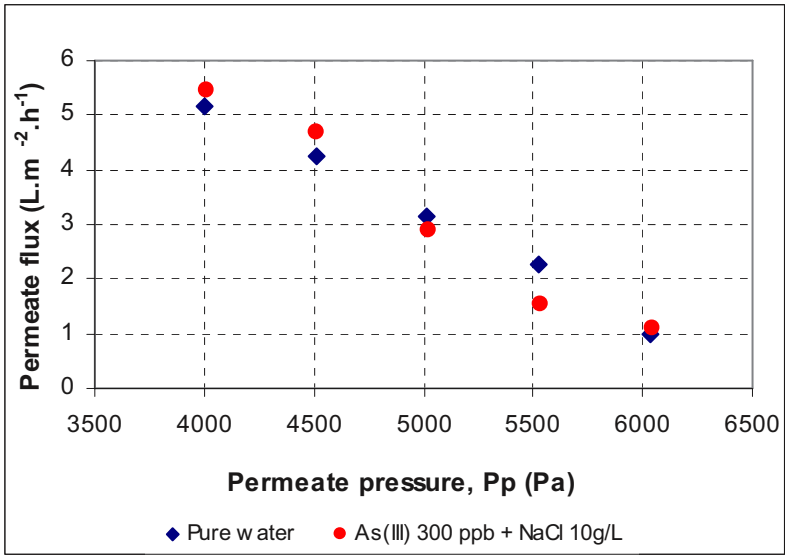

Fig 4.4 *Variation of VMD permeate flux as a function of permeate pressure (Fluoropore membrane, [NaCl] = 10 g.L^{-1}; T_f = 40^{0}C, Re = 3400).*

As observed in Fig 4.4 for given operating conditions (T_f = 40^{0}C, Re = 3400, Fluoropore membrane), the obtained permeate flux increased from 1 to 5.2 kg.m^{-2}.h^{-1} for a variation of the permeate pressure from 6100 Pa to 4000 Pa. Same tendency for both pure water and As(III) contaminated brackish water confirmed that presence of As(III) and NaCl at low concentration did not influence the permeate flux.

As the decrease of permeate pressure can also increase the trans-membrane pressure, it can enhance the risk of membrane pore wetting. Wetting phenomenon occurs when the trans-membrane pressure (TMP) is higher than liquid entry pressure (LEP), which can be determined either by Laplace equation or by experimental measurement. In this study, the feed side of the membrane was set at atmospheric pressure whereas the permeate side was maintained under reduced pressure (for example at an absolute pressure of 4000 Pa). Thus, the trans-membrane pressure, between the two sides of the membrane, was given by TMP = $P_{feed} - P_{permeate}$ = 0.96 bars (equivalent to absolute permeate pressure of 4000 Pa). This VMD trans-membrane pressure is much lower than LEP of the Fluoropore membrane employed (LEP = 4.2 bars as presented in Chapter 2) so wetting should not occur. Indeed no complete wetting phenomenon was observed in these experiments although a partial wetting may occurred.

In summary, for a certain hydrophobic membrane, all three operating parameters: feed temperature, vacuum pressure and Reynolds number have influences on the VMD permeate flux. Same trend of influence could be observed in previous publications as high feed temperature and low permeate pressure could provide a high permeate flux. Reynolds number also had influence on the permeate flux, but mainly in the laminar and a part of transition flow patterns. At the beginning of turbulent regime, the permeate flux reached asymptotic value and no longer increased. As a result, selected operating conditions (T_f = 40°C, Pp = 4500 Pa and Re = 3400) were applied for all the following experiments.

IV.2.3. VMD performance with As(III) contaminated brackish groundwater

IV.2.3.1. *Study on time variation of permeate flux: evaluation of fouling effects*

Aim was then to determine if membrane fouling is occurring. During the VMD operation, there are two possibilities to cause the decrease in permeate flux: (1) modification of water vapour pressure caused by increase of feed concentration and (2) fouling occurring on the membrane surface or inside the partially wetted pores. Indeed, as said before, the increase of feed concentration reduces the water molar fraction χ_{H2O} and the feed water activity coefficient α_{H2O}, and consequently decreases trans-membrane pressure difference. For the second case, membrane fouling could modify the membrane properties (i.e. pore size, porosity, hydrophobicity…) and could add a resistance to mass transfer thus causing a decline of trans-membrane flux.

In order to distinguish the effects of these two phenomena, a new Knudsen permeability, namely apparent Knudsen permeability, was proposed in equation 4-4 [*Mericq., et al, 2010*]. It represents permeability of the employed membrane at each certain time during the experiment, for the set of experimental conditions applied at that time. In this equation, the influence of feed solute concentration on the permeate flux was taken into account (i.e. water molar fraction χ_{H2O} and the feed water activity coefficient α_{H2O}). Thus, any decrease in apparent Knudsen permeability (if any) could be attributed to fouling.

$$K_M = \frac{J_{H2O}\sqrt{M_{H2O}}}{(\alpha_{H2O}\chi_{H2O}P_m^*(T_m) - P_p)} \quad (4\text{-}4)$$

It is worth noting that calculation of this parameter should be based on following assumptions:

- T_m is equal to the feed bulk temperature T_f (i.e. no temperature polarization effects);
- χ_{H2O} calculation is based on mass balance of feed solution density and mole fractions of contaminants.
- χ_{H2O} adjacent to the membrane surface is equal to χ_{H2O} in the bulk (i.e. no concentration polarization)
- α_{H2O} is calculated by the empirical equation 4-1.

In order to study possible effects of fouling on the VMD permeate flux, recorded operating conditions (feed temperature T_f, permeate pressure Pp and hydrodynamic condition Re) and their corresponding permeate fluxes within 3 hours were presented for three different As(III) concentrations (Fig 4.5, Fig 4.6 and Fig 4.7). Compositions of these feed solutions were listed in the Table 3.1. It is worth noting that all these experiments were carried out with the same Fluoropore membrane sample by cleaning the membrane sample (with clean water) between the experiments. This step was to ensure that the membrane sample with the same permeability was applied for all experiments.

During these experiments some fluctuations of the permeate pressures occurred as observed in Fig 4.5a, Fig 4.6a and Fig 4.7a, leading to instability of permeate fluxes as presented in Fig 4.5b, Fig 4.6b and Fig 4.7b. However, these variations could be considered insignificant and permeate fluxes fluctuated in range of 4 – 5 $kg.m^{-2}.h^{-1}$ for all three cases. Apparent permeability K_M and normalized permeate flux (i.e. the permeate flux divided by the one obtained at the steady state) at each point during the whole operation process were calculated and presented in Fig 4.8, for the three studied solutions.

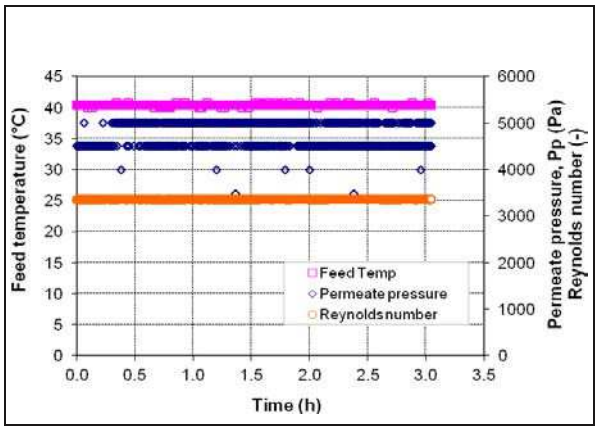

Fig 4.5a *Operating conditions for NaCl + As(III) 300 solution ([NaCl] = 10 g.L^{-1}; T_f = 40°C; Pp = 4,500 Pa; Re = 3400)*

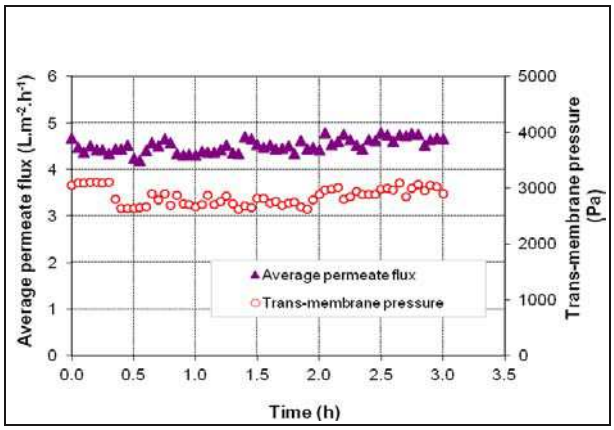

Fig 4.5b *Permeate flux and corresponding trans-membrane pressure for NaCl + As(III) 300 solution*

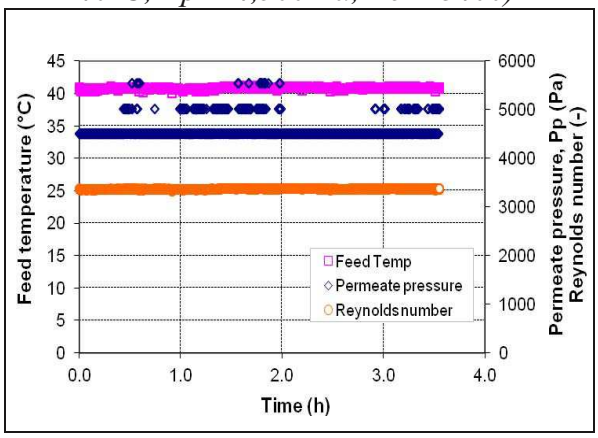

Fig 4.6a *Operating conditions for NaCl + As(III) 1000 solution ([NaCl] = 10 g.L^{-1}; T_f = 40°C; Pp = 4,500 Pa; Re = 3400)*

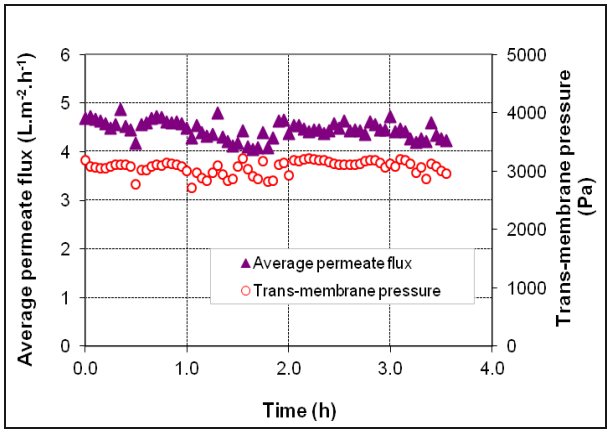

Fig 4.6b *Permeate flux and corresponding trans-membrane pressure NaCl + As(III) 1000 solution*

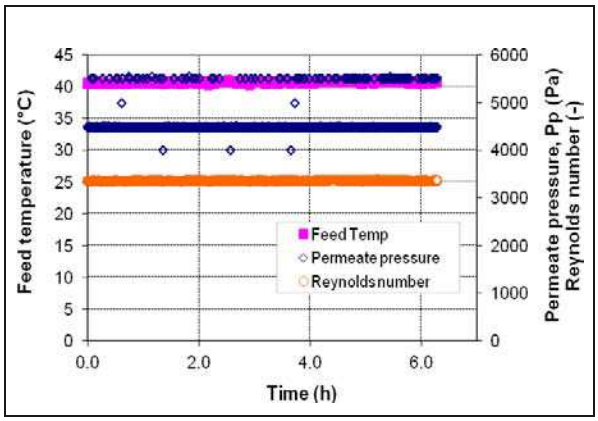

Fig 4.7a *Operating conditions for NaCl + As(III) 2000 solution ([NaCl] = 10 g.L^{-1}; T_f = 40°C; Pp = 4,500 Pa; Re = 3400)*

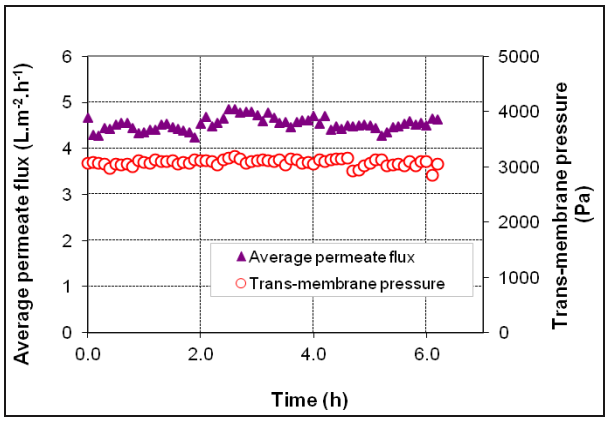

Fig 4.7b *Permeate flux and corresponding trans-membrane pressure for NaCl + As(III) 2000 solution*

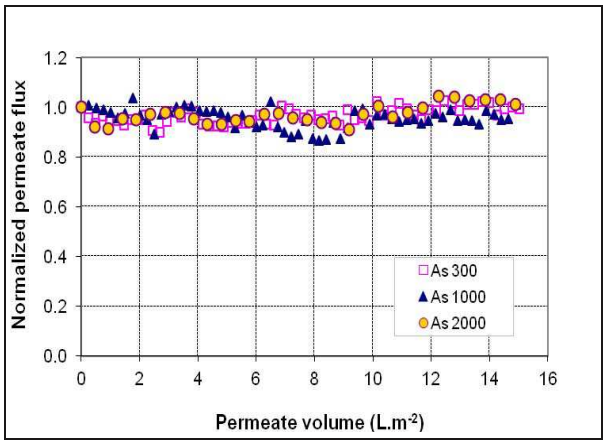

Fig 4.8a *Normalized permeate flux permeate volume for three feed brackish solutions: As(III) 300 – As(III) 1000 – As(III) 2000*

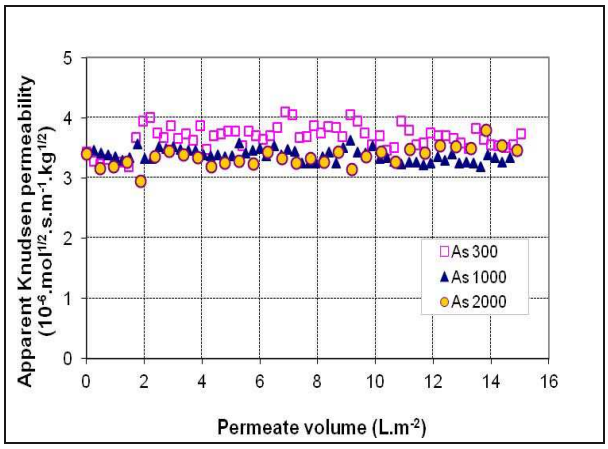

Fig 4.8b *Apparent Knudsen permeability versus permeate volume for three feed brackish solutions: As(III) 300 – As(III) 1000 – As(III) 2000*

Permeate fluxes obtained for the three feed solutions (i.e. As 300, As 1000 and As 2000) were plotted until a cumulated permeate volume of 15 $L.m^{-2}$ (corresponding to an operation duration of 3 hours). No decline of normalized permeate fluxes (Fig 4.8a) as well as stability of apparent Knudsen permeability values (Fig 4.8b) proved that no membrane fouling occurred within 3-hour operation time. In case of 3-hour operation, effects of feed As(III) concentrations could also be neglected. Two explanations could be given for this phenomenon: (1) concentrations of NaCl and As(III) in the feed solution were too low to be able to cause concentration polarization effects (as already seen in section 4.1), and (2) 3-hour operation time was too short for deposition or precipitation of salt and As(III) on the membrane surface or the deposition occurred but not much enough to affect to the permeate flux. In order to clarify this phenomenon, SEM and EDS analyses of the used membrane sample were carried out and are presented in the following part.

The deposition of undesirable materials on the membrane surface and/or membrane pores, known as fouling, may reduce the permeate flux and process efficiency. This fouling phenomenon may be formed by suspended particles, corrosion products, biological growth and variety of crystalline deposits [*El-Bourawi et al., 2006*]. Observation of the membrane (after use) aims to visualize the membrane surface as well as identifying which components deposited on the membrane surface. It can be done with SEM and EDS analysis, respectively. It is worth noting that precipitation may also occur during drying of the membrane as a sample preparation step for SEM and EDS analysis. Fig 4.9 and Fig 4.10 demonstrated an

example of SEM analysis for the membrane before and after As(III) 1000 experiment, respectively. Fig 4.10 showed presence of a deposited crystal on the membrane surface. EDS analysis then allowed to determine composition of the deposited crystal, which mainly consists of sodium and chloride as presented in Fig 4.11. It is worth noting that detection of carbon and fluoride is due to the membrane material itself. The EDS analysis also showed the presence of arsenic deposited on the membrane surface but in a very low quantity.

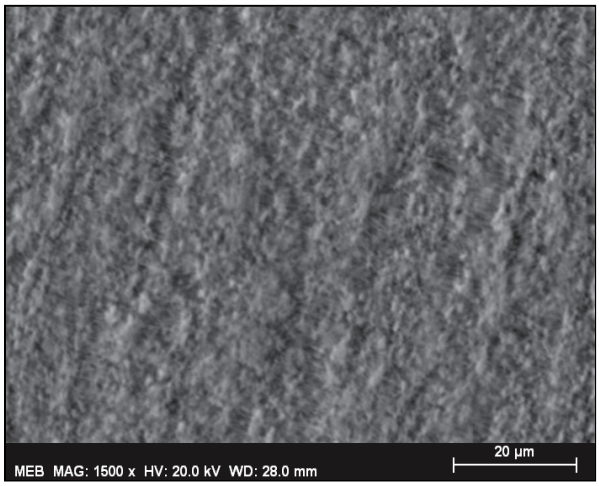

Fig 4.9 *SEM analysis of new Fluoropore membrane (x 1500)*

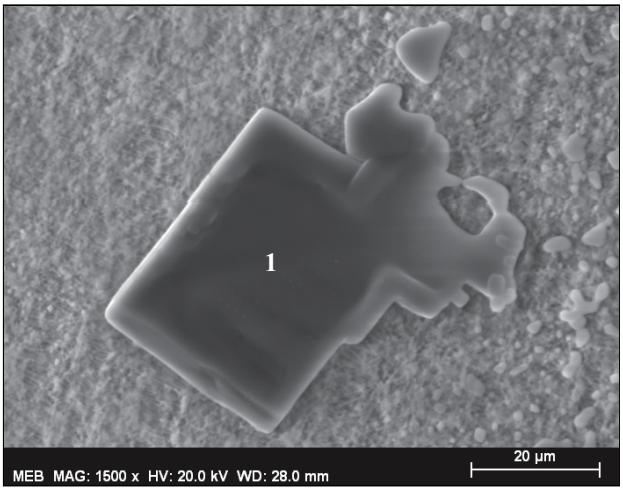

Fig 4.10 *SEM analysis of the membrane after As 1000 experiment (x 1500)*

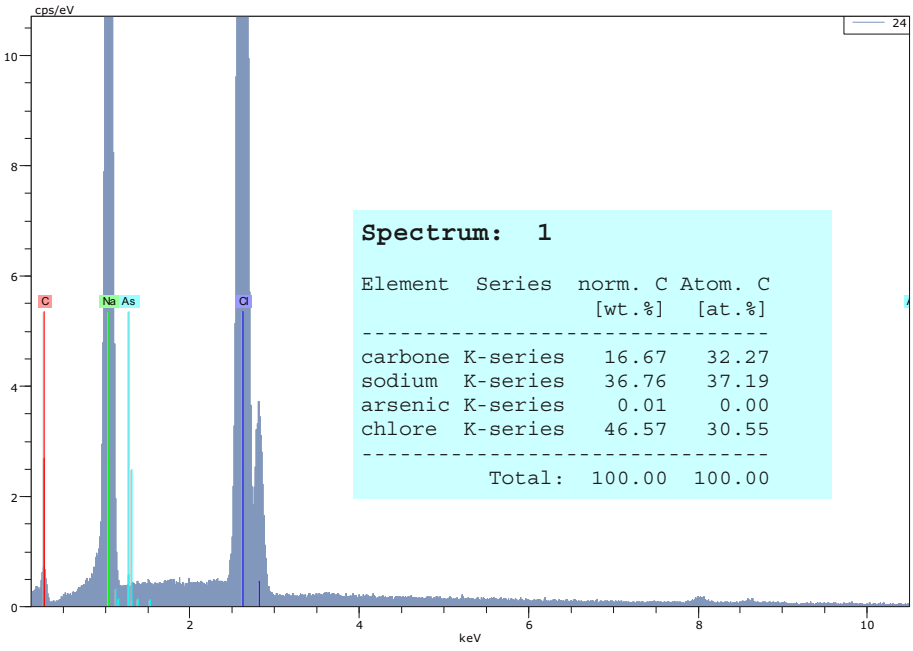

Fig 4.11 *EDS analysis of the deposited crystal.*

In summary, these experiments confirmed the independence of VMD performance on feed As(III) concentration with the same value of permeate flux for three different As(III) concentrations in the range [300 - 2000 ppb]. Within the operation time of 3 hours, depositions of small amounts of both NaCl and As(III) were observed on the membrane surface by SEM and EDS analyses. However, these deposits did not affect much the obtained permeate flux with high stability over 3 hours of normalized permeate flux as presented in Fig 4.8a. As no complete wetting was observed, it can be considered that the deposits occurred only on the membrane surface, but not inside the membrane pores. As a result, most of membrane pores were still available for mass transfer in all three cases. Besides that, 3-hour operation time of the experiment could be short for having significant deposits of NaCl and As(III) on the membrane surface. As a consequence, only small amount of both NaCl and As(III) depositions were found, which were not enough to cause permeate flux decline.

IV.2.3.2. *Study on permeate flux variation with presence of organic matter*

In this part, synthetic solution, with its composition similar to the one of groundwater in Vietnam, was prepared and studied. It was composed of As(III) at 300 ppb, NaCl at 10 $g.L^{-1}$ and organic matter at concentration of 20 $mg.L^{-1}$ (equivalent to TOC = 7.5 $mg.L^{-1}$). In this study, humic acid sodium salt (HASS), with its characteristic description in Table 4.3, was used as source of organic matter present in the water.

Table 4.3 *Characteristics of the employed humic acid sodium salt (HASS).*

Name	Unit	Value
Molecular formula		$C_9H_8Na_2O_4$
Appearance of colour		Black, amorphous acid
Molecular weight	$g.mol^{-1}$	226.14
Particle size	µm	20 - 120
Water soluble content (dry basic)	%	≥ 70
Water insoluble content (dry basic)	%	≤ 12
Content of Fe	%	≤ 0.45

***Source**: http://www.hewiki.com/view/790913.htm*

Although studies on fouling effect in MD have been carried out in many previous researches [*Khayet et al., 2004; Khayet and Mengual, 2004; Srisurichan et al., 2005; Mericq et al., 2010; He et al., 2009*], different types of membranes might exhibit different degree of fouling, which may depend upon membrane hydrophobicity, membrane surface structure, initial permeability and also on feed solution composition [*El-Bourawi et al., 2006*]. It is, thus, quite

necessary to evaluate fouling in case of a brackish water containing organics for the Fluoropore membrane.

In this part, experiments with three different feed solutions were carried out to determine if organic matter influenced the membrane fouling. Compositions of the three feed solutions were summarized in the Table 4.4. Same piece of membrane was used for all three experiments (after cleaning by clean water) to ensure that same membrane properties (hydrophobicity, surface structure and initial permeability) were applied. In this case, different degree of fouling (if any) will be attributed to different compositions of the feed solution. First of all, the experiments were carried out within a short-term operation (30 – 45 minutes) to determine permeate fluxes as well as apparent Knudsen permeability values obtained. After that, experiment with presence of organic matter (solution no.VI – Table 4.4) was performed during 5 days to evaluate influence of organic matter within a longer term operation.

Table 4.4 *Compositions of three feed solutions.*

No	Composition	As(III) (ppb)	NaCl ($g.L^{-1}$)	HASS ($mg.L^{-1}$)
IV	Pure water	-	-	-
V	As(III) + NaCl	300	10	-
VI	As(III) + NaCl + HASS	300	10	20

By applying the same method as presented in the previous part (i.e. section IV.2.3.1), normalized permeate fluxes and their corresponding apparent Knudsen permeability values were calculated for the three feed solutions. The results were presented in Fig 4.12a and Fig 4.12b, respectively. Within 45-minute operation time (corresponding to a cumulated filtered volume of 5 $L.m^{-2}$), permeate fluxes were almost the same for both arsenic contaminated brackish solutions, irrespective of being with or without presence of HASS. Apparent Knudsen permeability values showed in Fig 4.12b presented the same value (i.e. K_M = 3.2 x 10^{-6} $s.mol^{1/2}.m^{-1}.kg^{-1/2}$) for both cases. This means that, for short term operation, no fouling nor scaling effects are observed for brackish solutions with As(III) and brackish solutions containing both As(III) and organics. It also means that the presence of organics does not promote membrane wet ability. In fact, presence of As(III), NaCl in the feed solutions could theoretically contribute to permeate flux decline by lowering the water activity coefficient. Theoretical permeate fluxes in correspondence with membrane permeability and water activity coefficients are presented in Table 4.5. They indicated negligible impact of solute

concentrations on the permeate fluxes. Slightly lower permeate fluxes of the brackish solutions in comparison with the one of pure water as presented in Fig 4.12a could be attributed to variation of permeate pressure applied in this case.

Table 4.5 *Theoretical permeate fluxes as a function of water activity coefficients.*

Composition	As(III) (ppb)	NaCl ($g.L^{-1}$)	HASS ($mg.L^{-1}$)	α_{H20}	Km $s.m^{-1}.mol^{1/2}.kg^{-1/2}$	J_{H20} $L.m^{-2}.h^{-1}$
Pure water	-	-	-	1.000	$3.2x10^{-6}$	5.04
NaCl + As(III)	300	10	-	0.994	$3.2x10^{-6}$	4.98
NaCl + As(III) + HASS	300	10	20	0.994	$3.2x10^{-6}$	4.98

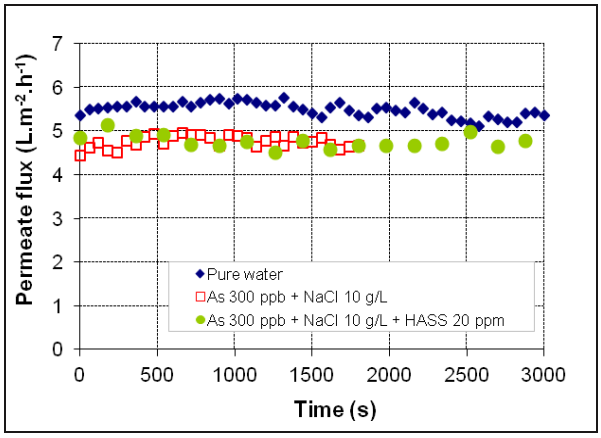

Fig 4.12a *Variations of the permeate fluxes for the three solutions*

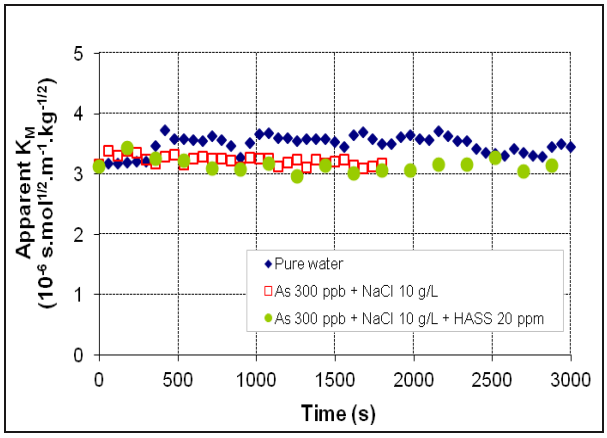

Fig 4.12b *Apparent Knudsen permeability values for the three solutions*

In order to fully evaluate influence of organic matter on membrane fouling, a longer term experiment (i.e. 5 days) of the feed solution no.VI (As(III) 300 ppb + NaCl 10 $g.L^{-1}$ + HASS 20 $mg.L^{-1}$) was carried out. All the operating conditions as well as the obtained permeate flux were presented in Fig 4.13. Similar to the previous experiments, the operating conditions in this test were set at T_f = 40°C, Re = 3400, Pp = 4500 Pa as shown Fig 4.13a. It is worth noting that the 5-day experiment had to be stopped at the end of each working day (average 8-hour operation) and was restarted in the next day because of electrical safety reasons. During the pause time (around 14 hours), the feed solution was maintained in the feed tank under stirring conditions. The tested membrane was kept intact inside the membrane cell for the next day without circulation and without operation of the vacuum pump during this duration.

Analysis of permeate flux, normalized permeate flux and apparent Knudsen permeability values were conducted and presented in Fig 4.13b, 4.13c and Fig 4.13d, respectively. It could

be observed that after a long-term operation, the obtained permeate flux was quite stable and only a slight decline was observed. Calculations with 6% decline of permeate and 5.8% decrease of apparent Knudsen permeability value proved that flux decline was linked to the modification of the apparent Knudsen permeability. It could be attributed to deposition of organic matter on the membrane surface, which modified the dynamic membrane structure by surface or inside pore deposit or adsorption and led to lower the membrane's permeability. However, at the given HASS concentration (equivalent to TOC = 7.5 mg/L) within time scale of the experiment, the influences of organic matter seems to be very small.

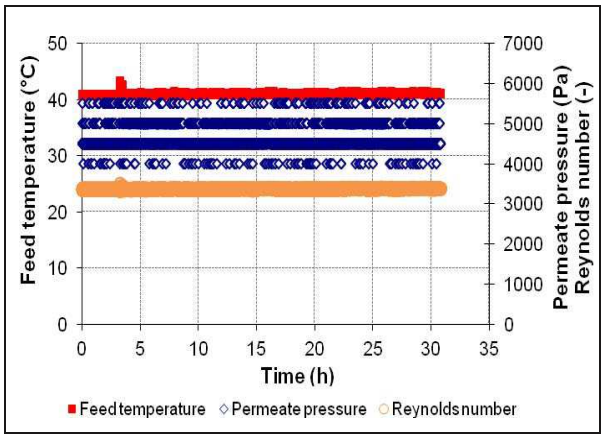

Fig 4.13a *Operating conditions for the 5-day experiment with solution VI (Fluoropore; [NaCl] = 10 g.L^{-1}; HASS = 20 mg.L^{-1}; T_f = 40°C; Pp = 4500 Pa; Re = 3400)*

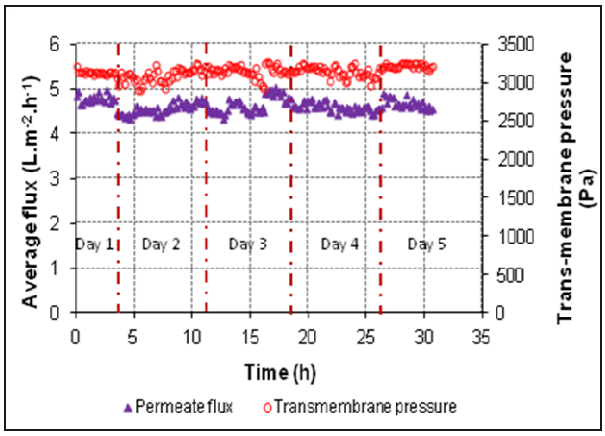

Fig 4.13b *Permeate flux and corresponding trans-membrane pressure versus time for the 5-day experiment with solution VI*

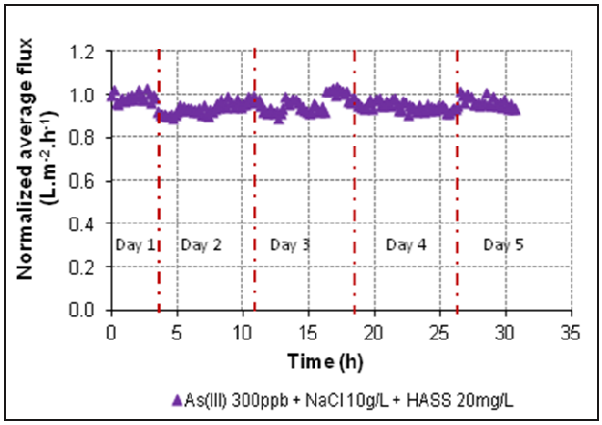

Fig 4.13c *Normalized permeate flux versus time for the 5-day experiment with solution VI*

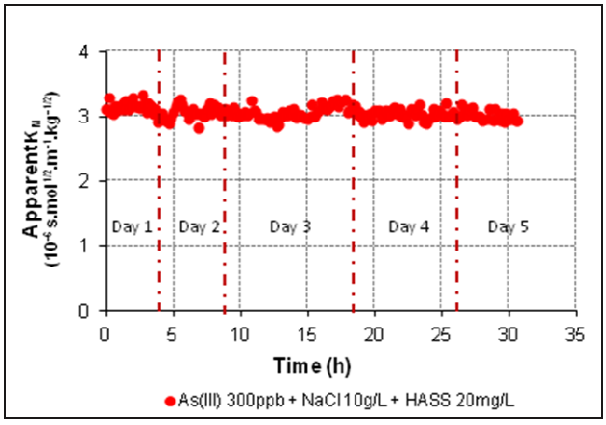

Fig 4.13d *Apparent Knudsen permeability versus time for the 5-day experiment with solution VI*

A SEM analysis was carried out to visualize whether there were any deposition of matter on the membrane surface and how the deposited crystals were modified in comparison with those

obtained without HASS. Fig 4.14 showed the used membrane after 5-day operation with presence of organic matter (solution no.VI). In case of the tested membrane samples, no deposition of arsenic was found on the membrane surface.

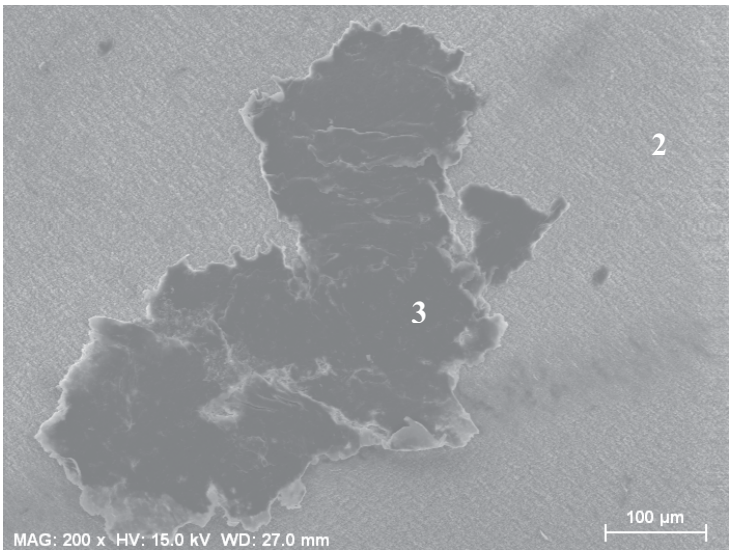

Fig 4.14a *Membrane surface after the 5-day experiment with solution VI (x 200)*

Observation on Fig 4.14a proved presence of some deposits on the membrane surface but in a small amount, which could explain the slight decline of the apparent Knudsen permeability. EDS analysis at points 3 indicated that the deposit was not NaCl with a very little presence of sodium and chloride. Higher amount of carbon at point 3 (Fig 4.15b) than the one at point 2 (Fig 4.15a) could indicate presence of organic matter on the membrane surface, which caused the slight fouling as above mentioned. As a complete wetting of the membrane did not occur, the liquid could not completely penetrate the membrane pores. In this case, two following assumptions could be proposed with their descriptive scheme in Fig 4.14b:

a) ***The first assumption***: The liquid/vapour interface stays at the membrane surface and the organic molecules cannot enter the pores. In this case, deposition of humic acid occurs only on the membrane surface;

b) ***The second assumption***: The liquid/vapour interface can partially penetrate the pores. In this case, a partial wetting could occur and some pores could be blocked by penetration and possibly adsorption of organics inside the pores, causing partial pore blockage.

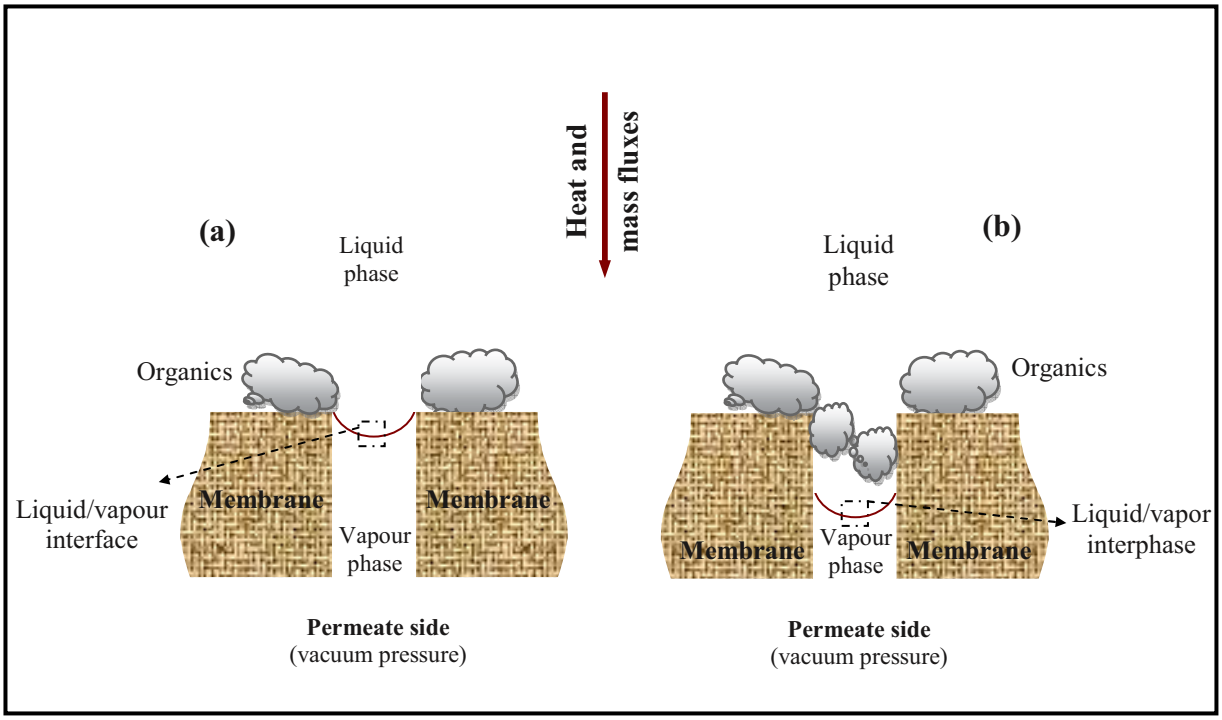

Fig 4.14b *Hypothesis of organic deposit: (a) at membrane surface or (b) inside the pore.*

However, the second hypothesis can be ignored due to larger size of HASS (20 – 120 µm) in comparison with average pore size (0.2 µm), unless if HASS can deform. It means that HASS cannot pass through the pores due to size exclusion mechanism. Finally, the hypothesis with only deposition of organic matter on the membrane surface is taken into consideration. In this case, due to low operating pressure of the process and the fact that mass transfer occurs by diffusion of the volatile compounds (not HASS) in vapour phase inside the pores, the deposition of humic acid on the membrane surface would be less compact and only slightly affect the transport resistance [*Srisurichan et al., 2005*]. Moreover, with lower 12% of water insoluble content (Table 4.3), the HASS is considered as a weak hydrophobe, leading a weak hydrophobic interaction with the Fluoropore membrane. By calculating difference between Knudsen permeability values at initial point and the end point of the experiment, the obtained value ΔK_M with 5.8%, referring to the percentage of inactive membrane surface area, was very small. It means that most of the membrane surface (around 94%) is still free for mass transfer. It could explain why the permeate flux was not be affected much by deposition of organics.

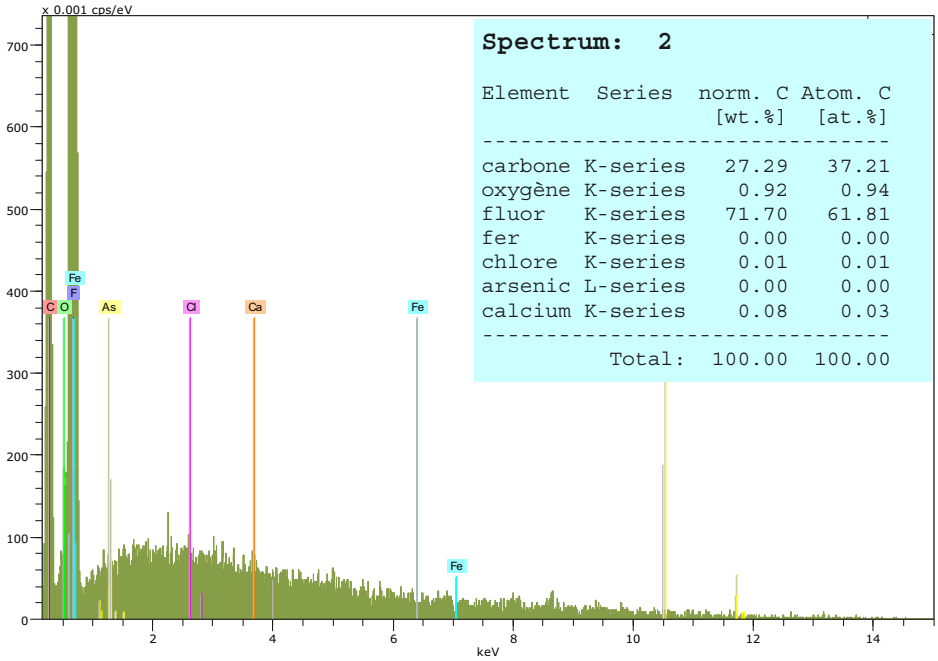

Fig 4.15a *EDS analysis of membrane after 5day - experiment with presence of HASS (point 2- Fig 4.14a)*

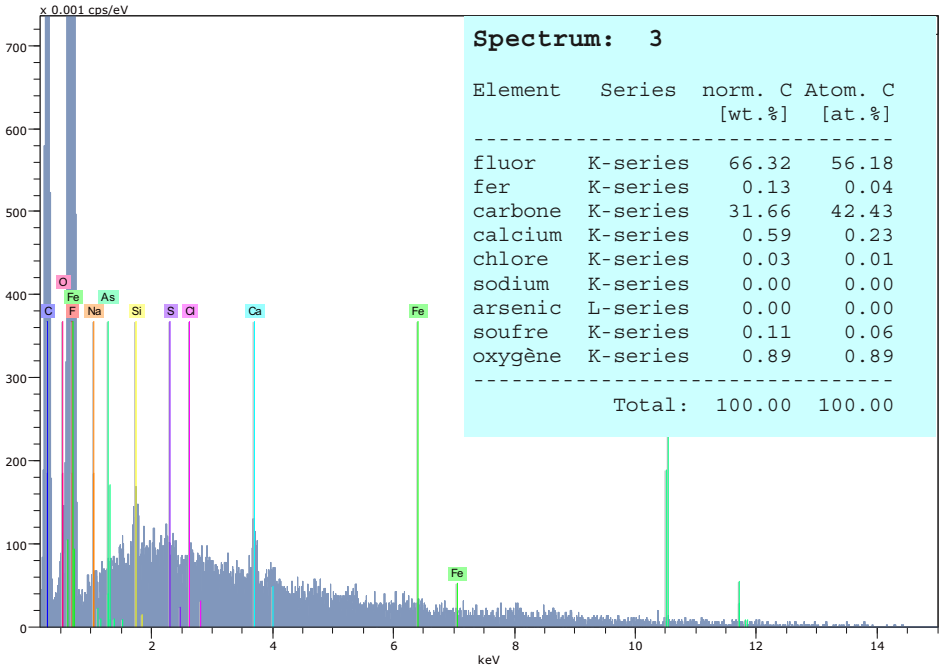

Fig 4.16b *EDS analysis of membrane after 5day - experiment with presence of HASS (point 3- Fig 4.14a)*

IV.2.3.3. *Permeate flux variation with presence of calcium*

The objective is now to study how the presence of calcium in brackish water can affect VMD permeate flux and fouling. For that purpose, $CaSO_4.2H_2O$ powder ($[Ca^{2+}]$ = 0.5 g/L) was added into the feed solution ([As(III)] 300 ppb + [NaCl] 10 $g.L^{-1}$) for a 4-day experiment. Same operating conditions as the previous tests were applied (Fluoropore membrane, T_f = 40°C, Pp = 4500 Pa, Re = 3400). Similar to the previous experiment with presence of HASS, this experiment was stopped at the end of each working day (average 8-hour operation) under the same condition as previously and was restarted in the next day. All operating conditions and the obtained permeate flux were shown in Fig 4.16a and Fig 4.16b. The normalized average and apparent Knudsen permeability were presented in Fig 4.16 c and Fig 4.16d, respectively.

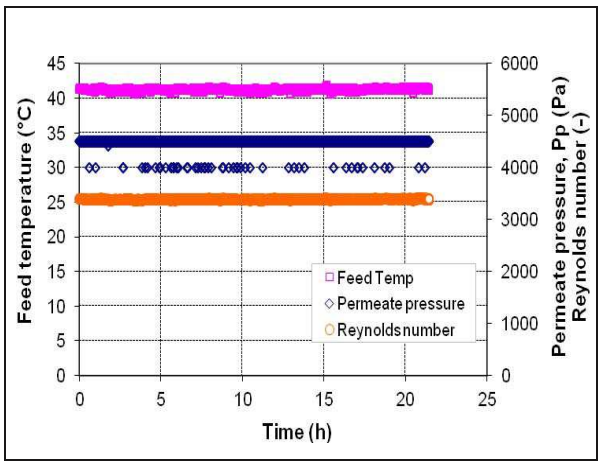

Fig 4.16a *Operating conditions for 4-day experiment with presence of $CaSO_4$ ([NaCl] = 10 $g.L^{-1}$; $[Ca^{2+}]$= 500 ppm; T_f = 40°C; Pp = 4,500 Pa; Re = 3400)*

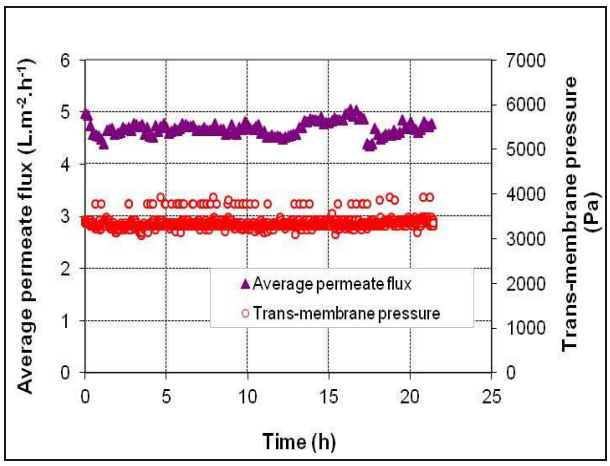

Fig 4.16b *Average permeate flux and corresponding trans-membrane pressure versus time for the experiment with presence of $CaSO_4$*

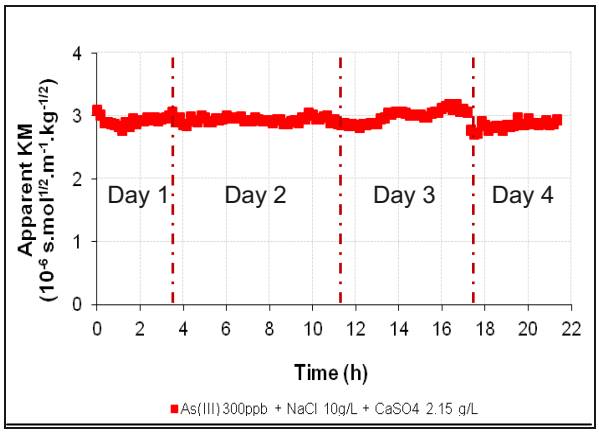

Fig 4.16c *Normalized permeate flux versus time for the 4-day experiment with presence of $CaSO_4$*

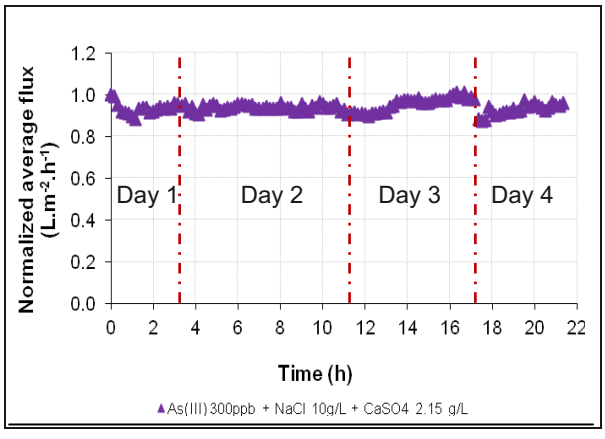

Fig 4.16d *Apparent Knudsen permeability versus time for the experiment with presence of $CaSO_4$*

After a 4-day operation (i.e. 22 hours in total), the results in Fig 4.16 showed that the permeate flux and the Knudsen permeability were nearly constant. A very slight decline of the permeate flux as well as the Knudsen permeability were observed (Fig 4.16c and Fig 4.16d) but could be neglected. Consequently, no scaling affect on the permeate flux was detected during the given operation time. Theoretically in order to study on possible precipitation of salts, saturation index (SI) of salt should be determined according to the following equation:

$$SI = \log\left(\frac{IAP}{K_T}\right)$$

where IAP is the ion-activity product of salt and K_T is the thermodynamic equilibrium constant at the measured temperature of the feed solution. If the SI is negative, the solution is under-saturated, and dissolution of the mineral is possible. If the SI is positive, the solution is over-saturated, and precipitation of salts occurs. A SI of zero indicates that the salt is in equilibrium with the water and that the tendency or rates of dissolution and precipitation should be equal.

In this case, two dissolved salts (NaCl and $CaSO_4$) and their crystals were considered as possible precipitation of halite and gypsum crystals, respectively [*He et al., 2008 – 2009*]. By using the PHREEQC software, saturation indexes of these two salts was estimated and listed in Table 4.6

Table 4.6 *Saturation index of NaCl and $CaSO_4$ salts*

Composition	**NaCl** ($g.L^{-1}$)	$CaSO_4$ ($g.L^{-1}$)	T_f (^0C)	α_{H20}	SI_f NaCl	SI_f $CaSO_4$	SI_f $CaSO_4.2H_20$
NaCl	10	0	40	0.994	-3.37	-	-
NaCl + $CaSO_4.2H_20$	10	2.15	40	0.994	-3.39	-0.63	- 0.49

Decrease of water activity coefficient was caused mainly by presence of NaCl in the feed solution. However, this decrease was very small and could be neglected. Negative values of saturation indexes of both NaCl and $CaSO_4$ indicated that these salts were under-saturated. It means that no precipitation of salts will occur. However, SEM analyses showed an opposite conclusion with deposit of some crystals of salts on the membrane surface as illustrated in Fig 4.17. EDS analyses continued to prove that the observed crystals are mainly composed of NaCl (Fig 4.17a) and a part of $CaSO_4$ (Fig 4.17c). Two possible reasons could explain this

observation: (1) influence of concentration polarization increases salts concentrations at the membrane surface, leading to a higher saturation at the membrane surface and precipitation occurs; and (2) during the drying of the membrane for the SEM and EDS analyses, evaporation of water in the brackish feed solution attached on the membrane surface after the experiment could leave some crystals of salts. Compositions of these deposits were illustrated in Fig 4.18 – Fig 4.21.

Fig 4.17a *Membrane surface after 4-day experiment with presence of $CaSO_4$ (x 750)*

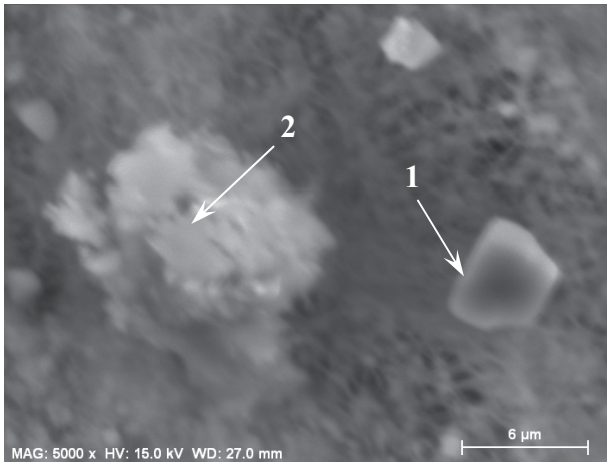

Fig 4.17b *Membrane surface after 4-day experiment with presence of $CaSO_4$ (x 5000)*

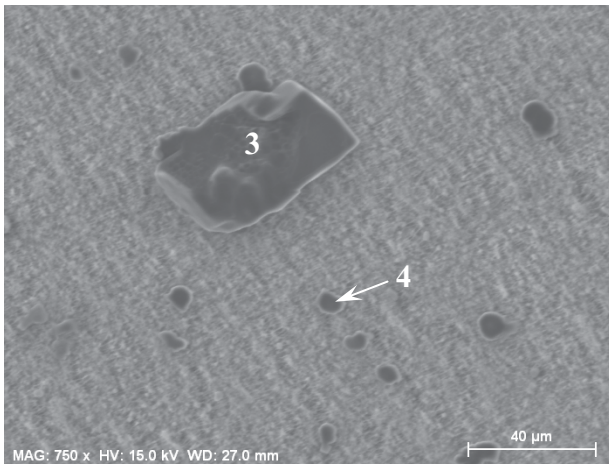

Fig 4.17c *Membrane surface after 4-day experiment with presence of $CaSO_4$ (x 750)*

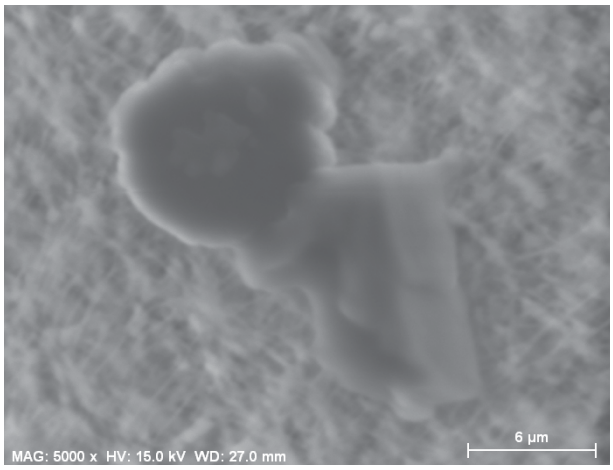

Fig 4.17d *Membrane surface after 4-day experiment with presence of $CaSO_4$ (x 5000)*

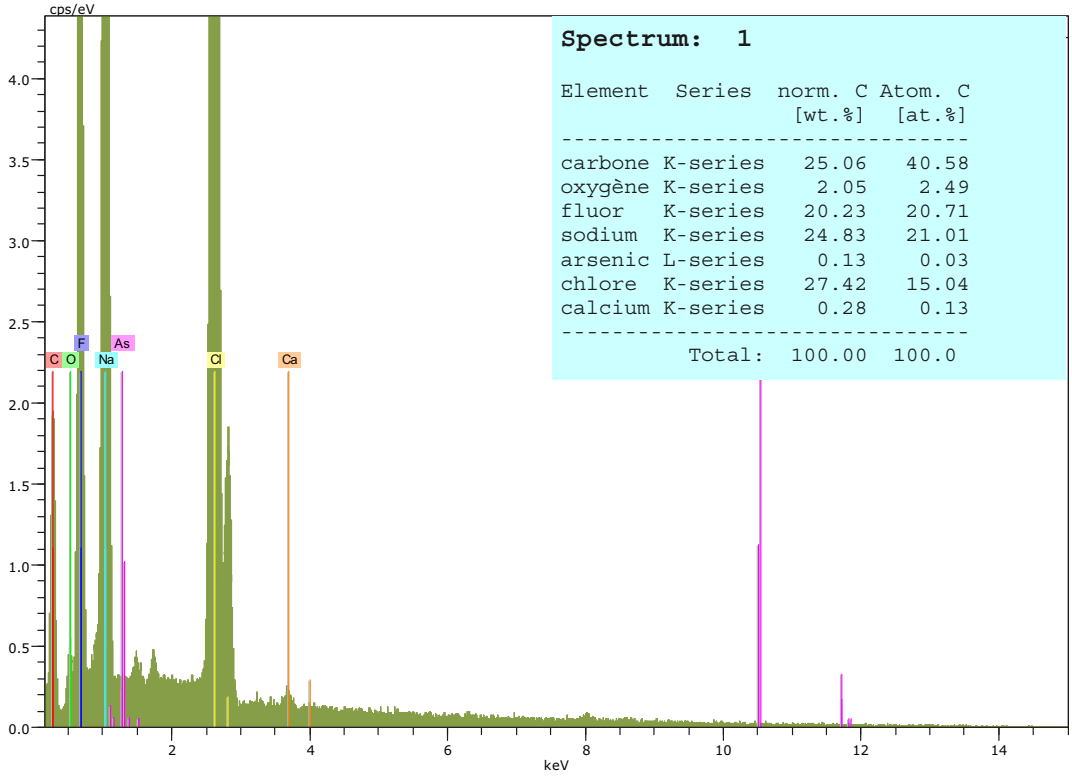

Fig 4.18 *EDS analysis on point 1(Fig 4.17a) for membrane after 4-day experiment with presence of $CaSO_4$*

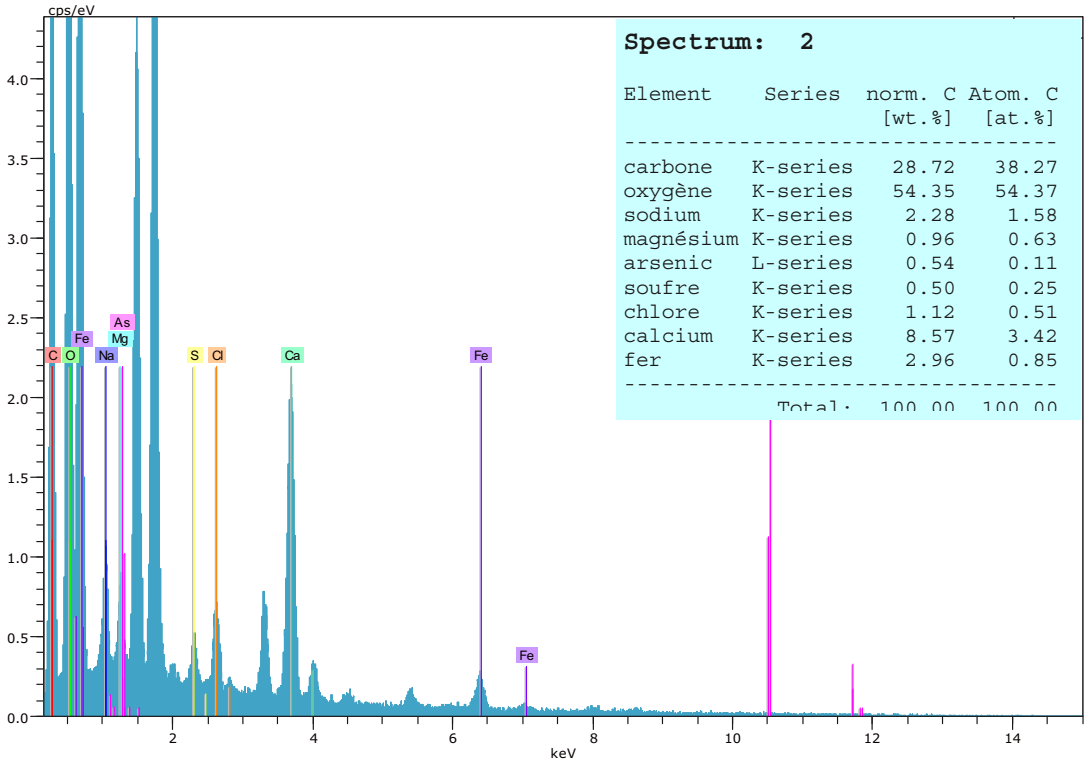

Fig 4.19 *EDS analysis on point 2(Fig 4.17a) for membrane after 4-day experiment with presence of $CaSO_4$*

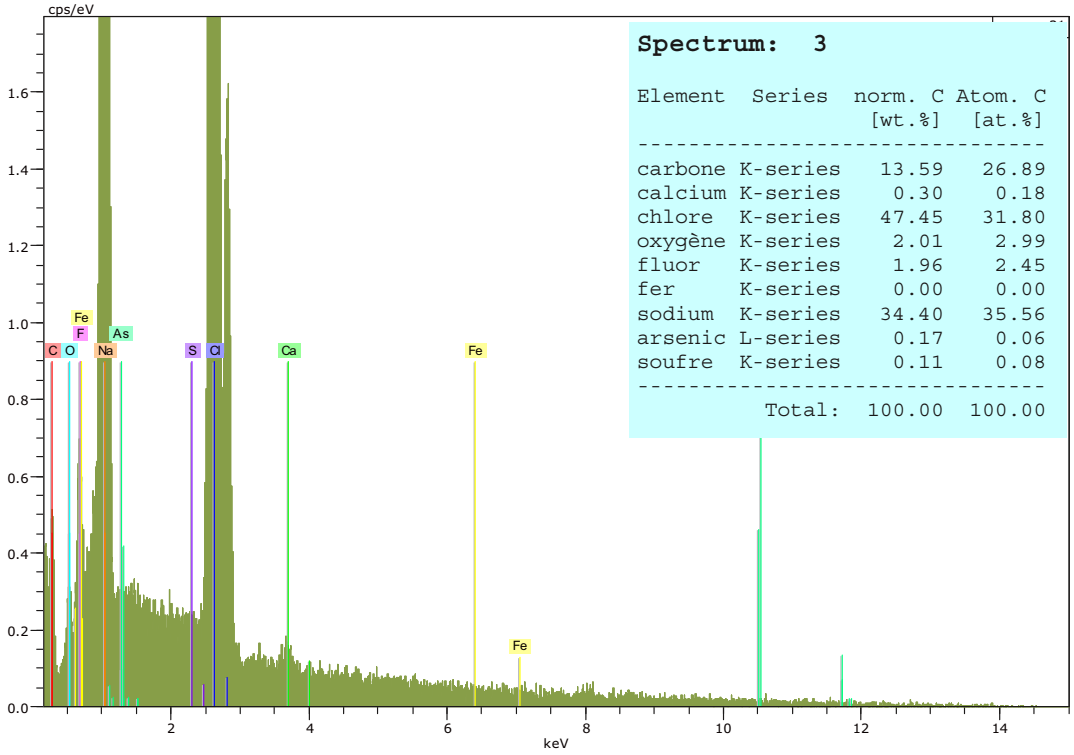

Fig 4.20 *EDS analysis on point 3(Fig 4.17c) for membrane after 4-day experiment with presence of $CaSO_4$*

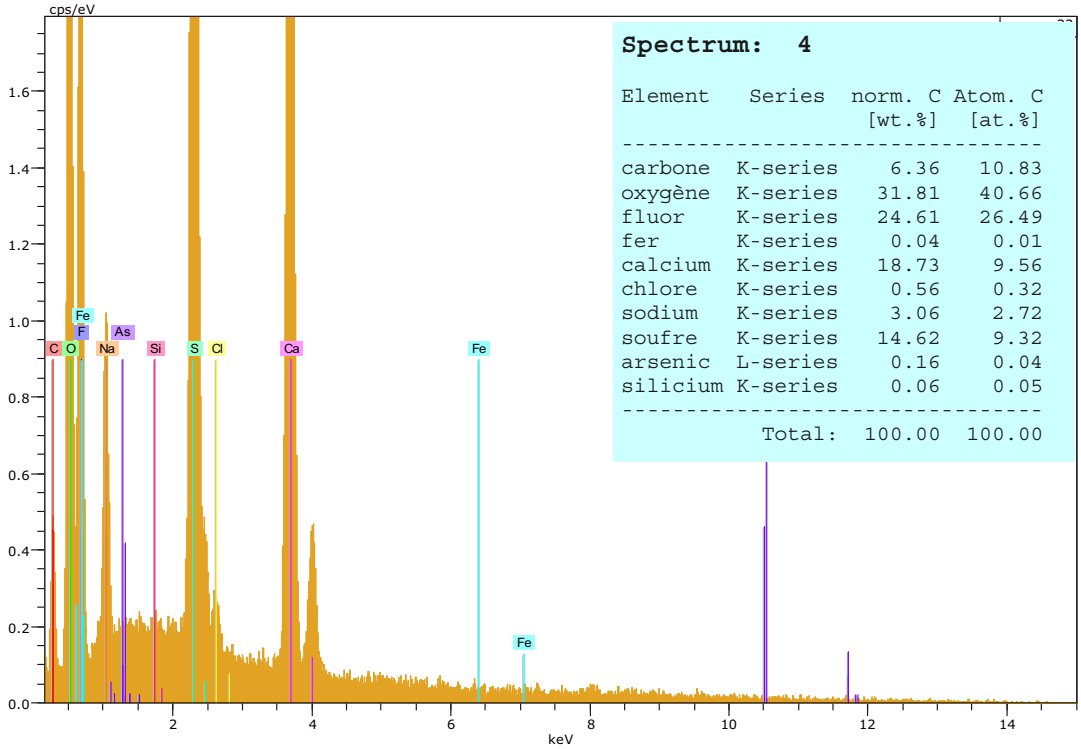

Fig 4.21 *EDS analysis on point 4(Fig 4.17c) for membrane after 4-day experiment with presence of $CaSO_4$*

SEM and EDS analyses proved that occasional scaling of salts could occur on the membrane surface in vacuum membrane distillation process or during their observation procedure. Crystals of NaCl and $CaSO_4$ could be observed on the membrane surface in both individual and integrated forms as illustrated in Fig 4.17b and Fig 4.17d, respectively. However at given operation time of the experiment (i.e. 22 hours of operation), no decline of the permeate flux occurred, which meant that effects of scaling was insignificant in this case. Scaling occurred on the surface of the membrane but not blocked the pores, leading to stability of the permeate flux obtained. However, influences of scaling for a longer term continuous operation could be significant and should be studied in more detail in the future.

IV.3. CONCLUSIONS

With the objective to test the applicability of the VMD technique for direct As(III) removal from brackish water, influences of the process operating conditions as well as possible fouling (with presence of organic matter and calcium) on the VMD performance were investigated. On the basis of experiments at lab scale, VMD has proved its feasibility on both direct arsenic and salt removal, helping to avoid the pre-oxidation step to convert As(III) into As(V) as for many other conventional treatment technologies. Permeate As(III) concentration was always lower than the standard for drinking water (MCL = 10 ppb), even at high feed As(III) concentration (i.e up to 2000 ppb). Same trend was observed for NaCl removal with over 99.5% rejection rate.

As expected, VMD permeate flux was strongly affected by the process operating conditions. At the selected operating conditions (Fluoropore membrane, $T_f = 40^0C$, Pp = 4500 Pa, Re = 3400), average permeate flux (5 $kg.m^{-2}.h^{-1}$) was obtained, irrespective of feed As(III) concentrations. Meanwhile, the highest permeate flux at 14 $kg.m^{-2}.h^{-1}$ could be obtained at $T_f = 55^0C$, Pp = 4500 Pa, Re = 3400. Hydrodynamic condition also has effect on the VMD permeate flux but mainly at the laminar and a part of transition flow patterns. At fixed feed temperature and vacuum pressure, permeate flux approached its asymptote value at Reynolds number of 3400. No effect of concentration polarization on the permeate flux was found at the given feed concentrations.

In presence of humic acid, deposition of organic matter could be observed on the membrane surface but its effect on the trans-membrane flux was very small with only 6% of permeate flux decline after 5-day operation. It was because of humic acid presents larger particle size (20 – 120 μm) than the pore size (0.2 μm) so the organics cannot pass through the pores due to size exclusion mechanism. As a consequence, only deposition of organic matter on the membrane surface was taken into consideration. Moreover, due to weak hydrophobic interaction with Fluoropore membrane, most of the membrane surface area (around 94%) was still free for mass transfer. It could explain why the permeate flux was not be affected much by deposition of humic acid.

Similar to the organic matter, effect of calcium (under the form of gypsum) on the membrane fouling was also limited. Crystals of NaCl and $CaSO_4$ could be observed on the membrane surface, but no decline of the permeate flux was observed. It indicated that effect of calcium under the form of gypsum could be insignificant. However, influences of scaling for a longer term continuous operation could be significant and should be studied in more detail in the future.

Chapter V:

Coupling of Reverse osmosis and Vacuum membrane distillation processes for direct arsenite removal from brackish groundwater

V.1. INTRODUCTION

As concluded in the Chapter 4, VMD process can directly remove arsenic in the brackish water to meet the standard without pre-oxidation step. One more advantage of this process is to treat As(III) effectively even at neutral pH (i.e. pH 7), without requirement to increase pH (i.e. pH 10) as for the conventional technologies. Although providing high arsenic and salt rejection efficiencies, the permeate flux achievement mainly depends on type of membrane employed and is still a big challenge for this advanced technology. In this study, at the given operating conditions (Fluoropore membrane, $T_f = 55^0C$, Pp = 4500 Pa, Re = 3400) for a brackish solution containing arsenic, highest permeate flux at 14 $kg.m^{-2}.h^{-1}$ was obtained (see Chapter 4). This value is in accuracy with other studies as presented in Chapter 1. Besides that, another main drawback of this VMD process is the high level of total energy requirement. By applying the same pilot plant for seawater desalination, *Mericq et al., 2010* classifies three types of energy requirement in VMD operation, including: (1) the vacuum energy; (2) the circulation energy and (3) the heat energy. Among them, the heat energy requirement represents more than 98% of the total energy requirements. In order to facilitate the feasibility of the VMD technology in the industry through lowering cost for energy, these two possibilities could be proposed:

- By using the low-grade, waste and/or alternative energy sources such as solar and geothermal energy as heat energy [*Lawson and Lloyd, 1997; Mericq et al., 2010*]. Typically, feed temperature in MD ranges from 60 – 90^0C (although temperatures as low as 30^0C have been used), these above-mentioned sources of energy could be a cost efficient solution. Indeed, MD systems powered by solar energy have been shown to be cost competitive with reserve osmosis in remote areas [Lawson and Lloyd, 1997] and also in VMD [*Mericq et al., 2011*]. In this case, this VMD technology could stand alone to treat all the feed flow;

- In case the alternative energies are inapplicable, another possibility is to focus VMD on feed previously concentrated by a low energy consuming process, for example reverse osmosis. Owing to this integration, a lower quantity of feed flow to be treated by VMD is required, and therefore decreases the energy cost as well as membrane area. This concept was proposed by *Mericq et al., 2010* for over-concentrate retentate of a RO plant with a 40% recovery factor and a 38.9 $g.L^{-1}$ feed salt concentration. As a

result, the feed volume can be reduced by a 1.6 factor and the water recovery increases from 40 to 89.1%. As the feed volume to be treated by VMD decreases, heat energy requirement is also reduced, leading to a lower energy cost.

Objective of this chapter is to study on a hybrid process by coupling of VMD and RO for further concentration of a RO retentate. On contrary to the RO process, the VMD is not limited by osmotic pressure. As a consequence, the coupling of RO and VMD processes (Fig 5.1) was expected to reduce the RO retentate volume as well as to increase global clean water recovery. As previously said the coupling of RO and VMD was already studied by *Mericq et al., 2010* for the desalination of seawater. The issue of this study is thus to check the feasibility of this coupling for brackish water containing arsenic.

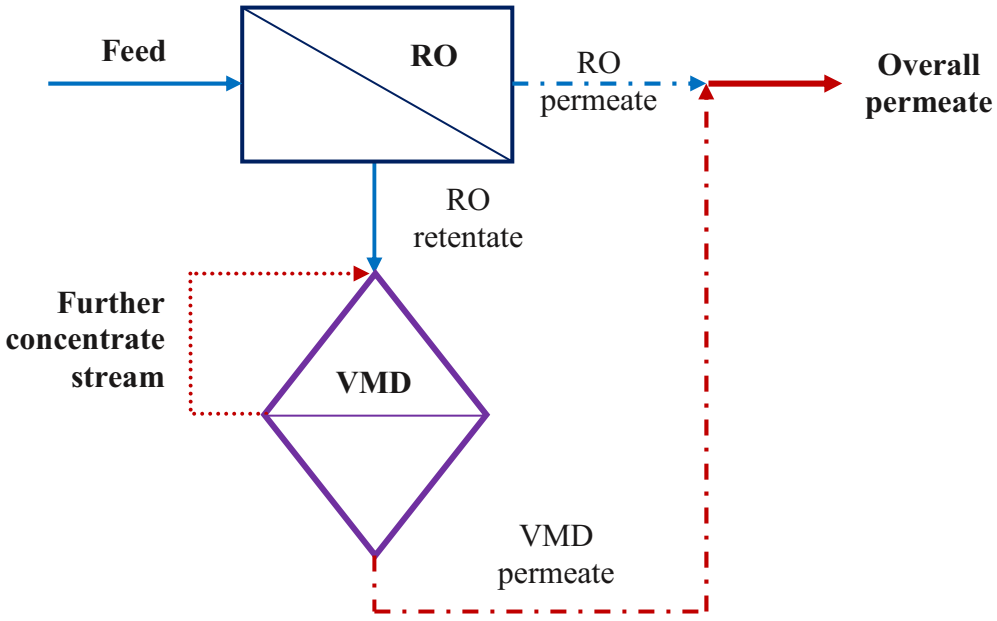

Fig 5.1 *Coupling of RO and VMD processes*

As presented in the previous studies, fort the same operating conditions, different RO membranes would provide different arsenic rejection rates, which should be experimentally determined. For this reason, the first step of this chapter is to test the efficiency of a given RO membrane for direct As(III) and NaCl rejections. Effects of operating conditions will also be studied to find out the optimal operating parameters. Then experiments of VMD to over-concentrate the RO retentate stream will be performed. All the data collected in these

experiments will be used to simulate a hybrid process by coupling RO and VMD. In general, three main parts will be introduced in this chapter:

a) RO experiments to determine influence of the operating conditions (i.e. pH value, trans-membrane pressure, recovery rate) on the rejections of As(III) and NaCl. SEM and EDS analyses will also be performed to find out whether any deposits of As(III) and NaCl occurring on the membrane surface or partially inside the pores;

b) VMD experiments with RO retentate to determine the VMD permeate flux and quality at high feed concentrations;

c) Simulation of the hybrid process to estimate the global recovery of the integrated process and to simulate a global hybrid RO + VMD process.

V.2. RESULTS AND DISCUSSIONS

V.2.1 Performance of the RO membrane process

V.2.1.1 Effect of pH, trans-membrane pressure and feed concentration

As reported in several previous studies, for the same process operating conditions, RO performance for As(III) removal depends on type of RO membrane employed [Shih, 2005]. These studies indicate that different membranes would provide different As(III) rejection rates, which should be experimentally determined.

- *Effect of pH and trans-membrane pressure TMP*

For this study, the osm-ESPA membrane, with its specifications as presented in Chapter 2, was used as a random sample. Influences of two operating parameters: (1) pH of feed solution; and (2) trans-membrane pressure (TMP) were investigated. Synthetic feed solution similar to the one of the VMD process was prepared as described in Chapter 2 with 10 $g.L^{-1}$ NaCl and 300 ppb As(III). According to *Kang et al., 2000*, rejection of As(III) is the same over the pH range of 3 to 7 and much higher at pH 10. For that reason, preliminary experiments (in batch-mode) at different pH values (i.e. pH 7 and pH 10) and at different trans-membrane pressures (TMP = 24 and 32 bars) were performed to determine the performance of the osm-ESPA membrane, towards rejections of both As(III) and NaCl. Fig 5.2 and Fig 5.3 showed respectively As(III) and NaCl rejection rates for two values of pH and two values of trans-membrane pressure. Rejection rate was calculated according to the equation 5-1.

$$R(\%) = \frac{C_f - C_p}{C_f} x100 \qquad (5\text{-}1)$$

where:

- ✓ R : rejection rate (%);
- ✓ C_f : feed concentration (ppb for As(III) and g/L for NaCl);
- ✓ C_p : permeate concentration (ppb for As(III) and g/L for NaCl).

The permeate concentration is the mean concentration in the permeate, determined for a cumulated volume of permeate of 250 mL, which corresponds to a recovery of 50%.

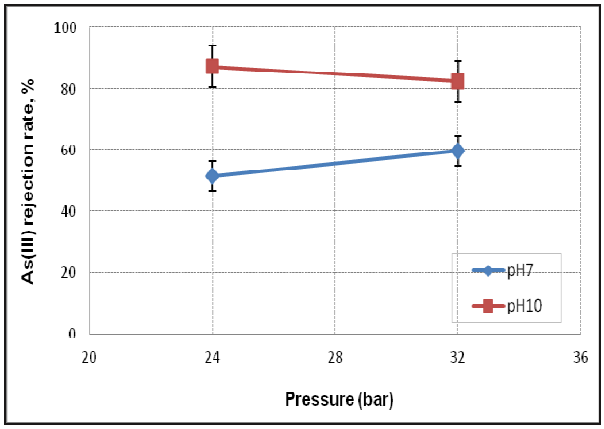

Fig 5.2 *As(III) rejection as a function of pH and TMP with* $[As(III)]_{initial}$ *= 300 ppb and* $[NaCl]_{initial}$ *= 10 g.L*$^{-1}$

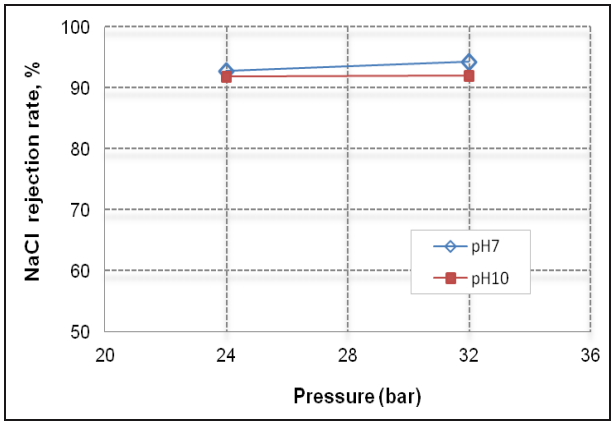

Fig 5.3 *NaCl rejection as a function of pH and TMP with* $[As(III)]_{initial}$ *= 300 ppb and* $[NaCl]_{initial}$ *= 10 g.L*$^{-1}$

These results confirmed that pH played an important role in As(III) rejection as observed in Fig 5.2. As(III) rejection increased sharply with increase of pH value from maximum 60% to 87% at pH7 and pH10, respectively. It was attributed to the electrostatic repulsion force between negative charges of the osm-ESPA membrane and arsenite anion ($H_2AsO_3^-$) at pH 10. Indeed, most of arsenite ions are in monovalent anion form at pH 10 (pKa = 9.1), while it is in neutral solute at pH 7 (see Fig 1.1 – Chapter 1). It led to a conclusion that As(III) rejection was affected by the charge of arsenite ions in the solution. Same tendency was observed in the study of *Urase et al., 1998* on As(III) rejection by nano-filtration. Observation in Fig 5.2 and Fig 5.3 indicated that the best compromise for As(III) rejection was obtained at pH10 and TMP = 24 bars. For this operating condition, the lowest permeate As(III) concentration (37 ppb) was obtained for a 300 ppb feed As(III) concentration. It led to the conclusion that as for a feed As(III) concentration of 300 ppb, the one-pass RO process with osm-ESPA membrane could not reject As(III) to meet the standard value (i.e. MCL = 10 ppb). Concerning NaCl rejection, it was quite stable with over 93%, regardless different pH and TMP values in the range of our study (Fig 5.3). In fact, salt passage is not affected by the trans-membrane pressure applied but by the salt concentration at the membrane surface [*Kucera, 2010*]. In our conditions, with a membrane that presents a high salt rejection rate, and for this concentration of NaCl which is quite low, no effect of TMP on NaCl rejection was observed.

Regarding permeate flux, Fig 5.4 showed influences of pH and TMP on the permeate fluxes, which were expressed as a function of recovery rate Y_{RO}, which was determined for batch-mode experiment by the equation 5-2:

$$Y_{RO}(\%) = \frac{V_p}{V_f} x100 \quad (5\text{-}2)$$

where:

- ✓ Y_{RO} : recovery rate (%);
- ✓ V_f : initial feed volume (V_f = 500 ml);
- ✓ V_p : cumulated permeate volume (ml).

As observed in this Fig 5.4, same decline trend of the permeate flux with increase of Y_{RO} was observed for all pH and TMP values. Two possibilities could explain the decline of permeate flux: (1) by increase of osmotic pressure inside the cell; and/or (2) by membrane fouling. To conclude on this point, permeability of the membrane was calculated (see chapter 2) by taking into account osmotic pressure in the cell. This osmotic pressure was calculated for each value of recovery, the salt concentration inside the cell being estimated by mass balance. As observed in Fig 5.5, permeability of the membrane at different pH values was quite stable, leading to the conclusion that membrane fouling did not occur in this case and the decline of the permeate flux was due to increase of osmotic pressure inside the cell .Slightly increases of permeability values at the end of the experiments were attributed to increase of solution temperatures (i.e. experiments were performed during the summer), which could decrease the viscosity of brackish solutions.

At the same TMP, it was found that permeate flux at pH7 was higher than the one at pH10. This observation was reinforced with higher value of apparent permeability at pH 7 in comparison with the one at pH 10 at the same TMP = 32 bars (Fig 5.5). Generally, RO flux was relatively constant over a range of pH, but it was reported that for some newer polyamide membranes, it is also a function of pH as its water transport coefficient (permeability) also varies with pH [*Kucera, 2010*]. So the dependence of the RO permeate flux on pH that was observed in the experiment can be linked to material of this osm-ESPA polyamide membrane.

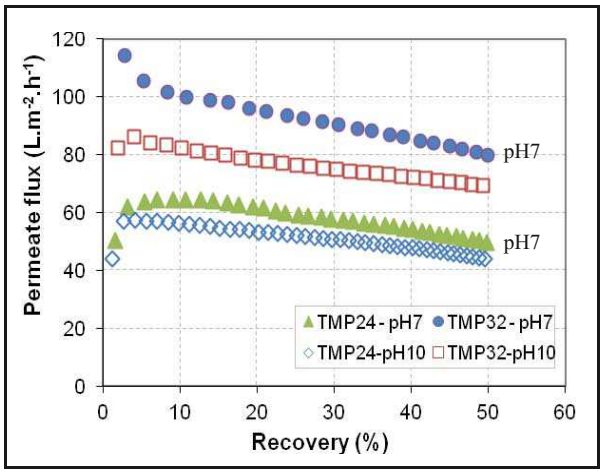

Fig 5.4 *Permeate fluxes as a function of Y_{RO} at different pH and TMP with $[As(III)]_{initial}$ = 300 ppb & $[NaCl]_{initial}$ = 10 g/L.*

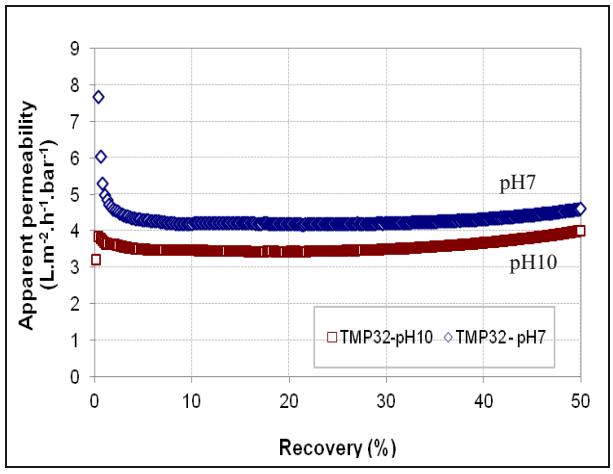

Fig 5.5 *Apparent permeability as a function of Y_{RO} at different pH and TMP with $[As(III)]_{initial}$ = 300 ppb; $[NaCl]_{initial}$ = 10 g/L*

❖ *Effect of As(III) concentration*

Feed concentration can also have influence on the RO performance. In order to test the As(III) rejection rate of the osm-ESPA membrane at different feed concentrations, a batch mode experiment was performed. As above-mentioned for the given RO membrane, feed As(III) concentration of 300 ppb was too high to meet the standard value in the permeate (in one-pass). As a consequence, the following experiment was started at a lower feed As(III) concentration of 107 ppb with 500 mL feed solution. Permeate was sampled after each 70 ml (i.e. minimum sample volume required for analysis of arsenic). By this way, at the end of the experiment, approximately 487 mL of permeate volume was collected, corresponding to a recovery rate of 97.4%. Retentate As(III) concentration (i.e. retentate available inside the reactor after each 70 ml permeate sampling) was calculated by the mass balance equation. In this calculation, quantity of As(III) deposited on the membrane surface (if any) was neglected what is quite consistent since the cell is continuously stirred. Both As(III) and NaCl rejection rates were estimated and presented in Fig 5.6, Fig 5.7, respectively.

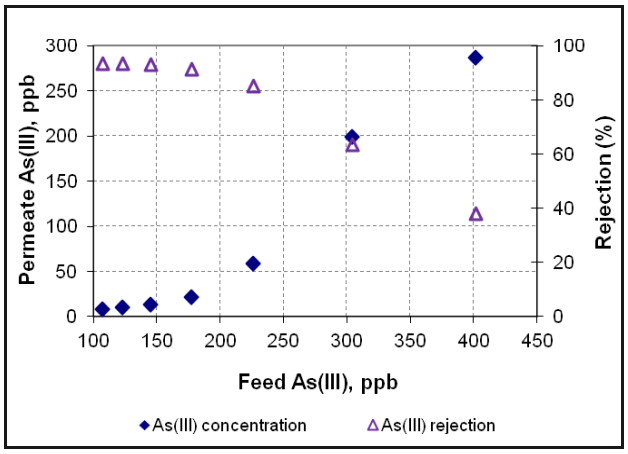

Fig 5.6 *As(III) rejection as a function of retentate concentration in the batch mode RO process ([As(III)]* $_{initial}$ *= 107 ppb; [NaCl]* $_{initial}$ *= 10 g.L*$^{-1}$*; pH 10; TMP = 24 bars)*

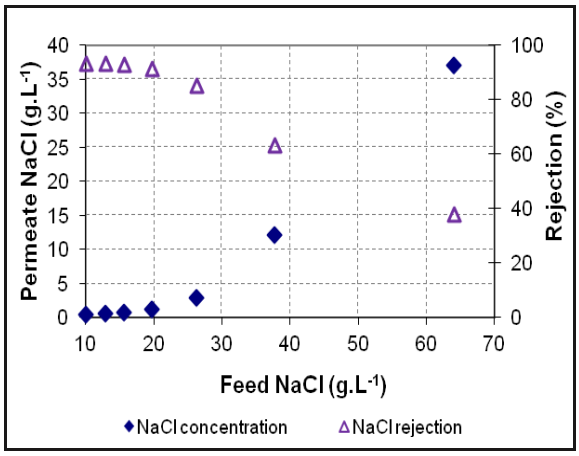

Fig 5.7 *NaCl rejection as a function of retentate concentration in the batch mode RO process ([As(III)]* $_{initial}$ *= 107 ppb; [NaCl]* $_{initial}$ *= 10 g.L*$^{-1}$*; pH 10; TMP = 24 bars)*

Effects of both retentate As(III) and NaCl concentrations were observed in Fig 5.6 and Fig 5.7, respectively. Same trend of decline for both As(III) and NaCl rejections was observed with increased retentate concentration. At the given operating condition (pH 10 and TMP = 24 bars), it was found that osm-ESPA membrane was able to treat maximum 123 ppb As(III) in solution to meet the standard value in the permeate (MCL = 10 ppb). However, this result should be considered in terms of variation of recovery rate since higher recovery applied will increase As(III) and NaCl concentrations at the membrane surface, leading to the decline of RO rejection rates. The following part of this chapter 5 will present influence of recovery on As(III) and NaCl rejection efficiencies for the osm-ESPA membrane.

Based on the volume and concentration of each permeate sample collected in the previous experiment, permeate As(III) and NaCl concentrations as well as its rejection rates as a function of recovery rates were calculated. These results were illustrated in Fig 5.8 and Fig 5.9.

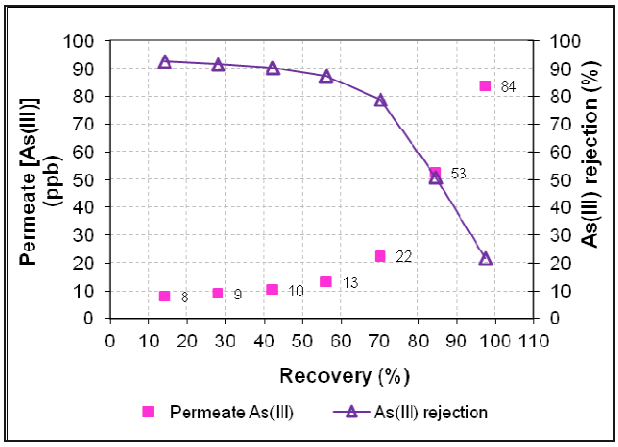

Fig 5.8 *Effect of recovery on As(III) rejection of batch mode RO process ([As(III)]* $_{initial}$ *= 107 ppb; [NaCl]* $_{initial}$ *= 10 g.L*$^{-1}$*; pH 10; TMP = 24 bars)*

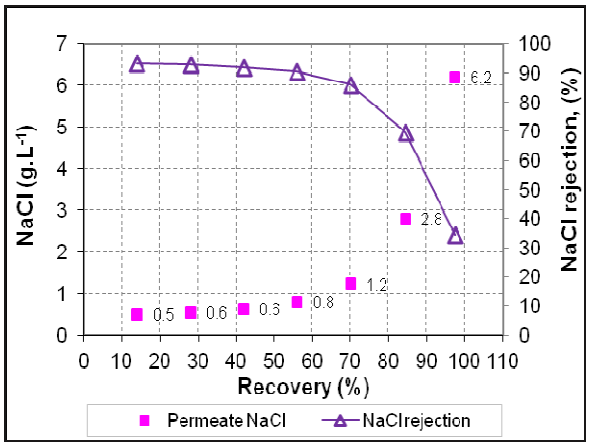

Fig 5.9 *Effect of recovery on NaCl rejection of batch mode RO process ([As(III)]* $_{initial}$ *= 107 ppb; [NaCl]* $_{initial}$ *= 10 g.L*$^{-1}$*; pH 10; TMP = 24 bars)*

By plotting the permeate As(III) concentration as a function of recovery as presented in Fig 5.8, it could be concluded that, with this osm-ESPA membrane, the RO process could treat 107 ppb As(III) in feed solution to meet the required standard (MCL = 10 ppb) at a recovery of Y_{RO} = 42%, equivalent to As(III) rejection rate of 90%. Meanwhile, same tendency was observed in Fig 5.9 with decline of NaCl rejection as increase of recovery. At initial NaCl concentration in feed solution of 10 g.L^{-1}, the osm-ESPA membrane could reach recovery at 70% to remove NaCl in the solution to meet Vietnamese standard for drinking water (i.e. equivalent to Ec = 2500 µS.cm^{-1}). In summary, with osm-ESPA membrane at the given operating condition (feed [As(III)] $_{initial}$ = 107 ppb, [NaCl] $_{initial}$ = 10 g.L^{-1}, pH 10, TMP = 24 bars), operation recovery of Y_{RO} = 42% was the maximum value possible to meet the standard in permeate.

V.2.1.2 Effect of organic matter on the RO performance for As(III) removal

As organic matter is normally available in the groundwater, this part studied on effect of feed As(III) concentration on RO performance with presence of organic matter in the feed solution. In this case, humid acid sodium salt (HASS) was used with its characteristic presented in Table 4.3 (chapter 4). Similar experiment was conducted with presence of organic matter by adding 20 mg.L^{-1} HASS (equivalent TOC = 7.5 mg/L) into the feed solution ([As(III)]$_{initial}$ = 104 ppb; [NaCl]$_{initial}$ = 10 g/L). Permeate were sample after each 100 ml (i.e. sample volume required for analysis of arsenic and TOC) until total permeate volume of 400 mL was

collected, equivalent to a recovery of 80%. Permeate As(III) and NaCl concentrations as well as rejection rates with presence of HASS as a function of recovery values were calculated by the same method as in section V.2.1. These results were compared with the one without presence of HASS (i.e section V.2.1) to see if the RO performance was affected by presence of organic matter. The comparison between the two cases was presented in Fig 5.10 and Fig 5.11.

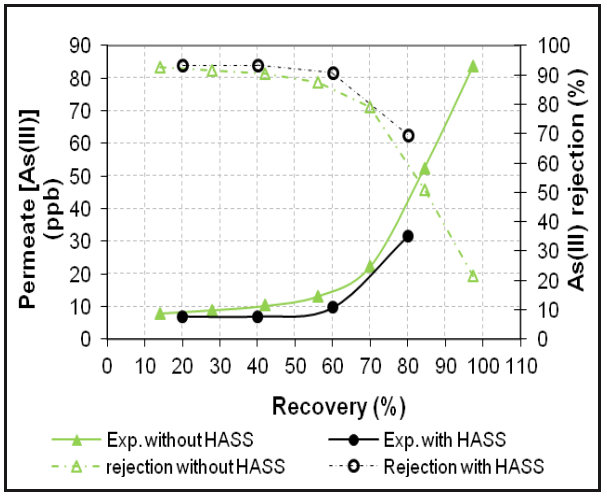

Fig 5.10 *The RO performance for As(III) removal with and without presence of HASS ($[As(III)]_{initial}$ = 104 ppb; $[NaCl]_{initial}$ = 10 g/L; $[HASS]_{initial}$ = 20 mg/L; pH 10; TMP = 24 bar)*

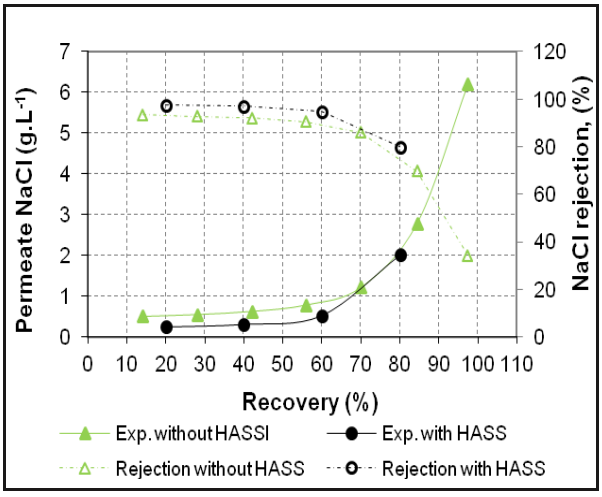

Fig 5.11 *The RO performance for NaCl removal with and without presence of HASS ($[As(III)]_{initial}$ = 104 ppb; $[NaCl]_{initial}$ = 10 g/L; $[HASS]_{initial}$ = 20 mg/L; pH 10; TMP = 24 bar)*

With the presence of organic matter (HASS) in the feed solution, same tendency as the previous experiment (without HASS) was observed with decline of As(III) rejection at higher As(III) concentration (also higher recovery). The As(III) rejections, however, were always higher than the one in case of no HASS. Regarding the recovery, permeate As(III) concentration at 10 ppb was obtained at higher recovery of 60% with presence of organic matter in comparison with 42% as in case of no organic matter (Fig 5.10). It revealed that presence of organic matter could increase the RO performance in terms of As(III) rejection for short-term experiments. It was attributed to association of arsenic with organic matter to create a hypothetical colloidal arsenic or organic/arsenic complex with larger size, which is better to be retained in the retentate side. It was reported in some studies [*Brandhuber and Amy, 2001*] that approximately 40 – 60% of the total arsenic in the waters was associated with organic matter in a size range between 500 and 10000 Daltons. Similar influence of organic matter on NaCl rejection was observed in Fig 5.11.

Regarding organic matter rejection, high TOC rejection of 94.6% was achieved with almost a same permeate TOC concentration at each recovery rate as observed in Fig 5.12. This indicated that in the range of the study, RO performance (in terms of TOC rejection) is independent of organic concentration. However, high feed organic concentration or longer term operation could create fouling or adsorption on the membrane surface and lead to decline of the RO permeate flux obtained.

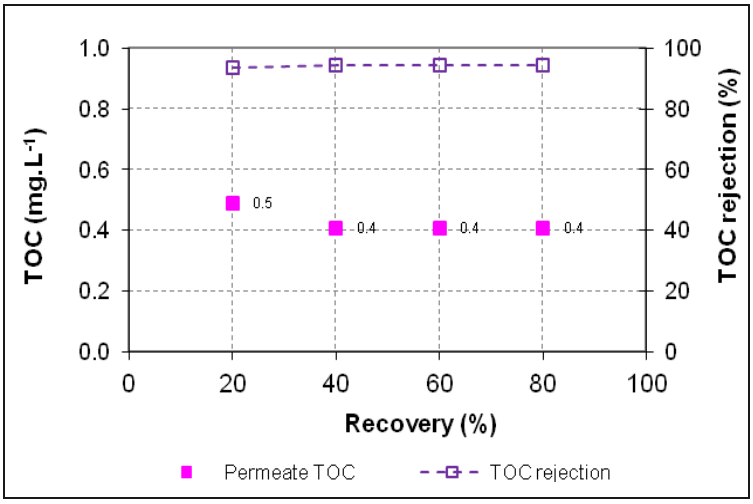

Fig 5.12 *Effect of recovery on batch mode RO performance with presence of HASS (osm-ESPA membrane, $[As(III)]_{initial}$ = 104 ppb; $[NaCl]_{initial}$ = 10 $g.L^{-1}$; $[HASS]_{initial}$ = 20 $mg.L^{-1}$, pH 10, TMP = 24 bars)*

Fig 5.13 showed variations of the RO permeate fluxes as a function of recovery with and without organic matter. Below a recovery of 50%, the presence of HASS did not affect significantly the permeate flux. For higher values of the recovery, the permeate flux appeared to decrease when HASS was added in the feed. The difference between permeate flux with and without HASS increased with the recovery. At the same maximum value of recovery (i.e. Y_{RO} = 80%), permeate flux declines of 67.6% and 62.3% were observed with and without HASS respectively. It was attributed to presence of HASS which created membrane fouling as observed in many published studies. In order to determine if any deposits of feed components on the membrane surface occurred, both SEM and EDS analyses were conducted. This will be presented in the next section.

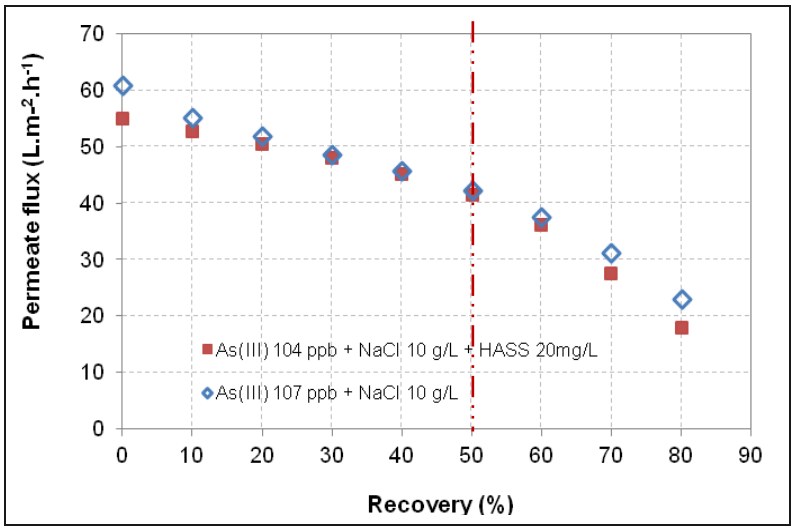

Fig 5.13 *Variation of RO permeate fluxes with and without presence of HASS as a function of recovery (osm-ESPA membrane, pH 10, TMP = 24 bars)*

In summary, on the basis of lab scale and short-term experiments, presence of organic matter in the feed solution could increase the RO performance, in terms of As(III) and NaCl rejections. In case of 100 ppb As(III) removal, higher recovery of 60% with the presence of organic matter in comparison with 42% in case no organic matter could be fixed to meet the standard in the permeate. However, an effect of feed organic matter on the RO permeate flux was found and need to be taken into consideration for recoveries higher than 50%.

V.2.1.3 Observation of membrane surface by SEM and EDS analyses

In order to determine whether any deposits of As(III), NaCl and HASS occurred, the RO membrane surface was observed and analyzed by both SEM and EDS analyses. Fig 5.14a and Fig 5.15a presented surface of the osm-ESPA membrane after the experiments without and with presence of HASS, respectively. As observed, the membrane surfaces were partially covered by non-uniform deposits. However, this phenomenon seems to be more significant in case of feed solution containing HASS, where larger areas of fouling appear on the membrane surface. Fig 5.14b and Fig 5.15b presented membrane surfaces at a larger magnification to show availability of some crystals. Composition of these crystals was analyzed with EDS probe as presented in Fig 5.16 – Fig 5.21. It is worth to noting that, except for its origin from

organics, some components as C, O and S also represent for basic material of polyamide membrane.

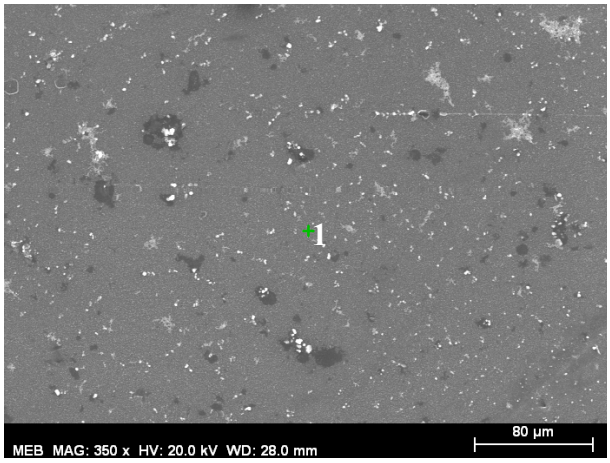

Fig 5.14a *Osm-ESPA membrane surface after the experiment without presence of HASS at pH 10, TMP = 24 bars (x 350)*

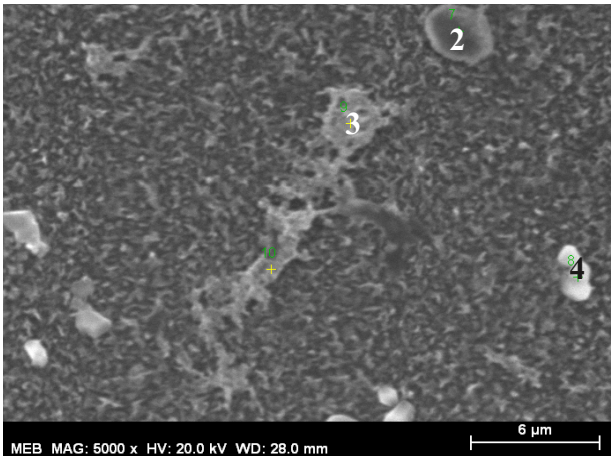

Fig 5.14b *Osm-ESPA membrane surface after the experiment without presence of HASS at pH 10, TMP = 24 bars (x 5000)*

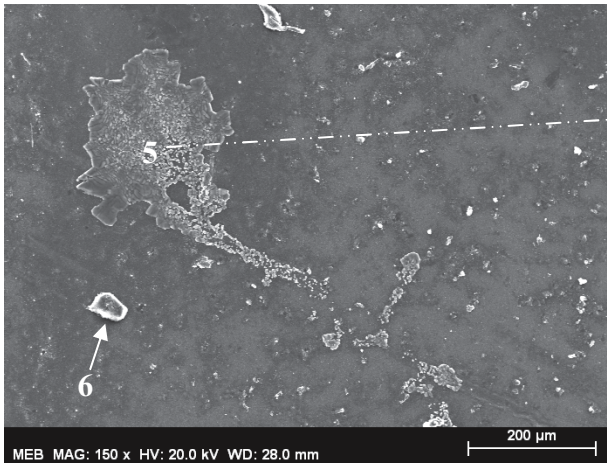

Fig 5.15a *Osm-ESPA membrane surface after the experiment with presence of HASS at pH 10, TMP = 24 bars (x 150)*

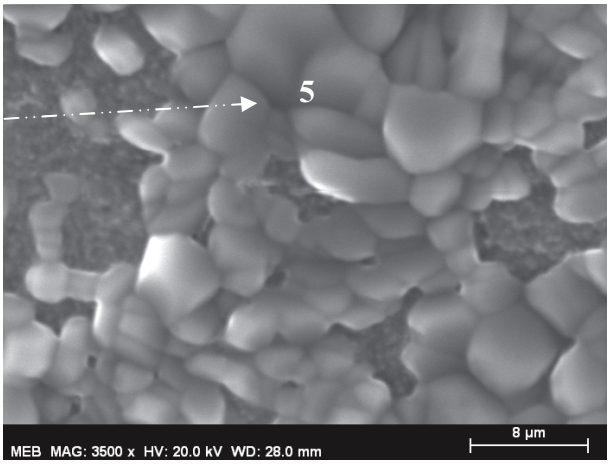

Fig 5.15b *Osm-ESPA membrane surface at larger magnification after the experiment with presence of HASS at pH 10, TMP = 24 bars (x 3500)*

EDS analysis proved that all crystals (points 4 and 6) and scale (points 2 - 3 and 5) on the membrane surface could be identified as NaCl deposition. Presence of Fe was also detected on the membrane surface (point 1). Its source was determined to originate from oxidation of the stirrer which was used for mixing inside the RO cell. Presence of As(III) was also detected at some points on the membrane surface (points 1 – 2 and 3), but in a small extent. However, As(III) deposition between two different cases (with and without presence of HASS) was still unclear and needed to be further identified.

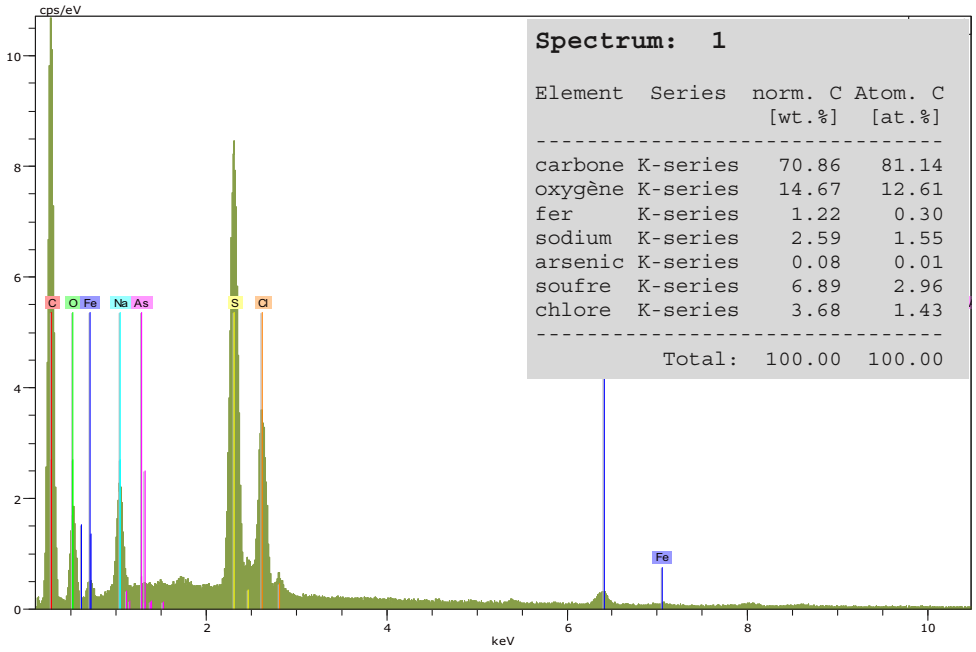

Fig 5.16 *EDS analysis of membrane surface at point 1 in Fig 5.14a after filtration without presence of HASS ($[As(III)]_{initial}$ = 107 ppb; $[NaCl]_{initial}$ = 10 $g.L^{-1}$; pH 10, TMP = 24 bars)*

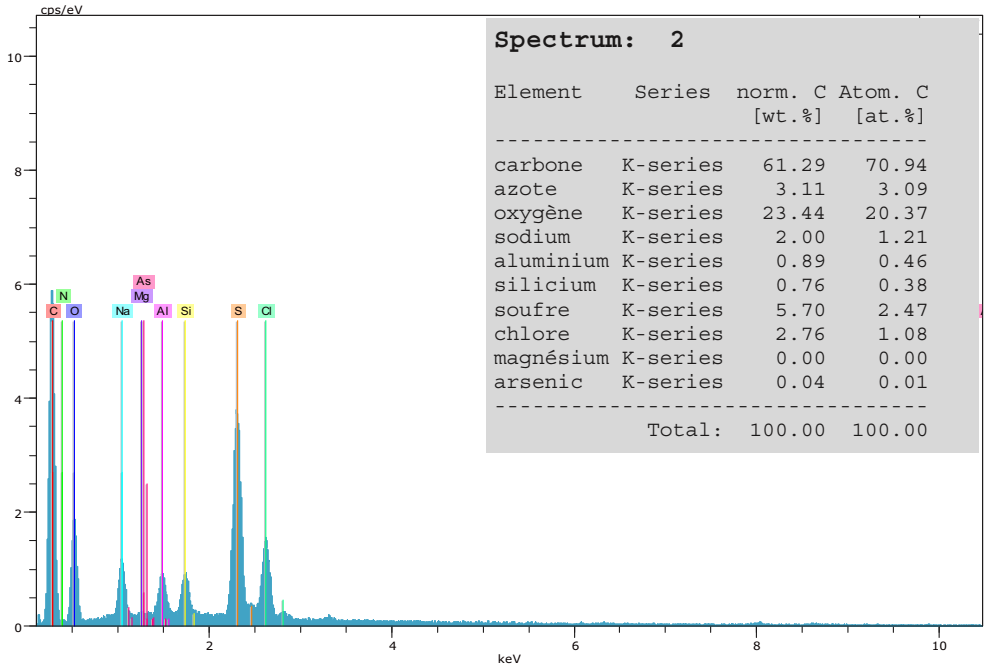

Fig 5.17 *EDS analysis of the deposit on the membrane surface at point 2 in Fig 5.14b after filtration without presence of HASS ($[As(III)]_{initial}$ = 107 ppb; $[NaCl]_{initial}$ = 10 $g.L^{-1}$; pH 10, TMP = 24 bars)*

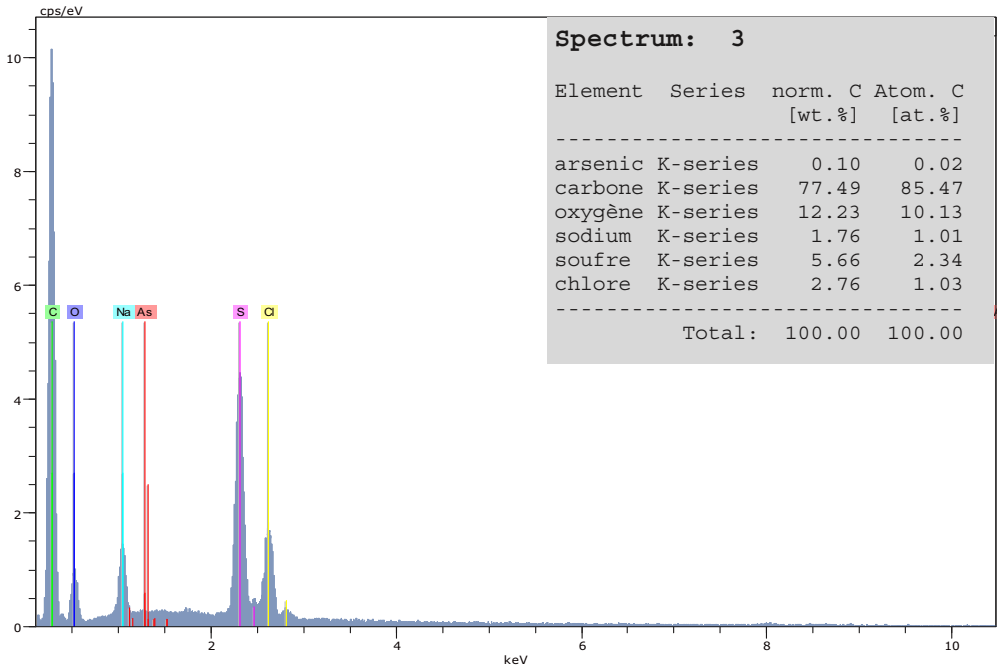

Fig 5.18 *EDS analysis of the deposit on the membrane surface at point 3 – Fig 5.14b after filtration without presence of HASS ($[As(III)]_{initial}$ = 107 ppb; $[NaCl]_{initial}$ = 10 g.L^{-1}; pH 10, TMP = 24 bars)*

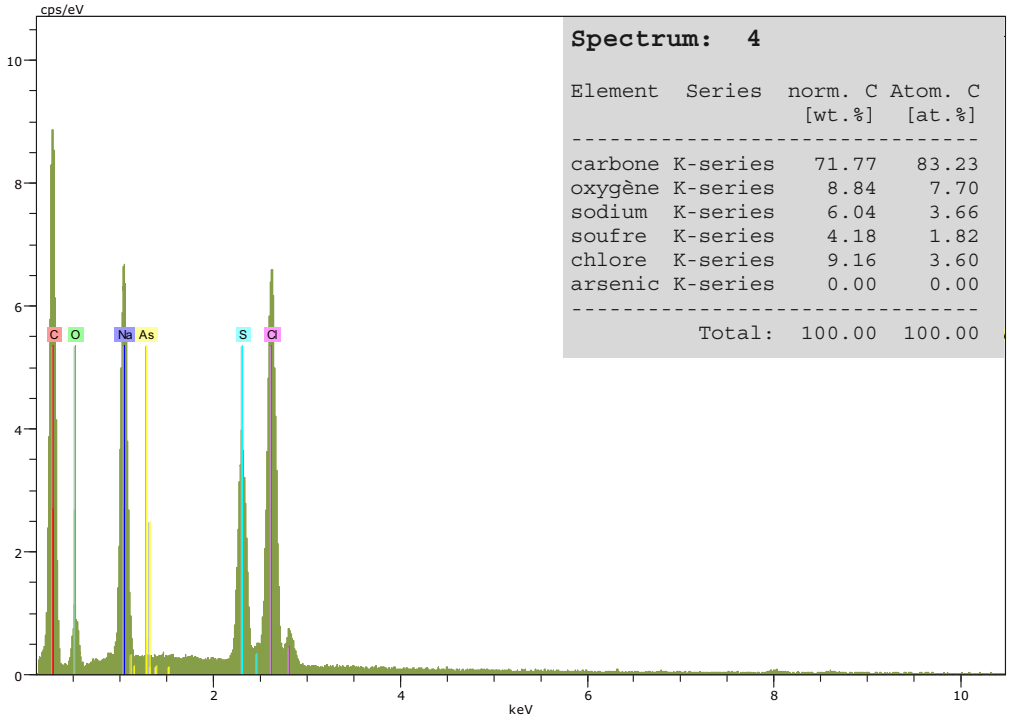

Fig 5.19 *EDS analysis of the deposit on the membrane surface at point 4 – Fig 5.14b after filtration without presence of HASS ($[As(III)]_{initial}$ = 107 ppb; $[NaCl]_{initial}$ = 10 g.L^{-1}; pH 10, TMP = 24 bars)*

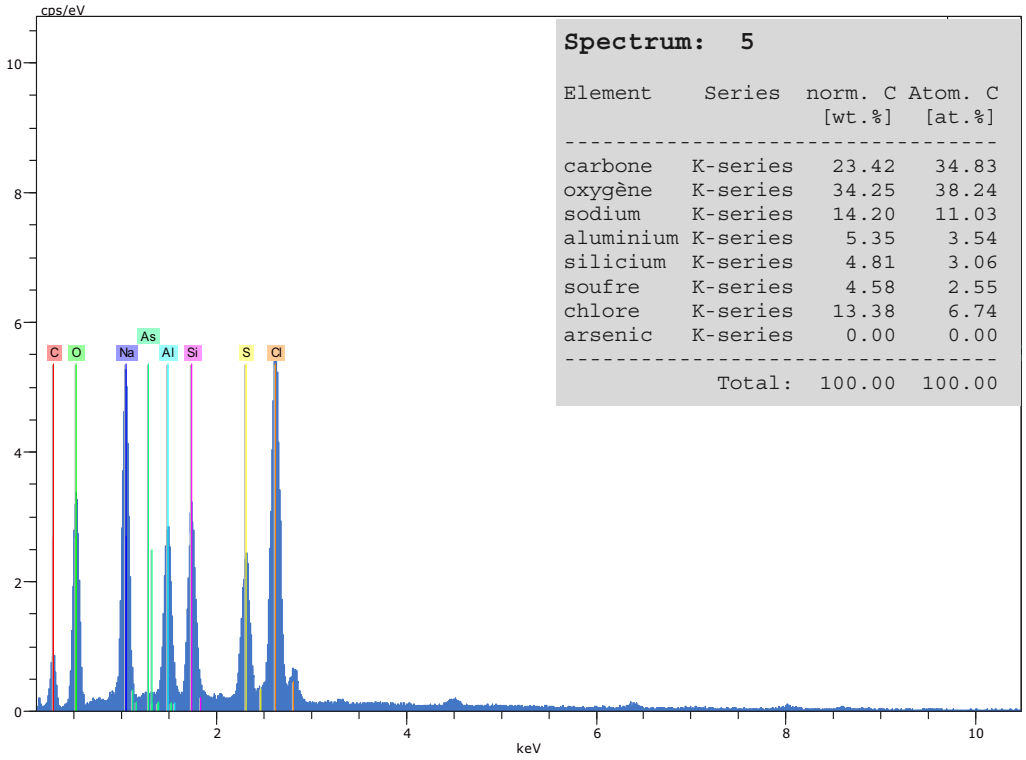

Fig 5.20 *EDS analysis of the membrane surface at point 5 - Fig 5.15a after filtration with presence of HASS*
($[As(III)]_{initial}$ = 104 ppb; $[NaCl]_{initial}$ = 10 $g.L^{-1}$; $[HASS]_{initial}$ = 20 $mg.L^{-1}$, pH 10, TMP = 24 bars)

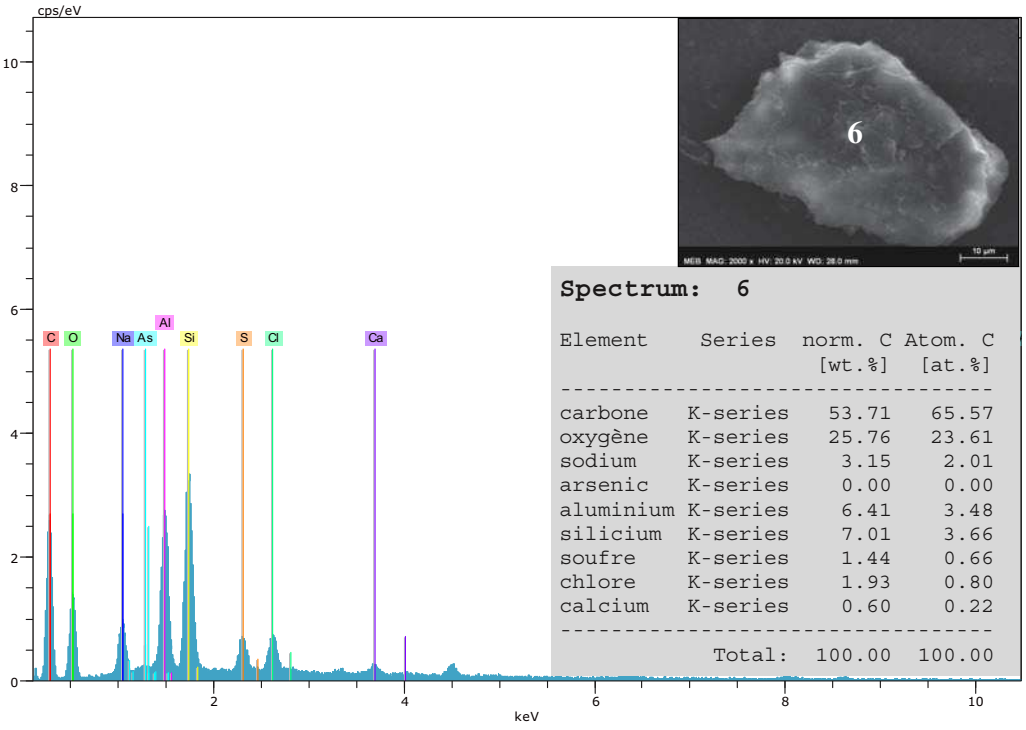

Fig 5.21 *EDS analysis of the deposit on the membrane surface at point 6 – Fig 5.15a after filtration with presence of HASS*
($[As(III)]_{initial}$ = 104 ppb; $[NaCl]_{initial}$ = 10 $g.L^{-1}$; $[HASS]_{initial}$ = 20 $mg.L^{-1}$, pH 10, TMP = 24 bars)

In order to identify the difference of As(III) deposition on the membrane surface in case without and with presence of HASS, two other samples of the tested membranes were investigated. Fig 5.22a and Fig 5.22b illustrated the surface of these two membrane samples after the filtrations without and with presence of organic matter, respectively. Similar to the previous membrane sample, presence of crystals could be also observed on the membrane surface in the two cases. However with presence of organic, the deposited crystals were covered by a layer of organic matter (Fig 5.22b). This observation could lead to hypothetic deposition of solutes on the membrane surface with first precipitation of NaCl and/or a few As(III), followed by deposit of organic matter. With presence of organic, more As(III) deposited on the membrane surface was observed due to adsorption. This phenomenon was confirmed by EDS analyses on the membrane surface (not on the crystal) at point 7 (without presence of HASS) and point 8 (with presence of HASS) showing that much higher As(III) deposit was found at the point 8. These EDS results were presented in Fig 5.23 and Fig 5.24.

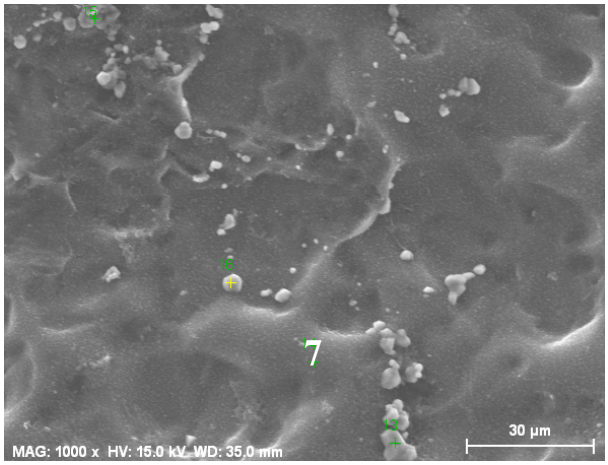

Fig 5.22a *The membrane surface after the experiment without presence of organic matter at pH 10, TMP = 24 bars (x 1000)*

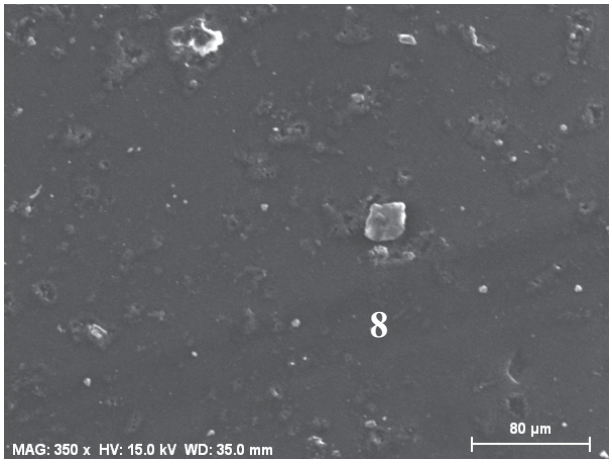

Fig 5.22b *The membrane surface after the experiment with presence of organic matter at pH 10, TMP = 24 bars (x 1000)*

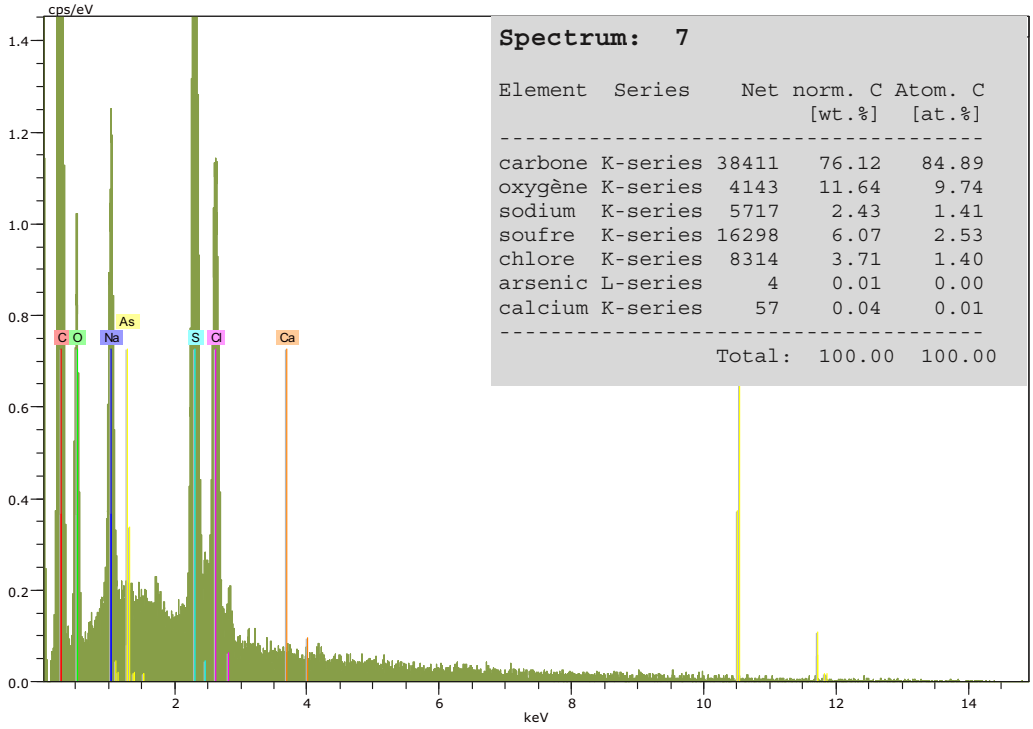

Fig 5.23 *EDS analysis of the membrane surface at point 7 – Fig 5.22a after the filtration without presence of HASS*
($[As(III)]_{initial}$ = 107 ppb; $[NaCl]_{initial}$ = 10 $g.L^{-1}$; pH 10, TMP = 24 bars)

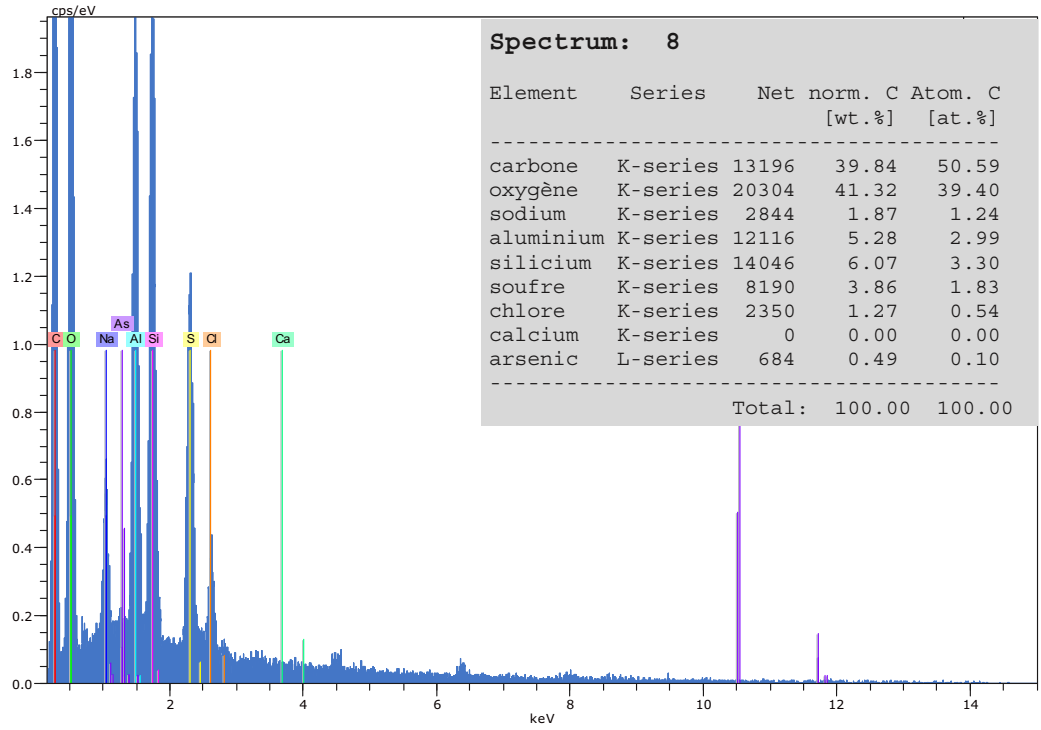

Fig 5.24 EDS analysis of the membrane surface at point 8 – Fig 5.22b after the filtration with presence of HASS
($[As(III)]_{initial}$ = 104 ppb; $[NaCl]_{initial}$ = 10 $g.L^{-1}$; $[HASS]_{initial}$ = 20 $mg.L^{-1}$, pH 10, TMP = 24 bars)

V.2.1.4 Summary

In this part, some preliminary RO batch-mode experiments for direct removal of As(III) contaminated in brackish ground water were performed. Influences of the operating parameters such as pH, trans-membrane pressure, feed concentration and feed composition (presence of organics) were investigated. These results were summarized in Table 5.1.

Table 5.1 *Influence of the operating parameters on the batch-mode RO performance.*

Parameters	Flux	As(III) rejection	NaCl rejection
pH	Effect	Strong effect	No effect
TMP	Strong effect	Unclear	No effect
Feed concentration	Effect	Effect	Effect
Presence of organics	Effect	Effect	Effect

Regarding possible membrane fouling, observations and SEM-EDS analysis of deposit composition were also performed. The results showed that membrane fouling occurred with primary presence of NaCl crystals on the membrane surface. Deposit of As(III) on the membrane surface was also detected , but in a small extent. However, this phenomenon became clearer with presence of organic matter. Stages of hypothetic deposition on the membrane surface was presumed and demonstrated in the Fig 5.25.

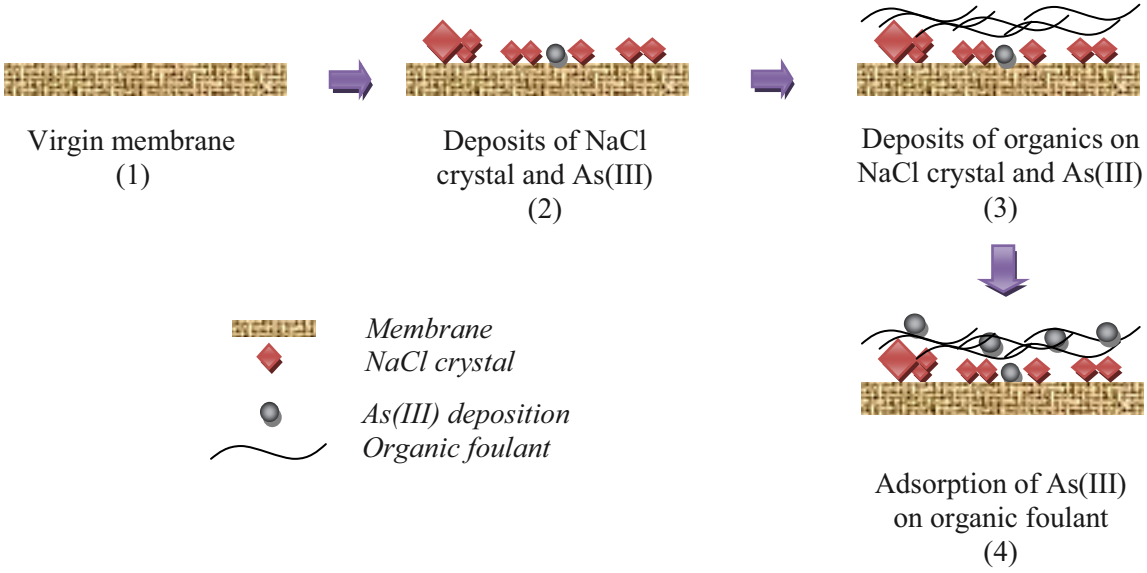

Fig 5.25 *Stages of solute deposition on the membrane surface.*

As above mentioned, in this study, an average recovery rate of 42% and 56% was respectively obtained in case without and with presence of organic matter to treat solutions containing 100 ppbAs(III) and 10 $g.L^{-1}$ NaCl. It also meant that a significant quantity of RO retentate at higher As(III) and NaCl concentrations would be produced. And further treatment for this stream should be seriously paid into attention. Solidification/stabilization method to solidify this stream before dumping was applied in the practice but, certainly, it required high treatment cost [*Sullivan et al., 2010*]. In order to reduce the cost for retentate treatment, a retentate volume reduction should be conducted. As presented in the Chapter 4, VMD performance was independent of feed As(III) concentration (i.e. up to 5000 ppb). It would lead to a proposition to use VMD as a further treatment step for the RO retentate volume reduction. This integrated process by coupling of RO and VMD processes was expected to provide a higher global recovery factor of clean water and lead toward zero liquid discharge treatment option. Further treatment of RO retentate by using VMD process as well as calculation of the global recovery will be presented in the next sections.

V.2.2 Hybrid process by coupling of RO and VMD for direct As(III) removal

V.2.2.1 VMD performance for a very high concentrated stream

This part focused on studying performance of the VMD process to treat the RO retentate. In order to test applicability of the VMD for a very high concentrated stream, and for different compositions of waters: three different feed solutions, namely concentrate A, concentrate B and concentrate C, were prepared and tested (see compositions listed in Table 5.2). It was worth noting that choice of NaCl concentration of 300 $g.L^{-1}$ was the maximum mixed salt concentration found in seawater, which used to be tested for VMD by *Mericq et al., 2010*; while As(III) concentration of 7000 ppb was chosen corresponding to initial feed As(III) concentration in resource of 1750 ppb (estimated by a concentration factor of 4), which was still in range of 1 – 3050 ppb of arsenic contamination in some places in the North of Vietnam [*Berg et al., 2001*].

- ✓ **Concentrate A**: Feed solution with As(III) only
- ✓ **Concentrate B**: Feed solution with As(III) + NaCl;
- ✓ **Concentrate C**: Feed solution with As(III) + NaCl + HASS.

Table 5.2 *Compositions of the three different solutions.*

Name	Compositions	As(III) (ppb)	NaCl (g/L)	HASS (mg/L)	pH	Ec mS/cm	TOC mg/L
Concentrate A	As(III) only	7000	0	0	6.8	-	0
Concentrate B	As(III) + NaCl	7000	300	0	6.8	230	0
Concentrate C	As(III) + NaCl + HASS	7000	300	165	6.0	247	50

As in Chapter 4, these VMD tests were conducted at the same operating conditions (Fluoropore membrane; $T_f = 40^0C$; Pp = 4500 Pa, Re = 3400). Experimental results showing the VMD performance are presented in the following section.

Regarding rejection efficiencies of the VMD, high NaCl rejection of 99.9%, for both Concentrate B and Concentrate C, were achieved with very low permeate conductivity (Ec = 20 µS/cm). For Concentrate C, high TOC rejection of 98.8% was also achieved with low permeate TOC of 0.6 $mg.L^{-1}$. As(III) concentration in permeate was only determined for Concentrate C. For this case, As(III) concentration of 8 ppb was found in the permeate, this value is still lower than the required standard (MCL = 10 ppb).

Regarding permeate flux achievement, operating conditions and corresponding permeate flux obtained from each feed solution were presented in Figs 5.26 – 5.28. Meanwhile, by applying the same analysis method as presented in the previous part (i.e. section IV.2.3.1), average normalized permeate flux and the corresponding apparent Knudsen permeability of the membrane for the three feed solutions were calculated versus time and used for comparing the three cases. These results are summarized and presented in Fig 5.29a and Fig 5.29b, respectively.

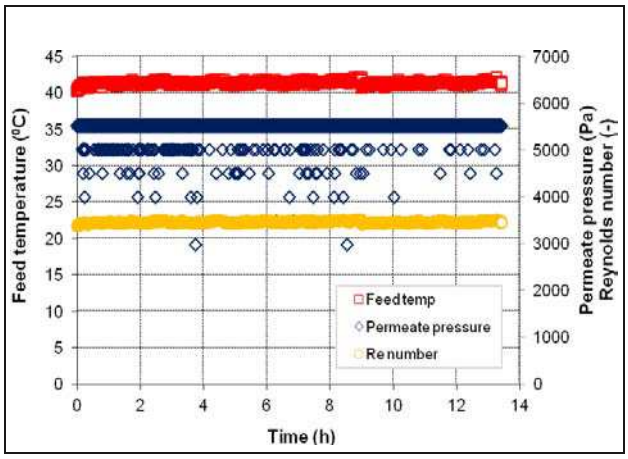

Fig 5.26a *Operating conditions for Concentrate A (Fluoropore; [As(III)] = 7000 ppb; [NaCl] = 0 g/L; T_f = 40°C; Pp = 4500 Pa; Re = 3400)*

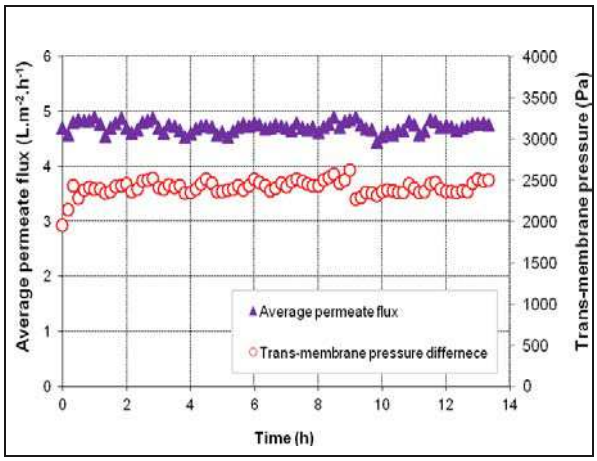

Fig 5.26b *Average permeate flux and corresponding trans-membrane pressure for Concentrate A*

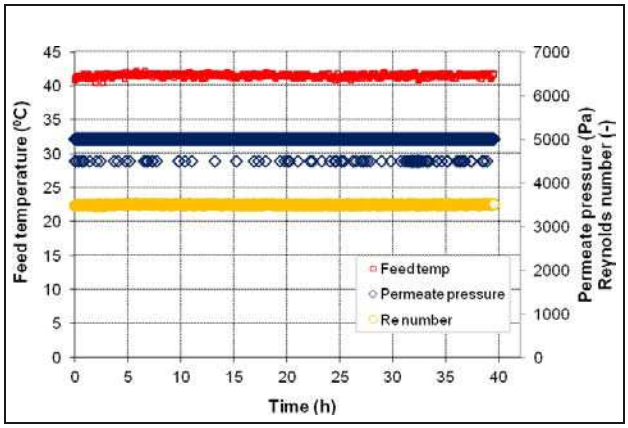

Fig 5.27a *Operating conditions for Concentrate B (Fluoropore; [As(III)] = 7000 ppb; [NaCl] = 300 g/L; T_f = 40°C; Pp = 4500 Pa; Re = 3400)*

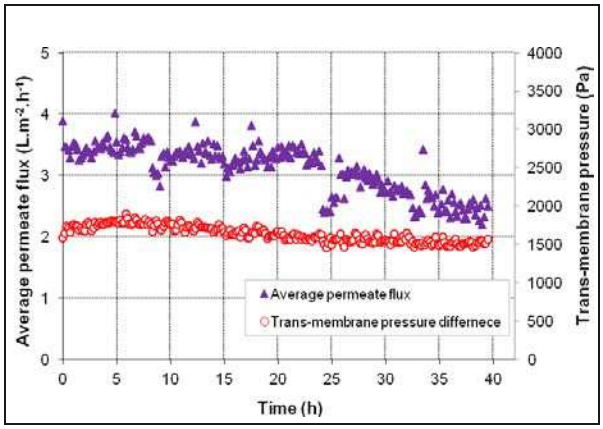

Fig 5.27b *Average permeate flux and corresponding trans-membrane pressure for Concentrate B*

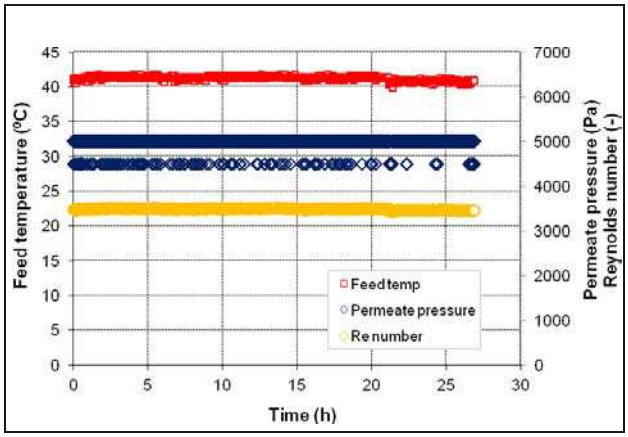

Fig 5.28a *Operating conditions for Concentrate C (Fluoropore; [As(III)] = 7000 ppb; [NaCl] = 300 g/L; [HASS] = 165 mg/L; T_f = 40°C; Pp = 4500 Pa; Re = 3400)*

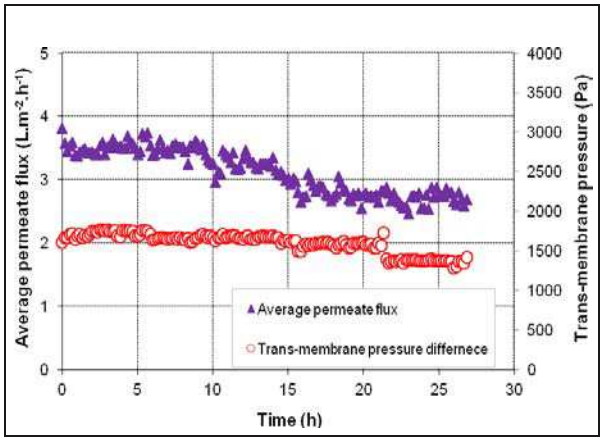

Fig 5.28b *Average permeate flux and corresponding trans-membrane pressure for Concentrate C*

Fig 5.26b showed stability of the permeate flux in corresponding with the Concentrate A during operating time of 13 hours: the VMD permeate flux seems to be not affected by presence of As(III) in the feed solution, even at a very high level (i.e. 7000 ppb) during a long-term operation. In comparison with average permeate flux (i.e. 5.0 $kg.m^{-2}.h^{-1}$) obtained in Chapter 4, an average permeate flux of 4.8 $kg.m^{-2}.h^{-1}$ confirmed independence of VMD permeate flux to feed As(III) concentration, even at high concentration within a long-term duration (i.e 13 hours).

On the contrary, decline of the permeate flux with presence of NaCl (Concentrate B) and with presences of both NaCl and HASS (Concentrate C) were observed in Fig 5.27b and Fig 5.28b, respectively. For these two experiments with the same salinity ([NaCl] = 300 $g.L^{-1}$) and within the same time scale (t = 26.8 hours), decline of permeate flux was more significant in case with presence of HASS (i.e. Concentrate C) with 29.5% of permeate flux decline in comparison with 21.3% in case of no HASS (Fig 5.29a). These decreases corresponded to 19.2% and 18.7% decline of apparent Knudsen permeabilities (K_M) for the Concentrates C and B, respectively that can indicate occurrence of membrane fouling. These observed declines of the apparent Knudsen permeability could thus be mainly attributed to the modification of mass transfer properties by deposits of NaCl or HASS. Theoretically, NaCl precipitation and HASS deposit could partially or totally block the membrane pores, and as the result, the membrane area available for the liquid-vapour interface decreased. Besides that, these deposits could also form scale on the membrane surface which increased the mass transfer resistance in the feed solution. However for these long-term experiments, two observations from Fig 5.29b could be taken into account:

- Decline of the apparent Knudsen permeability K_M was significant with 19.2% and 18.7% for Concentrate C and Concentrate B, respectively. It meant that fouling effects were measurable in these cases;

- The K_M decline was quite close for both Concentrate B and Concentrate C. It meant that fouling was mainly due to presence of NaCl in the feed solution and thus to scaling effect.

Based on these observations, it could lead to a conclusion that the deposit of HASS has a negligible effect on the permeate flux.

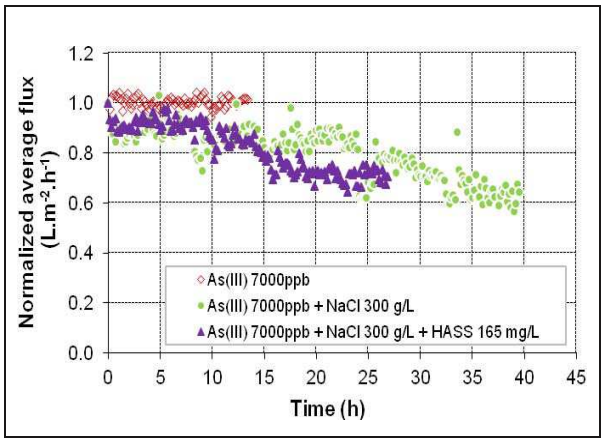

Fig 5.29a *Normalized permeate flux vs.time for three feed solutions: Concentrates A – B and C*

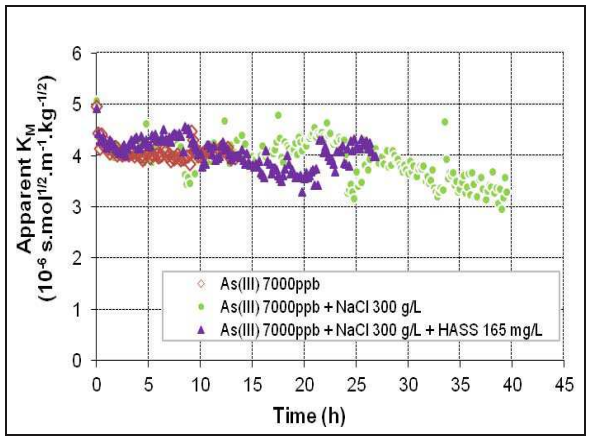

5.29b *Apparent Knudsen permeability vs. time for three feed solutions: Concentrates A – B and C*

Observations of the fouled membrane (after drying) with SEM and EDS analyses allowed to visualise the membrane surface and to identify some deposited compositions. First observation focused on HASS to check if HASS was deposited on the VMD. Fig 5.30 illustrated sample of a tested membrane after experiment with Concentrate C. As observed in this figure, the used membrane could be divided into two parts: (1) dead-zone parts (i.e. considered as the parts at two edges of the membrane, where there was no water-flow or water flowed at a very low velocity; and (2) working-zone part. As mentioned in Table 4.3 – Chapter 4, the HASS component contains maximum 12% water insoluble content of dry basic. That explained the presence of some visible non-soluble HASS component in the feed solution. However, it was interesting to see the difference between the dead-zone and the working-zone in terms of deposit of HASS. Different from the RO membrane, where organic matter was able to deposit on the RO membrane surface, no or very little deposit of organic matter on hydrophobic membrane (in the working-zone) was observed in Fig 5.30 , even at a very high feed HASS concentration (i.e. [HASS] = 165 $mg.L^{-1}$). It was attributed to hydrophobicity of the employed membrane to prevent water intrusion inside the pores. Furthermore, due to low trans-membrane pressure applied, the transport by convection of the organic matter (if any) towards the membrane surface was reduced, and the turbulent water flow allowed to entrain the non-soluble HASS.

Fig 5.30 *Membrane sample after experiment with Concentrate C [As(III)] = 7000 ppb, [NaCl] = 300 g.L^{-1}, HASS = 165 mg/L or TOC = 50 mg.L^{-1}).*

Fig 5.31a showed pictures of the membrane surface and its dead-zone and working-zone parts while Fig 5.31b, Fig 5.31c, and Fig 5.31d only illustrated some observations on the working-zone of the employed membrane. Crystals of NaCl were found on the both parts but at a higher density in the dead-zone part while HASS deposit was mainly gathered on the dead-zone area. EDS analyses at several points on the membrane surface to determine its compositions were presented in Fig 5.32 – Fig 5.37.

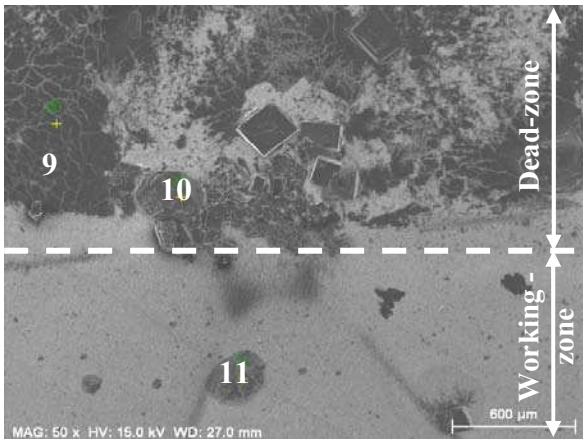

Fig 5.31a *Membrane surface after experiment with Concentrate C (x 50)*

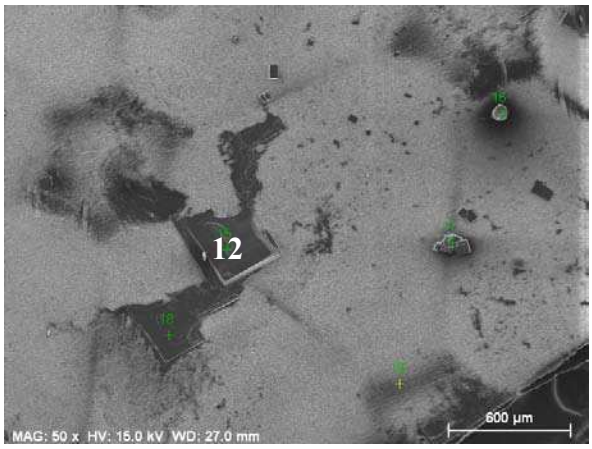

Fig 5.31b *NaCl crystal on membrane surface after experiment with Concentrate C (x 50)*

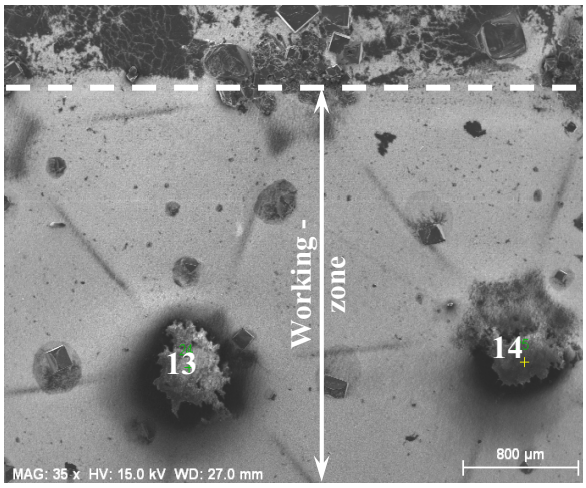

Fig 5.31c *Working zone of membrane surface after experiment with Concentrate C (x 35)*

Fig 5.31d *NaCl crystal on membrane surface after experiment with Concentrate C (x 200)*

Analyses with EDS probe at point No.9 and No.10 within the dead-zone are presented in the Fig 5.32 and Fig 5.33, respectively. Except for carbon, oxygen and fluor as the main material of hydrophobic membrane production, presence of sodium and chloride proved the precipitation of NaCl crystals on the dead-zone of membrane surface. Presence of organic matter was observed as illustrated in Fig 5.30 and Fig 5.31a but its composition was hard to determine by EDS probe since it was impossible to distinguish sources of carbon and sodium. Besides that, no deposit of As(III) was found on this area.

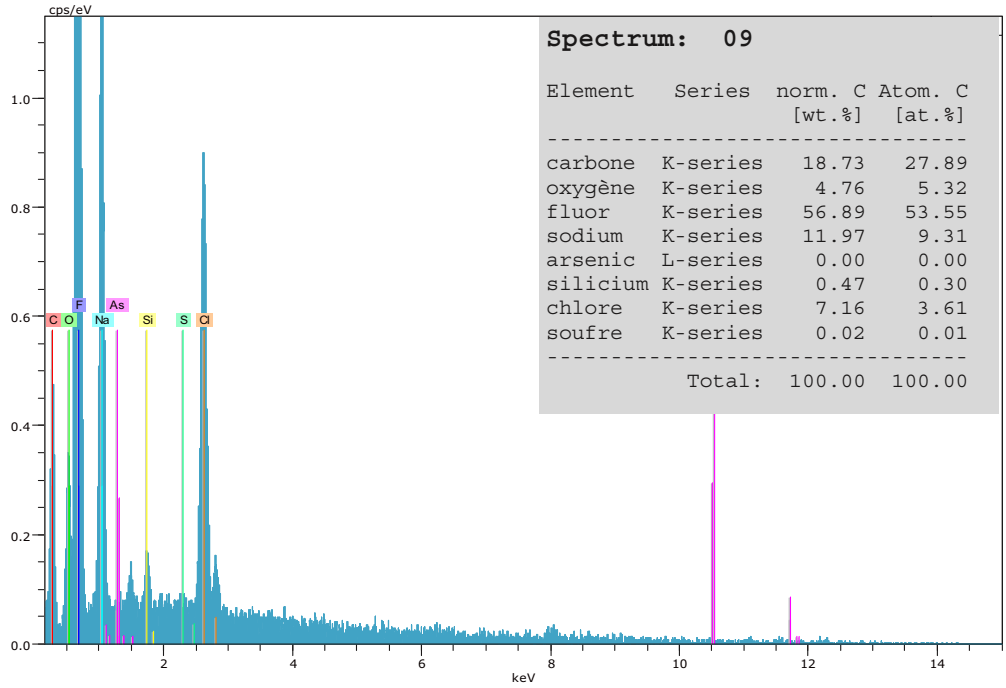

Fig 5.32 *EDS analysis of the dead-zone on the membrane surface at point 9 – Fig 5.31a*

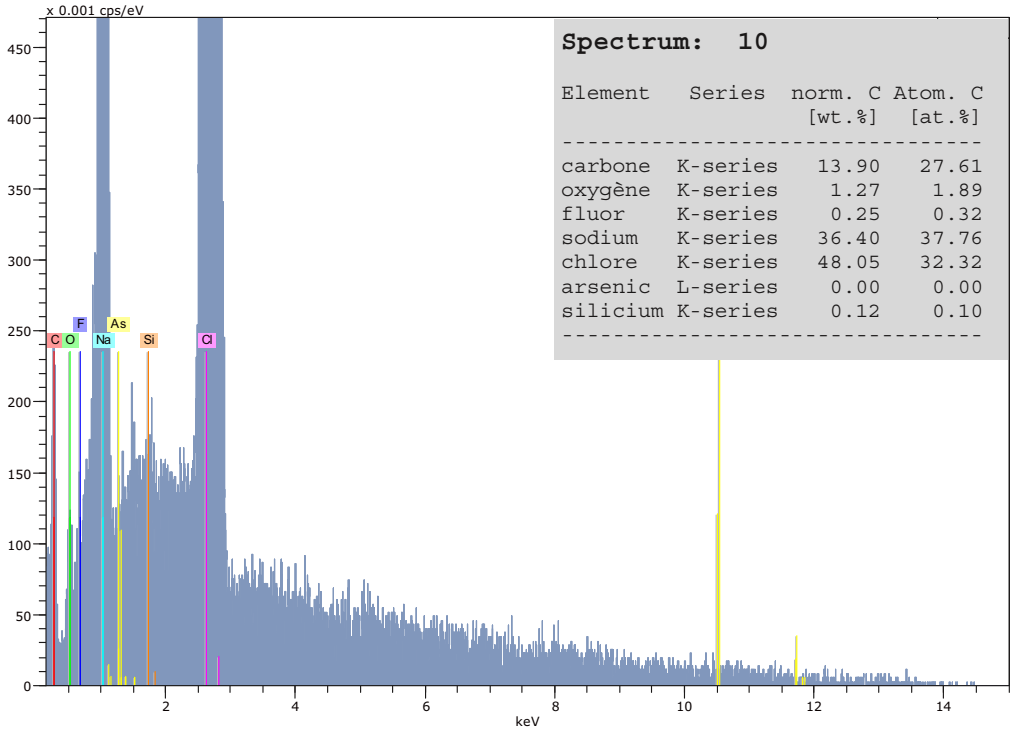

Fig 5.33 *EDS analysis of the dead-zone on the membrane surface at point 10 – Fig 5.31a*

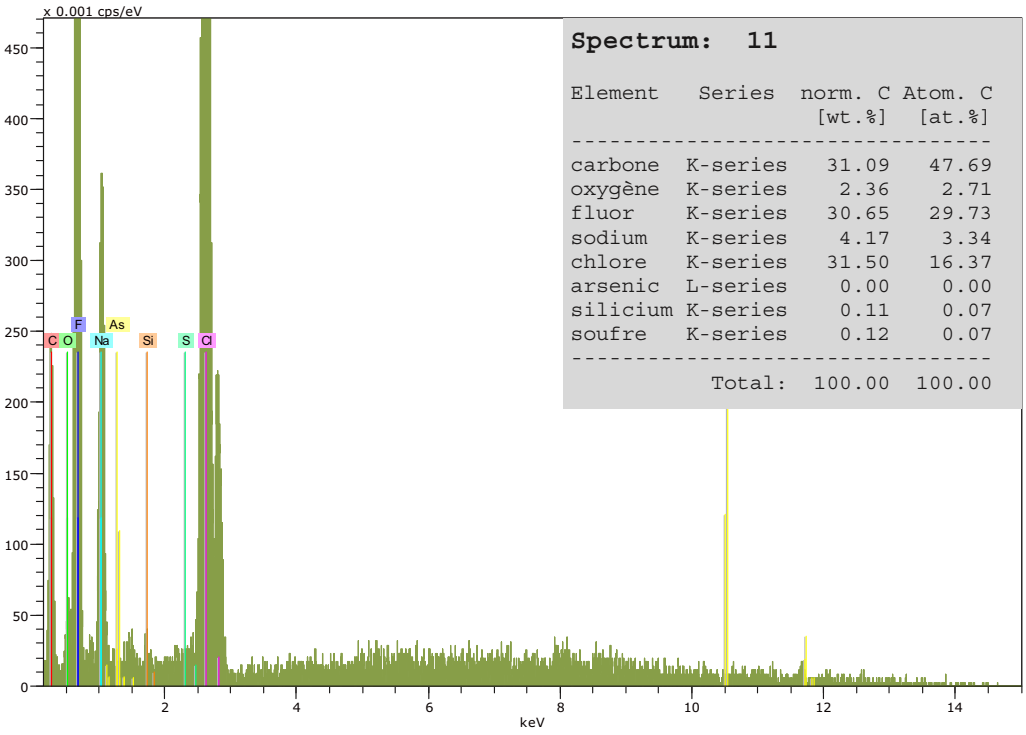

Fig 5.34 *EDS analysis of the working-zone on the membrane surface at point 11 – Fig 5.31a*

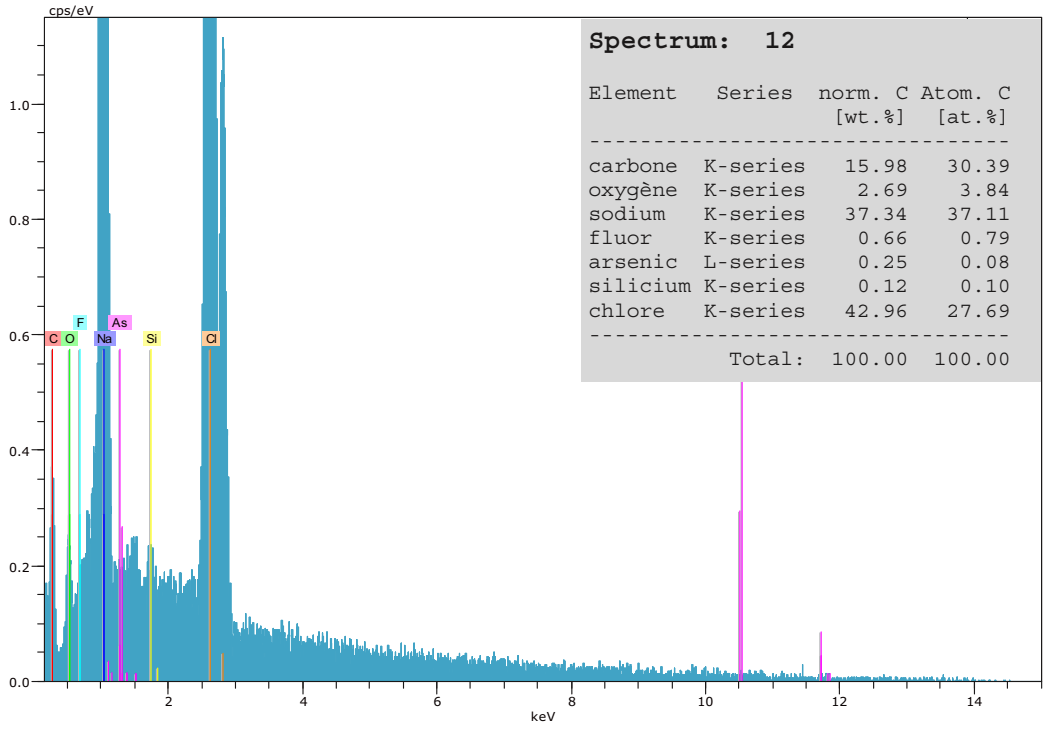

Fig 5.35 *EDS analysis of the crystal at the working-zone on the membrane surface at point 12 – Fig 5.31b*

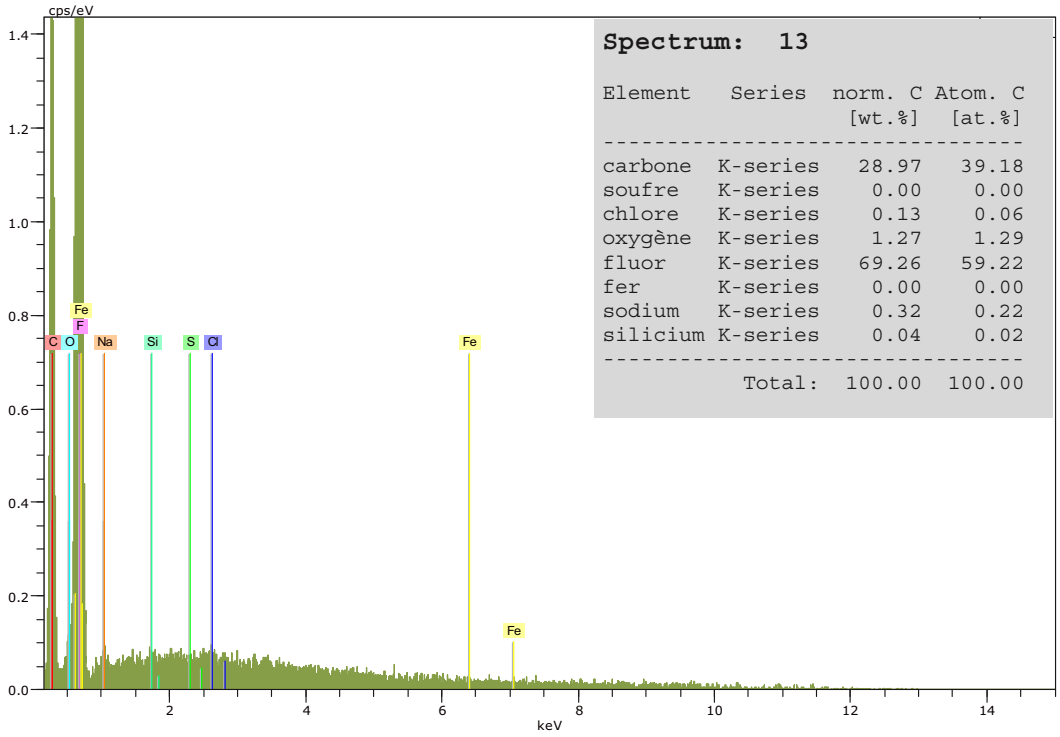

Fig 5.36 *Deposit composition at the working-zone on the membrane surface at point 13 – Fig 5.31c*

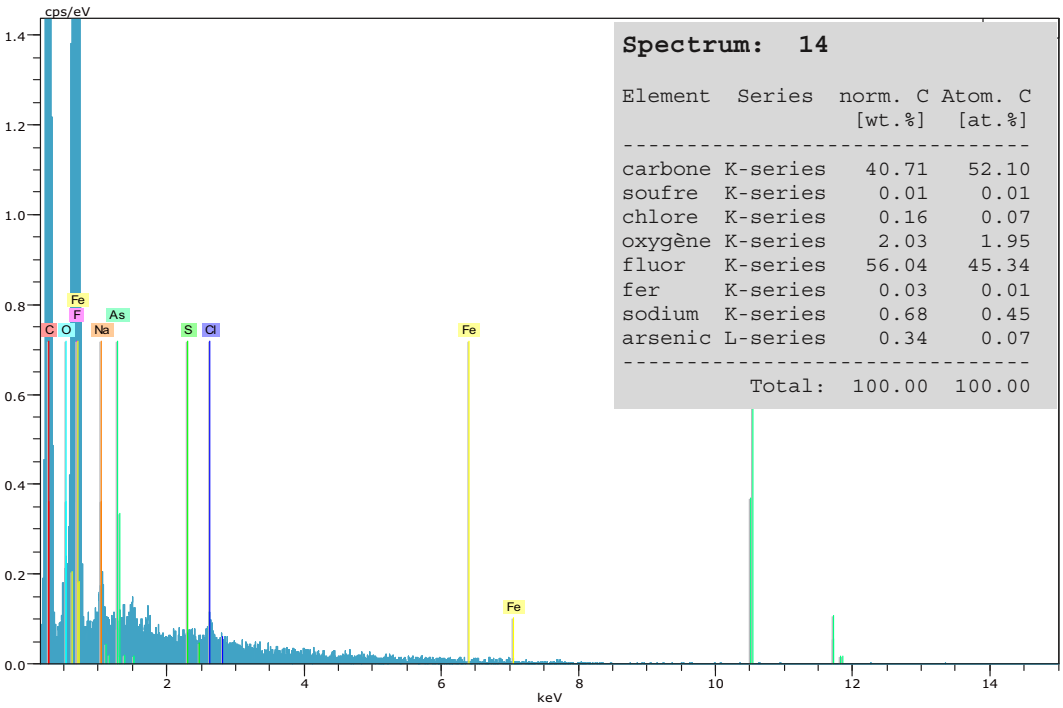

Fig 5.37 *Deposit composition at the working-zone on the membrane surface at point 14 – Fig 5.31c*

Different from the dead-zone, analysis with EDS probe at the working-zone at points 11 – 12 and 13 (as presented in the Fig 5.34 – Fig 5.36, respectively) revealed that only presence of NaCl crystal was found on the membrane surface. Deposit containing As(III) was found at several points on the membrane surface but in a very small extent.

In summary, the results showed that VMD process was able to remove effectively the RO retentate containing very high concentrations of As(III), NaCl and HASS. This observation allowed us to simulate an integrated system by coupling of VMD and RO to increase the global recovery factor of the process and reduce the energy cost.

V.2.2.2 Direct As(III) removal by coupling of RO and VMD process

In this part, a hybrid process by coupling of RO and VMD processes for direct As(III) removal was investigated. The RO process was used to treat directly As(III) contaminated brackish water while the VMD process was applied for further concentration of the RO retentate. Outline of the whole hybrid process was illustrated in Fig 5.38.

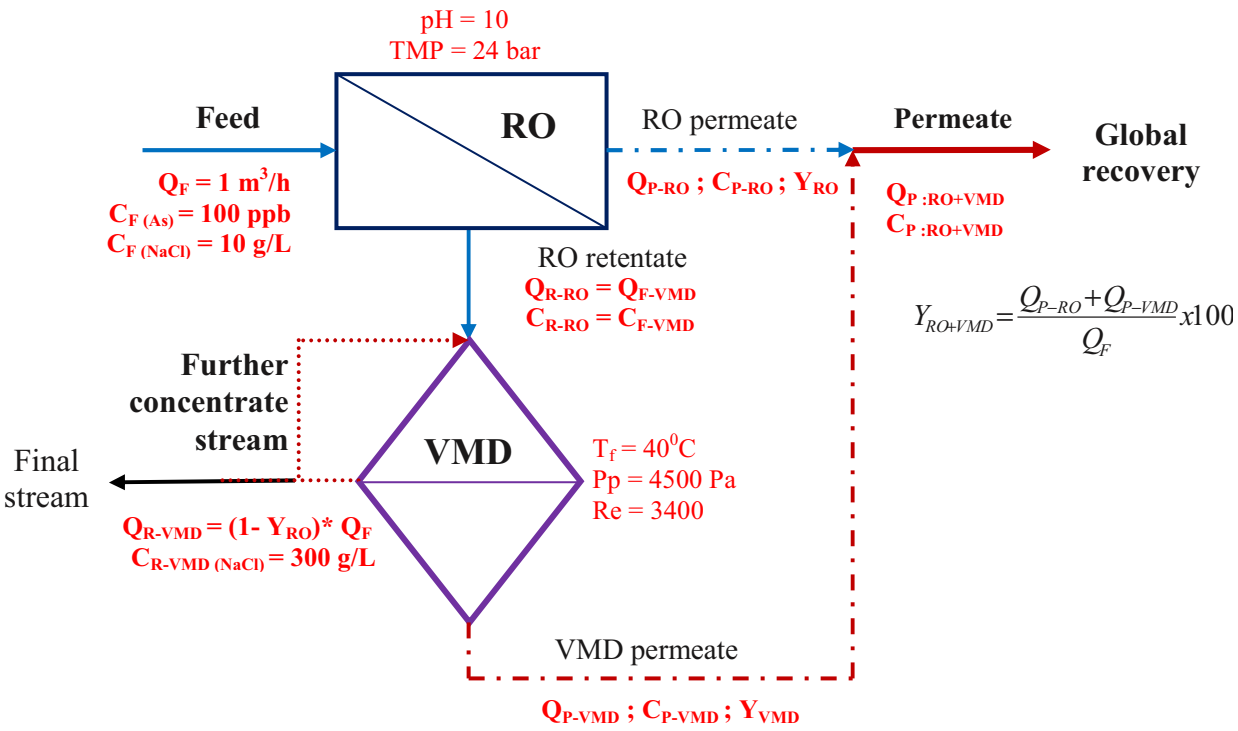

Fig 5.38 *Hybrid process by coupling of RO and VMD processes*

Simulation of this integrated process was based on following assumptions:

- Feed flow-rate at the inlet of RO is Q_F = 1 m^3/h;
- Feed concentrations at the RO inlet contain [As(III)] = 100 ppb and [NaCl] = 10 g/L;
- VMD performance in terms of NaCl rejection is 100%, equivalent to $C_{P\text{-}VMD\ (NaCl)}$ = 0 g/L;
- The VMD process is able to concentrate NaCl concentration up to level of 300 g/L, equivalent to $C_{R\text{-}VMD\ (NaCl)}$ = 300 g/L. It is equivalent to a global recovery rate of 96% ,which is fixed as an initial parameter;
- Fouling due to deposits of As(III) and NaCl on the membrane surface (for both RO and VMD membranes) is not taken into account;
- Amount of As(III) and NaCl lost by accumulation on the membrane surface is ignored, as a first approximation;

For the calculation, recovery rates for both RO and VMD processes are calculated by the equation 5-3 and 5-4.

$$Y_{RO} = \frac{Q_{P-RO}}{Q_F} x100 \tag{5-3}$$

and

$$Y_{VMD} = \frac{Q_{P-VMD}}{Q_{R-RO}} x100 \tag{5-4}$$

where

- ✓ Y_{RO} : the RO recovery (%);
- ✓ Y_{VMD} : the VMD recovery (%);
- ✓ Q_F : the inlet feed flow of the process ($m^3.h^{-1}$);
- ✓ $Q_{P\text{-}RO}$: the RO permeate flow-rate ($m^3.h^{-1}$);
- ✓ $Q_{P\text{-}VMD}$: the VMD permeate flow-rate ($m^3.h^{-1}$);
- ✓ $Q_{R\text{-}RO}$: : the RO retentate flow, equal to the VMD feed flow $Q_{F\text{-}VMD}$ ($m^3.h^{-1}$);

In order to calculate the recovery factor of each process (RO and VMD), experimental data obtained in chapter 4 and section 5.2 were used. Based on the above-mentioned assumptions,

mass balance equations 5-5 and 5-6 for NaCl component were applied to estimate the VMD retentate and permeate flow-rates ($Q_{R\text{-}VMD}$ and $Q_{P\text{-}VMD}$). After that, by merging both RO and VMD permeate flow-rates, overall permeate As(III) concentration was calculated according to the mass balance equation 5-7.

- Mass balance on NaCl on the VMD process:

$$Q_{R\text{-}RO} * C_{R\text{-}RO\ (NaCl)} = Q_{P\text{-}VMD} * C_{P\text{-}VMD\ (NaCl)} + Q_{R\text{-}VMD} * C_{R\text{-}VMD\ (NaCl)} \quad (5\text{-}5)$$

- Global mass balance on VMD process:

$$Q_{R\text{-}RO} = Q_{P\text{-}VMD} + Q_{R\text{-}VMD} \quad (5\text{-}6)$$

- Mass balance on As(III):

$$Q_P * C_{P\ (As)} = Q_{P\text{-}RO} * C_{P\text{-}RO\ (As)} + Q_{P\text{-}VMD} * C_{P\text{-}VMD\ (As)} \quad (5\text{-}7)$$

Simulated results were illustrated in Fig 5.39: As(III) concentration in the RO permeate and in the overall permeate as well as the VMD recovery are plotted versus RO recovery.

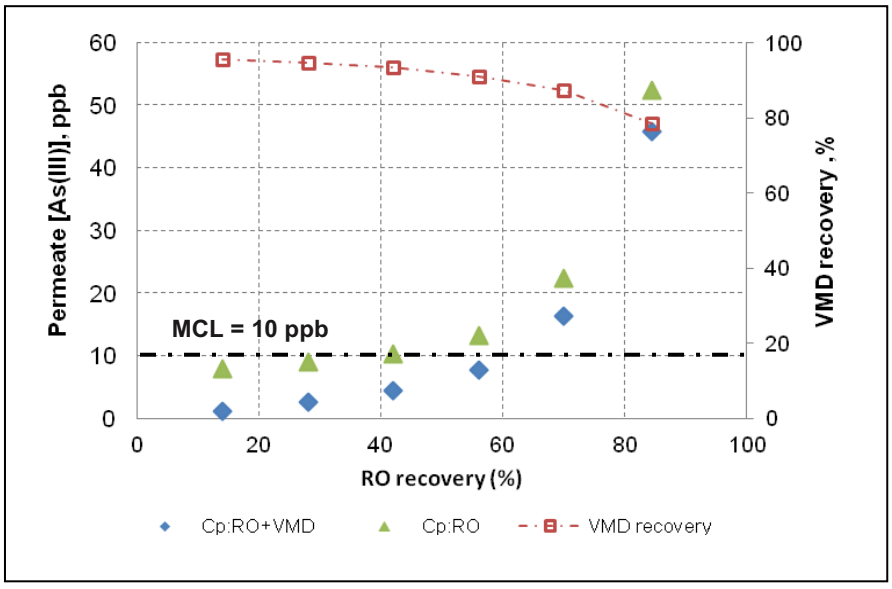

Fig 5.39 *Variation of VMD recovery, and of As(III) concentration in the RO permeate and in the outlet of the process as a function of RO recovery*

As reported in section V.2.3.1, for the given operating conditions (As(III) = 107 ppb, pH 10 and TMP = 24 bar), the RO process was able to reduce 107 ppb As(III) in the feed solution to meet the standard for drinking water (MCL = 10 ppb) at recovery Y_{RO} = 42%. By coupling

with VMD for further treatment of the RO retentate, a significant quantity of clean water could be recovered, which could help increase overall permeate flow-rate as well as to reduce As(III) concentration in the final permeate stream (i.e. $C_{P:RO+VMD}$). Fig 5.39 showed that the RO could be performed until a recovery Y_{RO} of 56% while the final permeate As(III) concentration was still lower than 10 ppb.

By coupling the RO and VMD processes, a global water recovery of 96% was proposed. It helped to reduce the RO retentate stream around 15 times. However, investment cost should be considered in terms of hydrophobic membrane area required. As increase of the RO recovery, decline of permeate VMD flow-rate could be observed (Fig 5.40), leading to a reduction of the required VMD membrane area. Fig 5.40 also showed an estimated requirement of the VMD membrane area (in case of Fluoropore membrane) as a function of the RO recovery and the VMD feed temperature for As(III) treatment at flow-rate of 1 $m^3.h^{-1}$. In all cases, around 50% of the required VMD membrane area could be reduced with increase of RO recovery from 14% to 56%. The VMD feed temperature also played an important role in reduction of the required VMD membrane area. Approximately 63% reduction of the required membrane area could be obtained in corresponding to increase of feed temperature from 40^0C to 55^0C. However, energy consumption, especially for heating should be taken into consideration.

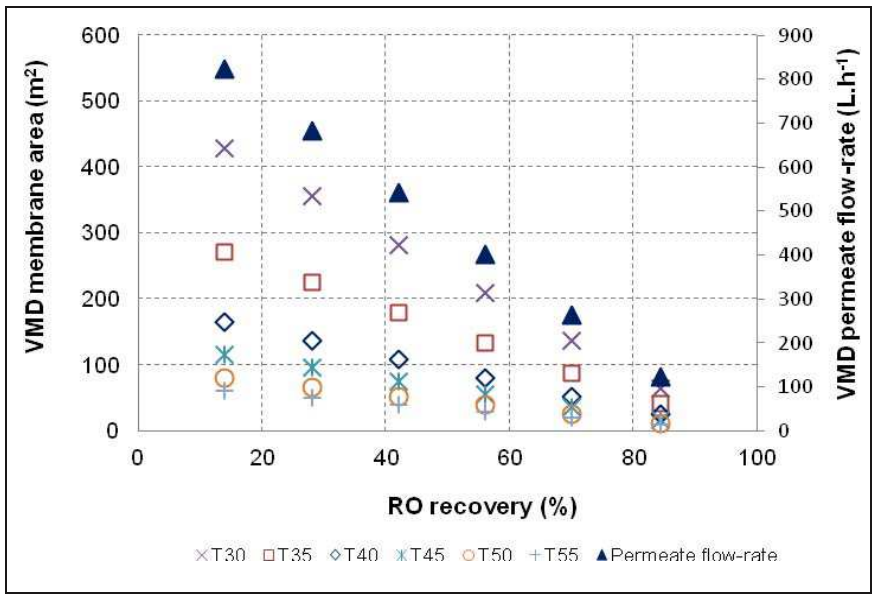

Fig 5.40 *VMD permeate flow-rate and required Fluoropore membrane area as a function of RO recovery and feed temperatures (between 30 and 55^0C)*

By applying the same VMD pilot plant for desalination of sea water, *Mericq et al., 2009* reported that heat energy requirement represents more than 98% of the total energy consumption. It means that operating at higher feed temperature could help reduce the membrane area requirement, but high energy consumption, especially for heating, could be required. In general, the heat energy requirement can be estimated by the following equation 5-8:

$$Q_h = C_p * m * \Delta T \quad (5\text{-}8)$$

where:

- ✓ Q_h : heat energy consumption (W);
- ✓ m : water mass flow-rate (g/h);
- ✓ ΔT : change in temperature (^0C);
- ✓ C_p : specific heat value; for water Cp = 4.18 (J/g.^0C);

Calculation of heat energy requirement for the simulated case was then carried out for a RO recovery of 56%. By mass balance, this value is corresponding to RO retentate flow-rate (also equal to VMD feed flow-rate) of 440 $L.h^{-1}$ and VMD permeate flow-rate of 401.5 $L.h^{-1}$. For the fixed recovery (Y_{RO} = 56%), membrane area as a function of feed temperature was reported in Table 5.3. Heat energy requirement was calculated by equation (5-8) also for a RO recovery of 56% (assuming an initial temperature of the feed solution of 20^{0}C) and presented in Table 5.3. Finally, specific heat energy consumption, as the ratio of heat energy consumption and permeate flow-rate, was calculated also. The obtained results were also illustrated in Fig 5.41.

Table 5.3 *Heat energy consumption and membrane area at different feed temperature.*

T_f (^0C)	$Q_{R\text{-}RO}$ ($L.h^{-1}$)	$Q_{P\text{-}VMD}$ ($L.h^{-1}$)	$J_{H2O\text{-}VMD}$ ($kg.m^{-2}.h^{-1}$)	Membrane area	Heat energy	Specific heat energy consumption
				m^2	W	kWh/m^3
30	440	401.5	1.9	209.2	5113	12.7
35	440	401.5	3.0	132.7	7669	19.1
40	440	401.5	5.0	80.4	10226	25.5
45	440	401.5	7.2	56.1	12782	31.8
50	440	401.5	10.3	39.0	15339	38.2
55	440	401.5	13.6	29.5	17895	44.6

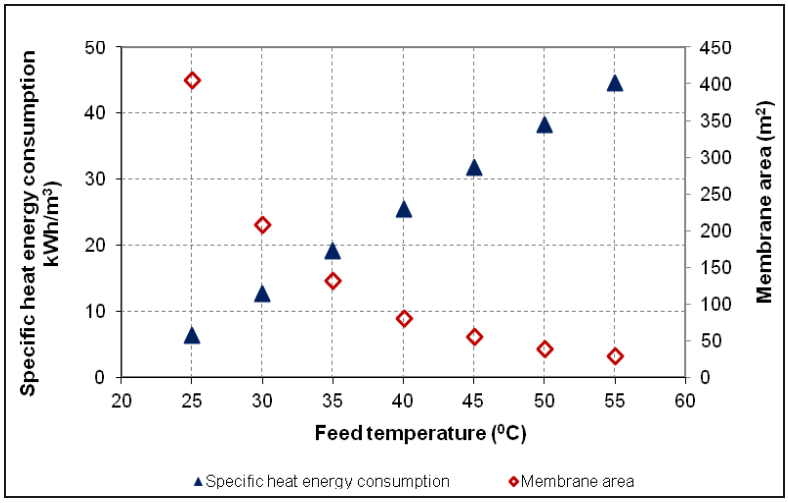

Fig 5.41 *Specific heat energy consumption and VMD membrane area as a function of feed temperature*

Concerning values of heat energy consumption, Table 5.3 showed that an increase of feed temperature from 30^0C to 55^0C led to an increase of heat energy consumption by a factor of 3.5. As the VMD permeate flow-rate was fixed in this case, when the VMD feed temperature increases, the specific heat energy consumption increases too (from 12.7 to 44.6 kWh.m^{-3}); but on the other hand the VMD membrane area decreases (from 209 to 29.5 m^2) (Fig 5.41). This observation indicated that the best VMD performance, in terms of membrane area requirement and heat energy consumption in this simulation, should be chosen at feed temperature of 35^0C, corresponding to 132 m^2 and 19 kWh.m^{-3}, respectively.

In summary, feasibility of coupling of RO and VMD processes for direct As(III) removal from brackish ground water was investigated. Global recovery at 96% could be achieved by this integration. Relative high VMD membrane area was required, which could increase the operation and treatment cost. Operating at high feed temperature ($T_f = 55^0$C) could help to reduce membrane area requirement, but it also requires higher specific heat energy consumption. As observed in Fig 5.41, feed temperature of $T_f = 35^0$C was selected as an optimal value which satisfies both heat energy consumption and membrane area requirement. Results of the simulation of coupling of RO and VMD process were summarized in the Table 5.4.

Table 5.4 *Simulation of coupling of RO and VMD process for initial values ([As(III) = 100 ppb and [NaCl] = 10 g/L^{-1})*

Parameters	Unit	RO process alone	RO + VMD		
			RO	VMD	Global
Feed flow-rate, Q_F	L.h^{-1}	1000	1000	440	1000
Water recovery, Y	%	42	56	91.3	96.15
Permeate flow-rate, Q_P	L.h^{-1}	420	560	401.5	961.5
Retentate flow-rate, Q_R	L.h^{-1}	580	440	38.5	38.5
Retentate As(III) concentration	ppb	177	226	2586	2586
Retentate NaCl concentration	g.L^{-1}	20	26	300	300

V.3 CONCLUSIONS

In this chapter, direct As(III) removal from brackish water was performed first by the RO process alone and then by coupling of the RO and VMD processes, in which the VMD process was used for further concentration of the RO retentate. In general, some following observations could be concluded:

V.3.1 For the RO process alone

- RO performance was quite dependent on pH value of feed solution. In terms of treatment efficiency, As(III) rejection rate was much higher at pH 10 with approximately 87% in comparison with 60% at pH 7. In terms of trans-membrane flux at the same TMP, a higher permeate flux was obtained at pH 7 in comparison with the one at pH 10;

- Influence of trans-membrane pressure on the permeate flux was quite clear with higher permeate flux obtained at higher trans-membrane pressure applied. However at the same recovery of 50%, no influence of trans-membrane pressure on NaCl rejection was found. Regarding As(III) rejection, there was a slight difference in rejection efficiencies at two trans-membrane pressures but no tendency was observed.

- For tested conditions, the RO process could be carried out at a maximum recovery factor of 42% to meet the standard for drinking water (MCL = 10 ppb) with 107 ppb As(III) in feed solution .

- High TOC removal was achieved with very low concentration of organic matter in the permeate (TOC = 0.4 mg/L), equivalent to 94.6% of TOC rejection rate;

- Presence of organic matter in the feed solution could have influence on the RO performance in terms of As(III) and NaCl removal. For As(III) rejection, to provide permeate As(III) concentration lower than 10 ppb, higher recovery of 60% was achieved with presence of organic matter in comparison with only 42% in case of no organic matter. On the contrary, a slight lower permeate flux was observed with presence of organic matter in the feed solution;

- SEM and EDS analysis showed that membrane fouling occurred with primary presence of NaCl crystal on the membrane surface. Deposit of As(III) on the membrane surface was also detected, but in a small extent.

V.3.2 For further concentration of the RO retentate by VMD process

- In this part, the results showed that VMD process was able to remove effectively the solution containing very high concentrations of As(III), NaCl and HASS. At high feed concentration (i.e. 7000 ppb), As(III) was found in the permeate with a 8 ppb concentration, which is still lower than the required standard for drinking water;

- Decline of VMD permeate flux was observed with increase of feed NaCl concentration: at the same given operating conditions (Fluoropore membrane, Tf = 40°C, Pp = 4500 Pa, Re = 3400), results showed a decline of VMD permeate flux from 5.0 $L.m^{-2}.h^{-1}$ to 3.5 $L.m^{-2}.h^{-1}$ with increase of feed NaCl concentration from 10 $g.L^{-1}$ to 300 $g.L^{-1}$. Slight decreases of the VMD permeate flux and of apparent Knudsen permeability were observed with presences of either NaCl or both NaCl and organic matter. This was attributed to fouling mainly due to salt precipitation, and not to the presence of organics.

- Membrane surface observation and analysis with EDS probe confirmed that precipitation of NaCl crystal was the main source of the flux decline and fouling of VMD. Deposit of organic matter could occur but it was avoided by tangential flow in a turbulent regime.

V.3.3 For the coupling of RO and VMD processes

Coupling of RO and VMD could be an interesting option with high global recovery rate of 96%. This option could help the RO process to be performed until a recovery Y_{RO} of 56% while the final permeate As(III) concentration was still lower than 10 ppb. Approximately 50% of VMD membrane area could be reduced with increase of RO recovery from 14% to 56%. Operating at medium feed temperature (T_f = 35^{0}C) for VMD could be the best VMD performance, in terms of both heat energy and membrane area requirement.

General conclusions and Perspectives

Removal of arsenic from water resources in order to obtain satisfying sanitary conditions for drinking water is a key issue in many countries worldwide. Contamination of water resources by arsenic-based species is notably drastic in Vietnam due to the anthropogenic activities during the Vietnam War. Some underground waters in other countries also contain arsenic naturally present in soils.

As a case-study on arsenic contamination in brackish groundwaters in Vietnam, this PhD work aimed to study the feasibility of integrating vacuum membrane distillation (VMD) technology in the treatment line, for both arsenic removal and removal of salts that are present together in the water resources. As a consequence, in comparison with most other relevant published studies on VMD, the originality of this study lies on the focus that was given to: a) arsenic removal with presence of sodium chloride at concentrations of about 10 g/L and b) influence of salts on the VMD permeate flux and fouling mechanisms.

Most of the conventional processes that can be used for arsenic removal (adsorption, precipitation + filtration, reverse osmosis) are requiring a preliminary oxidation step that aims to convert arsenite As(III) into arsenate As(V). This pre-oxidation step induces additional investment and operating costs and can also produce some non-desirable by-products by oxidation of the organic compounds that are present in the water resource.

As a consequence the choice was done at the beginning of the study to consider the direct removal of arsenite As(III), with the objective to avoid the pre-oxidation step.

In the following of Jean-Pierre Méricq's PhD thesis, the first step of the study (introduced in chapter 3) consisted in developing a new method for measuring membrane permeability through the Knudsen mass transfer coefficient (K_M) and to use this method (called INSA-K_M method) to select a convenient (more permeable) membrane for the application of interest in this PhD work.

For the conventional measurement methods (Gas permeation test and pressure variation test) the temperature is fixed and the permeate pressure varies to create the driving force for mass transfer. Moreover the gas permeation test is based on the measurement of gas permeation inside membrane pores without the presence of a liquid/vapour interface. This measurement does not consider the physico-chemical interactions between the liquid and the membrane

material (localisation of the interface). The idea of the INSA-K_M method was to propose a permeability measurement method based on the measurement of the flux of vaporised vapour while variation of feed temperature (in range of 25 – 60^0C) at fixed vacuum pressure and for controlled hydrodynamic conditions (Pp = 4500 Pa and Re = 3400). Comparison between the pressure variation test and the INSA-Km method for two different hydrophobic membranes (Durapore and Fluoropore) showed the greater stability and simplicity of the INSA-K_M as well as the similarity in permeability results for the two methods. This indicated that the INSA-K_M method could be an interesting tool for characterizing membrane distillation membranes. In addition, Fluoropore membrane showed a higher average permeability ($3.81x10^{-6}$ $s.mol^{1/2}.m^{-1}.kg^{-1/2}$) than the Durapore membrane ($3.41x\ 10^{-6}$ $s.mol^{1/2}.m^{-1}.kg^{-1/2}$). As a result, Fluoropore membrane was selected for the following parts of the study.

Precisely, two different ways of integrating VMD in the treatment line were then considered in this study:

- **Process A**: VMD as a direct treatment to remove both salts (NaCl in this study) and As(III) from brackish waters
- **Process B**: Coupling of reverse osmosis (RO) and VMD, in which RO had considered as a first step to concentrate NaCl and As(III) before this retentate stream was further concentrated by VMD.

Chapter 4 was focusing on process A. As a simulation of Vietnamese groundwaters some synthetic brackish waters showing concentrations of 10 $g.L^{-1}$ NaCl and 300 to 2000 ppb As(III) were used for VMD tests on a lab scale pilot plant. Influence of operating parameters (feed temperature, vacuum pressure, Reynolds number) on the VMD performance was studied. The effects of organic matter (humic acid sodium salt – $C_9H_8Na_2O_4$ at 20 mg/L) and $CaSO_4$ ($[Ca^{2+}]$ = 0.5 g/L) on membrane fouling were also investigated. Several important remarks could be done from the experiments, including:

- Within the given range of feed concentrations, VMD showed high rejection rates for both As(III) and NaCl, which proved high feasibility of VMD for this application

- *No arsenic was detected in the permeate, irrespective of feed As(III) concentration.*
- *Over 99.5% of NaCl rejection was observed.*

- No significant fouling (no modification of apparent Km) occurs for solutions containing NaCl and As(III) at any concentration, without organics or other salts. No membrane wetting was observed.

- As expected from the basic mass transfer equations describing the process, for a certain hydrophobic membrane, higher permeate flux could be obtained at higher feed temperature and at lower vacuum pressure. For the Fluoropore membrane, the highest permeate flux of 14 $Kg.m^{-2}.h^{-1}$ was obtained at T_f = 55°C, P_p = 4500 Pa and Re = 3400, both for pure water and for synthetic brackish waters containing 10 $g.L^{-1}$ NaCl and 300 ppb As(III);

- Hydrodynamics also influences the permeate flux, but mainly in the laminar and a part of transition flow patterns (Re < 3400). At the beginning of turbulent regime (Re = 3400), the permeate flux reached asymptotic value and no longer increased, which means that for our experimental conditions no polarisation concentration is occurring in turbulent flow.

- Considering energy consumption as well as stability of the VMD operation at high feed temperature, operating conditions at T_f = 40°C, Pp = 4500 Pa and Re = 3400 were selected and applied for all the following experiments. For this operating set of conditions, an average permeate flux of 5 $kg.m^{-2}.h^{-1}$ was obtained regardless of given feed As(III) concentration;

- In presence of organic matter (HASS) a slight decrease of K_M (5.8%) was observed which means that fouling is occurring even if its influence on the permeate flux was very small and could be neglected at the given feed concentrations. Considering the larger size of HASS (20 – 120 μm) in comparison with average membrane pore size (0.2 μm) membrane fouling can be mainly attributed to a deposit of organic matter on the membrane surface more than to internal pore fouling. Deposit of As(III) was

detected by SEM-EDS at some points on the membrane surface, but in a very small extent.

- In presence of $CaSO_4$ in the brackish water at concentration of 2.15 g/L (i.e. $[Ca^{2+}]$ = 0.5 g/L), some crystals of NaCl and $CaSO_4$ could be observed on the membrane surface. However after 22 hours of operation, no permeate flux decline occurred, which meant that effects of scaling was insignificant in this case. Negative values of saturation indexes of both NaCl and $CaSO_4$ indicated that these salts were under-saturated. It means that no precipitation of salts will occur. Influence of concentration polarization which increases salts concentrations at the membrane surface could be the reason for the crystal found on the membrane surface.

Chapter 5 was focusing on process B which involved a coupling of RO and VMD. For this integration, RO was considered as a first step to concentrate NaCl and As(III) before this RO retentate stream was further concentrated by VMD. Synthetic brackish waters at concentrations of 10 $g.L^{-1}$ NaCl and 100 ppb As(III) were used for RO batch-mode experiments at lab scale. Performance of RO and VMD for concentrating NaCl and As(III) and also for over-concentrating its retentate respectively were investigated. A simulation of coupling of RO and VMD for a feed flow-rate of $Q_{F\text{-}RO} = 1m^3/h$ was also proposed.

Several important remarks from the experiments and also from the simulation were as follows:

- For the tested optimal conditions (pH10 and TMP = 24 bars), RO process showed a lower rejection efficiencies than the one of VMD, even at the lower feed As(III) concentration of 107 ppb. Depending on recovery rate, RO could remove 107 ppb As(III) in brackish waters to meet the standard for drinking water (MCL = 10 ppb and Ec = 2500 µS/cm). However, its performance was inefficient at higher As(III) concentration (i.e 300 ppb) irrespectively of recovery rate.

- Concerning the influence of organic matter: at 107 ppb As(III) in a solution containing only NaCl, RO could be carried out at a maximum recovery of 42% to meet the standard for drinking water whereas higher recovery of 60% could be reached with presence of organic matter ([HASS] = 20 mg/L) in the feed brackish waters owing to adsorption of As(III) onto organics.

- For the given osm-OSPA membrane, RO could reach rejection efficiencies of 93% for NaCl, 87% for As(III) and almost 94.6% for TOC as the highest values at optimal conditions (pH 10 and TMP = 24 bars).

- In the presence of HASS in the feed brackish As(III) contaminated solution, approximately 60% of RO permeate flux decline was observed for the two cases: without and with presence of HASS. It was concluded that RO permeate flux decline was mainly due to presence of NaCl inside the cell. An effect of feed organic matter on the RO permeate flux was found and need to be taken into consideration for recoveries higher than 50%.

- RO membrane fouling occurred with primary presence of NaCl crystal on the membrane surface. Deposit of As(III) on the membrane surface was also detected, but in a small extent. However, this phenomenon became clearer with presence of organic matter as more As(III) deposition was detected. In this case, hypothetic deposition of solutes on the membrane surface was proposed with the order as follows:

    1) *Deposits of NaCl and a few As(III) on the membrane surface;*
    2) *Deposits of organic matter on NaCl crystal and also As(III);*
    3) *More adsorption of As(III) onto organic foulant.*

- As a further treatment step for concentrating the RO retentate, VMD could work efficiently with 99.9% of As(III) and NaCl rejections at a very high RO retentate concentrations ([NaCl] = 300 g/L and [As(III)] = 7000 ppb). Arsenic was found in the permeate of 8 ppb concentration, but was still lower than the required standard for drinking water.

- In comparison with average permeate flux (i.e. 5.0 $kg.m^{-2}.h^{-1}$) obtained in Chapter 4, an average VMD permeate flux of 4.8 $kg.m^{-2}.h^{-1}$ for feed solution containing only As(III) was obtained even at high concentration of 7000 ppb within a long-term duration (i.e 13 hours). It indicated that no effect of high feed As(III) concentration on VMD permeate flux was found.

- At the same given operating conditions (Fluoropore membrane, T_f = 40°C, Pp = 4500 Pa, Re = 3400), decline of VMD permeate flux from 5.0 to 3.5 $kg.m^{-2}.h^{-1}$ was observed with increase of feed NaCl concentration from 10 to 300 g/L. Slight decline of VMD permeate flux and also apparent Knudsen permeability with presences of either NaCl or both NaCl and organic matter during long-term operation (i.e. 26.8 hours) confirmed that fouling is mainly due to salt precipitation, and not to the presence of organics.

- By coupling of RO and VMD, a high global recovery of 96% could be achieved, together with increase of RO recovery from 42% to 56% for the RO process alone while the final permeate As(III) concentration was still lower than 10 ppb. It helped to reduce the RO retentate stream around 15 times.

- For the simulation, operating costs in terms of membrane area and energy consumption, especially for heating, were taken into consideration. Approximately 63% of the required membrane area was reduced with increase of feed temperature from 40 – 55^0C which confirmed the important role of feed temperature for the VMD performance.

- At a fixed RO recovery of 56% in this simulation, the best VMD performance, in terms of membrane area requirement and heat energy consumption, should be chosen at feed temperature T_f = 35°C, corresponding to 132 m^2 and 19 $kWh.m^{-3}$, respectively. For the simulation of feed slow-rate Q = $1m^3/h$, the coupling of RO and VMD could help to reduce specific heat energy consumption about 2.2 times in comparison with the one required for VMD alone. Schematic diagram of hybrid process by coupling of RO and VMD is described in the figure B below:

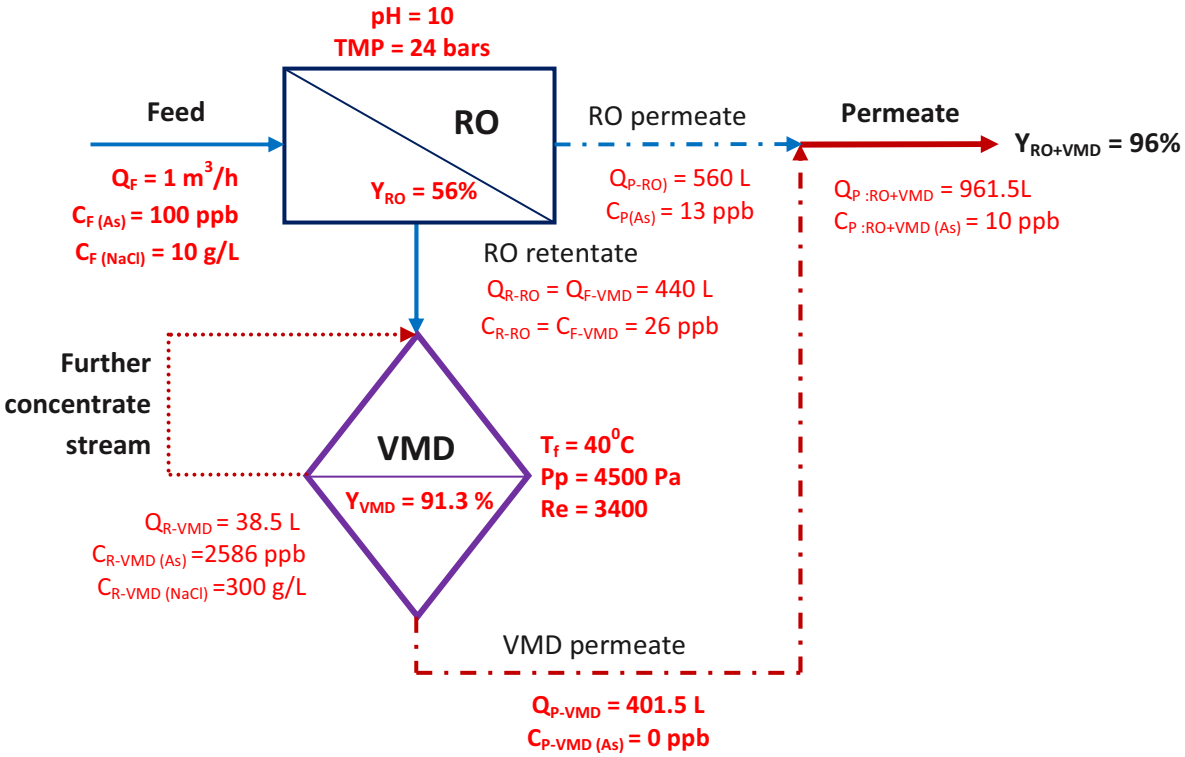

Figure B . *Hybrid process by coupling of RO and VMD processes*

Also, performance of hybrid process in comparison with RO and with VMD was illustrated in the Table below:

Parameters	RO	VMD	RO + VMD
As(III) rejection	+	+++	+++
Flux recovery	+	++	+++
Fouling by NaCl	+++	++	++
Fouling by HASS	+++	+	+
Energy consumption	+	+	++

+++ *: very high*
++ *: high*
+ *: low*

In summary, feasibility of VMD for direct As(III) removal in brackish groundwaters has been demonstrated. Coupling of RO and VMD could be an interesting option to be applied in the practice. However, following points of this research still remain to be explored in the future:

1. Since iron occurs regularly in the groundwaters in Vietnam, influence of iron concentration in the feed water on the arsenic rejection and on fouling and membrane wetting should be investigated.

2. Experiments during a very long term with real groundwaters should be done on site with different resource waters, in order to check viability of the process on long term operation and to check weather fouling or wetting can affect operation. Influences of organic matter and salts on the membrane fouling during a long-term operation must be further investigated, as well the possible effect of $CaCO_3$ or mixtures of $CaCO_3/CaSO_4$.

3. Higher permeable hydrophobic membrane should be tested to facilitate applicability of VMD in the practice; the possibility to test some locally manufactured membranes should also be explored.

4. As Vietnam is a tropical country, coupling with solar energy systems could be an interesting option to reduce operating costs in terms of energy consumption. Furthermore, this could also help to enhance mobility of VMD application in remote areas where there is no electricity supply system.

5. Further treatment of final retentate from the hybrid process should be taken into consideration.

Nomenclature

- C_b : concentration of non-volatile compound in the feed bulk ($mol.L^{-1}$)
- C_m : concentration of non-volatile compound at the membrane surface ($mol.L^{-1}$)
- c : molar concentration at bulk liquid phase ($mol.m^{-3}$)
- D : diffusive coefficient of the solute in the solution ($m^2.s^{-1}$)
- d : hydraulic diameter (m)
- I : the van't Hoff factor
- J_{H2O} : molar flux of water ($mol.s^{-1}.m^{-2}$)
- J_w : water flux passing through the RO membrane ($kg.m^{-2}.h^{-1}$)
- K_M : Knudsen permeability ($s.mol^{1/2}.m^{-1}.kg^{-1/2}$)
- $K_M(T_{ref})$: Knudsen permeability at reference temperature T_{ref} ($s.mol^{1/2}.m^{-1}.kg^{-1/2}$)
- K_w : water transport coefficient or membrane permeability ($kg.m^{-2}.h^{-1}.Pa^{-1}$)
- k_k : mass transfer coefficient in the membrane ($s.m^{-1}.mol.kg^{-1}$)
- k^T : thermal conductivity of liquid ($W.m^{-1}.K^{-1}$)
- h_f : heat transfer coefficient in the boundary layer of the feed side ($W.m^{-2}.K^{-1}$)
- h_p : heat transfer coefficient in the boundary layer of the permeate side ($W.m^{-2}.K^{-1}$)
- h_m : the heat transfer coefficient of the membrane ($W.m^{-2}.K^{-1}$)
- L : length of the feed channel (m)
- M_{H2O} : molar mass of water ($kg.mol^{-1}$)
- M : molarity ($mol.L^{-1}$)
- m : water mass flow-rate ($g.h^{-1}$)
- N : the mass transfer flux through the membrane ($mol.m^{-2}.s^{-1}$)
- N_A : Avogadro constant ($N_A = 6.02214129 \times 10^{-23}\ mol^{-1}$);
- P^*_m : vapour pressure of pure water at the membrane's conditions (Pa)
- P_p : partial pressure of water in the permeate side (vacuum pressure) for VMD (Pa)
- p : the mean pressure within the membrane pores (Pa)

- P_D : *applied driving pressure (Pa)*
- ΔP_{H2O} : *difference in partial pressure of water on both sides of the VMD membrane (Pa)*
- Q_F : *the inlet feed flow of the process ($m^3.h^{-1}$)*
- $Q_{P\text{-}RO}$: *the RO permeate flow-rate ($m^3.h^{-1}$)*
- $Q_{P\text{-}VMD}$: *the VMD permeate flow-rate ($m^3.h^{-1}$)*
- $Q_{R\text{-}RO}$: *the RO retentate flow ($m^3.h^{-1}$)*
- Q_h : *heat energy consumption (W)*
- q_f : *heat flux transfer through the thermal boundary layer of the feed side ($W.m^{-2}$)*
- q_v : *fraction of the heat energy transferred to the membrane surface and through the membrane in the form of latent heat ($W.m^{-2}$)*
- T_b : *temperature in the feed bulk (K)*
- T_{inlet} : *temperature at the inlet of membrane module (K)*
- T_{outlet} : *temperature at the outlet of membrane module (K)*
- $T_{permeate}$: *temperature at the permeate side of membrane module (K)*
- T_m : *temperature at the membrane surface (K)*
- T_{ref} : *reference temperature at 20^0C (K)*
- t_f : *feed temperature of aqueous solution at the bulk (K)*
- t_{fm} : *feed temperature of aqueous solution at the membrane surface (K)*
- t_p : *temperature at the permeate side (K)*
- R : *ideal gas constant ($R = 8.314\ J.mol^{-1}.K^{-1}$)*
- r : *radius of the pores (m)*
- Y_{RO} : *the RO recovery (%)*
- Y_{VMD} : *the VMD recovery (%)*
- μ : *bulk liquid viscosity (Pa.s)*
- μ_m : *liquid viscosity at the membrane surface (Pa.s)*

- ΔH : the latent heat of the volatile component ($J.mol^{-1}$)
- λ_m : the average heat conductivity of the membrane material ($W.m^{-1}.K^{-1}$)
- ε : the porosity of the membrane (-)
- δ_m : thickness of the membrane (m)
- λ_s : the heat conductivity of membrane material ($W.m^{-2}.K^{-1}$)
- λ_g : the heat conductivity the gas that fills the pores($W.m^{-2}.K^{-1}$)
- σ : the collision diameter or average diameter of water molecule (σ = 2.641 Å)
- χ_{fm} : the mole fraction of the solute at the membrane surface
- χ_f : the mole fraction of the solute at the bulk
- χ_p : the mole fraction of the solute at the permeate side
- $\Delta\Pi$: osmotic pressure difference across the membrane (Pa)
- Π : osmotic pressure (bar)
- χ : tortuosity factor
- ΔT : change in temperature (^0C);

Dimensionless numbers

- Nu : Nusselt number (-)
- Re : Reynolds number (-)
- Pr : Prandtl number (-)

Abbreviations

MCL	Maximum contaminant level
IWA	International Water Association
MONRE	Ministry of Natural Resources and Environment
VMD	Vacuum membrane distillation
RO	Reverse Osmosis
MD	Membrane distillation
WHO	World Health Organization
LD	Lethal dose

References

A

Ahmed, F., Jalil, M.A., Ali, M.A., Hossain, M.D., Badruzzaman, A.B.M., 2000. An overview of arsenic removal technologies in BUET. In: Ahmed, M.F, (Ed), Bangladesh Environment – 2000, Bangladesh Poribesh Andolon, pp.177-188.

Alkhudhiri, A., Darwish, N., Hilal, **N., 2012.** Membrane distillation: A comprehensive preview, Desalination 287, 2 – 18.

Al-Asheh, S., Banat, F., Qtaishat, M., Al-Khateeb, **M., 2006.** Concentration of sucrose solutions via vacuum membrane distillation, Desalination, Volume 195, Issues 1–3, Pages 60-68.

Altug, **T., 2003.** Introduction to toxicology and Food, CRC Press LLC, NewYork.

B

Banat, F., Al-Asheh, S., Qtaishat, **M., 2005.** Treatment of waters coloured with methylene blue dye by vacuum membrane distillation, Desalination, Volume 174, Issue 1, Pages 87-96.

Banat, F., Al-Rub, F.A., Bani-Melhem, K., 2003. Desalination by vacuum membrane distillation: sensitivity analysis, Separation and Purification Technology 33, 75-87.

Banat, F., Simandl, J., 1994. Theoretical and experimental study in membrane distillation, Desalination 95 (1), 39 - 52

Banat, F., Simandl, J., 1998. Desalination by membrane distillation: a parametric study, Separation science technology, 33 (2), 201 – 226.

Banat, F., Simandl, J., 1999. Membrane distillation for dilute ethanol: separation from aqueous streams, Journal of membrane science 163 (2), 333-348.

Bang, S., Meng, **X., 2004.** A review of arsenic interactions with anions and iron hydroxides, Environ.Eng.Res.Vol.9, No.4, pp. 184 – 192.

Bandini, S, Gostoli, C., Sarti, G.C., 1992. Separation efficiency in vacuum membrane distillation, Journal of membrane of science, 73, 217 – 229.

Bandini, S, Sarti, **G.C., 2002.** Concentration of must through vacuum membrane distillation, Desalination, Volume 149, Issues 1–3, Pages 253-259 .

Bandini, S, Saavedra, A., Sarti, G.C., 1997. Vacuum membrane distillation: Experiments and modelling, AICHe Journal 43, 398 – 408.

Benramdane, L., Accominotti, M., Fanton, L., Malicier, D., Vallon, J-J., 1999. Arsenic speciation in human organs following fatal arsenic trioxide poisoning – A case report, Clinical chemistry 45 :2, 301 – 306 .

Berg M., 2001. Arsenic contamination of groundwater ans drinking water in Vietnam: A human health threat, Journal of environmental science and technology, Vol.35, No.13.

Brandhuber, P., Amy, **G., 2001.** Arsenic removal by a charged ultrafiltration membrane – influences of membrane operation conditions and water quality on arsenic rejection, Desalination 140, 1-14.

Buschmann, J., Berg, M., Stengel, C., Winkel, L., Sampson, **M.L., 2008.** Contamination of drinking water resources in the Mekong delta floodplains: Arsenic and other trace metals pose serious health risks to population, Environment International 34,756–764

C

Cabassud, C., Wirth, **D., 2003.** Membrane distillation for water desalination: How to choose an appropriate membrane? Desalination 157, 307 – 314.

Cabassud C., 2000. Les contacteurs à membrane : principe, intérêts et perspectives, Colloque « Intégration des Membranes dans les Procédés », Lyon, 3-5 Mai 2000, Récents Progrès en Génie des Procédés, Vol 14 – 2000, pp. 167- 172

Cerneaux, S., Struzyn´skab, I., Kujawski, W.M., Persina, M., Larbot, **A., 2009.** Comparison of various membrane distillation methods for desalination using hydrophobic ceramic membranes, Journal of Membrane Science 337, 55–60.

Chilvers D.C., Peterson, P.J., 1987. 'Global cycling of arsenic' In T.C. Hutchinson and K.M. Meema, eds., Lead, Mercury, Cadmium and Arsenic in the Environment. Scientific Committee on problem on the Environment (SCOPE) 31. NewYork: John Wiley & Sons

Choong, T.S.Y., Chuah, T.G., Robiah, Y., Gregory Koay, F.L., Azni, **I., 2007.** Arsenic toxicity, health hazards and removal techniques from water: an overview, Desalination 217, 139 – 166.

Couffin, N., Cabassud, C., Lahoussine-Turcaud, **V., 1998.** A new process to remove halogenated VOCs for drinking water production: vacuum membrane distillation, Desalination, Volume 117, Issues 1–3, Pages 233-245.

Criscuoli, A., Carnevale, M.C., Drioli, **E., 2008.** Evaluation of energy requirements in membrane distillation, Chem. Eng. Process. 47, 1098-1105.

Criscuoli, A., Bafaro, B., Drioli, **E., 2012.** Vacuum membrane distillation for purifying waters containing Arsenic, Desalination, in press, corrected proof, available online 27 August 2012.

D

Dey, M., Williams, K., Coulton, **R., 2009.** Treatment of arsenic rich waters by the HDS process, Journal of Geochemical Exploration 100, 160 – 162.

Diban, N., Voinea, O.C., Urtiaga, A., Ortiz, **I., 2009.** Vacuum membrane distillation of the main pear aroma compound: Experimental study and mass transfer modeling, Journal of Membrane Science, Volume 326, Issue 1, Pages 64-75.

Driehaus, W., Jekel, M., Hildebrandt, U., 1998. Granular ferric hydroxide – A new adsorpbent for the removal of arsenic from natural water, Journal of Water SRT-Aqua, 47(1), 30 – 35.

E

Edwards, M., 1994. Chemistry of arsenic removal during coagulation and Fe-Mn oxidation, J.Am. Water Works Assoc.86 (9), 64-78.

EPA, 2003a. Arsenic treatment technology evaluation handbook for small systems. U.S.EPA 816-R-03-014, July 2003.

EPA website, http://cfpub.epa.gov/safewater/arsenic/arsenictradeshow/arsenic.cfm.

El-Bourawi, M.S., Khayet, M., Ma, R., Ding, Z., Li, Z., Zhang, **X., 2007.** Application of vacuum membrane distillation for ammonia removal, Journal of Membrane Science, Volume 301, Issues 1–2, Pages 200-209.

El-Bourawi, M.S., Ding, Z., Ma, R., Khayet, M., 2006. A framework for better understanding membrane distillation separation process, Journal of Membrane Science 285: 4-29.

Ergican, E., Gecol, H., Fuchs, **A., 2005.** The effect of co-occurring inorganic solutes on the removal of arsenic (V) from water using cationic surfactant micelles and an ultrafiltration membrane, Desalination 181, 9 – 26.

F

Fields, K., Chen, A., Wang, L., 2000. Arsenic removal from drinking water by iron removal plants, EPA 600R00086. Prepared by Battelle under contract 68C70008 for US.EPA ORD.

Figoli, A., Cassano, A., Criscuoli, A., Mozumder, M.S.I., Uddin, M.T., 2010. Influence of operating parameters on the arsenic removal by nano-filtration, Water research 44, 97 – 104;

Fogarassy, E., Galambos, I., Bekassy-Molnar, E., Vatai, **G., 2009.** Treatment of high arsenic content wastewater by membrane filtration, Desalination 240, 270 – 273.

G

Garcia-Payo, M.C., Izquierdo-Gil, M.A., Fernandez-Pineda, C., 2000. Air gap membrane distillation of aqueous alcohol solution, Journal of Membrane Science 169 (1), 61- 80.

Garcia-Payo, **M.C.,** 2002. Separation of binary mixtures by thermostatic sweeping gas membrane distillation: II. Experimental results with aqueous formic acid solutions, Journal of Membrane Science 198 (2), 197 – 210.

Geucke, T., Deowan, S.A., Hoinkis, J., Patzold, **Ch., 2009.** Performance of a small-scale desalinator for arsenic removal, desalination 239, 198 – 206.

Greenlee, L.F., Lawler, D.F., Freeman, B.D., Marrot, B., Moulin, **P., 2009.** Reverse osmosis desalination: water sources, technology, and it today's challenges, Water Research 43, 2317 – 2348.

Gunko, S., 2006. Concentration of apple juice using direct contact membrane distillation, Desalination 190 (1-3), 117 – 124.

H

Havezov, Tsekulov, **E., 2010.** Arsenic species iso-formation – A key problem for water purification, Springer Science + Business Media B.V.2010.

Hering, J.G., Chen, P., Wilkie, J.A., Elimelech, M., 1997. Arsenic removal from drinking water during coagulation, ASCE J.Env.Eng. 123 (8), 800 – 807.

Hoffmann, E., Odegaard, **H., 2012.** Chemical water and wastewater treatment, International Water Association publishing, London, pp 119 – 130.

Hug, S.J., Leupin, O.X., Berg, M., 2008. Bangladesh and Vietnam: Different groundwater compositions require different approaches to arsenic mitigation, Environmental science and Technology. Volume 42, no.17, p 6318 – 6323.

I

Izquierdo-Gil, M.A., Jonsson, **G., 2003.** Factors affecting flux and ethanol separation performance in vacuum membrane distillation (VMD), Journal of Membrane Science, Volume 214, Issue 1, Pages 113-130.

J

Jain, C.K., Ali, I., 2000. Arsenic: Occurrence, Toxicity and Speciation techniques, Water Research, Volume 34, Issue 17, pages 4304 – 4312.

Jain, C.K., Singh, R.D., 2012. Arsenic removal using adsorptive media treatment process, India water week 2012 – Water.

Jain, C.K., Singh, **R.D., 2012.** Technological options for the removal of arsenic with special reference to South East Asia, Journal of Environmental management 107, 1 – 18.

Jekel, M.R., 1994. Removal of Arsenic in drinking water treatment. In: Nriagu, J.O.(Ed), Arsenic in the environment, Part 1: Cycling and Characterization. John Wiley & Sons, Inc., New York.

Jessen, **S., 2009.** Groundwater arsenic in the Red river Delta, Vietnam: Regional distribution, release, mobility, and mitigation options, PhD thesis for Department of Environmental Engineering Technical University of Denmark.

Jin, Z., Yang, D.L., Zhang, S.H., Jian, **X.G., 2007.** Removal of 2,4-dichlorophenol from wastewater by vacuum membrane distillation using hydrophobic PPESK hollow fibre membrane, Chinese Chemical Letters, Volume 18, Issue 12, Pages 1543-1547.

Jones, H., Vissottiviseth, P., Bux, M.K., Foldenyi, R., Kovatsl, **N., 2008.** Case reports: Arsenic pollution in Thailand, Bangladesh, and Hungary, Reviews of Environmental Contamination Volume 197.

Jorgensen, R.B., Meyer, A.S., Pinelo, M., Varming, C., Jonsson, **G., 2011.** Recovery of volatile fruit juice aroma compounds by membrane technology: Sweeping gas versus vacuum membrane distillation, Innovative Food Science & Emerging Technologies, Volume 12, Issue 3, Pages 388-397.

K

Kang, M., Kawasaki, M., Tamada, S., Kamei, T., Magara, Y., 2000. Effect of pH on the removal of arsenic and antimony using reserve osmosis membranes, Desalination 131, 293 – 298.

Katsouiannis, I.A, Zouboulis, A.I., 2004. Application of biological processes foe the removal of groundwater: kinetic consideration and product characgerization. Water Res. 38 (7), 1922 – 1932.

Katsouiannis, I.A, Zouboulis, A.I., 2006. Use of iron and manganese oxidizing bacteria for the combined removal of iron, manganese, and arsenic from contaminated groundwater. Water Qual.Res.J.Can.41, 117 – 129.

Kartinen, E.O., Martin C.J., 2005. An overview of arsenic removal processes, Desalination 103, 79 – 88.

Khayet, M., Matsuura, T., 2011. Membrane distillation – Principles and applications, Elsevier Publication, Great Britain.

Khayet, M., Matsuura, T., 2004. Pervaporation and vacuum membrane distillation processes: Modeling and experiments, AIChE J.50, 1697 – 1712.

Khayet, M., Godino, M.P., Mengual, **J.I., 2003.** Possibility of nuclear desalination through various membrane distillation configurations: A comparative study, Int. J. Nuclear Desalination 1, 30-47.

Khayet, M., Velaszqez, A., Mengual, **J.I., 2004.** Direct contact membrane distillation of humic acid solutions, Journal of membrane Science 240, 123 – 128.

Khayet, M., Mengual, **J.I., 2004.** Effect of salt concentration during the treatment of humic acid solutions by membrane distillation, Desalination 168, 373 – 381.

Khayet, M., Godino, M.P., Mengual, **J.I., 2003.** Possibility of nuclear desalination through various membrane distillation configurations: A comparative study, Int. J. Nuclear Desalination 1, 30-47.

Khayet, M., Khulbe, K.C., Matsuura, **T., 2004.** Characterization of membranes for membrane distillation by atomic force microscopy and estimation of their water vapour transfer coefficient in vacuum membrane distillation process, Journal of Membrane Science 238, 199 – 211.

Khayet, M., 2001. Membranes and theoretical modelling of membrane distillation: A review, Adv.Colloid interface Science 164 (1-2), 56 – 88.

Koch membrane systems Inc, Reverse osmosis membranes remove arsenic and salt from water supplies, Membrane technology 140 (2001), 10 -11.

Kucera, **J., 2010.** Reverse Osmosis – Industrial applications and Processes, Copyright 2010 by Scrivener Publishing LLC.

L

Lawson, K.W., Lloyd, D.R., 1997. Membrane distillation: A review, Journal of Membrane Science 124, 10-025.

Lawson, K.W., Lloyd, D.R., 1996. Membrane distillation. I. Module design and performance valuation using vacuum membrane distillation, Journal of Membrane Science., 120, 111.

Lei, Z., Chen, B., Ding, Z., 2005. Special distillation processes, Elsevier publication, China

Li, B., Sirkar, **K.K., 2005.** Novel membrane and device for vacuum membrane distillation-based desalination process, Journal of Membrane Science 257, 60–75.

Li, J-M., Xu, Z-K., Liu, Z-M., Yuan, W-F., Xiang, H., Wang, **S-Y., 2003.** Microporous polypropylene and polyethylene hollow fibre membranes. Part 3. Experimental studies on membrane distillation for desalination, Desalination 155, 153-156.

Liang, C-P., 2009. An integrated GIS-based approach in Assessing Carcinogenic risks via Food chain exposure in arsenic-Affected groundwater areas, Wiley InterScience.

Ly, T.M., 2012. Arsenic contamination in groundwater in Vietnam: An overview and Analysis of the historical, cultural, economic, and political parameters in the success of various mitigation options. Pomona senior these. Paper 41. http://scholarship.claremont.edu/pomona_theses/41.

Loosveldt, H., Lafhaj, Z., Skoczylas, F., 2002. Experimental study of gas and liquid permeability of a mortar, Cement and Concrete Research 32:1357–1363.

Logsdon, G.S., Sorg, T.J., Symons, **J.M., 1974.** Removal of heavy metal by conventional treatment, paper presented at the 16th Water Quality Conference – University of Illinois, Urbana.

M

Mandal, B.K., Suzuki, **K.T., 2002.** Arsenic round the world: A review, Talanta 58, 201 – 235.

Manning, B.A., Fendorf, S.E., Bostick B., Suarez, D.L., 2002. Arsenite and arsernate adsorption reaction on synthetic birnessite, Environ.Sci.Technol., 36, 976 – 981.

Mericq, J-P, Laborie, S., Cabassud, C., 2010. Vacuum membrane distillation of seawater reverse osmosis brines, Water Research, Volume 44, Issue 18, October 2010, Pages 5260-5273.

Mericq, J-P, Laborie, S., Cabassud, C., 2011. Evaluation of systems coupling vacuum membrane distillation and solar energy for seawater desalination, Chemical Engineering Journal, Volume 166, Issue 2, 15 January 2011, Pages 596-606.

Mengual, J.I., Khayet, M., Godino, M.P., 2004. Heat and mass transfer in vacuum membrane distillation, International Journal of Heat and Mass Transfer 47, 865–875.

Mohan, D., Pittman Jr, **C.U., 2007.** Arsenic removal from water/wastewater using adsorbents – A critical review, Journal of Hazardous Materials 142, 1 – 53.

Mouchet, P., 1992. From conventional to biological removal of iron and manganese in France. J. Am. Water Works Assoc. 84 (4), 158 – 166.

Mohammadi, T., Akbarabadi, **M., 2005.** Separation of ethylene glycol solution by vacuum membrane distillation (VMD), Desalination, Volume 181, Issues 1–3, Pages 35-41.

Mohammadi, T., Safavi, **M.A., 2009.** Application of Taguchi method in optimization of desalination by vacuum membrane distillation, Desalination 249, 83-89.

Murcott, S., 2013. Arsenic contamination: A worldwide call for action, International Water Association Publishing (IWA).

N

Narasimhan, R., Thomson, B., Chwirka, J., Lowry, J., 2005. Chemistry and treatment of arsenic in drinking water. American water works association research foundation.

Ning, R.Y., 2002. Arsenic removal by reverse osmosis, Desalination 143, 237 – 241.

Nguyen P.K., 2008. Geochemical Study of arsenic behaviour in Aquifer of the Mekong Delta, Vietnam, A PhD dissertation in Kyushu Univerisity.

NSF International, 2001a, Environmental Technology Verification report: removal of arsenic in drinking water – hydranautics ESPA 2 – 4040 reverse osmosis membrane element module, NSF 0120EPADW395, March 2001.

NSF International, 2001b, Environmental Technology Verification report: removal of arsenic in drinking water – KOCH membrane system TFC – ULP4 reverse osmosis membrane element module, NSF 0120EPADW395, August 2001.

Nriagu, J.O., Pacyna, J.M., 1998. Quantitative assessment of worldwide contamination of air, water and soils by trace metals, Nature, 333(6169), 134 – 139, doi:10.1038/333134a0.

P

Pal, P and Manna, A.K., 2010. Removal of As from contaminated groundwater by solar-driven membrane distillation using three different membranes. Water Research 11/2010; 44 (19):5750-60.

Pontius, F.W., 1995. Crafting a new arsenic rule, J.Am. Water Works Assoc.87 (9), 6-10.

Pokhrel, D., Viraraghavan, **T., 2009.** Biological filtration for removal of arsenic from drinking water, Journal of environmental management 90, 1956 – 1961.

Q

Qu, D., Wang, J., Hou, D., Luan, Z., Fan, B., Zhao, C., 2009. Experimental study of arsenic by direct contact membrane distillation. Journal of Hazardous Materials, volume 163, Issues 2-3, 30 April 2009, pages 874 – 879.

S

Sato, Y., Kang, M., Kamei, T., Magara, Y., 2002. Performance of nanofiltration for arsenic removal. Water.Res.36:3371 – 3377.

Sarti, G.C., Gostoli, C., Bandini, **S., 1993.** Extraction of organic components from aqueous streams by vacuum membrane distillation, Journal of Membrane Science, Volume 80, Issue 1, , Pages 21-33.

Sarbatly, R., Chiam, C-K., 2013. Evaluation of geothermal energy in desalination by cavuum membrane distillation, Applied Energy xxx(2013)xxx-xxx.

Safavi, M., Mohammadi, T., 2009. High-salinity water desalination using VMD, Chemical Engineering Journal 149, 191 – 195.

Shih, M-C., 2005. An overview of arsenic removal by pressure-driven membrane process, Desalination 172, 85 – 97.

Shinkai, Y., Truc, D.V., Sumi, D., Canh, D., Kumagai, **Y., 2007.** Arsenic and other metal contamination of groundwater in the MeKong delta river, Vietnam, Journal of Health Science, 53(3), 344 – 346.

Smedley, P.L., Kinniburgh, **D.G., 2003.** Source and behaviour of arsenic in natural waters, British Geological Survey, Wallingford, Oxon OX10 8BB, U.

Smith, A.H., Smith, M.M.H., 2004. Arsenic drinking water regulations in developing countries with extensive exposure. Toxicology, 198(1-3), 39–44.

Sorg, T.J., Logsdon, G.S., 1974. Treatment technology to meet the interim primary drinking water regulation for inorganic: part 2. L.Am.Water Works Assoc.70 (7), 379 – 393.

Soni, V., Abildskov, J., Jonsson, G., Gani, **R., 2008.** Modelling and analysis of vacuum membrane distillation for the recovery of volatile aroma compounds from black currant juice, Journal of Membrane Science, Volume 320, Issues 1–2, Pages 442-455.

Srisurichan, S., Jiraratananon, R., Fane, **A.G., 2005.** Humic acid fouling in the membrane distillation process, Desalination 174, 63 – 72.

T

Tang, J., Zhou, **K., 2006.** Hydrochloric acid recovery from rare earth chloride solutions by vacuum membrane distillation, Rare Metals, Volume 25, Issue 3, Pages 287-292.

Tang, N., Jia, Q., Zhang, H., Li, H., Cao, **S., 2010.** Preparation and morphological characterization of narrow pore size distributed for vacuum membrane distillation via thermally induced phase separation, Desalination 256, 27 – 36.

Tanikawa, W., Shimamoto, T., Klinkenberg., 2006. Effect for gas permeability and its comparison to water permeability for porous sedimentary rocks, Hydrol.Earth Syst.Sci.Discuss., 3, 1315 – 1338.

Tomaszewska, M., Gryta, M., Morawski, A.W., 1995. Study on the concentration of acids by membrane distillation, Journal of Membrane of Science 102, 113 – 122.

U

Ujevic, M., Casiot, C., Duic, Z., Santo, V., Dadic, Z., Sipos, **L., 2010.** Distribution and speciation of Arsenic in groundwater and tap waters of eastern Croatia, Springer Science.

Urase, T., Oh, J., Yamamoto, K., 1998. Effect of pH on rejection of different species of arsenic by nanofiltration, Desalination 117, 11 – 18.

Urtiaga, A.M., Ruiz, G., Ortiz, I., 2000, Kinetic analysis of the vacuum membrane distillation of chloroform from aqueous solutions, Journal of Membrane Science, Volume 165, Issue 1, 17, Pages 99-110.

Urtiaga, A.M., Gorri, E.D., Ruiz, G., Ortiz, **I., 2001,** Parallelism and differences of pervaporation and vacuum membrane distillation in the removal of VOCs from aqueous streams, Separation and Purification Technology, Volumes 22–23, 1 March 2001, Pages 327-337.

V

Villaescusa, I., Bollinger, **J-C., 2008.** Arsenic in drinking water: sources, occurrence and health effects: a review, Rev Environ Sci Biotechnol 7:307-323.

W

Walton, J., Lu, H., Turner, C., Solis, S., Hein, H.,2004. Solar and waste heat desalination by membrane distillation, College of Engineering University of Texas, El Paso.

Wang, L., Chen, A., Fileds, K., 2000. Arsenic removal from drinking water by ion exchange and activated alumina plants. EPA 600R00088, prepared by Battelle under contract 68C70008 for U.S.EPA ORD.

Wang, X., Zhanga, L., Yanga, H., Chena, H., 2009. Feasibility research of potable water production via solar-heated hollow fiber membrane distillation system, Desalination 247, 403 –411.

Wang, Z., Gu, Z., Feng, S., Li, **Y., 2009.** Application of vacuum membrane distillation to lithium bromide absorption refrigeration system, International Journal of Refrigeration, Volume 32, Issue 7, Pages 1587-1596.

Wirth, **D., 2002.** Etude de la distillation membranaire sous vide pour le dessalement d'eau de mer: de l'analyse des mécanismes de transfert a l'optimisation énergétique de procédé, Thèse de Doctorat, INSA Toulouse.

Wu, B., Tan, X., Li, K., Teo, **W.K., 2006.** Removal of 1,1,1-trichloroethane from water using a polyvinylidene fluoride hollow fiber membrane module: Vacuum membrane distillation operation, Separation and Purification Technology, Volume 52, Issue 2, Pages 301-309.

X

Xu, Y., Zhu, B-K., Xu, Y-Y., 2006. Pilot test of vacuum membrane distillation for sea water desalination on a ship, Desalination 189, 165 – 169.

Y

Yasuda, H., Tsai, **J.T., 1974.** Pore size of micro-porous polymer membranes, Journal of Applied Polymer Sicence. 18, 805 – 81.

Yarlagadda, S., Gude, V.G, Camacho, L.M., Pinappu, S., Deng, S., 2011. Portable water recovery from As, U and F contaminated groundwater by direct contact membrane distillation process. Journal of Hazardous Materials 192 (2011) 1388 – 1394.

Z

Zhao, Z-P., Ma, F-W., Liu, W-F., Liu, **D-Z., 2008.** Concentration of ginseng extracts aqueous solution by vacuum membrane distillation. 1. Effects of operating conditions, Desalination, Volume 234, Issues 1–3, Pages 152-157.

Zhao, Z-P., Ma, F-W., Liu, W-F., Liu, **D-Z., 2011.** Concentration of ginseng extracts aqueous solution by vacuum membrane distillation 2. Theory analysis of critical operating conditions and experimental confirmation, Desalination, Volume 267, Issues 2–3, 15 February 2011, Pages 147-153.

Zouboulis, A.I., Katsoyiannis, I.A., 2002. Removal of arsenic from contaminated groundwater using combined chemical and biological treatment methods.

RESUME EN FRANÇAIS DE LA THESE :

Cette thèse de doctorat concerne l'étude de la distillation membranaire sous vide pour l'élimination de l'arsenic contenu dans les eaux souterraines. En effet, la contamination des nappes phréatiques par l'arsenic, à des concentrations largement supérieures aux valeurs recommandées par l'OMS, est une problématique majeure dans de nombreux pays, et en particulier au Vietnam. Avec des concentrations en arsenic comprises entre 1 et 1610 $\mu g.L^{-1}$ dans le delta du Mékong (au sud du Vietnam) et entre 1 et 3050 $\mu g.L^{-1}$ dans le du delta du fleuve rouge (au Nord du Vietnam), c'est entre 10 et 15 millions de vietnamiens (soit environ 13% de la population) qui se trouvent empoisonnés par ces eaux souterraines contaminées par l'arsenic. De plus, ces eaux présentent des salinités élevées (5-10 $g.L^{-1}$) dues à des infiltrations d'eau de mer dans les nappes.

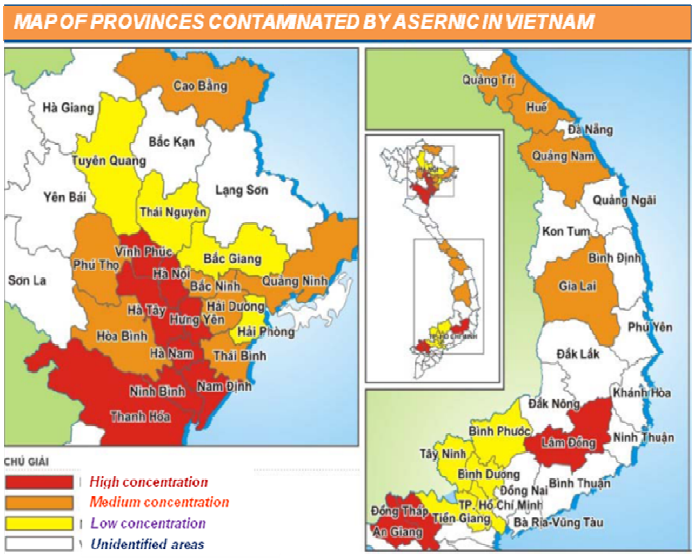

Répartition de la contamination en arsenic au Vietnam

Ce travail de thèse, qui prend pour cas d'étude la contamination par l'arsenic des eaux souterraines saumâtres au Vietnam, se propose d'étudier la faisabilité de la distillation membranaire sous vide afin de répondre à un double objectif : éliminer l'arsenic contenu dans ces eaux et réduire leur salinité afin de les rendre propres à la consommation humaine. Une partie du travail consistera également à l'étude du couplage de la distillation membranaire sous vide avec l'osmose inverse.

La thèse comporte 5 chapitres rédigés en anglais.

Le chapitre 1 est une revue bibliographique qui présente dans un premier temps les caractéristiques physico-chimiques de l'arsenic, sa toxicité et ses principales sources.

L'arsenic est un élément chimique métalloïde semi-métallique de la famille des pnictogènes, de symbole As et de numéro atomique 33, présentant des propriétés intermédiaires entre celles des métaux et des non-métaux. Il existe sous des formes organiques et inorganiques, les plus dangereuses étant ces dernières. On peut trouver de l'arsenic inorganique dans l'environnement sous plusieurs formes mais dans les eaux naturelles il se présente la plupart du temps sous forme d'arsénite trivalent (As(III)) ou d'arséniate pentavalent (AS(V)).

Un état des lieux des différentes techniques utilisées pour l'éliminer est ensuite dressé. Outre les techniques de traitement conventionnelles telles que l'adsorption, la précipitation ou l'échange d'ion, les procédés de filtration par membrane (nanofiltration, osmose inverse) font également l'objet d'études. Néanmoins, un inconvénient majeur de ces procédés est la nécessité de pré-oxyder l'arsenic(III) en arsenic (V) afin d'assurer une efficacité d'élimination suffisamment élevée et de produire ainsi une eau dont la teneur en arsenic est inférieure à la valeur limite fixée par les normes en eau potable, soit 10 $\mu g.L^{-1}$ au Vietnam. Un autre procédé membranaire, la distillation membranaire, montre en revanche de très fortes potentialités en termes d'efficacité d'élimination, sans nécessité une pré-oxydation de l'arsenic. La suite du chapitre développe alors les aspects théoriques de ce procédé membranaire qui sera mis en œuvre dans la suite de l'étude. La distillation membranaire (DM) est un procédé hybride combinant à la fois un procédé thermique et un procédé membranaire. La membrane met en contact direct un liquide côté alimentation et une phase liquide ou gazeuse côté perméat. La force de transfert du procédé est la différence de pressions partielles entre les deux côtés de la membrane qui provoque une évaporation du côté alimentation. La membrane sert uniquement de support à l'interface liquide-gaz et n'intervient pas dans le procédé séparatif. La membrane macroporeuse doit être hydrophobe afin d'empêcher le liquide de pénétrer à l'intérieur des pores de la membrane.

Le procédé de distillation membranaire comporte plusieurs étapes. Tout d'abord le fluide à traiter, sous forme liquide, s'évapore au voisinage des pores de la membrane à l'interface entre les phases liquide et vapeur du côté alimentation de la membrane. Les molécules du fluide sont ensuite transportées, sous forme vapeur uniquement, à travers les pores de la

membrane. Enfin, le fluide sous forme vapeur se condense de l'autre côté de la membrane par divers procédés.

Il existe quatre configurations possibles de distillation membranaire: la Direct Contact Membrane Distillation (DCMD), l'Air Gap Membrane Distillation (AGMD), la Sweeping Gas Membrane Distillation (SGMD) et la Vacuum Membrane Distillation (VMD) (Distillation Membranaire Sous Vide ou VMD). La différence entre ces configurations vient de la façon dont est générée la différence transmembranaire de pression partielle.

Dans cette thèse, la distillation membranaire est menée selon la configuration VMD, il s'agit donc d'une distillation membranaire sous vide.

Le chapitre 1 décrit quelques études ayant traité de la distillation membranaire pour éliminer de l'arsenic, ou pour dessaler de l'eau. Les conclusions de ces études divergent sur quelques points, en particulier sur les valeurs de flux de perméat obtenues qui dépendent très fortement du type de membrane hydrophobe utilisée. De plus, l'effet de la concentration en arsenic dans la solution d'alimentation n'est pas toujours le même, suivant les auteurs. D'autre part, la plupart de ces études ont utilisé des solutions synthétiques d'arsenic préparées dans de l'eau distillée (ou ultra pure), et donc, l'influence de la présence de sels ou de matière organique, sur le colmatage des membranes, ou sur leur mouillage, n'a pas été pleinement étudiée, en particulier dans le cas de la configuration sous vide.
Ce chapitre ce conclut par une présentation des objectifs du travail de thèse proposé : étudier l'influence des paramètres opératoires sur les performances de la DMV, afin d'éliminer de l'arsenic en présence de sels. Le colmatage de la membrane sera pris en considération, en présence de calcium et de matière organique.
D'autre part, un procédé global, intégrant DMV et osmose inverse (OI) sera également étudié, afin d'augmenter le taux de conversion global.

Dans la suite du travail, seul le cas de l'arsenic trivalent (As(III)) est pris en compte.

Le chapitre 2 est une synthèse des matériels et méthodes mis en œuvre dans ce travail de recherche. Les expériences de distillation membranaire sous vide ont été menées sur un pilote de laboratoire, équipé d'un débitmètre massique permettant de suivre l'évolution du flux de perméat en continu. Le pilote est schématisé sur la figure ci-dessous.

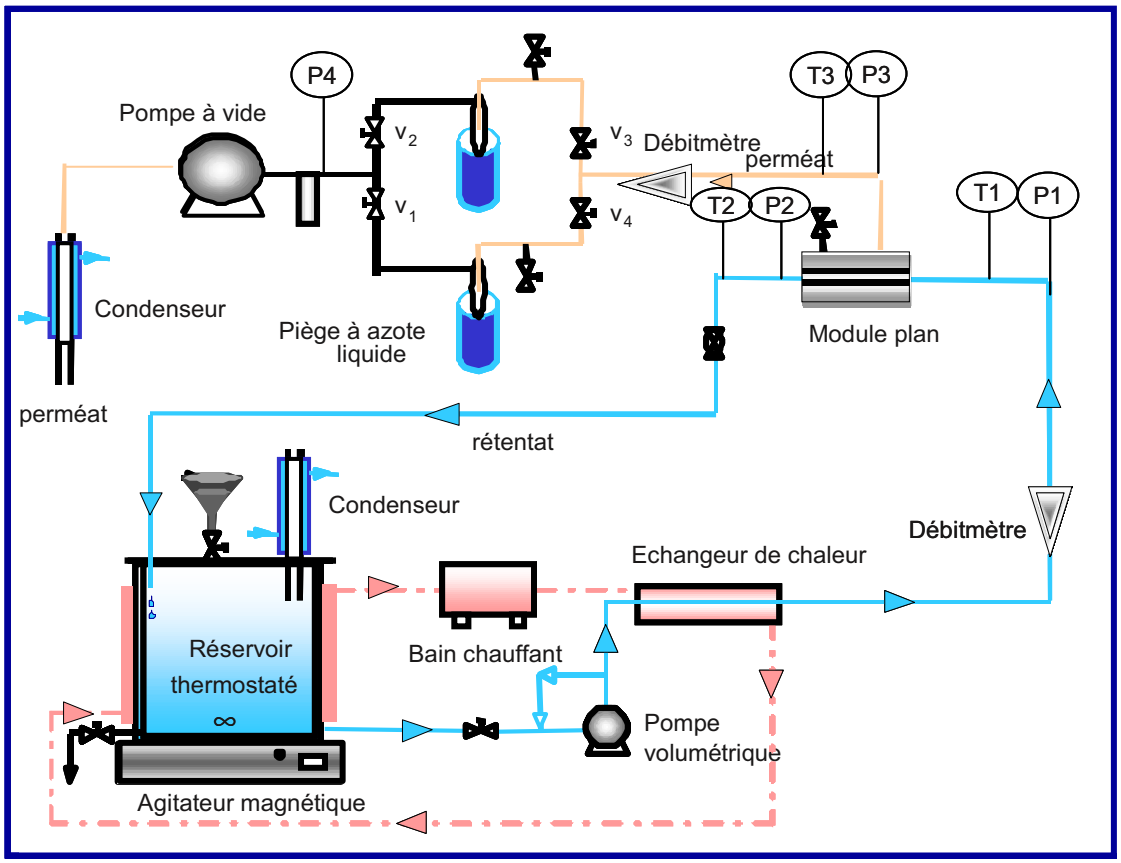

La membrane utilisée est une membrane plane, de surface $5{,}78.10^{-3}$ m^2.

Deux membranes hydrophobes commerciales (Durapore et Fluoropore de la société Millipore) ont été étudiées. Les caractéristiques de ces deux membranes sont présentées dans le tableau ci-dessous.

Membrane	Matériau	Epaisseur (mm)	Diamètre moyen de pores (µm)	Porosité (%)
Durapore	PVDF	0,125	0,2	75
Fluoropore	PTFE	0,175	0,2	70

Les expériences d'osmose inverse ont été menées dans une cellule agitée en acier inoxydable (Polymem, France) présentée sur la figure suivante.

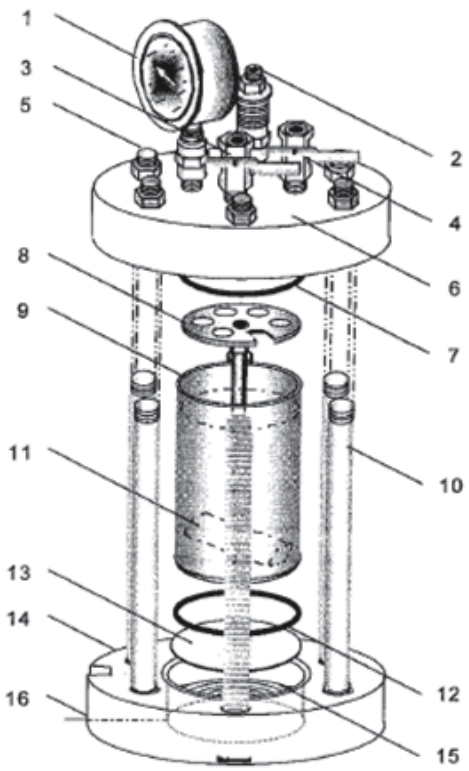

1. Manomètre
2. Soupape de sécurité
3. Vanne d'alimentation du liquide
4. Vanne d'alimentation d'air comprimé
5. Ecrou d'assemblage
6. Plaque supérieure
7. Joint supérieur
8. Tête de l'agitateur
9. Corps de la cellule
10. Pilier d'assemblage
11. Barreau alimenté
12. Joint inférieur
13. Membrane
14. Plaque inférieur
15. Support membranaire
16. Sortie du perméat

La filtration frontale est effectuée en discontinu. Des membranes planes de diamètre 9 cm sont utilisées. La cellule offre une surface active filtrante de 41,7 cm^2 et un volume total de 500 mL. Un circuit d'azote liquide est utilisé afin d'imposer une pression transmembranaire variant entre 0 et 36 bar. Un agitateur magnétique permet d'agiter en continu le liquide à la surface de la membrane afin d'éviter l'effet de polarisation de concentration. Le flux de perméat est déterminé par pesée de la masse du perméat récolté à intervalles de temps réguliers grâce à une balance électronique (Sartorius 1500S) connectée à un ordinateur.

Les caractéristiques de la membrane sont présentées dans le tableau ci-dessous.

Spécification	**Valeur**
Fabricant	Hydranautics
Matériau	Polyamide
Seuil de coupure ($g.mol^{-1}$)	< 200
Salt retention	> 98.7% $CaCl_2$
Perméabilité à l'eau à 20°C: (L.h-1.m-2.bar-1)	3.6

Tous les essais ont été menés sur des eaux synthétiques contenant de l'arsenic (III) (Gamme de concentration étudiée = [100-7000] $\mu g.L^{-1}$), du NaCl ([10-300] $g.L^{-1}$) et dans certains cas, de l'acide humique (AH) ([20-165] $mg.L^{-1}$) ou du $CaSO_4$. ([Ca^{2+}] = 0,5 $g.L^{-1}$).

Solutions étudiées	**As(III)** (µg/L)	**NaCl** (g/L)	**$CaSO_4$** (g/L)	**AH** (mg/L)	**pH** -	**Ec** (mS/cm)	**COT** (mg/L)
As(III) + NaCl	100	10	-	-	6.8	17.98	-
As(III) + NaCl	300	10	-	-	6.8	16.40	-
As(III) + NaCl + $CaSO_4$	300	10	0.5	-	6.5	15.92	-
As(III) + NaCl + AH	300	10	-	20	6.7	16.95	7.5
As(III) + NaCl + AH	7000	300	-	165	6.0	247	50

Les méthodes analytiques mises en œuvre au cours des expérimentations sont les suivantes : mesures de conductivité électrique (Ec), afin d'estimer la concentration en sels dans les échantillons, mesures de carbone organique total (COT) dans le cas des essais comportant de la matière organique, et enfin des mesures de spectrophotométrie à émission optique (ICP) afin de quantifier la teneur en arsenic. La limite de quantification de l'appareil utilisé est de 5 $\mu g.L^{-1}$.

Pour finir, des observations au microscope électronique à balayage, équipé d'une sonde d'analyse chimique élémentaire (EDS-X), ont été effectuées sur les échantillons de membrane recueillis après les expériences.

Le chapitre 3 est constitué par une publication parue dans la revue internationale Water Research et intitulée :

« A new method for permeability measurement of hydrophobic membranes in Vacuum Membrane Distillation process », T.D. Dao, J.-P. Mericq, S. Laborie, C. Cabassud, Water Research 47 (2013), 2096-2104.

Dans cette publication, l'objectif est de proposer une méthode de mesure de la perméabilité de la membrane à la vapeur d'eau, en s'appuyant sur une variation continue de la température d'alimentation, la pression de perméat étant maintenue constante. Cette méthode s'avère beaucoup plus adaptée au cas de la distillation membranaire sous vide que les méthodes classiques de mesure de perméation gazeuse, qui mettent en œuvre des variations discontinues de la pression à température constante. La méthode proposée est simple à mettre en œuvre, fiable et évite les fluctuations du système qui apparaissent lors d'une mesure de perméabilité effectuée par variation de pression. Cette méthode de mesure de perméabilité a été mise en œuvre et testée sur deux membranes (Fluoropore et Durapore de la société Millipore) afin tout d'abord de la comparer à la méthode « classique » par variation de pression. Cette comparaison a permis de valider la nouvelle méthode proposée et de montrer sa fiabilité.

Dans un second temps, la nouvelle méthode de mesure de perméabilité par variation de température a été utilisée pour comparer les performances des deux membranes, et a permis de choisir la plus perméable des 2, la Fluoropore, pour mener les essais suivants.

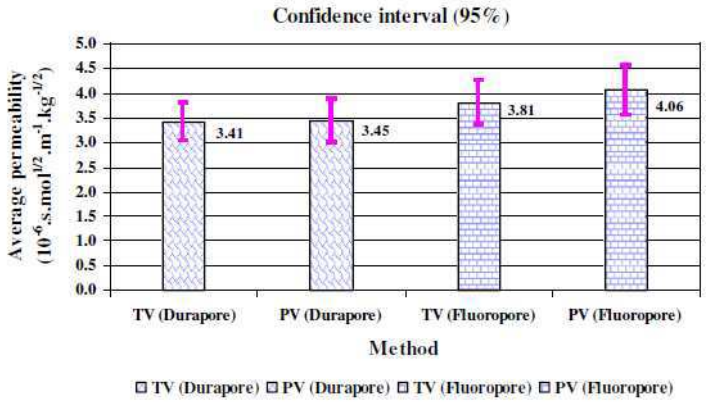

Fig. 8 – Average permeability values and confidence intervals (95%) obtained by two different methods (Durapore and Fluoropore membranes).

Extrait de la publication « A new method for permeability measurement of hydrophobic membranes in Vacuum Membrane Distillation process », T.D. Dao, J.-P. Mericq, S. Laborie, C. Cabassud, Water Research 47 (2013), 2096-2104.

Le chapitre 4 consiste en l'étude de la distillation membranaire sous vide pour le traitement direct d'une solution contenant des sels ([NaCl] = 10 $g.L^{-1}$) et de l'arsenic (III). Les résultats montrent que la DMV est un procédé qui permet d'éliminer directement à la fois l'arsenic et le chlorure de sodium, en évitant une étape de pré-oxydation de l'As(III) en As(V), étape nécessaire dans de nombreux procédés conventionnels de traitement. Les concentrations en As(III) dans le perméat de DMV sont toujours inférieures aux limites de la norme en eau potable (10 $\mu g.L^{-1}$), même pour de très fortes concentrations en As(III) dans l'alimentation (jusqu'à 2000 $\mu g.L^{-1}$). La même tendance est observée pour le NaCl avec un taux d'élimination de plus de 99,5%.

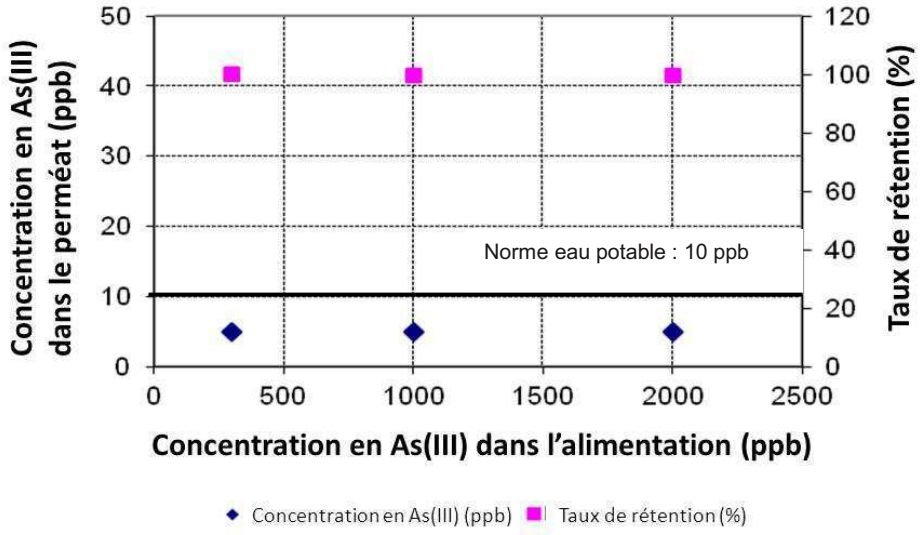

Effet de la concentration en As(III) dans l'alimentation sur les performances de la DMV (Membrane Fluoropore, [NaCl] = 10 $g.L^{-1}$, T_f = 40°C, Pp = 4500 Pa, Re = 3400).

Ces résultats permettent de confirmer que l'efficacité d'élimination de la distillation membranaire sous vide vis-à-vis de l'arsenic ne dépend pas de la concentration en arsenic dans l'alimentation.

Ce chapitre décrit en outre l'influence des conditions opératoires du procédé sur le flux de perméat obtenu. Pour les conditions opératoires retenues (Membrane Fluoropore, $T_{alimentation}$ = 40°C, P = 4500 Pa, Re = 3400), un flux de perméat moyen de 5 $L.h^{-1}.m^{-2}$ est obtenu, mais des valeurs de flux de 14 $L.h^{-1}.m^{-2}$ peuvent être atteintes pour une température d'alimentation de 55°C (autres paramètres identiques).

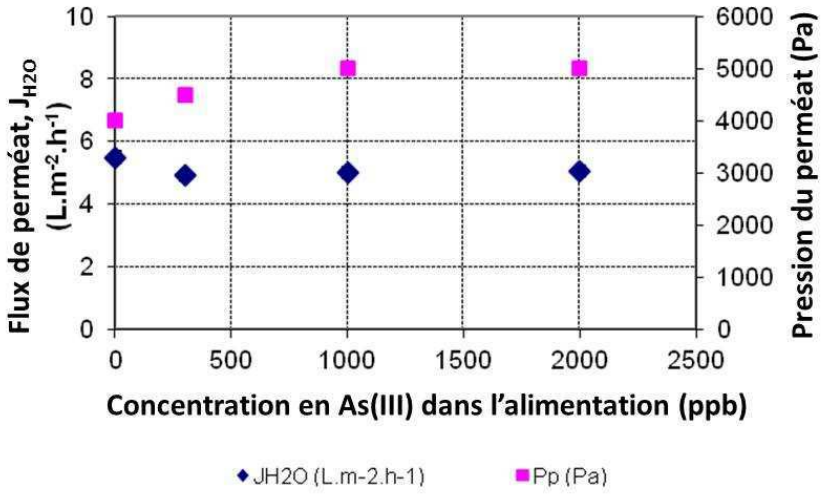

Effet de la concentration en As(III) dans l'alimentation sur les performances de la DMV (Membrane Fluoropore, [NaCl] = 10 g.L^{-1}, T_f = 40^{0}C, Pp = 4500 Pa, Re = 3400).

Enfin, l'étude démontre que le flux de perméat est peu affecté par les phénomènes de colmatage. En effet, des essais en présence de matière organique (acide humique à une concentration de 20 mg.L^{-1}) ont été menés tout d'abord sur une échelle de temps courte (1h).

Les résultats, présentés sur la figure suivante, montrent que le flux de perméat est le même pour les différentes solutions étudiées, que ce soit en présence ou pas de matière organique. Pour ces expériences de courte durée, aucun colmatage ni précipitation n'est observé. Cela signifie également que la présence de matière organique ne modifie pas l'hydrophobicité de la membrane puisqu'aucun mouillage n'est observé.

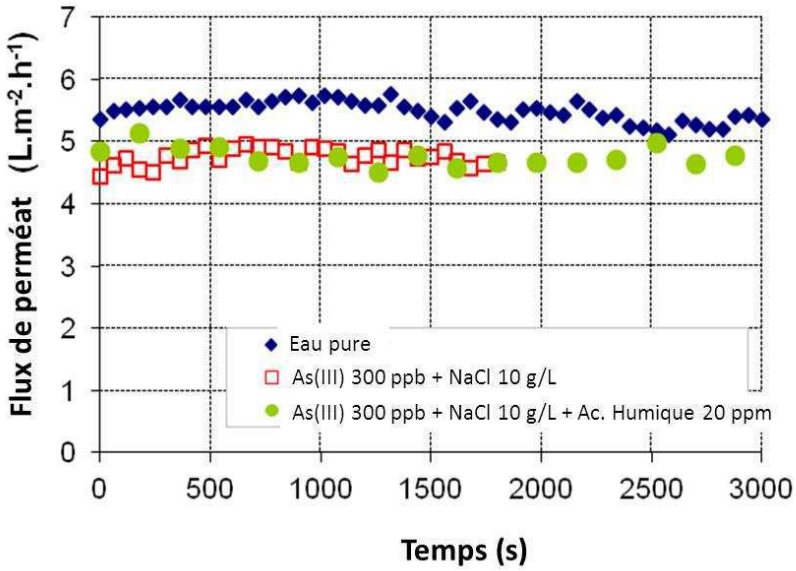

Enfin, des essais de plus longue durée (5 jours) ont également été menés avec une solution contenant de l'As(III) à 300 ppb, du NaCl à 10 g/L et de l'acide humique à 20 ppm. Le flux de perméat obtenu est relativement stable, avec une chute de flux de seulement 6% en 5 jours d'opération.

Cette légère chute de flux peut être attribuée à l'accumulation de matière organique à la surface de la membrane, qui peut modifier la structure de la membrane soit en surface soit à l'intérieur des pores, ou encore à de l'adsorption. Néanmoins, même à cette concentration élevée en matière organique (COT de 7,5 mg/L), et à l'échelle de temps de ces expériences (quelques jours), l'influence du colmatage par la matière organique semble faible.

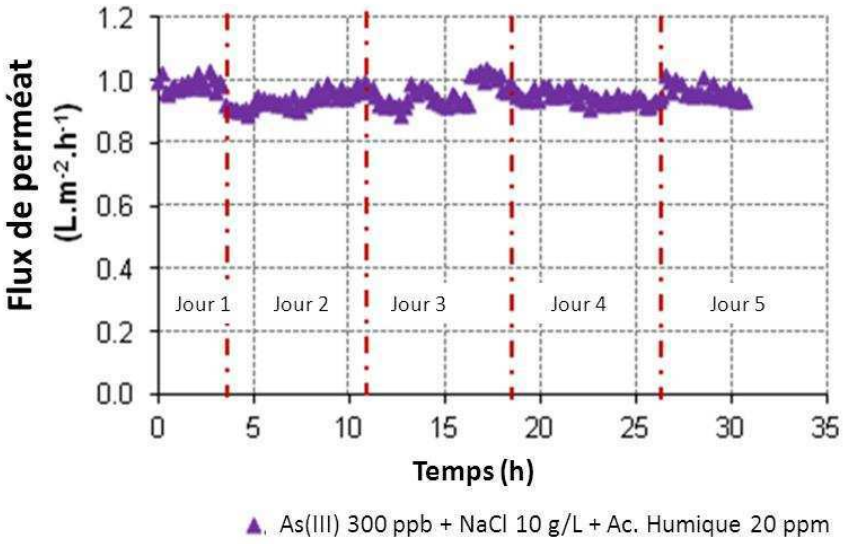

En résumé, le chapitre 4 démontre la faisabilité du traitement direct des solutions saumâtres contenant de l'arsenic par distillation membranaire sous vide.

Enfin, le chapitre 5 se propose de coupler l'osmose inverse (OI) et la distillation membranaire sous vide : l'étape d'OI est une première étape permettant une pré-concentration en NaCl et As(III), puis ce rétentat est alors sur-concentré grâce à l'étape de DMV.
L'objectif de ce couplage OI + DMV est de réduire le volume des rétentats d'OI et ainsi d'augmenter le taux de conversion global du procédé.

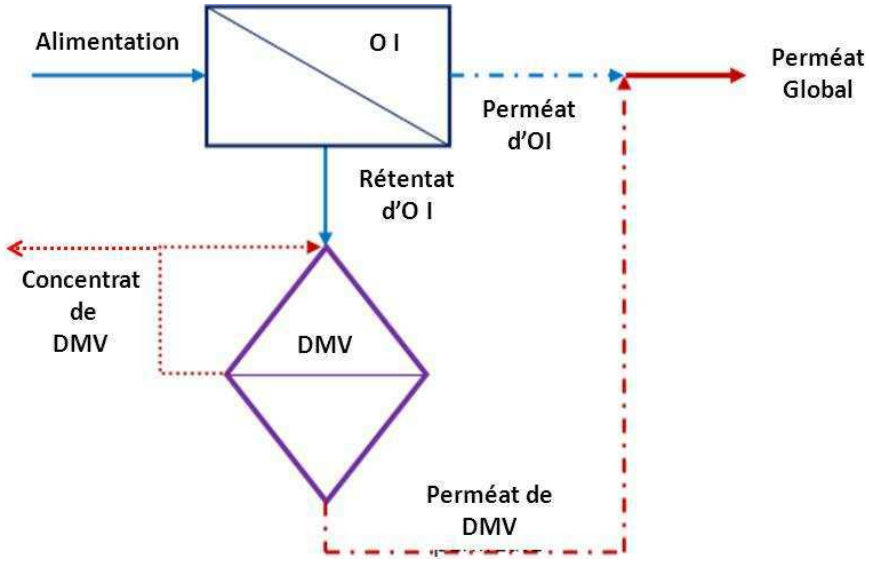

Ce chapitre est divisé en trois parties.

Dans une première partie, les performances de l'osmose inverse pour traiter directement l'arsenic sont étudiées. L'influence des conditions opératoires (pH, pression transmembranaire, taux de conversion…) est étudiée d'une part sur le taux de rétention de la membrane d'OI (en As(III) et en sels) ainsi que sur le flux de perméat obtenu.

Les figures ci-dessous présentent l'influence du pH et de la pression transmembranaire sur le taux de rétention en As(III) et en NaCl. Les résultats confirment le rôle important joué par le pH dans le cas de la retention en As(III), avec un taux qui augmente fortement de 60% (maximum) à 87% lorsque le pH augmente de 7 à 10.

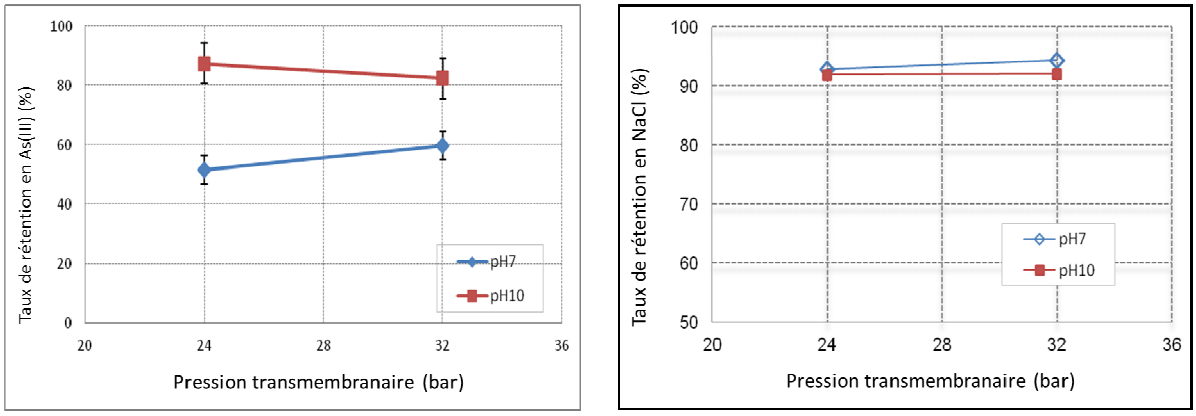

Taux de retention de l'As(III) et du NaCl en fonction du pH et de la pression transmembranaire ($[As(III)]_{initial}$ = 300 ppb et $[NaCl]_{initial}$ = 10 $g.L^{-1}$]

D'autre part, des expériences d'osmose inverse ont été menées en mode batch, en augmentant progressivement la concentration en arsenic dans la cellule d'alimentation, et en mesurant la concentration obtenue dans le perméat. Les résultats sont présentés sur la figure suivante :

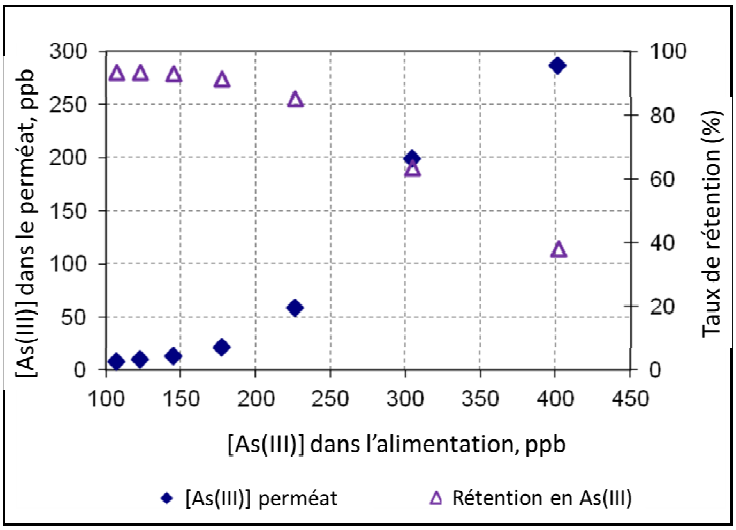

($[As(III)]_{initial}$ = 107 ppb; $[NaCl]_{initial}$ = 10 $g.L^{-1}$; pH 10; PTM = 24 bars)

Pour une concentration initiale en As(III) de 100 $\mu g.L^{-1}$, le taux de conversion maximum permettant d'atteindre la valeur cible dans le perméat (c'est-à-dire la valeur maximale autorisée de 10 $\mu g.L^{-1}$) est de 42% (Membrane osm-ESPA, pH = 10, PTM 24 = bars). Cette valeur maximale de taux de conversion passe à 60% en présence de matière organique (acide humique).

Dans une seconde partie, le chapitre 5 étudie les performances de la DMV pour traiter un concentrat d'osmose inverse, contenant de très fortes concentrations en espèces étudiées. Trois cas sont étudiés : un concentrat ne contenant que de l'As(III), un autre contenant de l'As(III) + NaCl et enfin un contenant As(III) + NaCl + Acide humique.

Concernant les taux de rétention obtenus grâce à la distillation membranaire sous vide, il est observé que même à une très forte concentration en As(III) (7000 µg/L), ce procédé permet toujours de limiter les teneurs en arsenic dans le perméat à des valeurs en-dessous de la norme (10 $\mu g.L^{-1}$).

Concernant les performances de la distillation membranaire en termes de flux de perméat, une chute de celui-ci est observée dans le cas de la solution contenant : As(III) + NaCl, ainsi que pour celle contenant As(III) + NaCl + Acide humique. Cette chute est du même ordre de grandeur pour ces deux solutions : de 5 à 3,5 $L.h^{-1}.m^{-2}$ pour une durée d'opération d'environ 27 heures. Cette chute de flux, due à la chute de perméabilité membranaire est attribuée à la précipitation de sels, et non à la présence de matière organique.

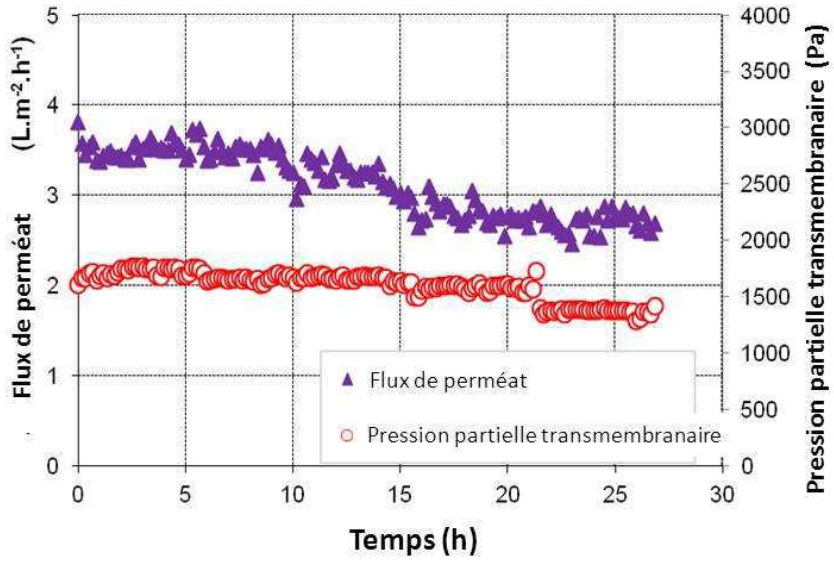

[As(III)] = 7000 ppb; [NaCl] = 300 g/L; [AH] = 165 mg/L; T_f = 40°C; Pp = 4500 Pa; Re = 3400

Enfin, dans une troisième partie, une simulation d'un procédé global, incluant osmose inverse et distillation membranaire, et fonctionnant à un taux de conversion global de 96%, est effectuée. L'osmose inverse peut être menée à un taux de conversion de 56% tout en obtenant un perméat répondant aux normes de rejet, et ce grâce au mélange du perméat d'OI avec celui de la DMV.

Le tableau ci-dessous synthétise la simulation du couplage OI+DMV, qui est comparé au procédé d'osmose inverse seul (pour lequel le taux de conversion maximum est de 42% comme présenté ci-dessus).

Paramètres	**Unité**	**Procédé d'OI seul**	**OI + DMV**		
			OI	DMV	Global
Débit d'alimentation, Q_F	$L.h^{-1}$	1000	1000	440	1000
Taux de conversion, Y	%	42	56	91.3	96.15
Débit de perméat, Q_P	$L.h^{-1}$	420	560	401.5	961.5
Débit de rétentat, Q_R	$L.h^{-1}$	580	440	38.5	38.5
Concentration en As(III) rétentat	ppb	177	226	2586	2586
Concentration en NaCl rétentat	$g.L^{-1}$	20	26	300	300

Pour ce taux de conversion global de 96%, un calcul de l'influence de la température d'alimentation en DMV sur la surface de membrane d'une part et sur la consommation spécifique d'énergie d'autre part est présenté. Les résultats sont présentés sur la figure ci-dessous. Une température de 35°C apparaît comme un bon compromis pour minimiser à la fois surface de membrane et consommation énergétique.

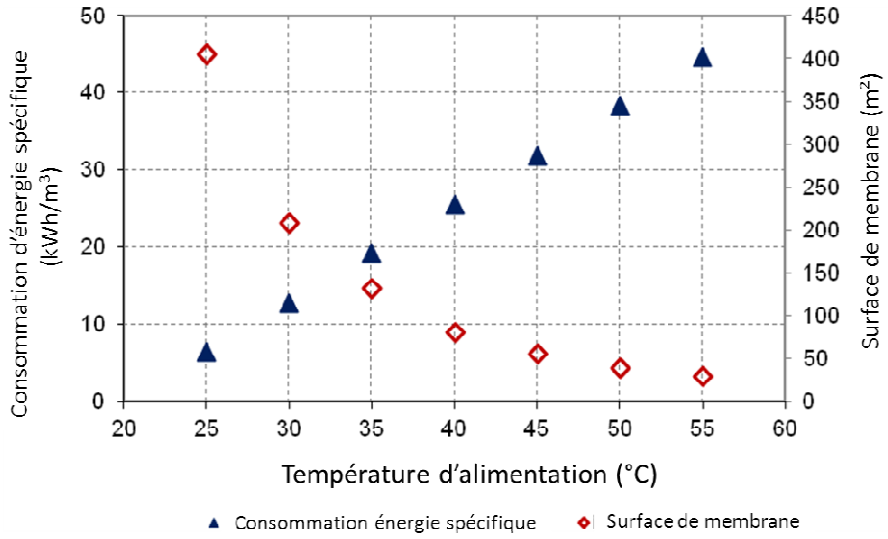

En résumé de ce chapitre, la faisabilité du couplage Osmose Inverse + Disitllation Membranaire sous Vide a été démontrée, pour le traitement direct d'eaux saumatres contenant de l'Arsenic (III). Un taux de rétention global du procédé de 96% pourrait être atteint grâce à ce couplage.

Des surfaces de membranes de DMV relativement importantes peuvent être nécessaires, mais celles-ci peuvent être réduites en augmentant la température d'alimentation. Un compromis peut être trouvé entre surface de membrane et consommation spécifique d'énergie, à une température de 35°C.

Enfin, ce mémoire de thèse se termine par une conclusion reprenant les principaux résultats du travail, et ouvrant la voie vers des perspectives de continuation. Parmi celles-ci, on peut citer les essais du procédé sur des eaux souterraines réelles, ce qui permettrait de prendre en compte la présence d'autres espèces dans le milieu (le Fer en particulier).

Des essais de plus longue durée, sur plusieurs mois, seraient également intéressants afin d'observer le colmatage ou un éventuel mouillage des membranes de distillation membranaire.

Egalement, un couplage de la distillation membranaire avec de l'énergie solaire serait à étudier afin de réduire le coût énergétique du procédé.